EXPERIMENTAL INVESTIGATION OF STRUCTURAL SYSTEMS MADE OF
SHEATHED COLD-FORMED STEEL WALL PANELS

A THESIS SUBMITTED TO
THE GRADUATE SCHOOL OF NATURAL AND APPLIED SCIENCES
OF
MIDDLE EAST TECHNICAL UNIVERSITY

BY

BARIŞ MERT PEHLİVAN

IN PARTIAL FULFILLMENT OF THE REQUIREMENTS
FOR
THE DEGREE OF DOCTOR OF PHILOSOPHY
IN
CIVIL ENGINEERING

JANUARY 2023

Approval of the thesis:

EXPERIMENTAL INVESTIGATION OF STRUCTURAL SYSTEMS MADE OF SHEATHED COLD-FORMED STEEL WALL PANELS

submitted by **BARIŞ MERT PEHLİVAN** in partial fulfillment of the requirements for the degree of **Doctor of Philosophy** in **Civil Engineering, Middle East Technical University** by,

Prof. Dr. Halil Kalıpçılar
Dean, Graduate School of **Natural and Applied Sciences**   _____

Prof. Dr. Erdem Canbay
Head of the Department, **Civil Engineering**   _____

Prof. Dr. Eray Baran
Supervisor, **Civil Engineering, METU**   _____

Examining Committee Members:

Prof. Dr. Kağan Tuncay
Civil Engineering, METU   _____

Prof. Dr. Eray Baran
Civil Engineering, METU   _____

Prof. Dr. Cem Topkaya
Civil Engineering, METU   _____

Assoc. Prof. Dr. Saeid Kazemzadeh
Civil Engineering, Atılım Uni.   _____

Asst. Prof. Dr. Burcu Güldür Erkal
Civil Engineering, Hacettepe Uni.   _____

Date: 12.01.2023

I hereby declare that all information in this document has been obtained and presented in accordance with academic rules and ethical conduct. I also declare that, as required by these rules and conduct, I have fully cited and referenced all material and results that are not original to this work.

Name, Last name: Barış Mert Pehlivan

Signature:

ABSTRACT

EXPERIMENTAL INVESTIGATION OF STRUCTURAL SYSTEMS MADE OF SHEATHED COLD-FORMED STEEL WALL PANELS

Pehlivan, Barış Mert
Doctor of Philosophy, Civil Engineering
Supervisor: Prof. Dr. Eray Baran

January 2023, 275 pages

Cold-formed steel (CFS) structural systems are considered to be an innovative and newly developing construction method. Because of advantages such as lower fabrication periods, high strength/weight ratio and ease of construction, CFS structural systems have been used increasingly all around the world, including seismically active areas. Although there have been many studies in the literature, CFS structural systems are relatively new for the civil engineering practice and few existing specifications regarding the subject still lack necessary detailing for safe and economical design and construction of these systems. As a result, there is a major concern regarding the performance of CFS structural systems especially under seismic actions. The current study aims at improving the understanding of the structural behavior of a specific type of CFS building system, where the lateral load resisting system is made of shear walls sheathed with oriented strand board (OSB) panels. An extensive and detailed experimental investigation on various components of a typical sheathed CFS shear wall system, as well as the connections between these components was conducted in this study. Experimental program consisted of several stages and various components of a lateral load resisting CFS system. Load testing of hold down devices, investigation of different sheathing and fastener

configurations for shear walls, tests on shear wall groups where wall panels are placed both horizontally and vertically and investigation of various connection details between wall panels, as well as experiments on three dimensional structural assemblies utilizing CFS shear walls and a floor system were included in the study. In addition to the extensive experimental part, a numerical study was also included in the thesis work. By using the experimental findings and load-displacement behavior data obtained from CFS shear walls, both single wall panels and full-scale buildings were modeled and analyzed. It was aimed to investigate the seismic response of CFS framed archetype buildings utilizing OSB sheathed wall panels with different levels of stiffness and shear resistance. Nonlinear time history analyses were conducted on archetype buildings and collapse performance evaluation was performed according to FEMA P695 methodology.

Keywords: Cold Formed Steel, CFS Shear Wall, Seismic Performance, Computational Modeling

ÖZ

HAFİF ÇELİK DUVAR PANELLERİNDEN OLUŞAN YAPISAL SİSTEMLERİN DENEYSEL OLARAK İNCELENMESİ

Pehlivan, Barış Mert
Doktora, İnşaat Mühendisliği
Tez Yöneticisi: Prof. Dr. Eray Baran

Ocak 2023, 275 sayfa

Hafif çelik yapı sistemler, yenilikçi ve yeni gelişen bir inşaat yöntemi olarak kabul edilmektedir. Düşük imalat süreleri, yüksek mukavemet/ağırlık oranı ve inşaat kolaylığı gibi birçok avantajı nedeniyle, hafif çelik yapısal sistemler sismik olarak aktif alanlar da dahil olmak üzere tüm dünyada giderek artan bir şekilde kullanılmaktadır. Literatürde birçok çalışma olmasına rağmen hafif çelik yapısal sistemler inşaat mühendisliği uygulamaları için nispeten yenidir ve konuyla ilgili mevcut az sayıdaki yönetmelikler, bu sistemlerin güvenli ve ekonomik olarak tasarlanması ve inşa edilmesi için yetersiz kalmaktadır. Sonuç olarak, özellikle sismik etkiler altında kalan hafif çelik yapı sistemlerinin performansına ilişkin soru işaretleri vardır. Mevcut çalışma, OSB kaplamalı hafif çelik duvar panellerinin yatay yük taşıyıcı sistem olarak kullanıldığı yapıların davranışını araştırmak amacıyla gerçekleştirilmiştir. Bu kapsamda, tipik bir kaplanmış hafif çelik duvar sisteminin çeşitli bileşenleri ve bu bileşenler arasındaki bağlantılar üzerinde ayrıntılı bir deneysel çalışma yapılmıştır. Deneysel program çeşitli aşamalardan oluşmaktadır ve yatay yük taşıyıcı sistem olarak kullanılan hafif çelik duvarların çeşitli bileşenlerinin incelenmesini kapsamaktadır. Çekme tutucu elemanları üzerindeki yükleme testleri,

hafif çelik duvarlar için farklı kaplama ve bağlantı elemanı konfigürasyonlarının incelenmesi, duvar panellerinin hem yatay hem de dikey olarak yerleştirildiği duvar sistemleri üzerinde testler ve duvar panelleri arasındaki çeşitli bağlantı detaylarının incelenmesi ve ayrıca hafif çelik duvarlar ve döşeme sisteminin beraber kullanıldığı üç boyutlu yapı modelleri üzerindeki deneyler çalışmaya dahil edilmiştir. Tez içerisinde deneysel çalışmanın yanısıra sayısal bir çalışma da yer almaktadır. Hafif çelik duvarlar üzerindeki yükleme testleriyle elde edilen deneysel bulgular ve yük-deplasman davranış verileri kullanılarak hem tekli duvar panelleri hem de tam ölçekli binalar modellenmiş ve analiz edilmiştir. Farklı rijitlik ve yük kapasitelerine sahip OSB kaplamalı duvar panelleri kullanılarak hazırlanan hafif çelik çerçeveli örnek bina modellerinin sismik etkiler altındaki davranışlarının araştırılması amaçlanmıştır. Model binalar üzerinde doğrusal olmayan zaman tanım alanı analizleri ve FEMA P695 metodolojisine göre göçme performansı değerlendirmeleri yapılmıştır.

Anahtar Kelimeler: Hafif Çelik, Hafif Çelik Duvar Panelleri, Sismik Performans, Modelleme

To my beloved mother and father, Filiz and Nail Pehlivan…

ACKNOWLEDGMENTS

First and foremost, I would like to express my deepest gratitude to my supervisor Prof. Dr. Eray Baran for his support, guidance, his endless patience and constant encouragement. He is one of the exceptional examples of an academician equipped with a great passion for his work, as well as willingness to share his knowledge and experience. Throughout the years, not only he has been a great guide, a mentor and a teacher, he also inspired me to become better at whatever I do. The work presented here would not be possible if it was not for his leadership and also companionship.

Many special thanks to my Prof. Dr. Cem Topkaya. He is one of the greatest minds that I have ever seen and working with him was such a privilege. His valuable insight, perspective and his contributions enhanced the every bit of this work.

Also, I would like to express my gratitude to Prof. Dr. Kağan Tuncay. He is such an inspiring person with his cordial attitude and many thanks to him as his contribution started this journey.

Although it is not possible to sufficiently express my gratitude with fancy words, many thanks to my beloved parents, Filiz and Nail Pehlivan. They have given endless love and support and made me who I am with their inspirational presence.

One of the biggest thanks goes to my dearest, İlke Togay. Your companionship is invaluable as well as the happiness and joy you bring into my life. Thanks for being at my side.

Special thanks to my favorite people, Berk Karakuş, Güncel Vara and Sinefin Gış. We suffered together, but in the end we thrived together. Pleasure to ride along with you.

TABLE OF CONTENTS

LIST OF TABLES

TABLES

LIST OF FIGURES

FIGURES

xx

xxi

xxiii

xxiv

CHAPTER 1

INTRODUCTION

1.1   General Overview

Cold-Formed Steel (CFS) structural systems are becoming more popular throughout the world especially for low to medium rise buildings. Advantages of this structural system include high strength-to-weight ratio, reduced time and cost of construction and low shipping costs. Manufacturing process of CFS members also allows reduced waste of materials and the recyclability of steel makes CFS structural systems environmentally friendly and energy efficient. CFS is basically structural steel rolled into sheets having 0.8 – 2.0 mm thickness and bent into various cross sections with roll-forming process. As a result, light-weight structural steel members are manufactured to be used as framing members such as studs, tracks and joists in a CFS-framed construction (Figure 1.1).

As a common construction method, a typical CFS structure is built by setting up walls on a foundation and placing CFS truss members or joists on top of walls to create lightweight floors (Figure 1.2). CFS framed shear walls are not only responsible for carrying gravity loads but also lateral load resistance is mainly provided by them. Typically, there are three types of shear wall configurations; strap-braced walls, walls sheathed with wood-based panels and walls sheathed with steel panels. Wood-based sheathing panels include Oriented Strand Board (OSB), gypsum board and plywood while the most popular and widely used type is OSB due to its cost-efficiency and favorable mechanical properties. A CFS wall panel consists of framing members (i.e., vertically placed stud members and horizontally placed track

members) and sheathing panels. Framing members are usually fastened together by rivets or self-tapping screws. Similarly, connection of sheathing panels to the framing is also made possible by using screws. Spacing of panel connecting screws is one of the main parameters affecting the structural performance of a shear wall. In conventional CFS structures, connection between wall panels at floor locations and connection of wall panels to the foundation are achieved with special devices called hold-downs. Along with shear walls, hold-downs are a part of the lateral force resisting system and they are responsible for resisting uplift forces caused by lateral loads and transferring them from wall panels to the foundation.

An important detail that affects the overall performance of CFS structures is the floor system and properties of connections between shear walls and floorings. The two commonly used construction method regarding the walls and floor system are shown in Figure 1.3: (i) platform framing; (ii) ledger framing. Platform framing refers to the detail where floor beams are placed on top of shear walls so that the continuity of shear wall studs are interrupted by beams. Ledger framing on the other hand, utilizes the method where floor beams are attached to the inside face of shear walls using a ledger member. This way, shear walls of neighboring stories are directly connected to each other, providing direct path for the transfer of horizontal forces.

1.2   Research Aim and Scope

As the use of CFS framed structures gradually increase, understanding the behavior of these systems especially under seismic effects is gaining prominence. In CFS structures, seismic loads are resisted by sheathed or braced wall panels, and this type of lateral force resisting system benefits from being light and having low seismic weight. This property makes CFS framing a valid option even for locations with high seismicity. Even this is the case, CFS can still be considered a relatively new system and even with several decades of research devoted, there is still room for

2

advancement in understanding the CFS system behavior both in local and global levels. Thus, main objective of this research program is to investigate the structural behavior of CFS framed structural systems that consist of shear walls sheathed with wood-based panels as the lateral load resisting system. In order to do so, an extensive and detailed experimental investigation has been conducted. Experimental effort consists of several stages and includes various components of a CFS structural system. The research starts from local scale experiments including investigation of the behavior of hold-down devices and continues up to a global scale where three-dimensional representations of a CFS framing system are tested. Load testing of single and double story CFS framed shear walls, as well as multiple horizontally placed shear walls are included in the research, which enabled a detailed investigation of wall response with different construction details.

In addition to experimental investigation of CFS shear wall systems, a detailed numerical study is also included in the thesis. In the first phase of numerical investigation, nonlinear numerical models of CFS wall panels were created based on reversed cyclic shear wall test data obtained through experiments. In the second phase, three dimensional models of CFS framed building archetypes were created by using numerical models of wall panels. The seismic response and collapse performance of these archetypes were evaluated based on the methodology described by Federal Emergency Management Agency (FEMA) P695 (2009) document.

1.3   Organization of Thesis

This thesis consists of ten chapters. The present chapter provides general information about CFS structures, details about their lateral force resisting systems and overall description of the research project.

Chapter 2 contains a literature review on CFS shear walls. In addition to that, design standards and guidelines related to CFS structures are also included.

In Chapter 3, the first part of the experimental study; load testing of hold downs, as well as finite element modeling of these devices are summarized.

Chapter 4 describes the experimental investigation conducted on a proposed hold down device. Results from load testing of the device itself, as well as results of tests on CFS wall panels utilizing this hold down are presented in this chapter.

Chapter 5 contains the investigation on CFS shear walls that are sheathed on both sides with a dense fastener layout. Details about test setup, instrumentation, loading protocol and evaluation methods used for test results are provided.

Chapter 6 describes the load tests on horizontally placed multi panel shear walls. Description of wall panel specimens, details of test setup and considered parameters are also provided.

In Chapter 7, the experimental investigation on two story CFS shear wall configurations is presented. Details of the tested specimens and discussion of test results are provided.

Chapter 8 describes details of the last step in experimental campaign, which is the load testing of three-dimensional CFS frame models.

In Chapter 9, numerical part of the study is presented. Nonlinear computational models are created based on experimental results to predict both single wall and representative archetype building behavior under seismic conditions. Details of models and results of analyses are provided in this chapter.

Concluding remarks of the thesis and highlights of the study are provided in Chapter 10.

Figure 1.1 CFS structural framing systems

CFS Shear Wall

Floor consisting of
CFS trusses and
sheathing

Hold down
connections
between floors

CFS Stud member

Hold downs connecting shear
wall to foundation
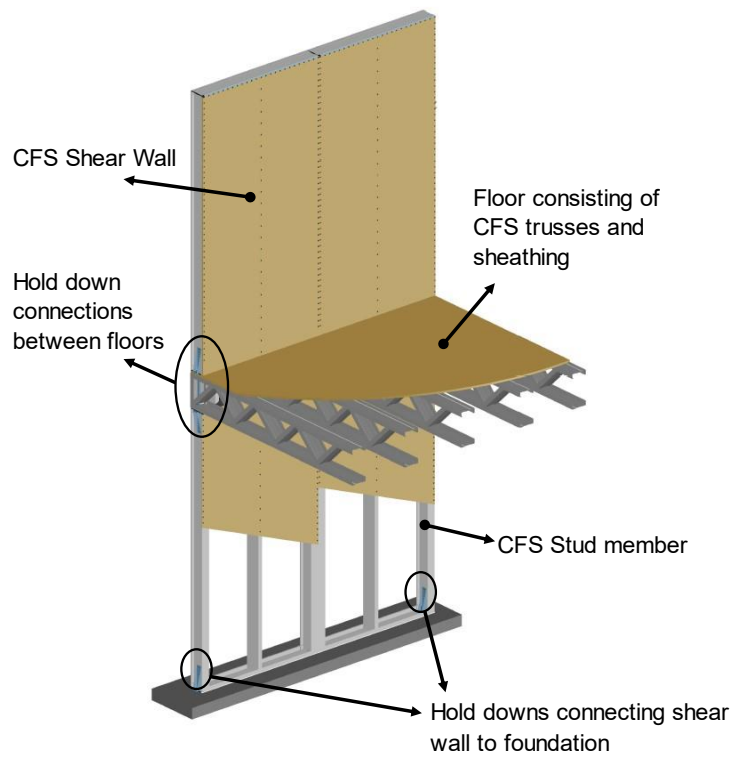
Figure 1.2 Details of a typical CFS framing
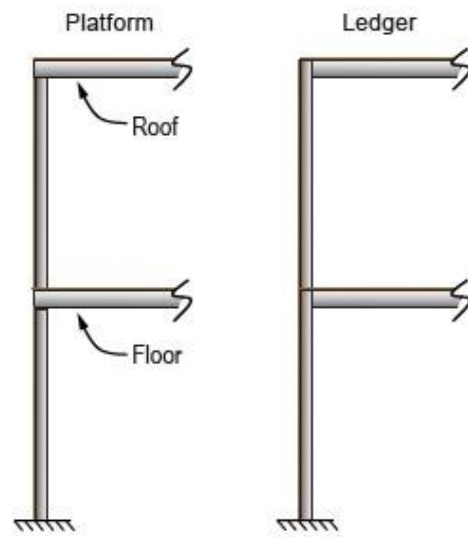
Figure 1.3 Framing types for CFS construction (Madsen et al., 2016)

CHAPTER 2

LITERATURE REVIEW

This chapter reviews current design standards and guidelines related with CFS framed structures as well as experimental and numerical studies on OSB sheathed shear walls. Various standards around the world describes methods for the design of CFS structural systems and sheathed CFS shear walls. Experimental studies from the literature that are presented here includes load testing of wall panel specimens, as well as testing of large scale CFS building representations. Similarly, numerical studies including different levels of detail and complexity are also presented, whether they include modeling of individual shear walls or detailed three-dimensional building models.

2.1   Specifications for the Design of CFS Framed Shear Walls

The research effort and many studies about CFS structural systems in the literature have led to development of design specifications in various countries. General design rules of CFS structural members are covered in specifications such as North American Specification for the Design of Cold-Formed Steel Structural Members (AISI S100, 2016) in North American countries, related parts of Eurocode for European countries (EN 1993-1-3, 2006) and Cold-Formed Steel Structures Specification (AUS/NZS 4600., 2005) for Australia and New Zealand. The recent Turkish Earthquake Code (TBDY, 2018) also includes design rules for CFS structural systems by mostly adapting the provisions from North American standards.

While general rules for design of CFS structural systems are described in aforementioned specifications, only North American standards specifically cover the seismic design rules for these structures. The North American Standard for Seismic Design of Cold-Formed Steel Structural Systems (AISI S400-15, 2015) describes design rules and guidelines in terms of limitations and mechanical properties of components of lateral load resisting systems in CFS structures. Following these rules and guidelines is expected to result in a proper design with plastic behavior localizing in energy dissipating components, which are basically sheathing-CFS connections in CFS framed shear walls. AISI S400-15 (2015) also presents shear strength values for predefined shear wall configurations. In addition to that, seismic design parameters such as the response modification coefficient (R), system over-strength factor (Ω_o) and deflection amplification factor (C_d) are clearly stated in North American specifications for CFS structural systems. For USA and Mexico, ASCE 7-16 (2017) defines these parameters whereas for Canada, these parameters are recommended in the National Building Code of Canada (NRCC, 2015). These standards also describe limits for the maximum height of buildings utilizing CFS framed shear walls as lateral load resisting systems. While seismic design parameters defined in these standards are based on studies considering past earthquakes and they are experimentally evaluated, Federal Emergency Management Agency describes a methodology (FEMA P695, 2009) to evaluate these parameters by non-linear analysis methods. Contrary to North America, earthquake specifications for Australia & New Zealand (AS1170.4, 1993) and Europe (EN 1998-1, 2004) do not explicitly cover structures with CFS lateral load resisting systems. The first one only describes a limiting response modification factor, while the latter one does not provide any behavior factor or design rules.

2.2 CFS Framed Shear Walls

Over the decades, there has been extensive research on sub-system components of CFS structural systems. Especially, studies on shear walls contribute to the literature by a great extent. In a CFS structure, shear walls sheathed with OSB or other sheathing materials provide the lateral force resisting capability of the structure. As a result, the overall seismic performance of a CFS building is directly related with the behavior of shear walls. For this reason, a considerable amount of experimental studies on CFS structural systems has actually focused on the lateral load response of CFS framed shear walls.

Several of these studies were conducted by Serrette and colleagues. CFS framed shear walls sheathed with plywood, OSB and gypsum boards that are connected to CFS framing with varying screw spacing values were tested under static and reversed cyclic loading conditions (Morgan et al., 2002; Nguyen et al., 1996; Serrette, 1997). In another study from the same research group, Morgan et al. (2002) further expanded the work on CFS shear walls with additional twenty tests on wall panel specimens with alternative configurations.

An extensive experimental research program has been conducted at the McGill University in Canada by several researchers. A total of 109 wall panel specimens were tested under monotonic and reverse cyclic loading conditions by Branston (2004), Boudreault (2005) and Chen (2004). Specimens were consisted of 16 different configurations. Various height to width aspect ratios, sheathing types and fastener spacings were investigated. The test setup used in the project for load testing of shear wall specimens is shown in Figure 2.1. Outcomes of this experimental research program are considered to be important milestones in the related literature. Not only the effects of different parameters on the overall behavior and shear strength of wall panels were evaluated, but also design parameters and test based

reduction factors were proposed. Branston (2004) investigated several methods to obtain design parameters from test data and suggested the Equivalent Energy Elastic-Plastic (EEEP) method, which has become a generally accepted and a widely used method.

Blais (2006) further extended the research effort by testing eighteen shear wall specimens sheathed with 9 mm thick OSB panels. Panels were connected to CFS framings with three different screw spacing configurations: 152 mm, 100 mm and 75 mm. Based on the findings and design values obtained from EEEP approach, R_o and R_d values were recommended as 1.8 and 2.5, respectively. In another study, Hikita (2006) investigated the effect of gravity loads on the lateral performance of sheathed CFS shear walls by conducting an experimental study on 32 wall specimens. These studies provided important insight on behavior of CFS framed sheathed shear wall panels under lateral loads and outcomes of these studies provided improvements and recommendations to the North American Design Specifications (AISI-S100, 2016).

In Johns Hopkins University, an extensive study was conducted under the name Cold-Formed Steel – Network for Earthquake Engineering Simulation (CFS-NEES) research project. Project focused on understanding and improving the performance of CFS framed buildings with OSB sheathed shear walls as lateral force resisting system. The investigation included load testing of CFS framed sheathed single walls (Liu et al., 2014) and tests on stud-sheathing connections (Peterman et al., 2014). One of the most important part of the project was shake table testing of a full scale two-story CFS framed building (Figure 2.2). Outcomes and findings of the research effort was summarized by Peterman (2014) and Schafer et al. (2016). Results obtained from this full-scale shake table testing indicated that presence of gravity load resisting systems and non-structural elements caused an increase in the lateral stiffness of the building. The experimentally determined stiffness was eighteen times

greater than the design value, which was calculated by only considering the effect of shear walls.

Many works have also been conducted by researchers from Europe. Fülöp and Dubina (2004) conducted an experimental study in which OSB sheathed shear walls with dimensions 360x244 cm were tested under monotonic and reversed cyclic loading conditions. This way, effect of loading type was investigated and it was reported that wall specimens acquired approximately 10% higher load capacity under monotonic loading compared to reversed cyclic loading. In addition to that, effect of openings and gypsum board interior cladding were also investigated.

Structural performance of CFS structures has been investigated extensively by researchers from Italy (Iuorio et al., 2014; Landolfo et al, 2006). The study by Fiorino et al. (2012) considered the seismic capacity of sheathed CFS walls and evaluated seismic design parameters and dynamic characteristics for various shear wall configurations. In addition to that, an alternative seismic design approach for sheathed CFS framed structures was proposed (Fiorino et al., 2009). A more recent study of the same research team was on the investigation of prefabricated CFS systems and it was a European Union funded project called ELISSA (Energy Efficient Lightweight-Sustainable-Safe-Steel Construction). The proposed system consists of CFS framed shear walls sheathed with gypsum panels. Seismic performance of the system was evaluated with experimental tests on connections, shear walls, and also shake table tests on a full-scale building specimen (Figure 2.3) (Fiorino, et al., 2017; Macillo et al., 2017).

Over the course of the last two decades, CFS framed wall panels have been the subject of many studies and these studies have been compiled by several researchers and discussed in various reports in order to establish databases on lateral behavior and strength of CFS wall panels (AISI, 2010; Ayhan et al., 2018; Sharafi et al., 2018; Zhang et al., 2021). Numerous parameters having strong influence on the behavior

11

of wall panels have been investigated with the studies available in the literature. These parameters include CFS member cross section and material properties, sheathing panel type and thickness, wall panel aspect ratio and presence of openings, connection screw type and spacing, and loading method used for testing.

2.3   Numerical Modeling of CFS Shear Walls

Significant research has been devoted during several past decades toward accurate modeling of CFS wall panel systems for lateral loading simulations. The existing numerical modeling methods are categorized as either micro modeling or macro modeling. In micro modeling approach all components of the structural system, including the CFS framing members, sheathing panels, and connectors are explicitly modeled in detail. As a result of the relatively high level of detail, micro models are capable of capturing all possible failure modes within the entire system provided that proper material behaviors and geometric relations are utilized for the components. Macro modeling, on the other hand, is considered to be more efficient approach, with reduced computation time and effort as compared to micro modeling. In this approach, components of the structural system are represented by equivalent simplified elements (Usefi et al., 2019).

One of the earlier studies that included modeling of CFS structures was the work of Boudreault (2005). In this study, CFS shear wall models were created using equivalent brace elements with the Stewart hysteresis model and results were validated against experimental results. These wall models were later used for creating two and three story structural models and evaluated under lateral loading conditions. Similar studies were conducted by Dubina (2008) and Fülöp and Dubina (2004b). Based on the results of experimental tests on CFS framed wood sheathed shear walls, numerical models were created by equivalent brace method capable of capturing the nonlinear behavior.

Another detailed study on modeling of CFS structures was completed by Shamim (2013). Based on the shear wall response obtained from single and double story test specimens (Shamim et al., 2013), numerical models were created for steel sheathed shear walls utilizing equivalent brace method and by using the Pinching4 element in OpenSees platform (Bian et al., 2015). Modeling effort was further continued with the development of archetype buildings (Figure 2.4) (Shamim and Rogers, 2015b) by utilizing the previous findings.

As mentioned before, the CFS-NEES project completed in the USA included shake table tests on a full scale two-story CFS framed building and outcomes from this project was reported by Peterman (2014) and Schafer et al. (2016). Following that, researchers of this project also conducted numerical studies by creating computational models of the tested CFS building (Leng, 2015; Leng et al., 2017; Schafer et al., 2016). In these studies, authors developed high fidelity numerical models to accurately predict the experimentally determined behavior of the test structure. In addition to that, another study evaluated different levels of complexity in modeling a CFS framed structure and evaluated its performance when subjected to nonlinear time history analysis (Leng et al., 2020). Linked to the same project, (-Bian et al. (2014) and Buonopane et al. (2015) conducted studies on fastener based numerical modeling approach in addition to a more conventional equivalent brace modeling approach. Instead of representing the shear wall behavior with brace elements, these models include spring elements for each individual fastener between sheathing and CFS framing. Obtained results were reported to be consistent with experimental findings.

Modeling of three dimensional archetype buildings were considered in several other studies with various types of CFS framed shear walls. In a study by Fiorino et al. (2017) strap braced shear walls were considered as lateral load resisting elements in typical CFS framed building archetypes, and performance evaluation was conducted

13

according to FEMA P695 (2009) methodology. In the numerical models, floor elements were considered as rigid and moment releases were defined between studs and rigid floors. Similar approach was used in other studies by Shakeel et al. (2019) on shear walls with gypsum board sheathing and wood sheathing (Shakeel et al., 2020a). A more recent study by Landolfo et al. (2022a) evaluated previous studies and results obtained from analyzing computational models of archetype buildings to propose new seismic design rules to be included in Eurocode 8.
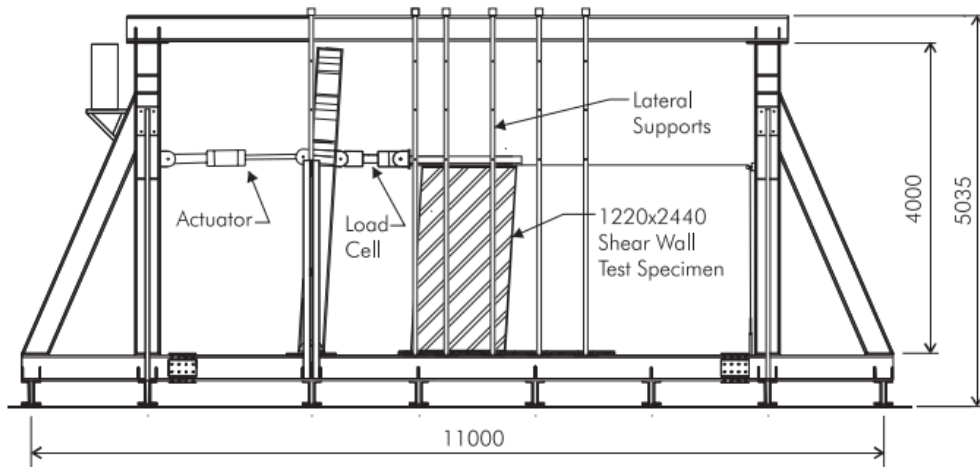
Figure 2.1 Schematic representation of the test setup used in McGill University
research program. All units in millimeters (Branston et al., 2006)

Figure 2.2 CFS-NEES Project full scale building (Peterman, 2014)
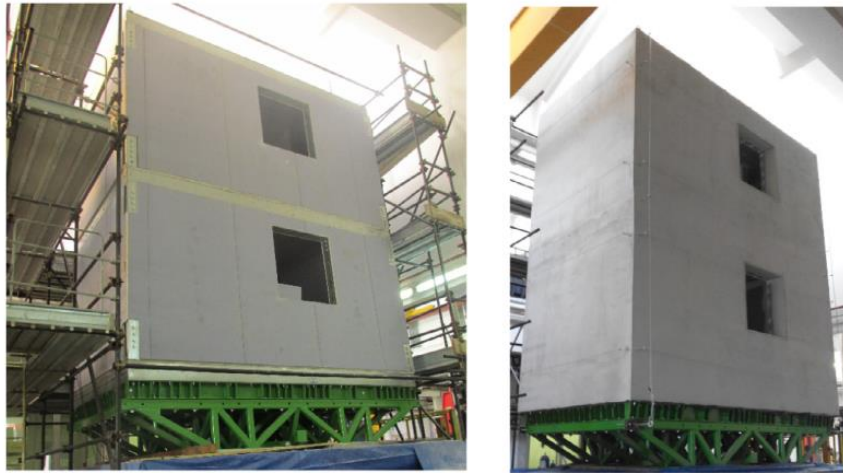
Figure 2.3 Shake table tests from ELISSA project (Fiorino, et al., 2017)
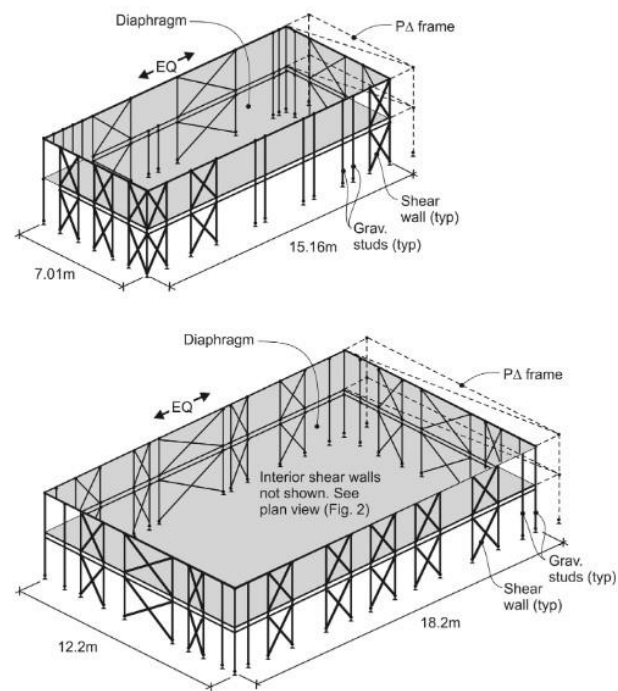
Figure 2.4 Modeling of archetype buildings (Shamim and Rogers, 2015b)

16

CHAPTER 3

TESTING AND ANALYSIS OF DIFFERENT HOLD DOWN DEVICES FOR CFS CONSTRUCTION

3.1   Introduction

Hold-down devices are used in conventional cold formed steel (CFS) structural systems as part of the lateral force resisting system for the purpose of transferring the CFS wall panel chord stud forces between adjacent floors and to the foundation system at the wall base. In order to provide a proper load transfer, these devices need to have adequate strength and stiffness characteristics (Madsen et al., 2016). Failure of the hold down devices to meet the strength and stiffness requirements may prevent the lateral force resisting system to utilize its entire capacity and will negatively affect the performance of the structure against seismic and wind forces.

The capacity-based design approach adopted in the current AISI Standard for Seismic Design of CFS Structural Systems (AISI S400-15, 2015) does not consider the hold downs as energy-dissipating elements in seismic force resisting systems of CFS structures. Accordingly, the hold downs are required to be designed based on increased seismic forces considering seismic overstrength or the expected strength of the designated energy-dissipating elements. Even though the AISI Standard requires the strength and stiffness of hold downs to be considered in design of seismic force resisting system, no method is provided explicitly for calculation of these properties. Therefore, laboratory testing is usually required in order to establish the mechanical response of such devices.

Another motivation for load testing of hold down devices, other than to obtain the design strength and stiffness, is to determine their mechanical response to use in

numerical modeling of wall panels or the structure as a whole. Accurate numerical modeling of the restraint against uplift of wall panels requires a full characterization of the mechanical response of hold down devices.

A two-phase study was conducted to investigate the mechanical behavior of different types of hold downs. The first phase of the study consisted of component testing of hold down devices and the second phase was based on testing of wall panels under lateral loading. In the component testing phase, monotonic and cyclic tensile load tests were performed on various types of hold down devices, in an attempt to reveal the hold down geometries that can enhance the performance of CFS framed buildings. The hold downs tested as part of the study represent devices that are commercially available as well as a simple hold down geometry that is made of a steel angle section. Some of the hold down geometries were studied with additional test parameters in order to come up with construction details that would result in improved performance. In the second group of tests, the hold down that is made of a steel angle section was further studied as part of oriented strand board (OSB) sheathed CFS framed wall panels. Monotonic and cyclic lateral loading were applied on wall panels, keeping the hold down devices under tensile force effects.

The main objectives of this study are to assess the performance of different hold downs produced by various manufacturers, as well as to demonstrate that simple hold down geometries that are relatively easy and less costly to fabricate can satisfy the necessary strength and stiffness requirements. Scope of the study extends to load testing of CFS framed wall panels incorporating such simple hold down devices in order to qualify the performance of these devices when used in a wall panel.

3.2   Hold Down Test Procedures and Loading Protocol According to AISI Specifications

AISI S913-13 (2013) Specification provides recommendations for load testing of hold downs, which is usually required in order to establish the strength and stiffness characteristics of these devices. In addition to the testing procedures, this specification also explains the procedures for evaluation of test results. Based on AISI S913-13 (2013), there are two recommended ways to test hold downs under tensile loads: hold down device test and hold down assembly test. Hold down assembly test simulates the field conditions, where the test setup includes cold formed steel members connected to hold down devices with fasteners and hold downs connected to test bed with anchor rods. In the current study, hold down test specimens were created in a similar way as the AISI hold down assembly test specimens, except that the CFS sections were sheathed with oriented strand board (OSB) plates on both sides, as shown in Figure 3.1.

As indicated, the specimen geometry represents the bottom corner of a CFS framed sheathed wall panel. Based on the experimentally determined load-deformation response obtained from hold down assembly tests, it is possible to determine the design load capacity of hold downs along with the maximum load capacity. In order to calculate the design load capacities, displacement limits are considered as stated in recommendations of AISI S913-13 (2013). These displacement limits are directly related with seismic design limits of CFS framed wall panel structural systems, where hold down devices are used as connectors. Accordingly, Load and Resistance Factor Design (LRFD) load capacity is taken as the smaller of 65% of maximum load attained by the hold down during testing or the load corresponding to 6.35 mm of vertical hold down deformation. Allowable Strength Design (ASD) load capacity, on the other hand, is taken as 70% of LRFD load capacity. Figure 3.2 shows a generic

load-displacement behavior of a hold down device and the definition of LRFD load capacity.

In the current study, both monotonic and cyclic loading protocols were used for hold down assembly testing phase. In monotonic tests displacement loading was applied on test specimens until failure occurred. Force controlled cyclic loading protocol recommended by CUREE (Consortium of Universities of Research in Earthquake Engineering) (Krawinkler et al., 2001) was chosen as the cyclic protocol. The CUREE force-controlled cyclic loading protocol involves a reference force value, which is the maximum force the test specimen is expected to experience, and cycles at incrementally increasing force levels are based on this reference force value. Accordingly, reference force values for the cyclic tests were taken as maximum force capacity of hold downs obtained from monotonic testing. Based on the experimentally obtained reference forces, the cyclic loading protocol was created, as shown in Figure 3.3.

3.3   Hold down Test Program

The geographical location of a CFS construction plays an important role in the selection of the type of hold down device used in a building. In North America patented off-the-shelf products are readily available and can be procured from department stores. These hold downs usually employ a special and sometimes complex geometry to increase the stiffness and strength of the device to meet the code requirements. Manufacturing of these devices usually require a special production line where cutting and bending of plates, drilling of holes and other necessary operations are automatically performed. While investing on development of such production lines is feasible for production of mass quantities of hold downs, it will not prove useful for economies where CFS construction is limited. In many parts of the world, off-the-shelf hold down devices are not available and the

contractors usually resort to in-house products that are produced by local CFS manufacturers. Unlike patented off-the-shelf hold down products, these in-house products do not come with any kind of capacity values or even material properties most of the time. Structural performance of such devices is a major concern because they are seldom subjected to proof load testing. For this reason, it is important to evaluate these in-house type of products and attain capacity values to be used for design purposes.

The main objective of hold down test program is to compare the performances of patented off-the-shelf devices and the in-house ones. In addition, the test program aims to propose cost effective hold down devices that can potentially be used in countries where off-the-shelf products are not available. Pursuant to these goals, a market survey among CFS manufacturers based in Turkey was conducted. Based on the results of this survey four hold down devices from three different manufacturers were included in the test program. In addition, an off-the-shelf type of product widely used in North America was experimented for comparison purposes. A new hold down device that consists of a hot rolled steel angle section was also manufactured and tested as a part of the experimental program. Since no information on the behavior of these specific manufactured angle type hold down devices is present in the literature, it is important to assess the performance of such devices by means of loading tests. The advantage of this angle type hold down is that it does not require costly bending or welding operations, which are required for the other hold down types.

The hold down test program included load testing of fourteen specimens representing seven hold down types named as HD-1 to HD-7. Monotonic loading was applied on eleven of the specimens while the remaining three specimens were tested under cyclic loading. As mentioned before, four of these hold down devices are products of three different manufacturers based in Turkey, one of the hold downs is an off-

the-shelf type of product which has a wide usage especially in North America, and two of them were hold downs made of available steel angle sections. Photographs of each of these hold down devices are given in Figure 3.4 while their technical drawings are provided in Figure 3.5 together with the weight of each device.

Hold downs HD-1 and HD-2 are composed of a bent steel plate as the body of the hold down and two triangular shaped stiffeners are welded at sides. Hold downs HD-3 and HD-4, are produced by bending of a single steel plate. In these hold downs the bottom parts of the two vertical triangles forming the sides of the device, as well as the bottom part of the back plate, were bent 90-degrees to form the bottom horizontal surface. This way, three pieces of steel plates rest on top of each other to form the bottom part of the device. In HD-4, edges of these three steel plates were fillet welded, while no such welding was provided in HD-3. Hold downs HD-1 to HD-4 are currently being used in CFS construction in Turkey, even though some of these devices have very poor structural behavior, as discussed in the following sections. These hold down devices were developed in-house by CFS construction companies and are not readily available to third party buyers. Therefore, technical information of these products is only kept in company files and is not made public.

Hold down designated as off-the-shelf (HD-5) was again made from a single steel plate and had a distinct geometry and a pre-deformed shape. This hold down has been widely used in CFS construction in North America.

HD-1 to HD-5 employ plates which are 2.5 to 3.0 mm thick. The amount of material used in each hold down differs due the thickness of the plate and more importantly due to the geometry of the side plates. HD-1 to HD-4 have comparable weights while the HD-5 has a considerably higher weight. All of these hold downs require bending of plates and in some cases welding of these plates as well. These operations adversely affect the cost of manufacturing. Furthermore, HD-5 requires two separate parts, one resting on top of the other, to be manufactured.

The proposed hold down HD-6 was manufactured in the laboratory from a 60 mm wide L120x12 steel equal leg angle section. The horizontal leg has an 18 mm diameter hole for the anchor rod and the vertical leg has multiple holes to accommodate the screws connecting the hold down device to the vertical CFS framing member. Hold down HD-7 was similar to HD-6, except that it was manufactured from a 60 mm wide L150x15 steel equal leg angle section. The width of the angle sections was selected similar to the width of other hold downs such that the hold down device can easily fit into the CFS track. The leg size and angle thickness were selected based on market availability. Because these angle sections are not reinforced by side plates, relatively thick angle sections should be selected to meet the stiffness and strength requirements. Although the thickness of the angle sections used in this study is 4 to 5 times the typical thickness used by off-the-shelf-products, the weights of HD-5 and HD-6 are almost identical. While selecting thicker angle sections has a negative impact, the absence of side plates greatly reduces the weight of the device. The angle section hold down employs similar amounts of steel material and does not require bending and welding operations. This hold down does not require any special production lines to be built and customary steel fabricators can produce this hold down in an automated fashion as the only operation needed is drilling of the holes. This enables mass production of this device by steel fabricators without any additional investments.

Coupon samples were taken from each hold down device and subjected to tensile testing. Results of these material tests in terms of yield (Fy) and tensile strengths (Fu) are given in Table 3.1.

Figure 3.6 shows the dimensions of test assemblies along with some of the details. Each specimen included an "L" shaped CFS framing made of 90 mm deep 1.2 mm thick lipped channel sections. Vertical leg of the framing has double channel sections connected back-to-back while the horizontal member has a single channel section.

23

The hold downs were attached to the vertical leg of CFS framing with either 4.2, 5.5, or 6.3 mm diameter self-tapping screws. Sheathing applied on both sides of CFS framing comprised of 11 mm thick OSB plates. These plates were attached to the CFS framing members using 4.2 mm diameter self-tapping screws placed at 150 mm spacing.

3.3.1 Test Specimen Selection and Hold Down Design

Table 3.2 shows details of test specimens. As evident, the number and diameter of screws providing the connection between hold down device and CFS framing were varied. The screw number and size used for hold downs HD-1 to HD-5 were dictated by those of the screw holes available on the devices. For these hold downs, the largest diameter screw that can fit inside the holes left on the devices was used. For hold down HD-6 connection screw size was used as a test parameter and this device was tested with two screw diameters of 4.2 and 5.5 mm. Having seen that the failure of HD-6 was due to shearing of connection screws, a larger screw diameter of 6.3 mm was used in hold down HD-7 in an attempt to improve the response of this device. The number of connection screws used in hold downs HD-6 and HD-7 was selected based on the maximum number of screws that can be accommodated by one leg of the steel angle sections.

As mentioned in the following sections, some of the hold-down devices exhibited limited damage during load tests and the failure of these specimens was due to shearing of connection screws. In order to determine screw strength, shear load tests were conducted on 6.3 mm diameter screws. The 6.3 mm screw diameter was chosen based on the fact that this diameter was used in majority of hold-down specimens that had screw shear off failure. In an attempt to reveal the effect of multiple fastener group action tests were conducted on single screws, as well as on groups of two, three and four screws. The test screws were subjected to double shear loading using

the setup shown in Figure 3.7. In order to prevent tilting of screws during load tests and measure the pure shear strength, the screws were driven into plywood pieces. Loading was applied in the form of monotonically increasing displacement and was continued until the test screws have sheared off. Screw shear capacities obtained from these tests are given in Table 3.3. The reported capacity values represent the average of three tests for each group. The measured shear strength values reveal the influence of group action among fasteners in which the shear capacity per screw reduces as the number of screws increases.

During the test program several modifications were applied in angle type hold downs (HD-6 and HD-7) in an attempt to improve their behavior. In Specimen HD6-M3, the total web thickness of the vertical leg of the CFS framing was increased at the hold down location by providing a 1.2 mm thick steel backing plate as seen in Figure 3.8, to reduce the tilting deformation of the connection screws. In order to eliminate the prying effect, measures were taken in specimens HD7-M2 and HD7-M3. For this purpose, 75 mm portion of horizontal leg of the hold down was cut in specimen HD7-M2 and a 50 mm gap was left between the hold down and the horizontal CFS framing member in specimen HD7-M3, as seen in Figure 3.8.

3.3.2   Hold Down Test Setup and Instrumentation

Details of the loading setup used in hold down tests are shown in Figure 3.9. The specimens were positioned in the loading frame in upside down orientation. A 20 mm thick steel base plate was fixed at the top of the loading frame. Hold down device was attached to the base plate with a 16 mm diameter steel threaded rod that has a yield strength of 480 MPa and tensile strength of 600 MPa. Displacement loading was applied at the free end of vertical CFS framing member by a screw jack that is driven by an electric motor. Tensile load acting on hold down was measured by a

25

200 kN capacity load-cell positioned between the mechanical loading assembly and the vertical CFS framing member.

In order to measure the deformation of specimens, a linear variable displacement transducer (LVDT) having a stroke of 100 mm was used. The LVDT measured the relative vertical displacement between the steel base plate and the vertical CFS framing member as shown in Figure 3.10.

3.4   Hold down Test Results

3.4.1   Deformation Modes

Several deformation modes were observed on specimens under applied tensile loading. Tilting of the screws connecting the hold down to the vertical framing member was common to almost all of the specimens. Such tilting deformation was followed by shearing of the screws in some of the tests. Deformations occurred in CFS framing members include local buckling, tearing, and punching, as shown in Figure 3.11.

Hold down devices themselves were also subjected to deformations shown in Figure 3.12. As evident, hold downs HD-1, HD-2, HD-3, and HD-4 particularly suffered from extensive damage during load tests. However, it should be mentioned here that the pictures in Figure 3.12 represent the hold down damage occurred at the end of load tests. Such deformations often correspond to significantly large uplift deformations and are usually not allowed at service load levels in CFS structural systems. The deformations observed in hold down devices near service load levels were much less severe than those depicted in Figure 3.12 and usually included tilting of the connection screws and local web bending of the vertical CFS framing member in the vicinity of screws.

3.4.2   Load-Deformation Response of Hold Downs

Measured tensile load versus uplift plots of hold down specimens are shown in Figure 3.13. The LRFD design load capacities determined as per AISI S913-13 (2013) are also indicated on the plots for each specimen. A summary of experimental results is given in Table 3.4. It should be mentioned that for each specimen the reported LRFD load capacities are controlled by the displacement limit of 6.35 mm, rather than the force limit of $0.65 \times P_{max}$. As evident in the plot given in Figure 3.13a hold down HD-1, which is known to be frequently used in CFS buildings constructed in Turkey, exhibited a limited load capacity and stiffness as a result of excessive deformation. Hold down HD-2 also suffered from extensive deformation and exhibited relatively small load capacity. The additional fillet welding provided along the folded plate edges in the bottom part of hold down HD-4 resulted in much favorable response compared to hold down HD-3. The ultimate failure of hold down HD-3 was due to plate rupture along all three edges of the bottom part of the hold down device (Figure 3.12), while for hold down HD-4 the failure mode became a combination of devise failure and pull out of the connection screws from the vertical CFS framing member. Close agreement between the monotonic and cyclic response of hold down HD-4 in terms of the maximum load capacity and stiffness is also evident in the plots given in Figure 3.13d. Hold down HD-5, which is a patented off-the-shelf device widely used in North America, showed no noticeable deformation during load tests as a result of its distinct geometry. Failure of the specimens utilizing this hold down device was due to shearing of the connection screws in both the monotonic and cyclic tests. The maximum and LRFD load capacities based on monotonic test results are in good agreement with nominal and LRFD load capacities reported in the manufacturer's technical specification. It should also be mentioned that no significant difference was observed in the response of this hold down device under monotonic and cyclic loading.

Among the hold down devices manufactured using a steel angle section, hold down HD-6 was used in three monotonic tests and the failure of all three specimens was due to shearing of the connection screws with some bending deformation on the horizontal leg of the angle (Figure 3.12). As evident in the plots shown in Figure 3.13f, improvement in the behavior due to increasing the screw size and providing a backing plate was insignificant. Due to its larger leg thickness and increase in screw capacity, hold down HD-7 had higher load capacity and stiffness than HD-6. Modifications such as shortening the leg of hold down and leaving a gap between the hold down and horizontal CFS framing member resulted in a reduction in both the load capacity and the stiffness of hold down HD-7. Plots in Figure 3.13g also depict the close agreement between the monotonic and cyclic load-displacement response of specimens utilizing hold down HD-7.

As mentioned earlier, specimens HD5-M1 and HD7-M1 utilized 6.3 mm diameter connection screws and the screws in these specimens were subjected to shear off at the end of load tests. For these specimens, load capacity based on screw shear off was calculated using the measured screw shear strength values. This capacity was calculated to be 75.1 kN for specimen HD5-M1 ($12 \times 6.26 = 75.1$ kN) and 100.2 kN for specimen HD7-M1 ($16 \times 6.26 = 100.2$ kN). The experimentally obtained load capacities for these specimens represent 96% and 76% of the calculated capacities, respectively. These values indicate that the load corresponding to the pure shear capacity of connection screws accurately represents the load capacity of specimen HD5-M1. For specimen HD7-M1, on the other hand, the total screw shear capacity overpredicts the hold down capacity by about 33%. The reason that screw shear off failure in specimen HD7-M1 occurred at a considerably smaller load level than the one corresponding to the pure shear capacity of connection screws is due to the fact that there was significant tensile force on connection screws in this specimen, in addition to shear. The reason for this additional screw tensile force is the presence of bending moment created by the eccentricity between the vertical CFS framing

28

member and the anchor rod in specimens. Such bending moment together with the relatively small moment arm of connection screws in hold down HD-7 results in significant tensile force effect. The connection screws in hold down HD-5 have much larger moment arm when compared to those in HD-7 (see screw locations on hold down devices in Figure 3.5). Therefore, the tensile force effect on screws remains small in the case of HD-5 and the total screw shear capacity accurately represents the load capacity of specimen HD5-M1.

3.4.3 Comparison among Hold Down Devices

Comparison of the maximum and LRFD load capacities of all hold down devices tested in this study is presented in Figure 3.14. In terms of the maximum load capacity, hold downs HD-4, HD-5, HD-6, and HD-7 performed better than the other hold down types. However, because the AISI Specification do not allow the use of maximum load capacity in design and recommends procedures to determine design load capacities, comparison of LRFD load capacities has a more significant practical meaning than that of maximum load capacities. When the LRFD load capacities are considered, hold downs HD-5, HD-6, and HD-7 seem to outperform the other hold down types with HD-5 having the largest capacity and HD-7 having a slightly smaller capacity.

Another important observation that is valid in the plots given in Figure 3.14 is that some of the hold down devices that have been used in CFS construction projects exhibited very poor behavior. These hold downs were observed to undergo significant deformations under tensile loading and as a result had limited load capacities. As an example, HD-1 used in the current study was also reported to undergo extensive deformation in wall panel tests by Baran and Alıca (2012). The hold down response in terms of deformation mode and load capacity observed during those wall panel tests was similar to the response of specimen HD1-M1 tested in the

current study. As Baran and Alıca (2012) reported, this hold down device became the weakest link in the entire wall panel system during their loading tests. The limited load capacity and stiffness obtained in the current study for hold down HD-1 is an evidence that this type of device is not suitable to be used in CFS structural systems for the purpose of transferring wall panel chord stud forces to the foundation system at the wall base.

Load-deformation response of specimens utilizing hold downs HD-5, HD-6, and HD-7 is shown in Figure 3.15. As explained earlier, one of these hold downs is a patented off-the-shelf hold down device widely used in North America while the other two hold downs were proposed as a part of this study and simply manufactured from pieces of steel angle sections without requiring much effort and cost. Even though HD-5 exhibited higher initial stiffness it had similar LRFD load capacity at 6.35 mm deflection as hold down HD-7. The main deformation and resistance mechanisms in these specimens were related with the deformation of CFS profile at screw locations and the deformation of screws themselves. Such mechanisms occurred mainly due to the fact that these hold down devices themselves possessed sufficient strength and stiffness such that the strength and stiffness of the system were dictated by the response of other components in the subassembly. Therefore, the thickness of steel parts and the number and size of connection fasteners in these devices can be adjusted by the designer to meet the required strength and stiffness demand dictated by the structural system.

Another point that is worth noting in Figure 3.15 is that specimens HD5-M1 and HD7-M1 exhibited similar load capacities even though the former specimen utilized 12 connection screws while the latter one utilized 16 screws of the same size. The discrepancy is related with the difference in layout of connection screws on hold down devices. As discussed earlier, the relatively smaller moment arm of connection screws on hold down HD-7 results in significant tensile force in these screws in

addition to shear force. This additional tensile force caused a reduction in shear capacity of connection screws and adversely affects the hold down capacity. Such phenomenon is a clear example that the layout of connection screws has a significant influence on the response of a hold down device. Because hold downs HD-1 to HD-5 were pre-manufactured the fastener layout for these devices was not a parameter that can be altered during the experimental program. For hold downs HD-6 and HD-7, on the other hand, as many screws as can be placed on one leg of steel angle sections were used and the layout of these screws was such that they are uniformly distributed within the angle leg. Deformation patterns and the experimentally determined load capacities suggest that had the fasteners been located close to the free edge of the vertical leg of steel angle sections to provide a larger moment arm, larger strength and stiffness values could have been obtained from these devices.

3.5   Numerical Study on Hold Down Devices

Finite element models of hold down devices tested as part of the experimental study were created using commercially available finite element program ANSYS (2015) and analysis was conducted on these models. Finite element modeling offers the advantage of studying the performance of hold down devices themselves, without concentrating on the assembly behavior. In other words, in order to provide a comparison of the response of hold down devices themselves without the influence of the finite strength and stiffness of the connection fasteners as well as that of the fastener layout, the screws providing the connection between hold down device and CFS member were not included in these models. Furthermore, accurate modeling of the screw connection between hold down devices and CFS profiles would require the response of screws under the combined effects of shear and tension, as well as the interaction between the screw threads and the CFS profiles. Modeling of these mechanisms is relatively complex and requires experimental data to calibrate the FE

models and verify the results. Because of the absence of such experimental data, the screws were not included in FE models whether as distinct elements or simplified global springs.

3.5.1   Description of FE Models

Each model included a hold down device, a 20 mm thick steel base plate, a 16 mm diameter anchor rod and a nut attached to the lower end of anchor rod (Figure 3.16). Welding present in some of the hold down devices was not included in models, instead the parts welded together were modeled as rigidly connected. It should be noted that in order to obtain accurate results and correctly represent the complex deformation mode of hold down devices, the base plate and anchor rod were included as discrete bodies in FE models. Although it may be possible to simulate the base connection arrangement by means of spring elements, such a modeling approach would require the knowledge of exact load-deformation relationship to be used for these elements. Use of such a simplified model might not be able to capture some of the deformation modes observed during experiments, either. For example, the contact algorithm employed in FE models allows the transfer of compressive forces between the hold down device and the base plate only through the bent part of the hold down. This way, the models accurately capture the influence of prying of hold downs on axial force develop in anchor rods. Such a complex mechanism may not accurately be represented with the use of a simple spring element. All parts were meshed with a combination of 20-node brick and 10-node tetrahedral solid elements. Fixed boundary condition was assigned at all nodes located at the lower face of base plate and linearly increasing vertical displacement was applied at nodes corresponding to screw locations on hold down devices. Contact surfaces were defined at all interfaces between different parts. The contact between anchor rod and nut was set as bonded type, while frictional type contact with a friction coefficient

value of 0.2 was used for all other contact surfaces. For the formulation of contact surfaces, Augmented Lagrange method was used. Nonlinear stress-strain behavior of steel parts was implemented using isotropic hardening. Material properties for hold down devices were specified based on the measured steel strengths given in Table 3.1. Other parts in models (i.e., base plate, anchor rod and nut) were assigned a yield strength of 480 MPa and an ultimate strength of 600 MPa. For all steel parts the elastic and hardening moduli were taken respectively as 200 GPa and 2 GPa with a Poisson's ratio value of 0.3.

3.5.2   Results of FE Analysis

Numerically determined deformed shape of each hold down device together with the corresponding equivalent plastic strain distribution is shown in Figure 3.17. A comparison of the numerically determined and experimentally observed deformed shapes indicates the accuracy of FE models in correctly capturing the deformation mode of all hold down device types. Resulting load-displacement behavior of hold down devices are shown in Figure 3.18. The plots given in this figure generally shows a similar trend as those in Figure 3.13 and Figure 3.15, confirming the agreement between the experimentally determined and numerically predicted response. Poor response of hold down devices HD-1 and HD-2 with limited stiffness and load capacity is evident in Figure 3.18. The beneficial effect of attaching the folded plate edges in the bottom part of hold down HD-4 as compared to HD-3 is also clearly seen. Along with that, both of the proposed angle section hold down devices have comparable stiffness to off-the-shelf type of hold down HD-5.

A comparison of the numerically obtained load-displacement response of hold down devices with the experimentally determined behavior is given in Figure 3.19. The hold downs can be investigated in two groups based on their main deformation and resistance mechanisms. The first group includes hold down devices HD-1, HD-2 and

HD-3. These devices suffered from extensive damage during load tests and the strength and stiffness of specimens were mainly controlled by those of the hold down devices themselves. For these devices the numerically obtained load-displacement response agrees acceptably with the experimentally determined response of test specimens.

In the second group of devices, which includes hold downs HD-4 to HD-7, the main deformation mechanism was tilting and shear deformation of connection screws as well as the bearing deformation of vertical CFS framing member localized around these screws. These hold down devices themselves were subjected to minor deformations. Finite element analysis indicates substantially high initial stiffness for these devices when compared to the experimentally determined response of test specimens. This was an expected result considering that the FE models included only the hold down devices themselves without the CFS framing members and connection screws. Therefore, the discrepancy present between the numerical and experimental response of these devices arises from the deformation of components that were not present in FE models. The inset pictures in Figure 3.19 show some of these deformations.

Plots in Figure 3.19 also show that within the second group of hold downs (HD-4 to HD-7) the degree of strength overprediction is larger for angle type hold downs (HD-6 and HD-7). This observation suggests that the response of specimens with angle type hold down devices is influenced more significantly from the behavior of connection screws. This situation was also explained by comparing the calculated and experimentally determined load capacities, as discussed in Section 3.4.2. Consequently, significant improvement in structural performance of this type of hold downs can be achieved by increasing the number and diameter of connection screws rather than the thickness of angle section.

Another observation that is valid in the plots presented in Figure 3.19 is that contrary to the other devices, FE analysis underestimated the response of hold down HD-1 as compared to the experimentally determined response. During testing of hold down HD-1 extensive deformation occurred on the horizontal plate forming the bottom part of the device. The washer and nut used at the end of the anchor rod was observed to punch through the bottom horizontal plate. Hold down damage of such extent was unique to only hold down HD-1. The FE models, on the other hand, did not include the washer piece. The underestimation of specimen stiffness for HD-1 could be attributed to the absence of washer piece in FE models.

3.6   Wall Panel Tests

Wall panel tests presented below are part of a larger experimental work investigating the structural performance of CFS framed sheathed wall panels under lateral reversed cyclic loading. Details of the work on CFS framed shear walls are presented in the following parts of the thesis. In this chapter, results from two wall panel specimens utilizing the hold down devices designated as HD-7 are presented. These two wall panels were tested in order to substantiate the use of this hold down device that is fabricated relatively easily with a small cost from a piece of steel angle section. A comparison of the hold down response from these wall panel tests and the tension tests explained in the previous sections is provided in order to elucidate the differences and similarities in the behavior from the two test series.

Figure 3.20a shows the details of test specimens. Specimens had dimensions of 1.22 m x 2.44 m and both stud and track members were made of S350 grade 1.2 mm thick 140 mm deep C-shaped section shown in Figure 3.20b. In order to connect stud and track members, lips of track sections were bent outwards during manufacturing process at locations of stud-track connections. This way, stud member ends were placed inside track members and the connection between these members was

35

provided by blind rivets. Exterior studs were formed by connecting two CFS C-shaped sections back-to-back, whereas interior stud and track members were comprised of a single C-shaped section. Hold downs were connected to wall panels through exterior studs by 16 screws having 6.3 mm diameter and 50 mm length as shown in Figure 3.21. Wall panels reported in this paper were sheathed with 11 mm thick OSB sheets. Sheathing panels were attached to the CFS framing members using self-tapping screws having 4.2 mm diameter and 50 mm length. Screw spacing of 50 mm was used for boundary members while 100 mm spacing was used for interior stud. The 50 mm screw spacing used along the boundary CFS members represents the minimum spacing value specified in Nominal Shear Strength Table E1.3-1 in North American Standard for Seismic Design of Cold-Formed Steel Structural Systems, AISI S400-15 (2015). The reason behind the use of such small screw spacing was to put the hold downs and anchor rods into test by increasing the force and deformation demands imposed on these members under lateral loading. The only difference between the two wall panel specimens reported here was the presence of a 16.08 kN/m of gravity load applied on one of the specimens in order to simulate the effect of gravity loads existing in typical CFS structures.

3.6.1   Wall Panel Test Results

Both wall panels were able to sustain loading cycles of up to 4% drift in both loading directions. Photos of wall panels at 4% lateral drift are shown in Figure 3.22. Wall panels mainly underwent rocking motion with limited deformation in CFS framing and OSB sheathing. Deformation modes common to both wall panels were (1) tilting of the screws between sheathing panels and boundary CFS members, (2) tilting of the screws connecting hold downs to studs, and (3) uplift at the base of tension stud due to elongation of anchor rod and bending of hold down. It was also realized during dismantling of the specimens that anchor rods experienced excessive bending

deformation. In the wall panel tested with gravity load, local flange buckling, as indicated in Figure 3.23, occurred on exterior studs at 4% drift cycles.

Load-drift response of wall panels is given in Figure 3.24. The presence of gravity load reveals itself in the form of a minor increase in lateral stiffness of wall panel. Both specimens exhibited a stable behavior with similar maximum load capacities. The severely pinched hysteresis response, which results from tilting of screws at boundary CFS framing members and local bearing deformation of OSB sheathing panel around these screws, is considered to be an inherent property of these systems. The pinched response results in an almost zero-stiffness region in hysteresis curves following unloading of specimens. In other words, upon load reversal bearing between OSB panel and screws does not start immediately and certain amount of screw pivoting is required. The amount of screw pivoting required to obtain the contact condition also increases with increasing displacement amplitudes.

The bilinear load-drift responses determined based on the Equal Energy Elastic-Plastic (EEEP) approach as specified in AISI S400-15 (2015) are also given in Figure 3.24 for both wall panel specimens. A comparison of these responses indicates that the two wall panels showed comparable stiffnesses and load capacities.

Maximum load capacities both specimens have reached are in good agreement with nominal load capacities presented in Nominal Shear Strength Table E1.3-1 in AISI S400-15 (2015) as well as the measured load capacity of sheathed CFS wall panels tested by other researchers. As stated in the AISI S400-15 Specification, the wall panel configuration utilized in the current study in terms of sheathing type, stud and track thickness, fastener spacing and fastener type is expected to result in a nominal load capacity of 30 kN/m. As indicated on the plots given in Figure 3.24, for both wall panels the measured load capacities are slightly larger than the nominal strength specified by AISI S400-15 in the push direction, while slightly smaller capacities were measured in the other direction. Morgan et al. (2002) also reported that a 1.22

m x 2.44 m wall panel specimen sheathed with 11 mm thick OSB, consisting of 350S162-54 stud and 350T125-54 track members has reached a maximum lateral load capacity of 34.3 kN/m when the panel was sheathed with 4.2 mm diameter screws spaced at 50 mm. Hold downs used in those tests were of Simpson S/HD15 type attached with 48 screws having a diameter of 4.8 mm. Considering that the two wall panels tested in the current study exhibited maximum load capacity of 32 kN/m, it could be concluded that these specimens were able to reach the expected level of load capacity based on the related specification and test results available in the literature. These results are valid indicators that the angle type hold down device provides proper load transfer between the wall panel and the foundation system, and has adequate mechanical performance to develop the expected strength of wall panel. It can be concluded that this type of hold down device, which requires less workmanship and fabrication cost than some of the widely used devices, is promising and can be an alternative to more traditional hold down devices currently being used in CFS structural systems.

3.6.2 Comparison of Hold Down Response from Wall Panel and Tension Tests

Tensile force developing in hold downs during wall panel tests was determined by considering the equilibrium of external forces and moments acting on panels and with the relationship as follows:

$$T = H * h/w_n \hspace{4cm} [3.1]$$

where, T is the tensile force developed in hold down device; H is the horizontal load applied at the top of wall; h is the wall height, which is equal to 2440 mm; and w_n is the distance between the center of anchor rod connecting hold down to base and far end of the wall specimen, which is equal to 1120 mm. Hold down forces determined

this way were plotted against the uplift measured at the base of tension stud for the corresponding wall panel and the plots are shown in Figure 3.25. Superimposed on the same plots are the load-displacement responses of hold downs recorded during the monotonic hold down tension tests explained earlier in the paper. As evident, there is a remarkable agreement between the hold down response from the two series of tests and such agreement is valid for both cases of wall panels tested with and without gravity load. This observation is an indication that the specimen geometry and loading method used in hold down tension tests accurately represent the conditions that these hold downs are subjected to when used in CFS framed sheathed wall panels.

Table 3.1 Material properties of hold down devices

	F_y (MPa)	F_u (MPa)
HD 1	302	360
HD 2	313	400
HD 3	360	385
HD 4	363	392
HD 5	280	350
HD 6	377	524
HD 7	366	550

Table 3.2 Details of hold down specimens

Specimen name	Hold down device	Number of screws	Screw dimensions (diameter x length)	Loading type
HD1-M1	HD-1	14	5.5 x 50 mm	Monotonic
HD2-M1	HD-2	14	5.5 x 50 mm	Monotonic
HD3-M1	HD-3	16	5.5 x 50 mm	Monotonic
HD4-M1	HD-4	16	5.5 x 50 mm	Monotonic
HD4-C1		16	5.5 x 50 mm	Cyclic
HD5-M1	HD-5	12	6.3 x 50 mm	Monotonic
HD5-C1		12	6.3 x 50 mm	Cyclic
HD6-M1		13	4.2 x 50 mm	Monotonic
HD6-M2	HD-6	13	5.5 x 50 mm	Monotonic
HD6-M3[a]		13	5.5 x 50 mm	Monotonic
HD7-M1		16	6.3 x 50 mm	Monotonic
HD7-M2[b]	HD-7	16	6.3 x 50 mm	Monotonic
HD7-M3[c]		16	6.3 x 50 mm	Monotonic
HD7-C1		16	6.3 x 50 mm	Cyclic

[a] 1.2 mm thick backing plate was used to increase web thickness.
[b] Horizontal leg of the hold down was shortened to 75 mm.
[c] 50 mm gap was left between the hold down and horizontal CFS member.

Table 3.3 Results of screw shear tests

Number of fasteners	1	2	3	4
Shear capacity per screw (kN)	6.91	6.78	6.40	6.26

Table 3.4 Results of hold down tests

Specimen	Maximum Load, P_{max} (kN)	$0.65 \times P_{max}$ (kN)	Load at 6.35 mm deformation (kN)	LRFD load capacity (kN)	Deformation at LRFD load capacity (mm)
HD1-M1	33	21	11	11	6.35
HD2-M1	30	19	9	9	6.35
HD3-M1	56	36	21	21	6.35
HD4-M1	80	52	30	30	6.35
HD4-C1	78	51	26	26	6.35
HD5-M1	72	47	44	44	6.35
HD5-C1	65	42	36	36	6.35
HD6-M1	55	36	34	34	6.35
HD6-M2	64	41	33	33	6.35
HD6-M3	65	42	39	39	6.35
HD7-M1	76	49	41	41	6.35
HD7-M2	72	47	28	28	6.35
HD7-M3	50	32	26	26	6.35
HD7-C1	78	51	44	44	6.35
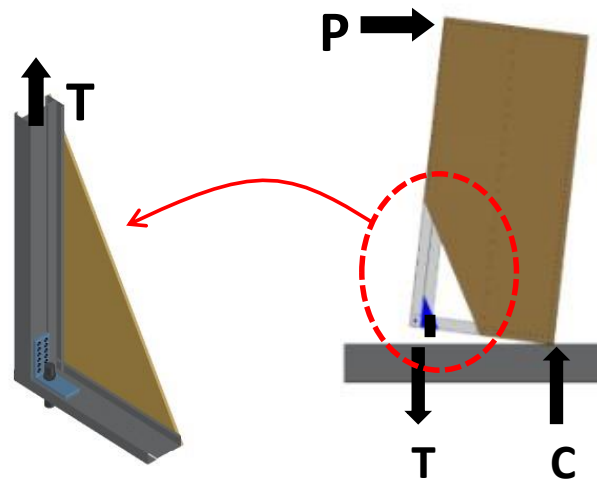
Figure 3.1 Representation of specimens on CFS framed wall panel
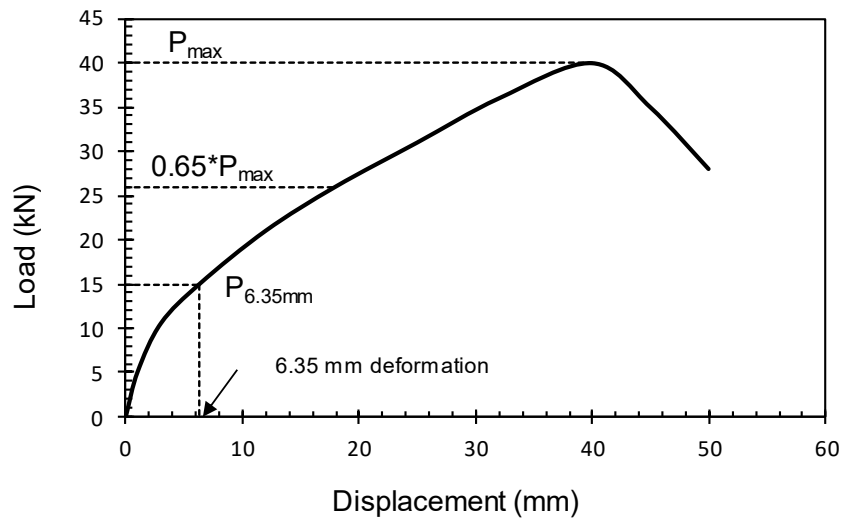
Figure 3.2 Generic hold down load-displacement behavior
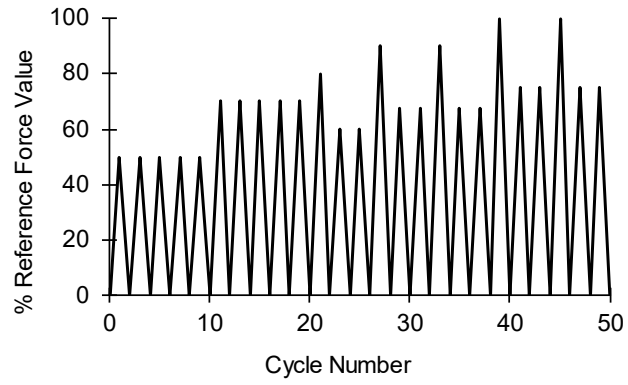
Figure 3.3 Cyclic loading protocol used in hold down assembly tests

| HD - 1 | HD - 2 | HD - 3 | HD - 4 |

| HD - 5 | HD - 6 | HD - 7 |

Figure 3.4 Hold down devices tested in the study

* All dimensions are in mm.
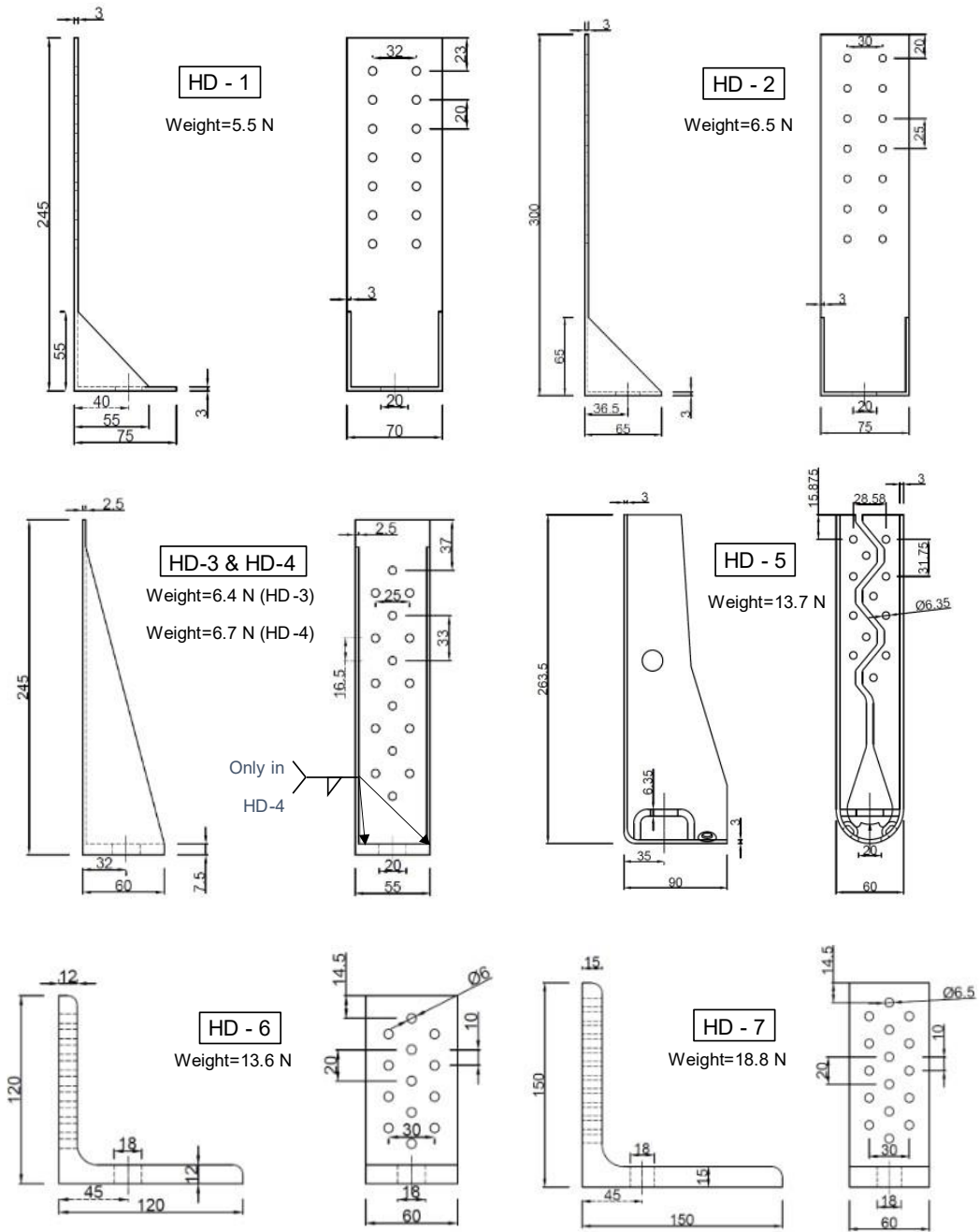
Figure 3.5 Details of hold down devices

44

(a)   (b)
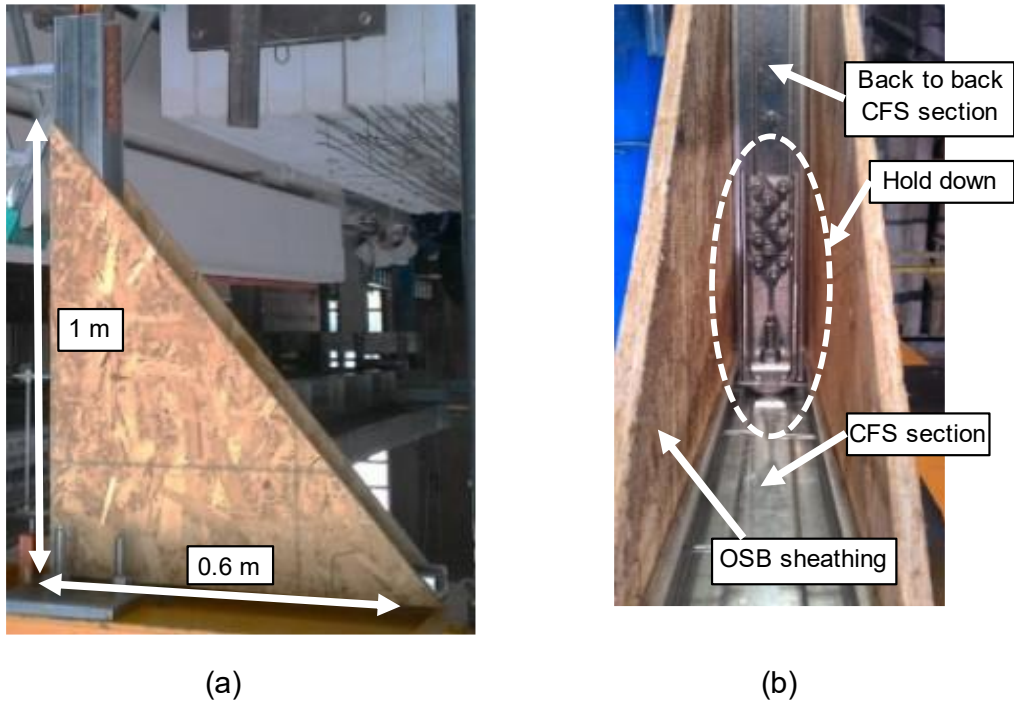
Figure 3.6 Details of hold down test specimens: (a) dimensions; (b) details
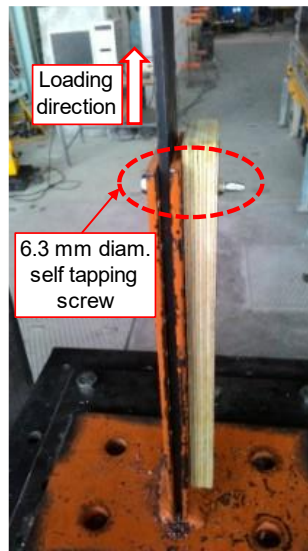
Figure 3.7 Screw shear test setup
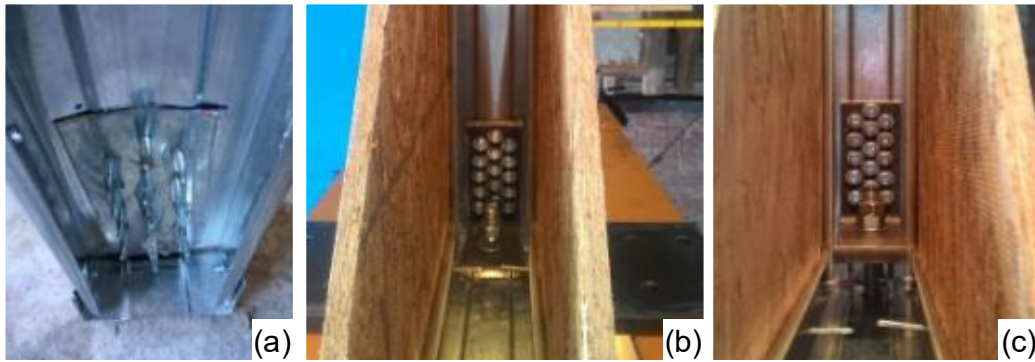
Figure 3.8 Additional construction details used in specimens; (a) HD6-M3 (steel backing plate); (b) HD7-M2 (hold down cut short); (c) HD7-M3 (gap between hold down and CFS framing member)
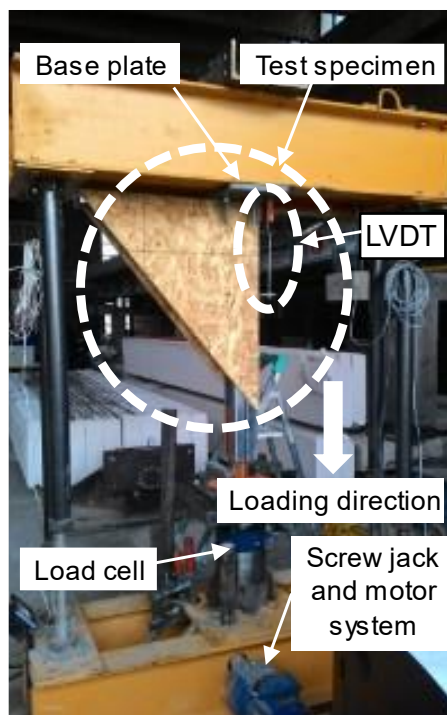
Figure 3.9 Hold down assembly test setup
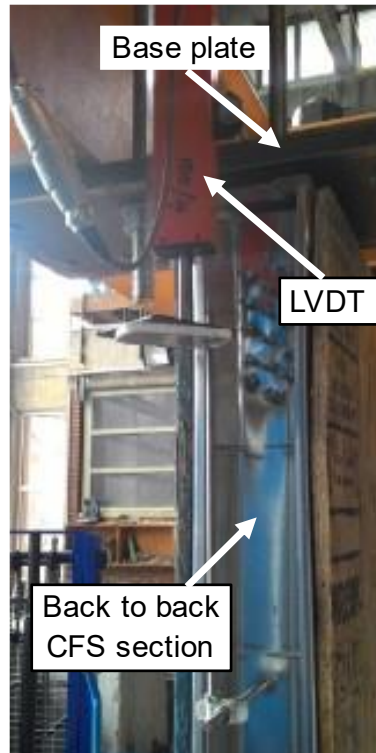
Figure 3.10 LVDT measuring the relative vertical displacement
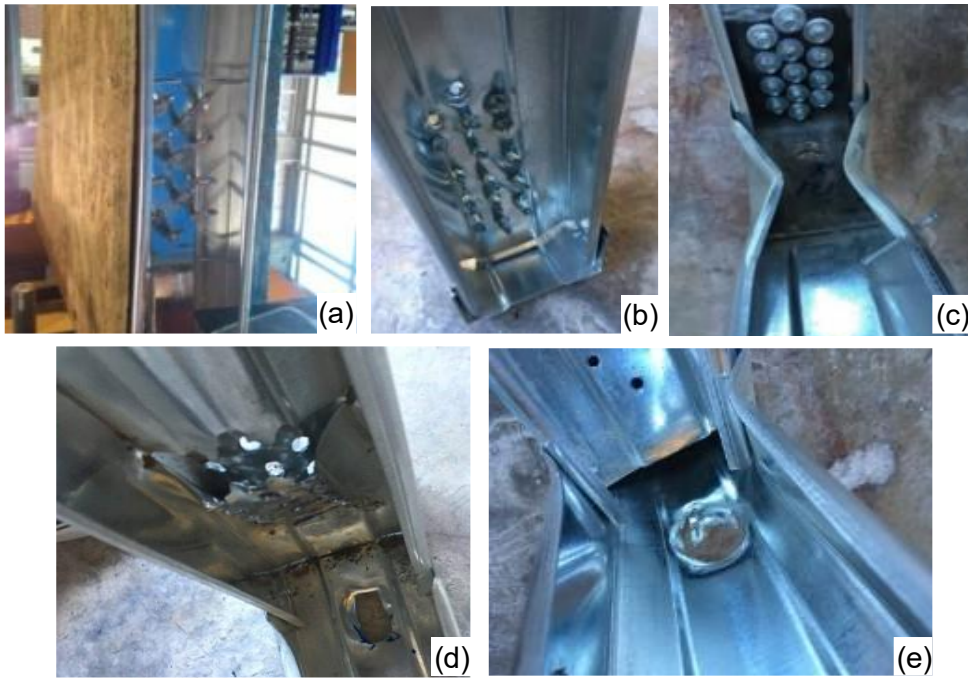
Figure 3.11 Observed deformation modes at the end of load tests: (a) tilting of screws; (b) shearing of screws; (c) local buckling of horizontal framing member; (d) tearing of vertical framing member; (e) punching of horizontal framing member

Figure 3.12 Deformations observed in hold down devices at the end of load tests
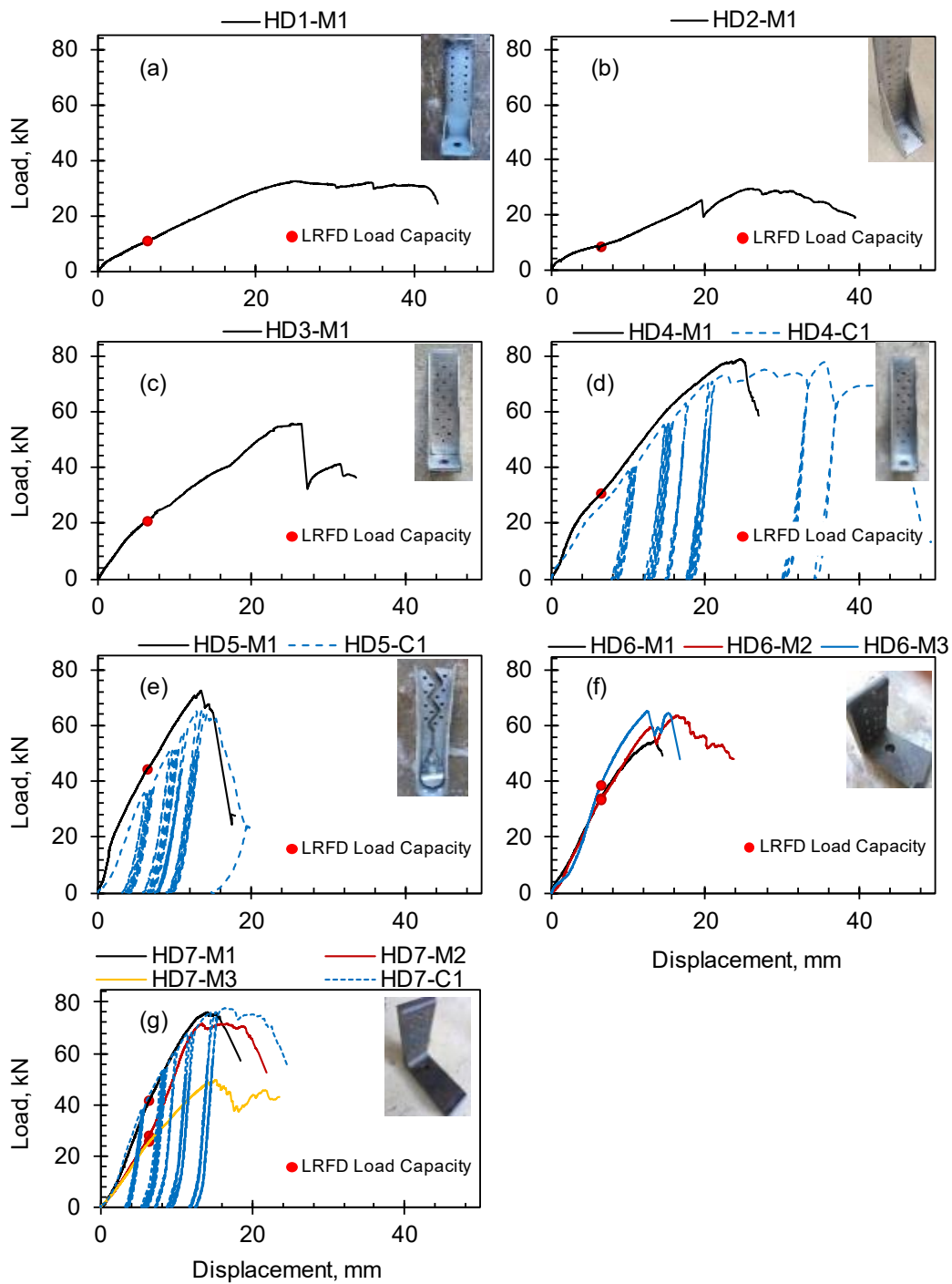
Figure 3.13 Load-deformation behavior of hold downs: (a) HD-1; (b) HD-2; (c) HD-3; (d) HD-4; (e) HD-5; (f) HD-6; (g) HD-7
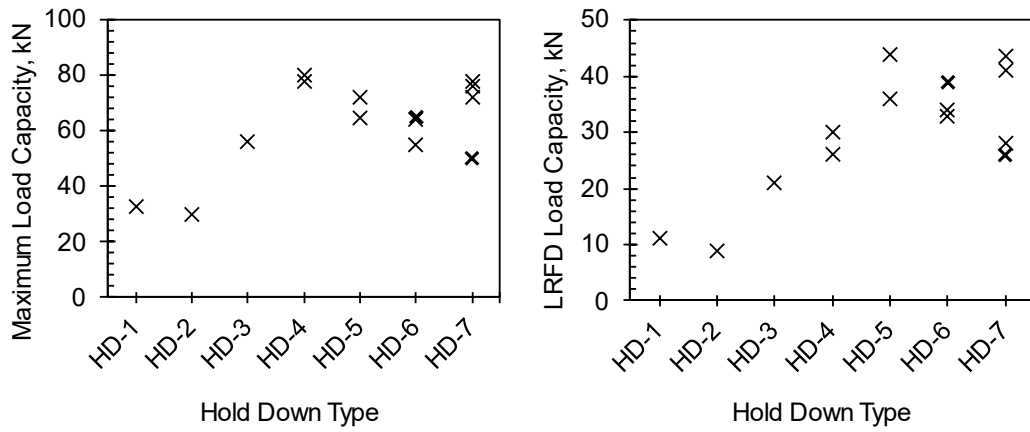
Figure 3.14 Comparison of load capacities for different hold down types
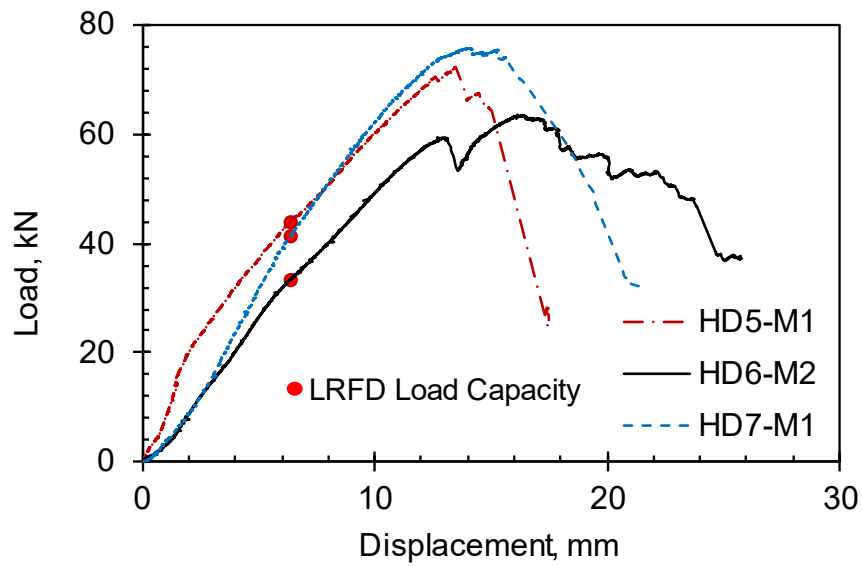
Figure 3.15 Load-deformation response of specimens with largest load capacities

51
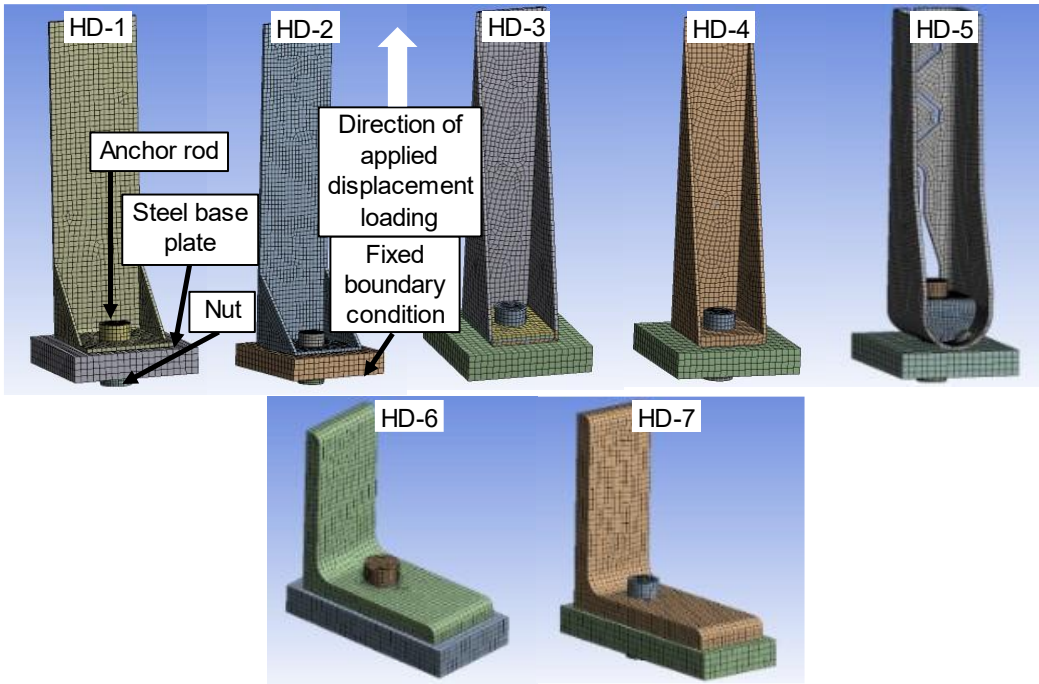
Figure 3.16 Finite element model of hold down devices
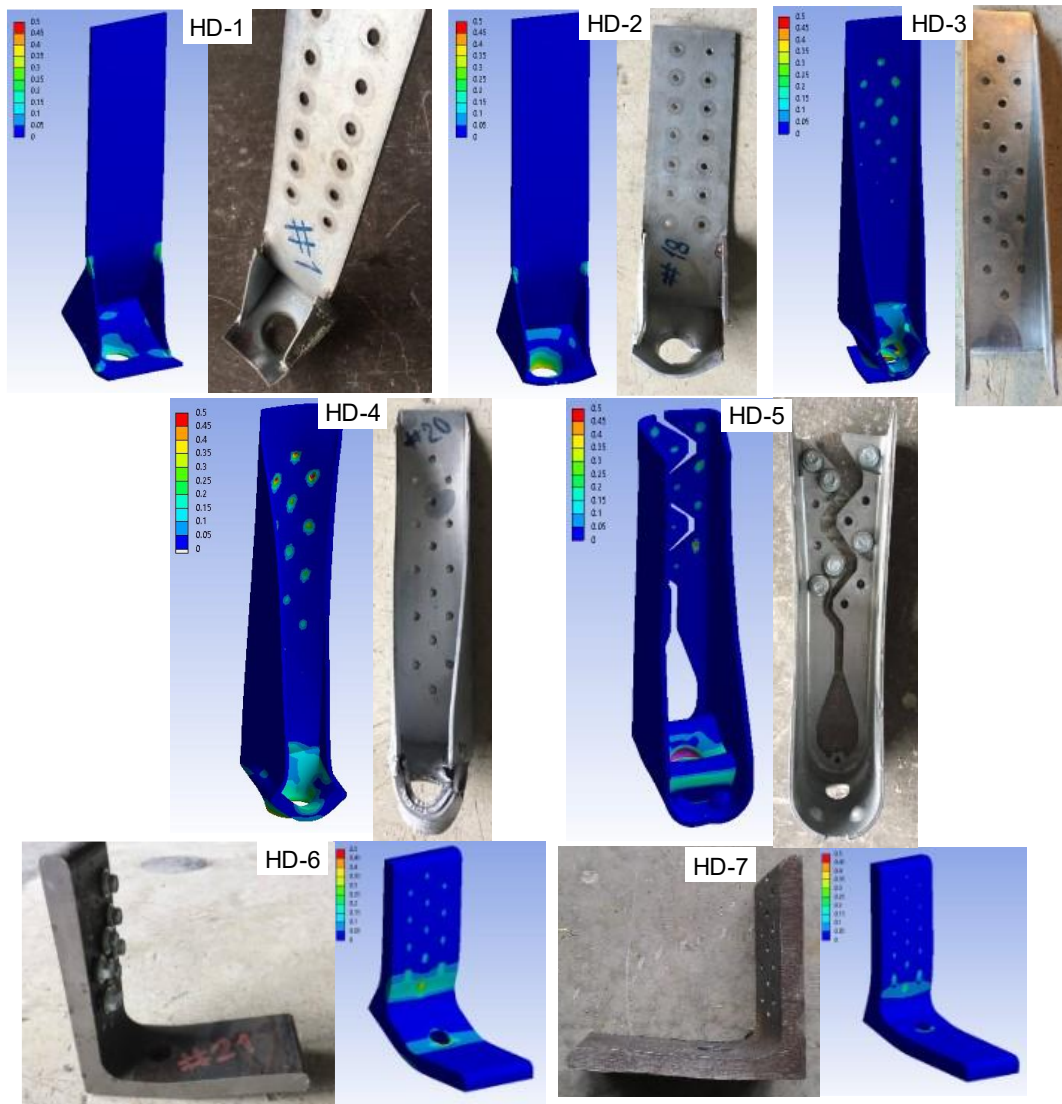
Figure 3.17 Deformed shape and equivalent plastic strain distribution of hold downs
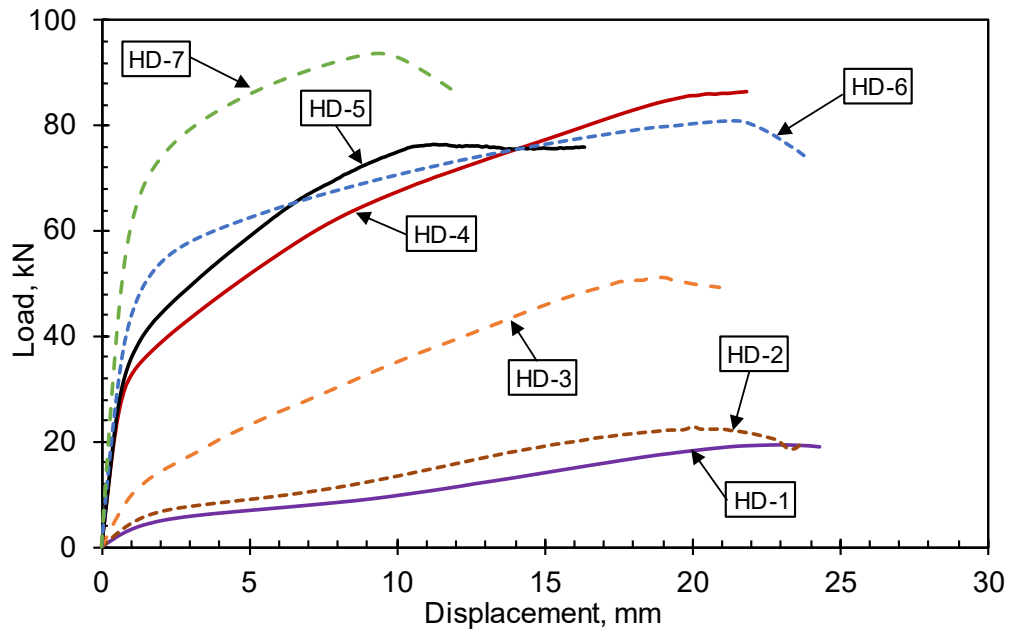
Figure 3.18 Load-deformation response of hold down devices obtained from finite element analysis
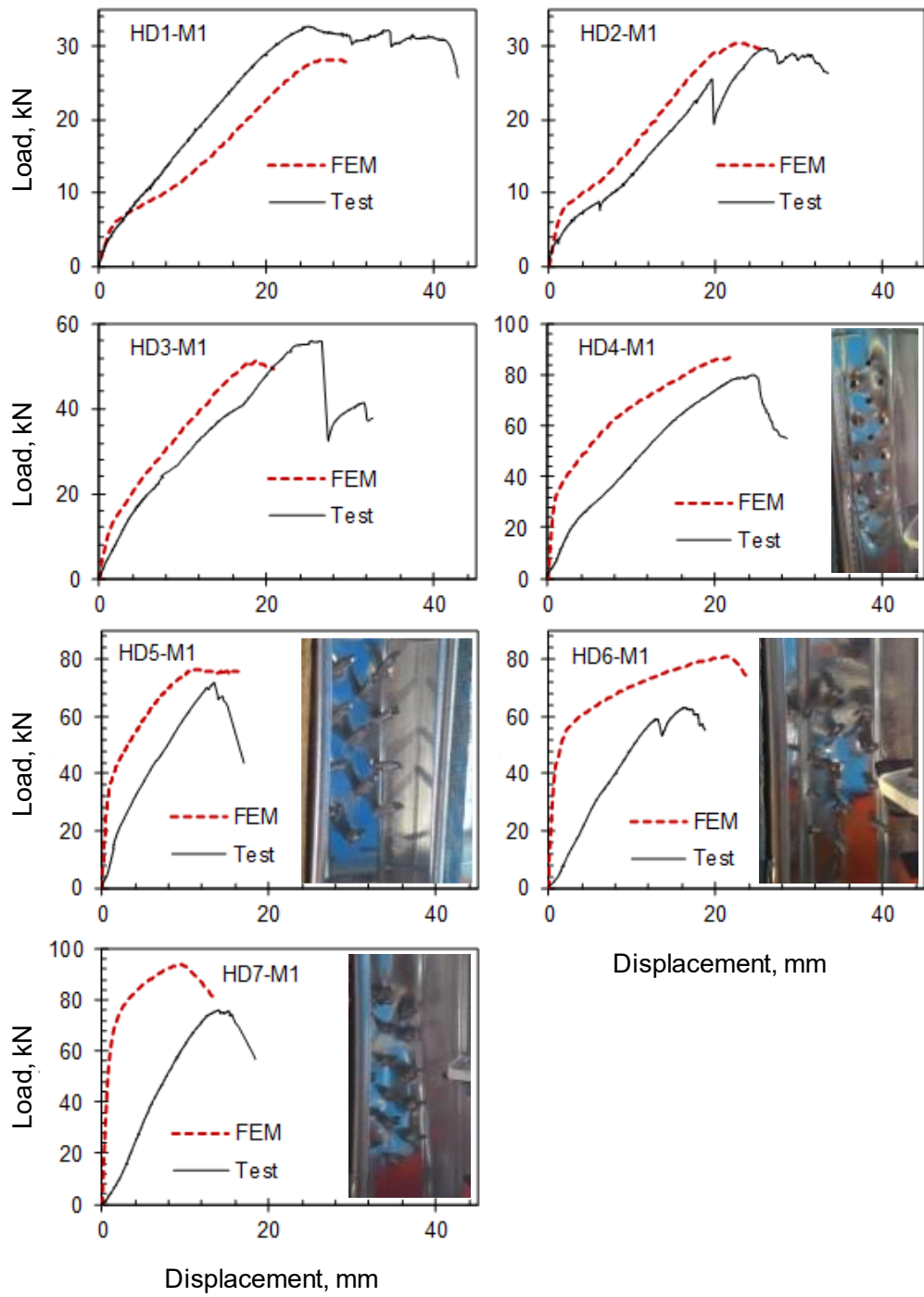
Figure 3.19 Measured and predicted load-deformation response of hold down devices
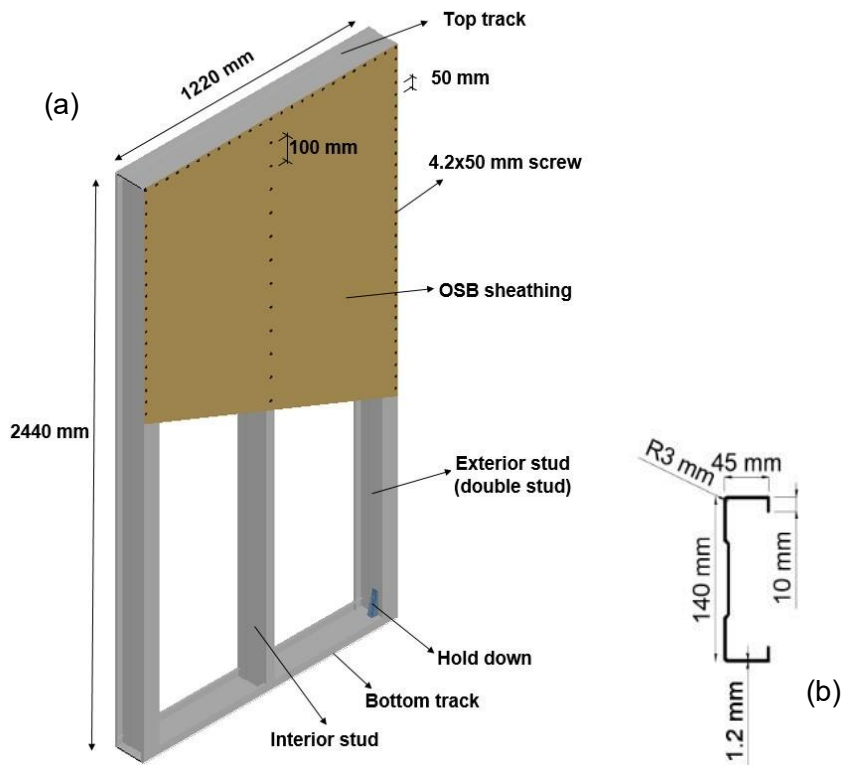
Figure 3.20 (a) Framing details of wall panels; (b) CFS section used in the study
for tracks and studs
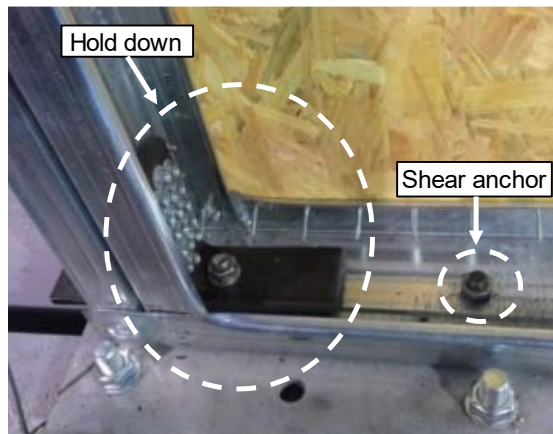
Figure 3.21 Connection and placement details of hold downs in wall panels
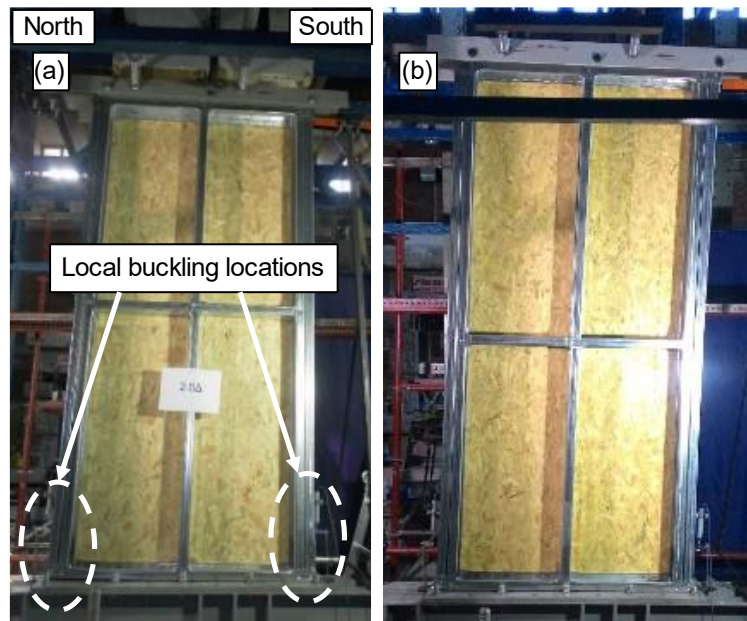
Figure 3.22 Wall panels at 4% lateral drift: (a) with gravity load; (b) without gravity load
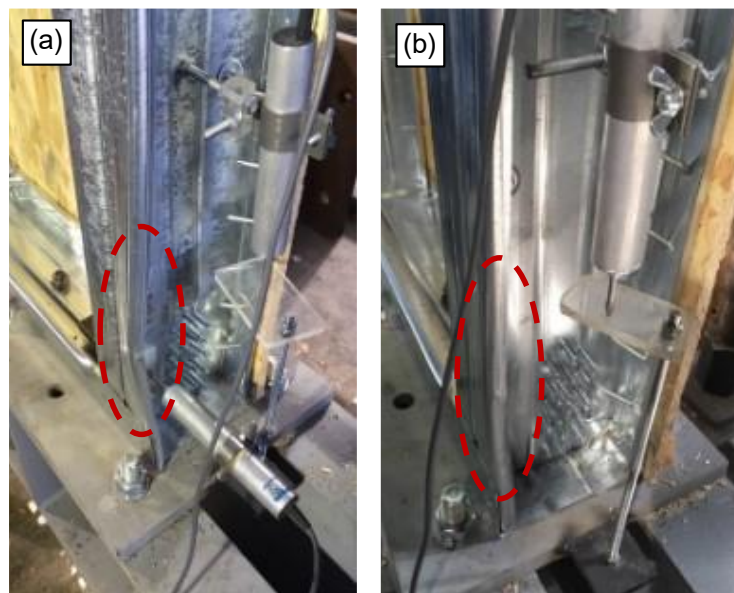
Figure 3.23 Buckling of exterior studs: (a) south side; (b) north side
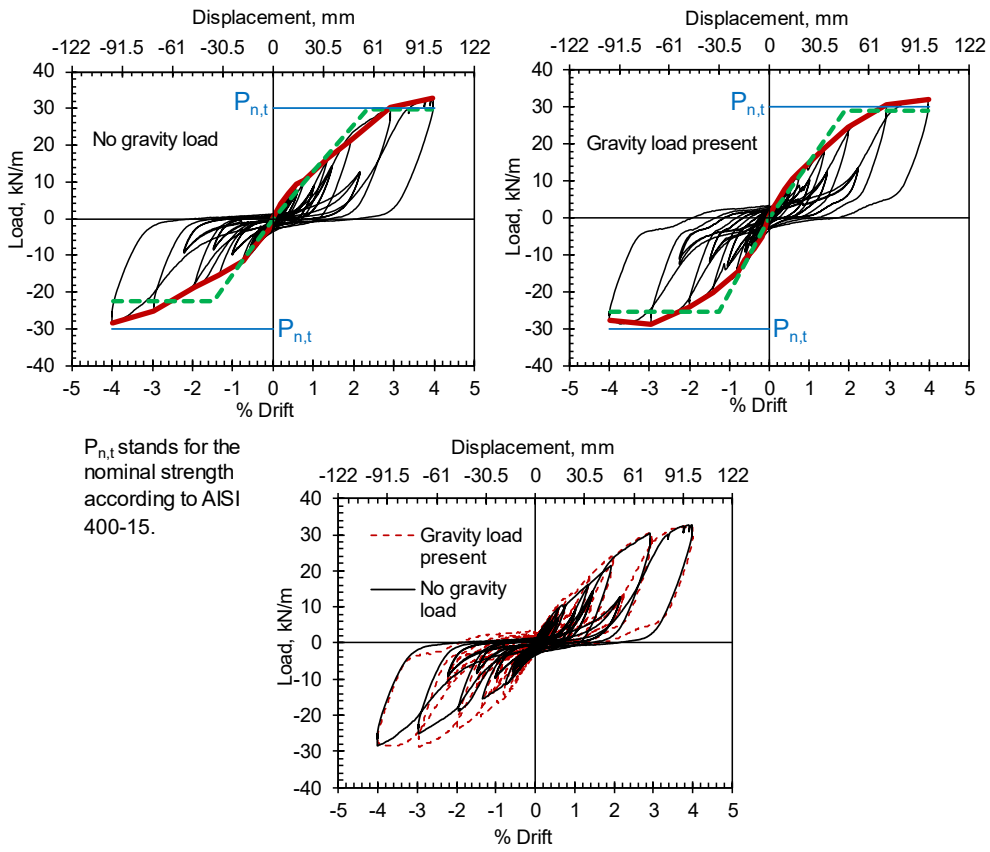
Figure 3.24 Load-lateral displacement behavior of wall panel tests
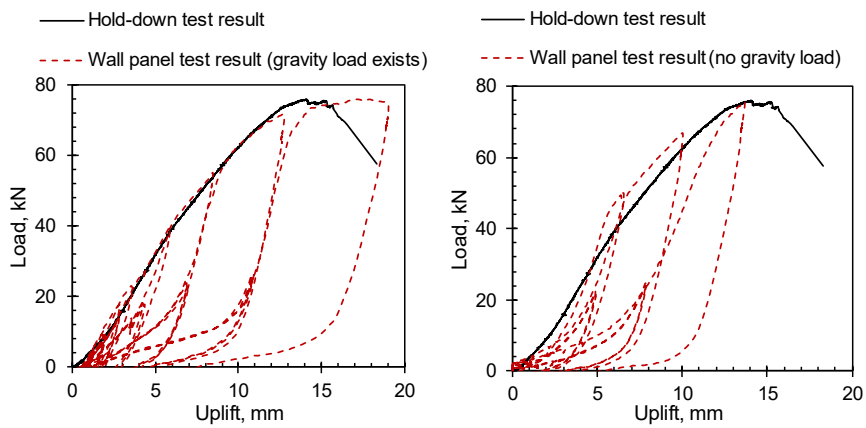
Figure 3.25 Comparison of hold down and wall panel test results

CHAPTER 4

AN ENERGY DISSIPATING HOLD DOWN DEVICE FOR COLD-FORMED STEEL STRUCTURES

4.1   Introduction

Structural performance of various types of hold down devices were investigated and presented in Chapter 3 of the thesis. Some of these tested hold downs particularly suffered from extensive damage during load tests. Test results indicated that load capacity of some of these devices remain well below the force demand levels which typically occur in CFS wall systems. The limited load capacity and stiffness exhibited by these low-performance hold down devices make them unsuitable for CFS structural systems for the purpose of transferring the wall panel forces to the foundation system at wall base. The test results also proved that a superior performance in terms of strength and stiffness can be obtained from simple hold down geometries as compared to an off-the-shelf hold down device that has wide use in North America. Even though these high performance hold down devices proved themselves to have the ability to produce adequate strength and stiffness, they lack energy dissipation mechanisms. Providing energy dissipation capability at wall base through the use of specially designed hold down devices would improve the structural performance under reversed cyclic loading and promote the use of CFS structural systems in seismic regions.

The objective of this part of the thesis work was to develop and evaluate the structural performance of a hold down that can be used as an energy dissipating device in CFS construction. The proposed idea was to have a hold down device that has high strength and stiffness and allows controlled yielding of anchor rod over a

predetermined length. The hold down device to be used for this purpose was designed to be easy to fabricate and low-cost. The device is also easy to install at the base of CFS wall panels and replace after a major seismic event.

Experimental work described in this chapter consists of two phases. In the first phase, the focus was on the development of the aforementioned hold down device that can be used to provide force transfer at the base of CFS wall panels and at the same time serve as an energy dissipation mechanism. The second phase of the experimental work concentrated on the investigation of the performance of this device when used in a sheathed CFS wall panel that is subjected to reversed cyclic lateral loading.

4.2   Proposed Hold Down Device

Details of the investigated hold down device are shown in Figure 4.1. The device was formed by welding two steel angles to a steel square tube together. Holes were drilled on free legs of angles for placement of screws to connect the hold down device to CFS members. An anchor rod runs through the square tube to provide connection to the base.

In commonly used hold down devices, bottom leg of the device allows for the placement of an anchor rod to provide connection to the foundation system and the vertical leg is connected to CFS studs with screws. This type of geometry results in significant eccentricity between the anchor rod and the connection interface where CFS stud force is transferred to the hold down device. Additional moment caused by this eccentricity introduces additional tensile forces in connection screws and contributes to deformation of the hold down device itself. Because of the unique geometry of the proposed hold down device, eccentricity between the anchor rod and the connection interface is minimized. Thus, the resulting adverse effects of the eccentricity are reduced.

The length of the proposed hold down device can be adjusted to accommodate the required number of screws. Similarly, the square tube size can be increased to allow for the placement of an anchor rod with required diameter. As indicated in Figure 4.1 the connection screws were placed as close to the top part of the hold down device as possible. This way, the moment arm of each screw was reduced and the level of tensile force developing in screws as a result of load eccentricity was minimized.

Hold down devices tested in this study were fabricated from 30x30x3 mm angle sections and a 20x20x1.2 mm square tube. The devices allow the use of anchor rods with a diameter of 16 mm. However, for most of the wall panel specimens tested in the second phase of the study, anchor rods having diameters larger than 16 mm were used. In order to accommodate these larger diameter rods 30x30x1.2 mm tubes were adopted in some of the hold downs used in wall panel tests.

4.3   Hold Down Test Program

Test procedures, loading protocol, test setup and the instrumentation used in the load testing of proposed hold down device, as well as the methodology used in preparation of specimens were same as described in the Chapter 3 of the thesis.

4.3.1   Hold Down Test Specimen Details

Hold down assembly test specimens are similar with the previously tested hold down specimens and they are shown in Figure 4.2a and Figure 4.2b along with some of the details. Specimens included an "L" shaped CFS framing made of 90 mm deep and 1.2 mm thick lipped channel section shown in Figure 4.2c. Similar to CFS wall panels, vertical leg of the framing was formed by connecting two channel sections back-to-back, whereas a single channel was used for the horizontal member. OSB panels with 11 mm thickness were attached on both sides of CFS framing using 4.2

mm diameter self-tapping screws placed at 150 mm spacing. Hold downs were attached to the vertical leg of CFS framing with 6.3 mm diameter self-tapping screws. As mentioned earlier, the connection screws were placed as close to the top part of the hold down device as possible in order to minimize the level of tensile force developing in screws as a result of load eccentricity.

All of the hold down devices tested as part of the assembly specimens were fabricated using a 20x20x1.2 mm steel square tube and two 30x30x3 mm angle sections. These hold downs were attached to a base plate in the testing machine with a 16 mm diameter steel threaded anchor rod. The yield and tensile strengths for the anchor rods were measured to be 480 and 580 MPa, respectively.

As mentioned earlier, the proposed hold down device was intended to be used as an energy dissipating mechanism. Such energy dissipation capability is achieved by significant plastic deformation of anchor rod under tensile loading. In order to have controlled yielding, diameter of the anchor rod can be reduced in the middle portion over a certain length. This approach was not implemented in hold down assembly tests. These tests were conducted with anchor rods that had a constant diameter of 16 mm over the entire length. In other words, the energy dissipation feature of the hold down was investigated only in the wall panel tests, while the assembly tests focused solely on the characterization of the strength and stiffness properties under various parameters.

The parameters used in each hold down assembly specimen are given in Table 4.1. The first number in specimen designation represents the number of screws connecting hold down device to CFS stud. The letters "M" and "C" indicate whether the specimen was subjected to monotonic or cyclic loading. The last number in specimen designation is the test number of corresponding specimen.

The main parameter for hold down assembly specimens was the number of screws connecting hold down devices to vertical CFS members. In three of the specimens,

OSB pieces were provided at the back side of the vertical CFS framing members at hold down location in an attempt to reduce the tilting deformation of connection screws (Figure 4.2d). Influence of the layout of connection screws on hold down response was investigated in one of the specimens. This specimen was prepared in such way that the screws were distributed evenly along the length of the hold down device instead of placing them near the upper part of the device. Layout of connection screws used on hold down devices tested as part of the study is shown in Figure 4.3.

4.4   Hold Down Test Results

4.4.1   Deformation Modes and Load-Deformation Response of Hold Downs

The main deformation mode observed on all specimens was the tilting of screws connecting the hold downs to the vertical CFS framing members. This tilting action was eventually followed by the shearing of screws as shown in Figure 4.4. The hold down devices themselves were observed to remain mostly undamaged. No distinct difference was observed on deformation response of specimens tested under monotonic and cyclic loading.

Figure 4.5 shows the measured tensile load versus uplift plots of hold down specimens. LRFD design load capacities determined as per AISI S913-13 (2013) are also shown on the plots. The corresponding numerical values are presented in Table 4.2. It should be noted that for all specimens, LRFD load capacities were governed by the force limit of $0.65 \times P_{max}$, rather than the displacement limit of 6.35 mm. This is an indication that the stiffness should not be a consideration for these devices when the strength requirements are satisfied.

Providing an OSB plate at the back side of vertical CFS framing member at hold down location increased the load capacity of hold down specimens as a result of reduced screw tilting. The increase in load capacity was 15% for the specimen with 8 screws, 12% for the specimen with 12 screws, and 6% for the specimen having 22 screws.

Another important observation that should be mentioned is the effect of screw layout on the response of hold down device. Specimen HD-16-M1, which utilized 16 screws evenly distributed along the full height of the hold down device, was able to reach a maximum load capacity of 74 kN. On the other hand, when screw placement was arranged such that the same number of screws were placed closer to the upper edge of the hold down, as it was the case for Specimen HD-16- M2, a maximum load capacity of 91 kN was achieved. The proposed hold down geometry minimized the eccentricity between the anchor rod and the connection interface. However, even though the magnitude was small, there was still an eccentric force transfer through the hold down device between the CFS framing and the anchor rod. This force eccentricity created moment effects on the hold down device, which caused additional tensile force in connection screws. Presence of tensile force in these screws resulted in a reduction in their shear resistance. The 23% increase in load capacity between specimens HD-16-M1 and HD-16-M2 is a clear indicator that increased moment arm for screws delayed the failure by reducing the screw tensile force and thereby increasing the shear resistance.

Test results indicate that increasing the number of connection screws results in an increase in hold down load capacity but the rate of change gets smaller as the number of screws is increased. Both the maximum load capacity and LRFD load capacity increased for the cases of 8, 12 and 16 screws, and remained virtually the same between the cases of 16 and 22 screws. The reason for such a reduction in the effectiveness of screws in improving the load capacity of hold down device was

related with two effects. The group action effect among multiple screws is a well known phenomenon. As explained in Chapter 3, the interaction among closely spaced screws results in the reduction of the shear capacity of each screw, as the number of screws increases. The second reason for the observed reduction in the effectiveness of screws was related with the screw layout used in test specimens. When the number of screws was increased, the newly added screws were placed below the already existing ones. In this case, the newly added screws, which were located lower on the hold down, were not as effective to resist the moment effects as the ones that were located further above. Therefore, increasing the number of screws by a certain amount did not provide an increase in total shear resistance by the same amount. Figure 4.5 also provides a comparison of load-displacement plots obtained from monotonic and cyclic testing of companion specimens. For all four cases the cyclic curves closely follow the monotonic response.

4.4.2 Comparison of Hold Down Response with Previous Test Data

The load-deformation behavior of the hold down device developed and presented in this chapter can be compared with other hold down devices investigated in the Chapter 3. Two hold down devices were selected for this comparison. First one is the off-the-shelf device designated as "HD-5" and the second one is the "HD-4". Because HD-5 and HD-4 were connected to CFS framing with 12 and 16 screws respectively, it is suitable to compare the behavior of these hold downs with specimens HD-12-M1 and HD-16-M2. Such a comparison is presented in Figure 4.6. It can be seen that the proposed hold down device outperforms the other devices in terms of LRFD load capacity and stiffness. Specimens HD-12-M1 and HD-16-M2 exhibited 23% and 94% higher LRFD load capacity compared to devices HD-5 and HD-4, respectively. This comparison is a good indicator that the proposed hold down

geometry offers a favorable mechanical response with superior strength and stiffness.

Higher deformations exhibited by hold down devices HD-4 and HD-5 during load tests (Figure 4.6) make these devices absorb more energy than the proposed device. However, it should be remembered that the approach adopted here is to have the hold down device itself to remain undamaged and have the anchor rod to undergo controlled yielding during a major seismic event. From this perspective, the high strength and stiffness together with the limited deformation exhibited by the proposed hold down make this device an appropriate alternative to be used together with the controlled yielding anchor rod concept.

4.5   Wall Panel Test Program

As the second phase of this part of thesis work, seven full scale sheathed CFS wall panel specimens were tested under cyclic loading conditions in order to investigate the structural performance and energy dissipation feature of the developed hold down device when used in a CFS wall panel system.

Different from the hold down assembly tests, which focused on the characterization of the strength and stiffness response of the proposed hold down device, focus of the wall panel tests was on the energy dissipation ability of the device. Aligned with this focus, the anchor rods used to connect the hold downs to the foundation system in wall panel specimens were altered to provide controlled rod yielding under tensile forces. For this purpose, the anchor rods were altered by either reducing their diameter in the middle portion or by using rods having different type of steel properties. The approach was to create an energy dissipating mechanism within the wall structure by letting the wall panel undergo rocking motion and having the anchor rods undergo significant plastic deformation. Such energy dissipation

mechanism and its effect on the overall wall panel behavior were investigated by testing seven wall panel specimens. In addition to that, a comparison was made between the response of hold down devices observed from both the hold down assembly tests and the wall panel tests.

Details of wall panel specimens are already given in Chapter 3. Wall panels had dimensions of 1.22 × 2.44 m and the CFS framing members were made of S350 grade 1.2 mm thick 140 mm deep C-shaped section. Details of wall panel specimens and CFS section are shown in Figure 3.20. Wall panel framing consisted of exterior studs that were formed by connecting two CFS C-shaped sections back-to-back and track members comprised of a single C-shaped section. Hold downs were attached to the bottom part of exterior studs by 22 self-tapping screws having 6.3 mm diameter and 50 mm length, as shown in Figure 4.7. Layout of the screws used to attach hold downs to CFS wall studs was similar to the layout used during hold down assembly tests (Figure 4.3). Bottom track member in each wall specimen was connected to the foundation system with two 16 mm diameter shear anchors in order to transfer the wall base shear force.

OSB sheathing panels with 11 mm thickness were attached to the CFS framing members by means of self-tapping screws having 4.2 mm diameter and 50 mm length. For this purpose, screw spacing of 50 mm was used for boundary members while 100 mm spacing was used for interior stud. These spacing values were taken from Nominal Shear Strength Table E1.3–1 in North American Standard for Seismic Design of Cold-Formed Steel Structural Systems, AISI S400-15 (2015). The 50 mm screw spacing represents the designated minimum spacing value to be used for boundary CFS members. By using such small screw spacing value, the shear force capacity of wall panels was increased. This way, increased force and deformation demands were imposed on hold downs and anchor rods during wall panel tests.

4.5.1 Wall Panel Test Parameters

Details of wall panel test specimens and the investigated parameters are given in Table 4.3. One of the specimens was tested with single-sided OSB sheathing while double-sided sheathing was used in the remaining six specimens. In Specimens S1 and S2 16 mm diameter threaded anchor rods with measured yield and tensile strengths of $F_y = 480$ MPa and $F_u = 580$ MPa (Batch A) were utilized. These rods were the same as those used in hold down assembly tests. In order to preclude any type of anchor rod related failure, Specimen S3 was tested with 24 mm diameter threaded anchor rods. In Specimens S4–S7 the middle portion of anchor rods were weakened by reducing the diameter in order to have controlled yielding of the rods. The rod diameter within these yielding portions were adjusted such that the lateral load acting on wall panels at the initiation of anchor rod yielding would remain below the expected load capacity of the wall panels.

Geometries of anchor rods used in Specimens S4–S7 are given in Figure 4.8. In S4 and S5, diameter within the middle portion of anchor rods was reduced to 15 mm and 13 mm respectively. Length of the yielding portion within the anchor rods was adjusted to 400 mm in Specimen S5, as opposed to a yielding length of 200 mm used in S4, S6, and S7.

The anchor rods used in Specimens S3–S5 had measured yield and tensile strengths of $F_y = 500$ MPa and $F_u = 575$ MPa (Batch B). Specimens S6 and S7 utilized anchor rods manufactured from AISI 1040 grade steel (Batch C). This grade of steel was chosen based on the relatively large ratio between the tensile and yield strengths it offers. The measured yield and tensile strength values were $F_y = 415$ MPa and $F_u = 645$ MPa. Diameter of the yielding portion within the anchor rods was 15 mm in S6 and 13 mm in S7.

The proposed hold down device allows the replacement of damaged anchor rods after a major seismic event. In order to investigate such application, a slightly different sheathing configuration was used in Specimen S7. The wall panel used in this specimen was sheathed with two separate pieces of OSB panels on one side, while the other side was conventionally sheathed with a single panel. In order to allow for access to the anchor rods, the lower 350 mm portion of the wall panel was initially left unsheathed. This portion was sheathed with a separate OSB panel after the wall was connected to the foundation base plate with anchor rods and shear anchors, as illustrated in Figure 4.9.

Specimen S7 was tested with 31.4 kN of vertical load placed on the wall panel as shown in Figure 4.9. Amount of vertical load was selected based on the severe loading condition acting on a wall panel of a conventional CFS building. Axial capacity of studs in wall panels were computed to be 33.9 kN and 90.7 kN, respectively for the interior and end studs, following Direct Strength Method approach (AISI S100, 2016) and incorporating the stiffness contribution of OSB sheathing panels (Vieira and Schafer, 2012, 2013). Based on these computed values, the vertical load applied on Specimen S7 corresponds to 15% of the total axial load capacity of the wall panel.

4.5.2   Test Setup, Instrumentation and Loading Protocol

Test setup configuration is shown in Figure 4.10. The wall panel specimens rested on a 20 mm thick steel foundation plate that was connected to steel support beams, which themselves were attached to the laboratory strong floor. Lateral load transfer to wall panel specimens was achieved by using a 1.6 m long steel channel which was connected to the wall top track by self-tapping screws. This load distribution beam was connected to a hydraulic actuator having 300 kN load capacity and ± 250 mm stroke through a steel plate and bolts. On top of the load distribution beam, another

steel channel with 1.5 m length was placed and connected to this beam with bolts. This second steel channel supported the weight blocks simulating the gravity loading in Specimen S7. Also, two ball bearing rollers on each side supported wall panels laterally in the out-of-plane direction through this steel channel as indicated in Figure 4.10.

Lateral force applied on wall panels was measured by a load cell that was placed between the hydraulic actuator and the load distribution beam. Four LVDT's were used to measure the lateral displacement at the top of wall panel, lateral slip at the wall base and base uplift at hold down locations. Middle portion of each anchor rod was also instrumented with strain gauges in order to monitor the variation of hold down force under lateral loading.

All wall panel specimens were tested under reversed cyclic loading in displacement controlled mode at a rate of 60 mm/min. The loading history of the cyclic tests was defined according to the CUREE specification (Krawinkler et al., 2001). Based on a reference lateral deformation of 2% of the total wall height, cyclic loading history shown in Figure 4.11 was applied on wall panel specimens. Loading was terminated at 4% drift ratio or specimen failure, whichever occurred first.

4.5.3   Wall Panel Test Results

Figure 4.12 shows the lateral load versus top displacement response of all wall panel specimens with the corresponding key load and displacement values presented in Table 4.4. It should be noted that lateral load values for wall panels are presented in terms of 1 m unit wall length. As evident in these plots, severely pinched load-displacement behavior, which is a characteristic property of CFS framed shear walls, is common to all specimens.

70

Lateral load levels corresponding to the expected anchor rod yielding and anchor rod maximum force are also indicated in each plot in Figure 4.12. Superimposed on the same plots are cyclic backbone curves based on primary loading cycles and bilinear load-displacement curves determined based on the Equal Energy Elastic-Plastic (EEEP) approach as specified in AISI S400-15 (2015). EEEP model is a simple and commonly used approach to define the nonlinear response of CFS framed shear walls based on measured load-deformation response. Relation between a generic cyclic backbone curve and the corresponding EEEP curve is illustrated in Figure 4.13.

In EEEP approach the yield point and the corresponding elastic stiffness K_e are calculated as follows:

$$K_e = \frac{0.4P_{peak}}{\Delta_e} \tag{4.1}$$

$$P_{yield} = \left(\Delta_u - \sqrt{\Delta_u^2 - \frac{2A}{K_e}} \right) K_e \tag{4.2}$$

$$\Delta_{yield} = \frac{P_{yield}}{K_e} \tag{4.3}$$

where A represents the area under the cyclic backbone curve of specimen between zero and ultimate displacement (Δ_u). Equivalent yield load capacities and elastic stiffnesses determined based on the EEEP approach provide means for the comparison of response among wall panel specimens, as presented in Table 4.4.

4.5.3.1   Comparison of Hold Down Response

Local hold down response obtained from the wall panel specimen S1 is compared with the load-deformation behavior obtained from the hold down assembly test HD-16-M2 in Figure 4.14. In order to acquire the hold down response from wall panel tests, tensile force developing in hold downs was determined by considering the equilibrium of external forces and moments acting on panels. The following relation was used to calculate the hold down force:

$$T = H * h/w_n \qquad\qquad [4.4]$$

where, T is the tensile force developed in hold down; H is the horizontal load applied at the top of wall panel; h is the height of wall panel, which is equal to 2440 mm; and w_n is the distance from the tension side anchor rod to the end of the wall panel on compression side, which is equal to 1120 mm. As evident in Figure 4.14 the hold down response obtained from the wall panel tests closely followed the monotonic response from the hold down assembly test. Even though the initial stiffnesses differ slightly, both sets of response agreed well in terms of general behavior and force levels. Such agreement indicates that the specimen geometry and loading method used in hold down assembly tests accurately represented the conditions of hold down devices in CFS framed sheathed wall panels.

4.5.3.2   Comparison of Wall Panel Response

During wall panel tests Specimens S1, S6, and S7 were able to complete target 4% drift cycles in both directions, while premature failure occurred in Specimens S2, S4, and S5 due to fracture of the anchor rods located on the tension side of wall panels. The maximum drift ratio cycles completed prior to anchor rod fracture was 2% for S2, 3% for S4 and 2% for S5. Specimen S3 suffered from failure due to extensive

72

deformation in CFS stud members near wall base in both loading directions shortly before reaching the 4% target drift ratio.

Even though a significant increase in load capacity would be expected due to the presence of double-sided sheathing in Specimen S2 when compared to S1, these two specimens exhibited similar load capacities. As evident in Figure 4.12, S2 failed at a load level that is significantly smaller than the expected load capacity. The wall panel capacity in this specimen was limited by the tensile capacity of anchor rods. In order to overcome such limitation, the anchor rod size was increased in Specimen S3. The use of larger diameter anchor rods resulted in significant improvement in wall response in the form of increased load capacity with no anchor rod fracture in S3. However, the increased axial force levels that the CFS studs were subjected to in this specimen resulted in stud buckling failure near wall base prior to 4% drift ratio.

The main energy dissipation mechanism in conventionally designed CFS wall panels is through tilting deformation of screws providing the connection between the sheathing panel and the CFS framing members, as well as the resulting bearing deformation of the sheathing material around these connection screws. With the proposed hold down device, on the other hand, an additional energy dissipation mechanism can be provided through controlled tension yielding of anchor rods.

Performance of walls designed based on controlled yielding concept of anchor rods can be investigated by studying the experimentally determined response of Specimens S4–S7. Damage in these specimens was observed to localize mostly in anchor rods. Anchor rod fracture occurred in Specimens S4 and S5 before reaching the 4% target drift ratio, mainly due to relatively low tensile strength to yield strength ratio of anchor rod steel material used in these specimens. As evident in the plots presented in Figure 4.12, there is a narrow window for Specimens S4 and S5 between the lateral load levels corresponding to the expected anchor rod yielding and anchor rod fracture. As a result, the anchor rods in these specimens exhibited somewhat

nonductile response by fracturing shortly after the onset of yielding. The reason for Specimen S5 to be able to maintain a smaller maximum drift ratio compared to S4 is related with the additional anchor rod bending deformation occurring in S5 as a result of longer rod used in this specimen. Such a significant bending deformation promoted early fracture of anchor rod in Specimen S5. Use of anchor rods with more favorable material properties in Specimens S6 and S7 eliminated rod fracture and both of these specimens were able to maintain the target 4% drifts in both directions. Measurements from the strain gages attached on anchor rods indicate that the middle portion of the anchor rods in these specimens yielded when wall panels reached 2% drift ratio and were able to sustain plastic deformations until the end of cyclic loading.

Energy dissipated by each wall specimen is presented in Table 4.5. The values represent the cumulative energy dissipated by specimens at the end of each drift ratio cycle considering only the main cycles of loading. Specimens S3, S4, S6 and S7 dissipated more energy than the rest of the specimens. Among these specimens, S3 had the largest energy dissipation ability, even though the controlled anchor rod yielding concept was not utilized in this specimen. This specimen was tested with a 24 mm diameter anchor rod, and as a result it was able to maintain higher lateral load than the other specimens in all drift ratio cycles. Such high load levels resulted in higher dissipated energy values than the rest of the specimens. Even though it dissipated more energy, the overall ductility (defined as Δ_u/Δ_y in Table 4.4) of Specimen S3 was considerably smaller than those of Specimens S6 and S7, which utilized controlled anchor rod yielding concept with favorable material properties.

4.5.3.3 Comparison of Wall Damage between Conventional and Controlled Yielding Concepts

For wall panels that were able to maintain 3% drift ratio (i.e., Specimens S3, S4, S6, and S7), damage in CFS compression stud members after 3% and 4% drift cycles is shown in Figure 4.15. The extent of CFS stud damage near wall base after completing the 3% drift cycle in Specimen S3 is evident in the figure. For Specimens S6 and S7, controlled yielding of the anchor rod on tension side contributed to meet the deformation demand imposed on wall panel. Consequently, damage on CFS stud members remained minimal. Pictures showing the compression stud members in Specimens S6 and S7 after completing the 3% drift cycle indicate very minor stud damage located at approximately quarter of wall height from the base. These specimens were able to maintain the target 4% drift ratio in both loading directions with the CFS stud members damaged slightly when compared to those in the conventionally designed Specimen S3. The slight wall damage even after maintaining 4% drift ratios implies that the concept of replacing the damaged anchor rods after a strong seismic event is a viable option.

Table 4.1 Details of hold down specimens

Specimen Name	Number of Screws	Additional Parameters	Loading Type
HD-8-M1	8	-	Monotonic
HD-8-M2	8	Backing OSB piece	Monotonic
HD-8-C	8	-	Cyclic
HD-12-M1	12	-	Monotonic
HD-12-M2	12	Backing OSB piece	Monotonic
HD-12-C	12	-	Cyclic
HD-16-M1	16	Evenly distributed screws	Monotonic
HD-16-M2	16	-	Monotonic
HD-16-C	16	-	Cyclic
HD-22-M1	22	-	Monotonic
HD-22-M2	22	Backing OSB piece	Monotonic
HD-22-C	22	-	Cyclic

Table 4.2 Results of hold down tests

Specimen Name	Maximum Load, P_{max} (kN)	0.65xP_{max} (kN)	Load at 6.35 mm deformation (kN)	LRFD load capacity (kN)	Deformation at LRFD load capacity (mm)
HD-8-M1	53.6	34.8	-	34.8	3.6
HD-8-M2	61.8	40.1	57.6	40.1	3.5
HD-8-C1	52.9	34.4	52.0	34.4	4.0
HD-12-M1	82.7	53.8	57.4	53.8	6.1
HD-12-M2	92.8	60.3	60.0	60.0	6.4
HD-12-C1	64.0	41.6	44.0	41.6	5.4
HD-16-M1	74.3	48.3	61.5	48.3	4.9
HD-16-M2	91.4	59.4	66.0	59.4	5.7
HD-16-C1	92.0	59.8	64.0	59.8	5.9
HD-22-M1	86.7	56.3	70.0	56.3	5.0
HD-22-M2	91.6	59.5	74.0	59.5	5.1
HD-22-C1	86.6	56.3	70.5	56.3	4.9

Table 4.3 Details of wall panel specimens

Specimen	Sheathing	Anchor Rod	Controlled Yielding?
1	Single-sided	Ø16_threaded, Steel Batch A (F_y = 480 MPa, F_u = 580 MPa)	No
2	Double-sided	Ø16_threaded, Steel Batch A (F_y = 480 MPa, F_u = 580 MPa)	No
3		Ø24_threaded, Steel Batch B (F_y = 500 MPa, F_u = 575 MPa)	No
4		Ø15, Steel Batch B (F_y = 500 MPa, F_u = 575 MPa)	Yes
5		Ø13 - 1 m length, Steel Batch B (F_y = 500 MPa, F_u = 575 MPa)	Yes
6		Ø15, Steel Batch C (F_y = 415 MPa, F_u = 645 MPa)	Yes
7[a]		Ø13, Steel Batch C (F_y = 415 MPa, F_u = 645 MPa)	Yes

[a] Bottom 35 cm part of sheathing was cut and screwed back. A vertical load of 31.4 kN was applied to simulate gravity loads

Table 4.4 Results of wall panel tests

Test Specimen	P_{peak} (kN/m)		Δ_{peak} (mm)		Δ_{u} (mm)/% drift				P_{yield} (kN/m)		Δ_{y} (mm)		Δ_u/Δ_y		K_e (kN/m/mm)		
	Push	Pull	Push	Pull	Push		Pull		Push	Pull	Push	Pull	Push	Pull	Push	Pull	Average
1	31.66	30.21	91.73	73.20	97.60	4.0	73.20	3.0	28.93	26.04	50.26	39.87	1.9	1.8	0.58	0.65	0.61
2	29.97	28.92	48.80	48.80	61.20	2.5	48.80	2.0	28.79	26.10	37.22	27.98	1.6	1.7	0.77	0.93	0.85
3	46.60	47.00	71.22	70.64	87.65	3.6	87.65	3.6	42.84	42.77	47.69	47.78	1.8	1.8	0.90	0.90	0.90
4	37.60	41.55	73.20	65.03	87.18	3.6	65.03	2.7	33.81	36.93	35.97	39.78	2.4	1.6	0.94	0.93	0.93
5	26.17	24.94	49.76	48.80	57.58	2.4	48.80	2.0	24.21	22.67	31.22	22.67	1.8	2.2	0.78	1.00	0.89
6	40.00	40.00	87.57	94.13	97.60	4.0	97.60	4.0	35.69	34.08	44.61	46.87	2.2	2.1	0.80	0.73	0.76
7	37.24	33.00	97.60	97.60	97.60	4.0	97.60	4.0	30.83	27.92	35.18	33.84	2.8	2.9	0.88	0.83	0.85

Table 4.5 Cumulative energy dissipated by wall panel specimens (joule)

Specimen	Drift ratio, %								
	0.15	0.2	0.4	0.6	0.8	1.4	2.0	3.0	4.0
1	6	16	62	152	272	700	1437	3037	4596
2	8	26	87	198	375	913	1935	[a]	[a]
3	9	25	98	218	390	963	2048	4541	[a]
4	9	23	78	189	360	972	2013	4216	[a]
5	9	23	95	223	397	964	1789	[a]	[a]
6	8	23	81	201	363	869	1756	3522	5948
7	12	31	100	228	430	1022	1976	3656	5893

[a] Specimen failed without completing drift cycles

Figure 4.1 Details of the proposed hold down device
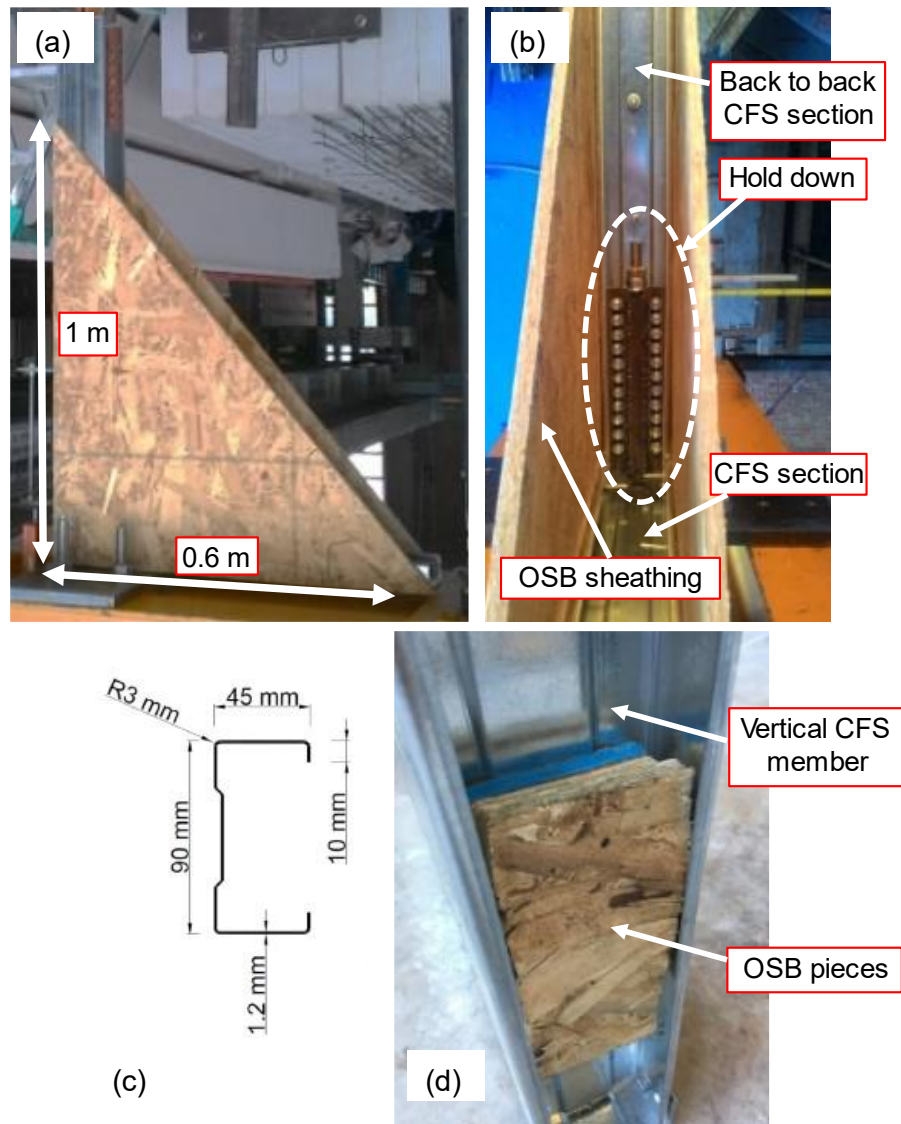
Figure 4.2 Details of hold-down test specimens: (a) dimensions; (b) details; (c) CFS section used for framing members; (d) OSB pieces at back side of vertical CFS framing member
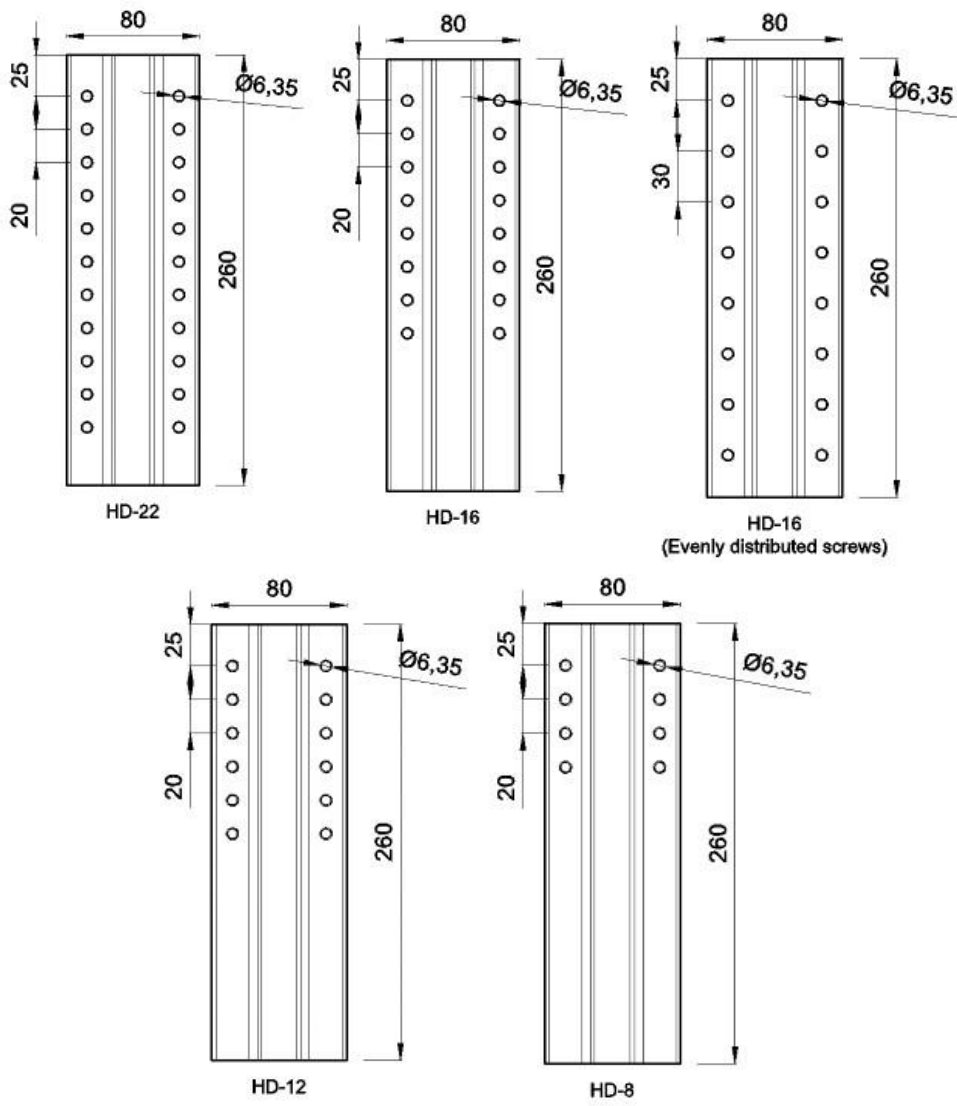
Figure 4.3 Connection screw layouts used on hold down devices
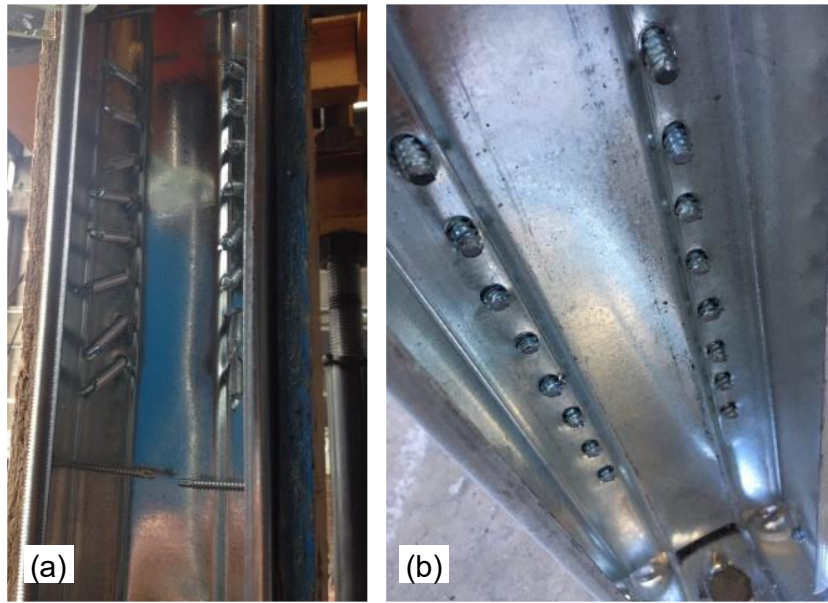
Figure 4.4 Observed deformations: (a) tilting of connection screws during testing;
(b) shearing of screws
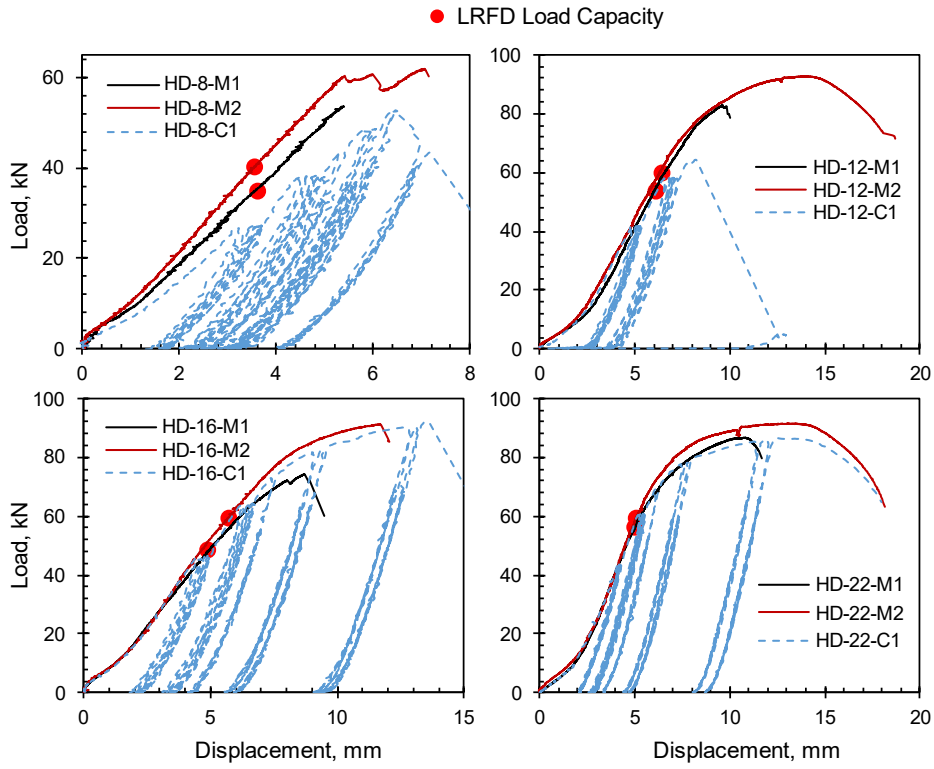
Figure 4.5 Load-deformation behavior of hold down specimens
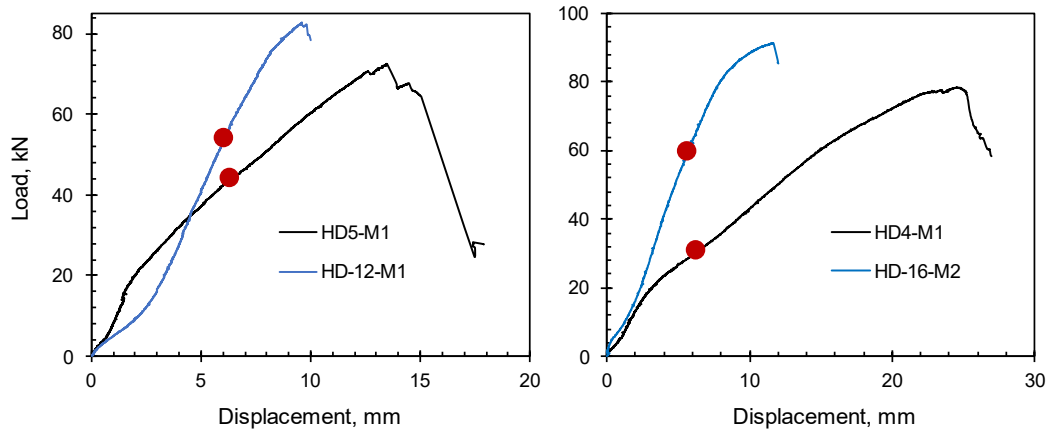
Figure 4.6 Load-deformation behavior of hold down specimens
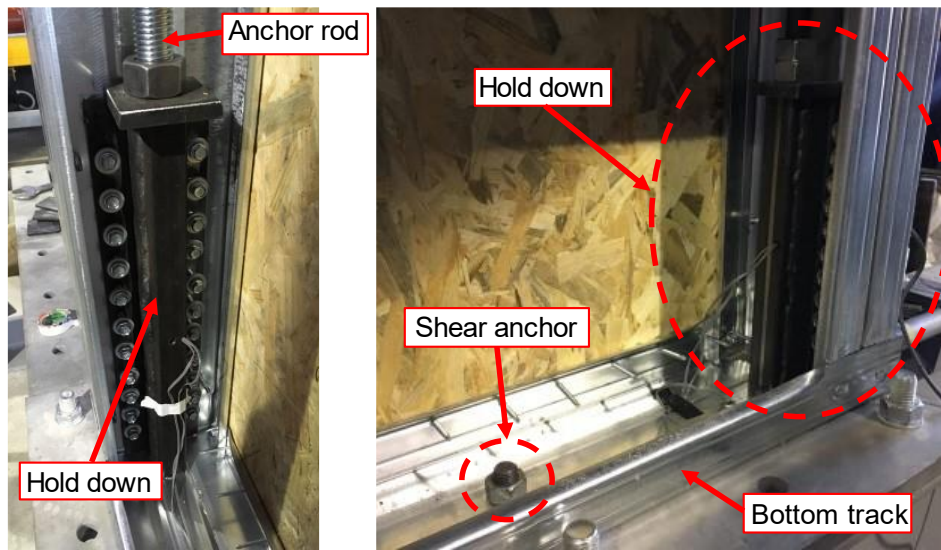
Figure 4.7 Connection and placement details of hold downs in wall panels

*All dimensions are in mm
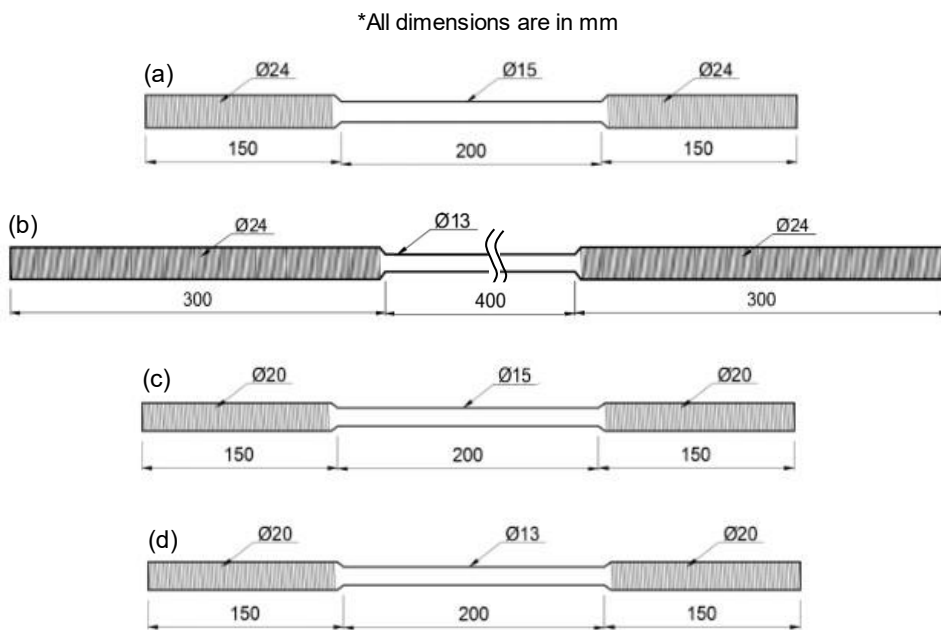
Figure 4.8 Geometry of anchor rods used: in (a) Specimen-4; (b) Specimen-5; (c) Specimen-6; (d) Specimen-7
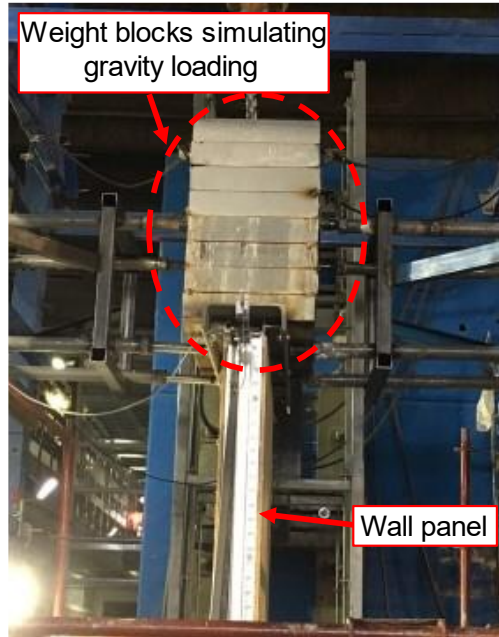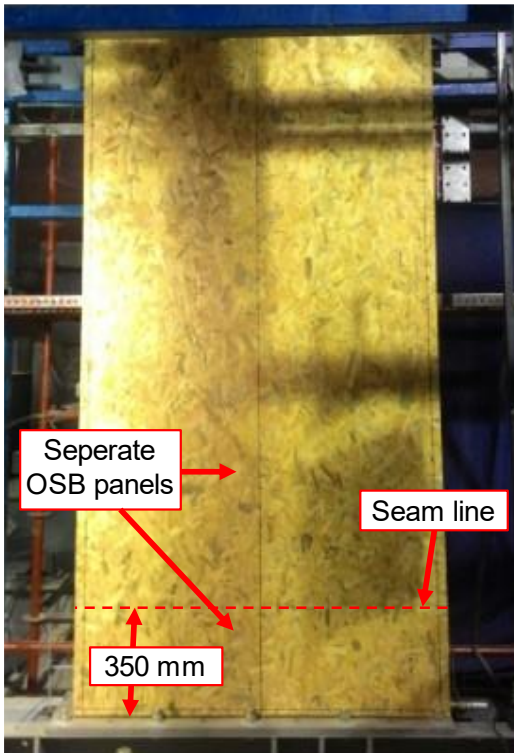
Figure 4.9 Sheathing configuration and gravity loading used in Specimen-7
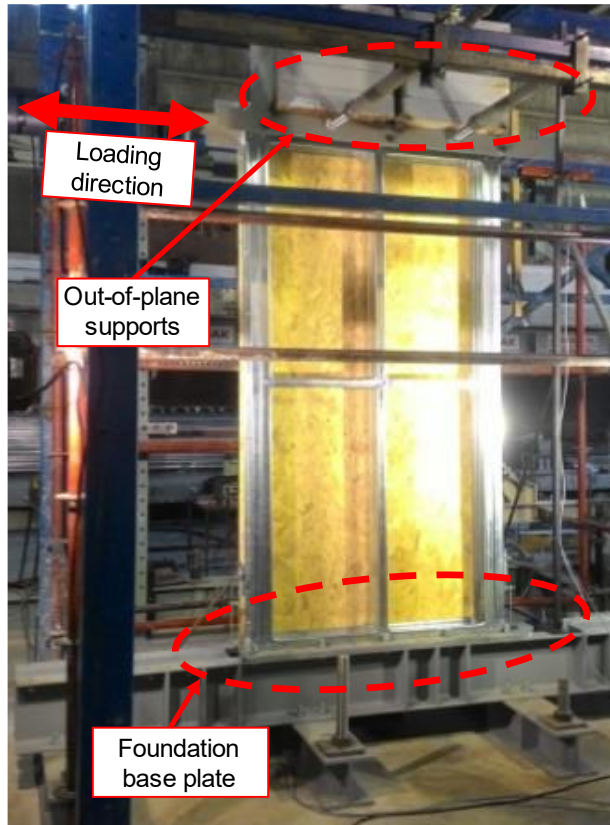
Figure 4.10 Details of wall panel test setup
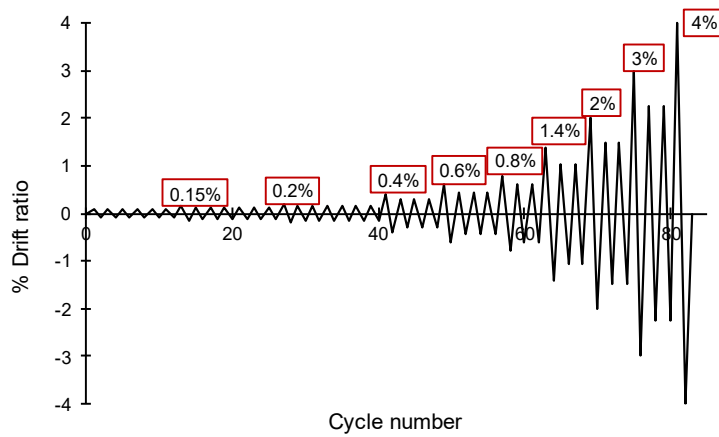
Figure 4.11 CUREE cyclic load pattern used in wall panel tests
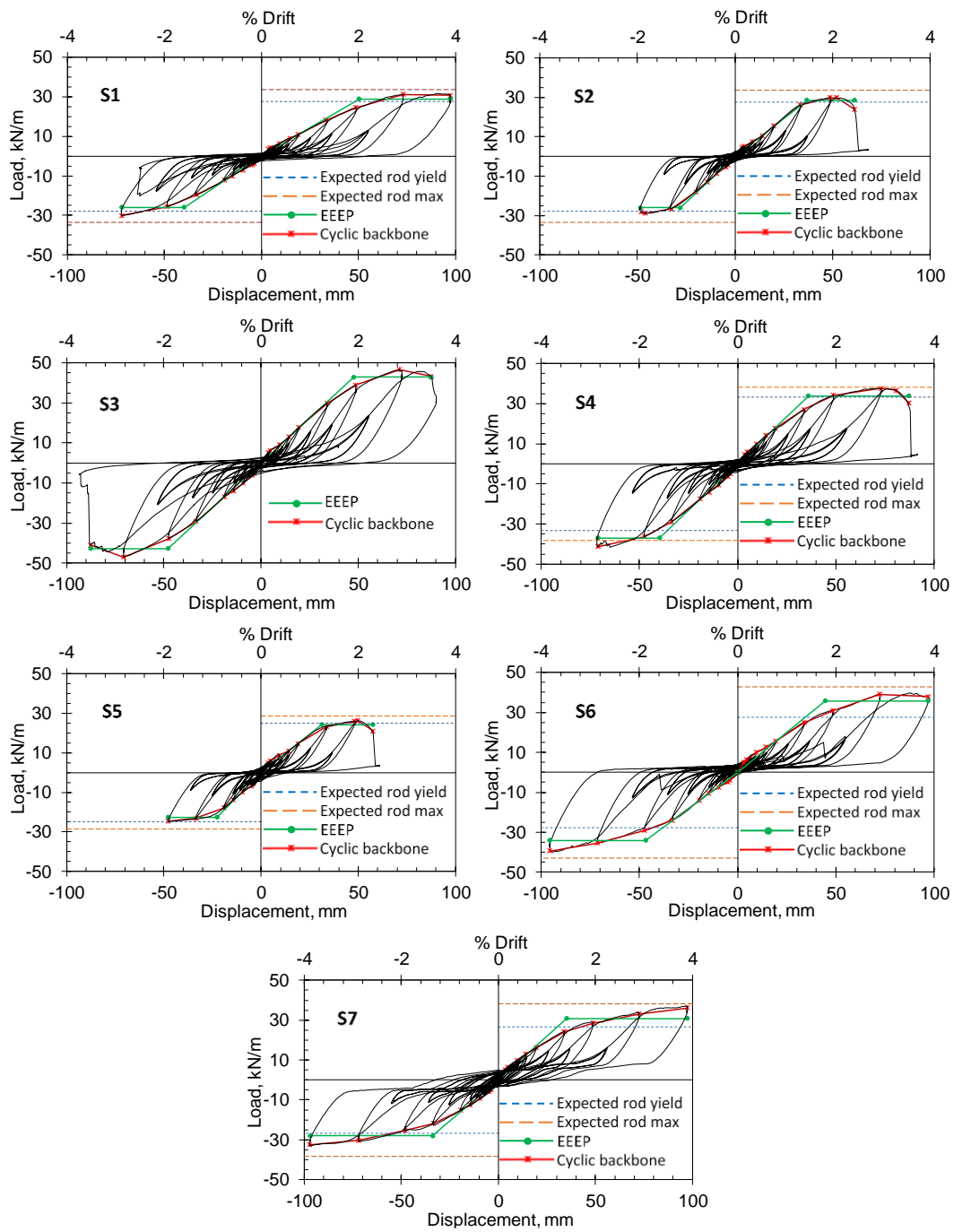
Figure 4.12 Load-lateral displacement behavior of wall panels
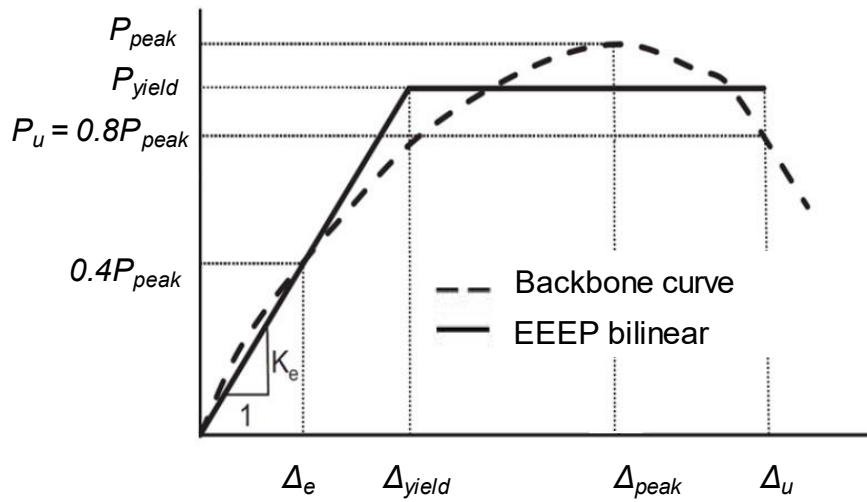
Figure 4.13 Relation between cyclic backbone curve and EEEP model
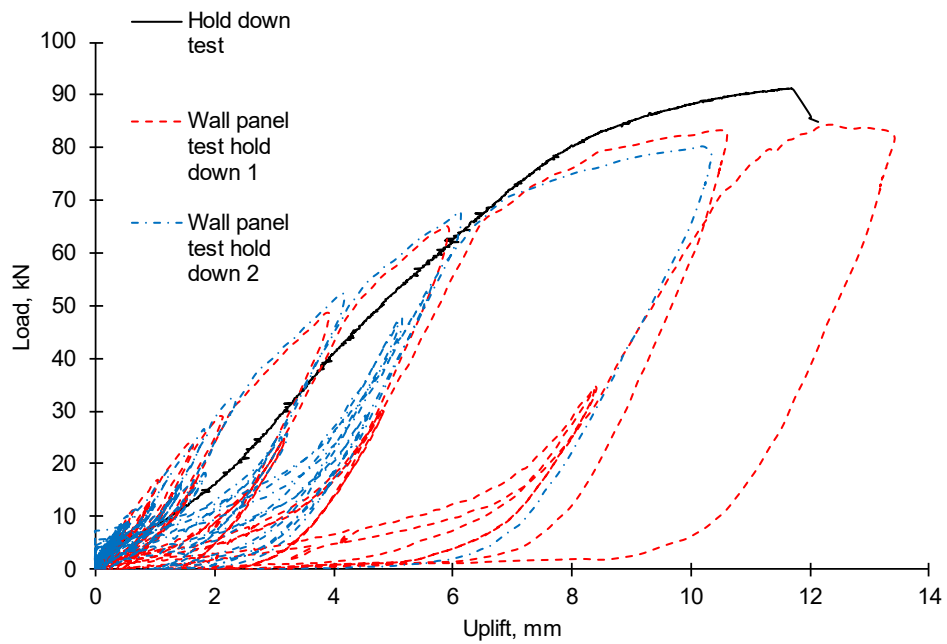
Figure 4.14 Comparison of hold down response from subassembly and wall panel tests

Drift ratio	Specimen			
	S3	S4	S6	S7
3%				
4%		Failure prior to 4% drift		

Figure 4.15 CFS compression stud damage after 3% and 4% drift cycles

CHAPTER 5

INVESTIGATION OF CFS SHEAR WALLS WITH TWO-SIDED SHEATHING AND DENSE FASTENER LAYOUT

5.1   Introduction

The lower and upper bound screw spacing values specified in the shear wall capacity tables given in AISI S400-15 (2015) Standard are 50 mm and 150 mm, respectively. Even though the lateral load response of CFS framed and OSB sheathed wall panels has been the subject of much research, the vast majority of these studies focused on walls constructed with a typical screw spacing of 150 mm. With the increasing use of CFS building systems in high seismic regions one way to address the need for higher lateral load capacity is by providing sheathing on both sides of wall panels with a relatively small fastener spacing. Despite extensive research in the field of CFS shear walls, there is still a need to understand the behavior of CFS framed walls with dense screw layout and double-sided OSB sheathing. A detailed review of the literature reveals that this wall panel configuration has only been considered by Morgan et al. (2002) with a total of four experimental tests. Moreover, wall panels with single-sided OSB sheathing and dense fastener layout have been investigated in a few studies (Blais, 2006; Branston, 2004; Hikita, 2006; Li, 2012; Morgan et al., 2002; Nguyen et al., 1996; Serrette, 1997). The current part of the thesis study aims to address the gap in the literature by investigating the cyclic response of cold formed steel shear walls sheathed on both sides with a relatively small fastener spacing.

Main objectives of this part of the study can be summarized as follows: (i) determine the load capacity of CFS wall panels sheathed with OSB on both sides with closely spaced screws, (ii) improve the drift capacity of such wall panels with the help of

hold down devices enabling the controlled yielding of anchor rods, (iii) obtain seismic response parameters for such wall panels, (iv) evaluate the local response of fasteners with locally available OSB sheets and develop a fastener-based numerical model of wall panels, and (v) develop an equivalent brace wall model to be employed in seismic performance assessment of CFS framed OSB sheathed building systems.

5.2   Shear Wall Test Program

The shear wall tests presented here includes eight full scale CFS wall panel specimens sheathed on both sides and one supplementary specimen sheathed on a single side. The first seven wall specimens shown here are the shear walls considered in the Chapter 4 in order to evaluate the proposed hold down device's behavior when utilized for a shear wall. These wall specimens are considered again in this chapter, but this time in terms of overall behavior and performance. Also, configuration of these walls (double side sheathing and dense fastener layout) is the main property that is being investigated in the current chapter of the thesis.

Parameters used in wall panel specimens are given in Table 5.1. All of the specimens were sheathed with OSB panels and were tested under cyclic loading. Vertical loading was applied on three specimens in order to simulate the effect of gravity loading transferred to wall panels from flooring members. Axial capacity of CFS studs used in wall panels was calculated to be 50 kN and 139 kN for interior and end studs, respectively, using the Direct Strength Method (AISI S100, 2016) and also incorporating the stiffness contribution of OSB sheathing panels by considering full composite action between sheathing and CFS member. The utilized method is a new design approach named ''Direct Stiffness–Strength Method'' and it was presented by Selvaraj and Madhavan (2019a, 2019b, 2021) based on numerous experimental tests on sheathed CFS members. A similar approach was also suggested by Vieira and Schafer (2012, 2013). Based on the computed axial capacity values, the 25.7

kN/m vertical load used in three of the specimens corresponds to 10% of the total axial load capacity of wall panels.

As shown in Figure 5.1 and presented in Chapter 4 previously, each specimen represents a 1220 mm wide and 2440 mm high shear wall panel. All CFS framing members were made of a 1.2 mm thick 140 mm deep C-shaped section with a specified yield strength of 350 MPa. Field stud and track members were comprised of a single C-shaped section, while back-to-back C shaped sections were used for boundary studs. Lip parts of the track cross section were straightened in order to fit stud member at track-stud connections.

Wall panels were sheathed with 11 mm thick OSB sheets. All of the sheathing panels were attached to the CFS framing members using self-tapping screws having 4.2 mm diameter and 50 mm length. A 50 mm screw spacing was used along the boundary CFS members, while for the field stud the spacing was 100 mm. The 50 mm screw spacing represents the lower bound spacing values specified in Nominal Shear Strength Table E1.3-1 in North American Standard for Seismic Design of Cold-Formed Steel Structural Systems, AISI S400-15 (2015) for boundary framing members. The connection screws were driven into OSB sheathing with a typical edge distance of 25 mm.

The hold down device presented in Chapter 4 was used for all shear wall specimens. As explained before, various anchor rods were used along with this hold down device. Properties of anchor rods are also shown in Table 5.1. Along with hold downs, two 16 mm diameter shear anchors were used in each wall panel, except for Specimen S9, to connect the bottom track member to the foundation base plate. In Specimen S9 no shear anchor was used and the wall panel was connected to the base plate with only two hold downs in order to investigate the influence of shear anchors on the base slip response of the wall panel. Locations of the shear anchors along the

bottom track member were adjusted such that there is equal distance between the two shear anchors as well as between each shear anchor and hold down.

Test setup, placement of specimens, instrumentation used on wall panels and details of the utilized cyclic loading history are already presented in Chapter 4.5.2 of the thesis.

5.3   Test Results

5.3.1   Damage and Failure Modes

The deformation modes that were commonly observed during cyclic load testing of wall panels include (1) tilting and pull through of the screws between sheathing panels and CFS framing members, (2) tilting and pull out of the screws connecting hold downs to boundary studs, (3) bending of hold downs and anchor rods, and (4) distortion of boundary studs in the vicinity of hold down location. Examples of these deformation modes are shown in Figure 5.2. Failure of the tested wall panel specimens was typically initiated by buckling of boundary studs. All of the wall panels were able to reach a drift ratio of 2% without experiencing significant damage on sheathing or framing. With further increase in drift ratio, boundary studs suffered from local/distortional buckling near wall base as shown in Figure 5.2(d–f).

For the wall panel that was sheathed on one side (specimen S1), the predominant failure mechanism was related with the failure of sheathing panel and fasteners. Tilting of screws between sheathing panels and CFS framing members indicates relative slip at the OSB CFS interface in the plane of the wall. With increasing drift ratio OSB sheathing panel was observed to separate from the CFS members at corner locations. Such separation finally led to the pulling of screw heads through the OSB panel.

5.3.2   Load-Displacement Behavior

Typical lateral load versus top displacement responses of wall panel specimens are given in Figure 5.3 and Figure 5.4. Lateral load values indicated on these plots are for 1 m of wall length. Cyclic hysteresis curves for all wall panel specimens exhibit severe pinching. This pinched response is a characteristic property of CFS framed shear wall systems and mainly results from the local behavior of connection screws between the sheathing panel and CFS framing members.

5.3.3   Comparison of Response among Wall Panels

A comparison of wall panels based on load capacities and elastic stiffnesses determined from the EEEP model approach is presented in Table 5.2, along with key load and displacement values. The wall panel sheathed on one side (specimen S1) exhibited a maximum load capacity of 31.7 kN/m. For comparison, the load capacity of a similar wall panel tested as part of this research project with a much wider screw layout of 150/300 (150 mm screw spacing along boundary CFS members and 300 mm screw spacing along field stud) was measured to be 12.5 kN/m. Both of these wall panels exhibited similar deformation modes including separation of OSB sheathing from CFS framing at corner locations and pulling of screw heads through the OSB panel. The measured load capacities (i.e., 31.7 and 12.5 kN/m) for the panels with 50/100 and 150/300 screw layout are in good agreement with nominal shear strength values specified in AISI S400-15 (2015) Standard, which are 30 and 12.0 kN/m, respectively. These results indicate that for the same wall configurations, the panel that was constructed with three times more connection screws experienced approximately 2.5 times increase in lateral load capacity. It should be mentioned that validity of the shear wall capacity values specified in AISI S400-15 (2015) Standard is subjected to CFS material grade requirement. Accordingly, the standard requires

ASTM A1003 Structural Grade 33 steel (yield strength of 230 MPa) for CFS thickness of 1.1 mm and Grade 50 steel (yield strength of 345 MPa) for CFS thickness of 1.4 mm. The CFS members used in the current investigation had a thickness of 1.2 mm and a yield strength of 350 MPa.

The AISI S400-15 (2015) Standard suggests that with double-sided sheathing, load capacity of the panel can be considered to be two times the nominal shear strength of the panel sheathed on a single side, provided that minimum stud and track thickness and fastener size are satisfied. The specimen S2 was able to maintain a peak load capacity of only 30.0 kN/m due to premature failure of an anchor rod. By providing a larger size anchor rod in specimen S3, peak load capacity of the wall panel increased to 47.0 kN/m. This was the largest load capacity among all wall panels tested as part of the current study. This load capacity value represents 1.5 times increase between the cases of single-sided and double-sided sheathing. The corresponding increase in elastic stiffness of wall panels is also 1.5 times.

As evident in Table 5.2, for the wall configurations considered in this study, providing double-sided sheathing resulted in less than two times improvement in wall response when compared to the corresponding single-sided sheathing case due to deformation of other components of the wall panel. It should be noted that providing stud and track thicknesses in accordance with the designated values in AISI S400-15 (2015) Standard did not prevent stud buckling in the current wall panels. Therefore, special attention should be paid to the fact that the designated CFS thickness values in the Standard do not guarantee a stable condition for framing members under gravity and seismic loading. The direct use of the tabulated shear wall capacity values without consideration of CFS member buckling may result in unsafe designs especially for the case of wall panels sheathed on both sides.

5.3.4 Hold Down Contribution on Shear Capacity

The current practice in CFS construction is to use hold downs and shear anchors, respectively, for transferring the tension and shear forces at wall base. In order to reveal the shear transfer ability of hold downs in addition to resisting the uplift effects, no shear anchors were used in specimen S9. As evident in Figure 5.3 and Table 5.2, there is no appreciable difference in the response of this specimen and the companion specimen tested with two shear anchors in addition to hold downs (specimen S8). These two wall panels exhibited almost identical responses in terms of load capacity, stiffness, and overall shape of load–displacement curves. This observation suggests that hold down devices not only resist uplift effects but also provide significant shear resistance at wall base.

5.3.5 Effect of Gravity Loading

The effect of gravity loading on lateral behavior of wall panels is visible in the response of specimens S8 and S3. Specimen S8 was tested under 25.7 kN/m of vertical loading while the companion specimen S3 was tested with no vertical loading. The presence of vertical loading in specimen S8 resulted in a 16% increase in elastic stiffness with a small reduction in peak load capacity and peak displacement. The reason for the increase in wall stiffness is due to the fact that gravity loading opposes the overturning effect of lateral loading. The gravity loading in specimen S8 resulted in stud buckling at a smaller drift ratio than the companion specimen tested with no gravity load.

5.3.6 Comparison of Wall Response with Earlier Studies

The measured drift capacities of wall panels tested in the current study were compared to those of walls tested earlier by other researchers (Blais, 2006; Branston, 2004; Hikita, 2006; Li, 2012; Morgan et al., 2002; Nguyen et al., 1996; Serrette, 1997). For this purpose, a database of OSB-sheathed CFS-framed wall panel tests was created. The database includes cyclic tests on 27 wall panels from seven different studies with fastener spacing values of 50 and 75 mm and with similar wall dimensions as the ones used in the current study. Out of these 27 wall panels only four of them had double-sided sheathing. Details of the wall panels in the database are shown in Table 5.3. For each study in the database, the average values of wall drift ratio at peak load and the maximum wall drift ratio were calculated in both loading directions. The maximum wall drift ratio was taken as the value of the drift ratio at 80% of wall load capacity in post-peak region. Wall drifts for the specimens in the database are provided in terms of net wall lateral displacement. For the sake of comparison, net lateral displacements were calculated for the wall panel specimens of the current study. For this purpose, lateral displacements due to lateral slip and uplift at wall base were subtracted from the total lateral displacement measured at the top level of panels.

Figure 5.5 provides a comparison of average drift values from the database with the corresponding values obtained in the current study. As evident, there is a relatively large variation among the drift values obtained in different studies. Such variation can be attributed to variation in several factors among studies; such as material properties, construction details used in test specimens, and the loading method used for testing. The average drift capacity of wall panels tested in the current study is 2.0% and 1.9% in two loading directions. The maximum and minimum of these values from the database are 3.0% and 1.4%. For the wall panels tested as part of the current study the average drift ratio at peak load is 1.7% in two loading directions.

98

The corresponding maximum and minimum values from the database are 2.8% and 1.1%. Both the net maximum drift capacity and peak load drift capacity of wall panels tested in the current study are within the maximum and minimum values obtained earlier by other researchers for similar wall panels. The values obtained in the current study represent the somewhat average values of the similar wall panels available in the literature.

The four double side sheathed wall panels tested by Morgan et al. (2002) utilized 1.4 mm and 1.7 mm stud thicknesses. For these walls, the increase in load capacity compared to the companion single side sheathed panels was 77% and 70%, respectively. The failure mode for the single-sided walls tested by Morgan et al. (2002) was reported to be OSB fracture along panel edges at fastener locations, irrespective of the stud thickness used for the framing. For double-sided walls, stud buckling occurred on walls framed with 1.4 mm thick studs and screw failure occurred at hold down-stud connections on walls framed with 1.7 mm thick studs. This response is similar to the one observed in the current study in a sense that with double-sided sheathing the axial force demand on CFS studs increases and such a demand increase leads to failure of other components of the wall panel. As a result of such premature failure, the increase in lateral load capacity remains below 100% between the cases of single-sided and double-sided sheathing (i.e., only 77% and 70% increase in load capacity). The tests by Morgan et al. (2002) also indicated a decrease in drift capacity of wall panels when the walls were sheathed on both sides instead of on a single side. For walls framed with 1.4 mm studs, the average max drift decreased from 1.7% to 1.2%, while for walls framed with 1.7 mm studs, the decrease was from 2.0% to 1.2%. It should be noted that drift capacities for the double side sheathed panels tested by Morgan et al. (2002) (i.e., 1.2%) are significantly smaller than the average net drift capacity of 2.0% obtained in the current study. The reason for the double side sheathed wall panels tested in the current study exhibiting higher net drift capacity than the similar walls tested by

Morgan et al. (2002) can be attributed to the reduced drift demand on wall panels due to the controlled yielding concept utilized in the current study.

The wall panels tested in the current study exhibited asymmetric load–displacement response with the load capacity being higher in the direction that was first loaded than the other direction. During testing when the loading was applied in the push direction screw tilting and a resulting local bearing deformation of OSB occurred. When the loading was reversed, the screws were able to resist a smaller level of force as a result of already existing OSB damage. This mechanism showed itself in the form of reduced load capacity and stiffness in the positive displacement direction as compared to the negative displacement direction. Similar asymmetric wall response is also valid in Figure 5.5 in the form of unequal drift capacity values in two loading directions measured by other researchers.

5.3.7 Seismic Response Parameters

Seismic response parameters, including ductility ratio (μ), ductility related modification factor (R_μ), and overstrength factor (R_O) were determined based on the load and displacement capacities determined using the EEEP model. Ductility ratio and ductility related modification factor represents the structure's ability to dissipate energy through inelastic deformations. Overstrength factor is a crucial parameter for capacity based design and it is usually involved in the design of elements other than the energy dissipating components within the system. Such an approach ensures that these components remain elastic while energy dissipation is provided by ductile deformation of sheathing to framing connections.

The relatively low natural periods (i.e., $T_n < 0.5$ sec) of structures utilizing wood sheathed wall panels, as suggested by Boudreault (2005), require the use of equal energy approach rather than the equal displacement approach to determine the

ductility related modification factor. The seismic response parameters can be derived by utilizing the equal energy rule and by using the experimentally determined response of wall panel specimens as follows (Boudreault, 2005; Newmark and Hall, 1982):

$$\mu = \frac{\Delta_u}{\Delta_{yield}} \qquad\qquad [5.1]$$

$$R_\mu = \sqrt{2\mu - 1} \qquad\qquad [5.2]$$

$$R_o = \frac{P_u}{P_y} \qquad\qquad [5.3]$$

It should be noted that the overstrength factor determined by Equation 5.3 does not include the overstrength present in the design due to conversion between the nominal and design capacities. This part of the overstrength factor depends on the design methodology used, as well as the value of safety factor utilized in design.

Seismic response parameters determined for the investigated wall panels are given in Table 5.4. It should be noted that these parameters represent the response of individual wall panels, and that the effects of other components have to be considered as well when evaluating the seismic response of an entire CFS structural system. The average $R\mu$ for double-sided walls is 1.75 with a coefficient of variation of 0.11. For wall panels sheathed with OSB on a single side, Boudreault (2005) determined a test based average $R\mu$ value of 2.9. Based on cyclic testing of a three-dimensional model structure with CFS framed OSB sheathed walls Landolfo et al. (2006) reported an $R\mu$ value of 2.6. As evident, the $R\mu$ values obtained in the current study for double-sided walls are smaller than those reported by other researchers for single-sided shear walls. The discrepancy is probably due to premature failure of some of the wall

panels in the current study due to increased demand on CFS studs resulting from the presence of double-sided sheathing.

As indicated in Table 5.4 the overstrength factors, as determined by Equation 5.3, range between 1.08 and 1.19 (average = 1.12, coefficient of variation = 0.03). For wall panels sheathed with OSB on a single side, Boudreault (2005) determined a test based average overstrength factor of 1.18 and 1.09, respectively from monotonic and cyclic load tests. A relatively large material overstrength factor of 2.6 was reported by Landolfo et al. (2006) based on cyclic testing of a three-dimensional model structure with CFS framed OSB sheathed walls.

5.4   Numerical Modeling of Wall Panels

In this part of the study, two methods of macro modeling approach, namely fastener-based method and equivalent brace method, was utilized for numerical modeling of the wall panel specimens. Numerical modeling and analysis were conducted using OpenSees (Open System for Earthquake Engineering Simulation) (McKenna, 2011) platform. Both the fastener based and equivalent brace models were developed in a 2D environment. For the equivalent braced model corner nodes were defined, while for the fastener-based model nodes at each fastener location were considered. Representation of framing elements was achieved by including beam–column elements. Pinched response of wall panels was obtained by defining truss members in the equivalent brace model, while for the fastener-based model zero-length elements were defined to represent fastener-sheathing connections. The fastener-based model was calibrated based on the physical test results on fastener-sheathing connection screws. The equivalent braced model was calibrated based on the load testing results of full-scale shear wall panels. It should be noted that numerical modeling work done by the fastener based method and fastener testing program

given in the following chapters are the work of Topçuoğlugil (2019), and presented in this chapter of the thesis for comparison purposes.

The cyclic loading protocol described by CUREE (Krawinkler et al., 2001) was utilized both in physical tests and numerical models. Details of the numerical models and the obtained results are discussed in the following sections.

Although it is possible to determine the level of imperfections exist in CFS members (Selvaraj and Madhavan, 2018), such geometric imperfections that are known to exist in CFS members were not considered in modeling of stud and track members in this study. This is mainly because of the fact that the current computational models aim to represent CFS shear wall behavior with minimum possible complexity. Many other studies in the literature adapt the same philosophy for numerical modeling of CFS shear walls and ignore the effect of imperfections while utilizing macro modeling approach (Bian et al., 2014, 2015; Buonopane et al., 2015; Leng, 2015; Leng et al., 2017; Padilla-Llano, 2015). This approach usually involves the use of simple beam–column elements available in OpenSees, which are not suitable for representing geometric imperfections of CFS members.

5.4.1 Fastener-Based Modeling of Wall Panels

The fastener-based model represents a 1.22 m by 2.44 m wall panel with the general layout provided in Figure 5.6. The model is based on the simulation of the nonlinear behavior of each screw providing the connection between the CFS framing members and the sheathing panel. Two sets of nodes were defined at the fastener locations. At each fastener location, one node belongs to the CFS member while the other one belongs to the sheathing panel. These two nodes, sharing the same physical location, were then connected by zero-length spring elements simulating the screw connection. These zero-length elements act in two orthogonal directions.

Stud and track CFS members were divided into small-size frame elements. These frame elements were defined between adjacent fastener nodes as non-linear displacement-based beam–column elements. For these elements, sections defining flexural and axial behavior were combined using section aggregator option to define sectional properties to elements. While flexural behavior was considered as linear-elastic, axial behavior was defined as an elastic perfectly plastic material model. This way, stud failure due to tension or buckling was incorporated in the model. Similar modeling approach has been utilized previously by other researchers (Leng, 2015; Leng et al., 2017). The limiting tension capacity was taken as the tensile strength of steel. The compression limit was defined in terms of the buckling capacity of studs calculated using the Direct Strength Method (AISI S100, 2016) and incorporating the stiffness contribution of OSB sheathing panels. The intermediate stud available between two end studs in wall panel specimens was not included in the numerical model since the effect of these members on overall wall response is negligibly small (Padilla-Llano, 2015). Stud-to-track connections at the top corners of wall panels were modeled with rotational springs. These springs were assigned a linear moment–rotation behavior, with a stiffness of 11.3 kN-m/rad based on a similar study of Bian et al. (2015).

Tension flexibility provided by hold down devices at wall base were modeled by using zero-length elements defined between the bottom of CFS chord studs and the fixed foundation nodes (Figure 5.6). These elements were assigned linear elastic material behavior, with the tension stiffness values based on experimental findings that are presented in the Chapter 4 of the thesis. The tension stiffness values for hold downs were equal to 10,000 kN/m for single side sheathed specimen utilizing 16 mm diameter anchor rod and 20,000 kN/m for double side sheathed specimen with 24 mm diameter anchor rod. Stiffness assigned to these elements in compression was 1000 times larger than the corresponding tension stiffness. With the boundary

conditions used at wall base in numerical models, rocking motion of wall panels was allowed, while base slip was restrained.

Screws providing the connection between the sheathing panel and CFS framing members were modeled using CoupledZeroLength element available in OpenSees. Material model for these elements was assigned by using Pinching4 model, which is a special hysteretic material model available in OpenSees. The Pinching4 material model is capable of capturing softening, strength degradation, and cyclic pinching responses and is defined with four positive and four negative backbone points shown in Figure 5.7.

The OSB sheathing panel was modeled as a rigid diaphragm including a master node defined at the center of the panel, and the nodes at panel edges were slaved to this master node. This type of modeling approach is consistent with the rigid in-plane behavior of sheathing panels observed during shear wall load tests. Such a rigid diaphragm assumption is a common method in numerical modeling of sheathed CFS shear walls and has previously been used by others (Buonopane et al., 2015). It should be noted that even though the sheathing panel was assumed to have infinite in-plane stiffness, local damage of the panel around the connection screws is reflected in the numerical model through the Pinching4 material model used for the connection elements.

5.4.2   Fastener Testing Program

A physical testing program was performed as part of the current investigation for the characterization of the local load-deformation response of connection screws by Topçuoğlugil (2019). A total of five tests under monotonic loading and three tests under cyclic loading were conducted using the setup shown in Figure 5.8. Similar setups have previously been used by other researchers for load testing of screw

connections (AISI, 2017; Derveni et al., 2021; Fiorino et al., 2007; Kechidi et al., 2021; Peterman et al., 2014). Each test specimen included two pieces of 600×300 mm OSB pieces attached on both flanges of two CFS C-shaped members. Three self-tapping screws were provided between the OSB sheathing and each flange of the bottom CFS member. A stronger connection was provided between the sheathing and the top CFS member with more screws in order to prevent any damage at this location during load testing. The connection screws were driven into OSB sheathing with a typical edge distance of 25 mm, which represents the edge distance provided in wall panel specimens. The OSB thickness, CFS section dimensions, screw size, and the material properties used in these fastener test specimens were the same as those used in the wall panel specimens. All monotonic and cyclic tests were carried out as displacement-controlled with a constant loading rate. For cyclic loading tests CUREE loading protocol (Krawinkler et al., 2001) was used. Relative displacement between the OSB pieces and the bottom CFS member was determined at corner locations by using four displacement transducers.

The setup used for the tests is based on simultaneous loading of six fasteners. In this type of arrangement, even though there is a possibility of one screw failing before the others, the load capacity of each screw is usually determined based on the assumption of equal force share among the screws (Derveni et al., 2021; Fiorino et al., 2007; Peterman et al., 2014). In the current study, load capacity ($Pmax$) of each screw was taken as one-sixth of the maximum load achieved during testing. Screw displacement was taken as the average of readings from four transducers positioned at specimen corner locations. Load–displacement curve for a single fastener was obtained and stiffness of each screw was determined as the slope of the secant line passing through the point corresponding to the load level of $0.6*Pmax$ on fastener load–displacement curve. Similar criteria has previously been utilized by other researchers (Derveni et al., 2021; Fiorino et al., 2007; Peterman et al., 2014). It

106

should be noted that the assumption of equal force share among the screws may result in overprediction of individual screw response.

Tilting of screws and pulling of screws through OSB sheathing were the main failure modes observed during fastener tests. The monotonic and cyclic load–displacement responses representing a single screw are shown in Figure 5.9. For the monotonic response, the load capacity changes between 1.71 and 2.23 kN, and the displacement at peak load changes between 8.54 and 9.36 mm. As evident, there is a marked variation in response of the screws from repeat specimens under monotonic loading. Such a variation can be attributed to nonuniform structure of the OSB sheets. Because the strands forming the OSB sheets are randomly oriented, the relative position of the connection screw with respect to these strands has a major influence on local screw response.

The level of variation in local fastener response is smaller in the case of cyclic loading when compared to the monotonic tests, as evident in Figure 5.9b. All three cyclic specimens exhibited asymmetric load–displacement response with the load capacity being higher in the direction that was first loaded than the other direction. During testing when the loading was applied in the positive displacement direction screw tilting and a resulting local bearing deformation of OSB occurred. When the loading was reversed, the screws were able to resist only a smaller level of force as a result of already existing OSB damage. This mechanism showed itself in the form of reduced load capacity and stiffness in the positive displacement direction as compared to the negative displacement direction. Another observation that is valid in Figure 5.9b is the significantly pinched hysteresis curves. The reason for the pinched response is again related with the tilting of screws and the resulting local OSB damage in the vicinity of screws. As discussed earlier, similar asymmetric and pinched behavior was also valid in experimentally determined response of wall panel specimens.

The Pinching4 material models for the monotonic and cyclic loading cases were calibrated based on the test data as shown in Figure 5.10. The monotonic response was characterized by the four points given in Table 5.5. For the cyclic response, four points are required for each loading direction to define the backbone curve, and six additional parameters are required to define the unloading/reloading stiffness (Figure 5.7 and Table 5.5). A comparison of the monotonic fastener response used in the current numerical models with similar responses reported by other researchers (AISI, 2017; Derveni et al., 2021; Fiorino et al., 2007; Peterman et al., 2014) is shown in Figure 5.11. The relatively large variation in the reported screw responses is evident in the figure. The current fastener response represents the lower bound of the data available in the literature. The relatively small stiffness of the current fastener test specimens as compared to the available data could be related with the mechanical properties of the locally supplied OSB sheets being different than those used by other researchers.

5.4.3   Equivalent Brace Modeling of Wall Panels

Schematic representation of the equivalent brace wall model is shown in Figure 5.12. Similar to the fastener-based models, the chord studs were modeled using non-linear beam–column elements with elastoplastic behavior and by neglecting geometric imperfections. Considering that during load testing, CFS tracks of wall panels were connected to a rigid test frame at the base and a loading beam at the top of the wall, rigid beam–column elements were used for tracks in the numerical model. Hold down devices were incorporated in the model in the same way and with the same stiffness values as in the fastener-based model.

In the equivalent brace model inelastic response of all connection screws was lumped into two brace elements. The Pinching4 material property assigned to these brace elements was calibrated to represent the measured lateral load-drift response of the

corresponding wall panel specimen. Load-drift response of wall panel specimen S1, which was sheathed on one side, was used to create the initial model. Afterwards, by using this single side sheathed model, force capacity of the brace elements were doubled to create a double side sheathed model of specimen S3. The parameters used to define the Pinching4 material model for test specimen S1 are provided in Table 5.5.

5.4.4   Comparison between Experimental and Numerical Wall Responses

In order to demonstrate the relation between the local fastener response and the global response of the wall panel, a wall model was analyzed under monotonic loading. Numerical results from this model were compared with the existing experimental results from monotonic testing of a wall panel that was sheathed with OSB panel on one side with 150/300 mm screw layout. For this wall panel the lateral load–deflection response obtained from the fastener-based numerical model under monotonic loading is compared with the experimentally determined response in Figure 5.13. The global load–displacement plot in Figure 5.13a shows the agreement between the measured and numerically predicted responses. The initial stiffness of the wall panel from the numerical model matches exactly with the measured response, while the lateral load capacity is overpredicted by 7%.

In order to investigate the relation between the global response of the wall panel and the local fastener response, the Pinching4 material model used in the numerical analysis was divided into four regions, as shown in Figure 5.13b. The numerically determined load–deflection response of the wall panel was also divided into 20 loading steps with 5 mm wall displacement increments (Figure 5.13a). Figure 5.13c shows the individual connection fasteners used in the wall numerical model. Each dot in Figure 5.13c corresponds to a connection fastener in the numerical model, as well as in the test specimen. The colors used for the fasteners in Figure 5.13c indicate

at which region the fasteners are located in the local fastener response curve given in Figure 5.13b.

As evident in Figure 5.13c, all fasteners remain in the initial linear region (indicated with the blue color) during the first 6 loading steps. This region is characterized by a linear increase in wall lateral load resistance with displacement. The first major reduction in wall stiffness occurs at approximately 35 mm lateral displacement (loading step 7). This reduction in wall lateral stiffness corresponds to transition of the fasteners at wall corners from the initial linear region to the pre-peak linear region. The increase in wall lateral load resistance with displacement continues up to 60 mm of lateral displacement (loading step 12). As evident in Figure 5.13c, at this stage the corner fasteners already entered into the post-peak region. As the local fastener response on wall studs enters into the post-peak region, the lateral load resisting ability of the wall panel deteriorates rapidly. Beyond this stage, the global response of the wall panel is dictated by the local post-peak response of the fasteners. The region characterized by a constant fastener resistance following the post-peak region in Figure 5.13b actually corresponds to failure of the fasteners. For this reason, the part of the numerical wall response curve in Figure 5.13a for displacement values higher than 70 mm (i.e., beyond loading step 14) does not represent the actual behavior, as wall failure has already initiated at this stage.

The measured and numerically predicted load–displacement responses of wall panels are compared in Figure 5.14 for specimens S1 and S3. These specimens, respectively, represent a wall panel sheathed on one side with a dense fastener layout, and a wall panel sheathed on both sides with a dense fastener layout. There is an acceptable agreement between the overall shapes of the load–displacement hysteresis curves from both numerical models and the measured response. In particular, the fastener-based model underpredicts the wall load capacity for the single-sided specimen. Overprediction of wall stiffness in the fastener-based model

up to 2% drift cycles can be due to the local fastener response inside the wall panels somehow being different than the response obtained from fastener tests. Ignorance of CFS member geometric imperfections in the fastener-based numerical model may also have contributed to overprediction of wall stiffness. It should be mentioned that discrepancy between the numerically predicted and experimentally determined wall responses is also evident in data reported by other researchers (Bian et al., 2014; Buonopane et al., 2015).

Another observation valid in Figure 5.14 is that the equivalent brace model is able to predict the load capacity and stiffness of these wall panels with a higher accuracy than the fastener-based model. This is an expected result, considering that the material model calibration in the equivalent brace modeling is performed directly with data from wall panel testing. The material model used in the fastener-based model, on the other hand, is based on the fastener tests and the numerical model is expected to predict the global wall response using this local fastener data. The numerical and experimental hysteresis curves for the 1.4, 2, 3, and 4% drift ratios in the CUREE cyclic loading protocol are presented in Figure 5.15 for specimen S1.

5.4.5 Efficiency of Fastener-Based Modeling and Equivalent Brace Modeling

Both the fastener-based and the equivalent brace modeling approaches have some advantages and disadvantages over each other. The fastener-based modeling approach does not require full-scale wall panel testing, as the Pinching4 material data is obtained from small scale fastener tests. Even though the modeling can be completed with information from small scale fastener tests, the fastener-based modeling approach is not computationally efficient due to the need for modeling of each individual connection fastener. The equivalent brace modeling approach, on the other hand, utilizes a relatively simple numerical wall model with only CFS framing

members and equivalent brace elements. However, calibration of the Pinching4 material model for equivalent brace elements requires load testing of full scale wall panels, which involves a significant effort. For this reason, the equivalent brace method would be more suitable for modeling large and three dimensional CFS structures than the fastener-based method, provided that the material model for the brace elements are calibrated with data from wall panel testing. As a matter of fact, this type of modeling approach is currently being used in a numerical investigation by the authors for seismic performance assessment of CFS framed OSB sheathed building systems.

5.4.6   Effect of Stud Inelastic Behavior on Overall Wall Panel Response

Buckling deformation observed in wall panel studs during load testing has been simulated in the numerical models by using inelastic material model that limits the stud compression capacity. For the case of single side sheathed wall panel the force demand in wall studs remain below the stud compression capacity. In the numerical model of double-sided wall panel, on the other hand, axial force developing in studs exceeded the stud compression capacity. In this case, the lateral load capacity of the wall panel was limited by the stud compression capacity, rather than the capacity of the equivalent brace elements in the model. This behavior is depicted in Figure 5.16, where wall responses with both elastic and inelastic stud behavior from the equivalent-brace model are plotted together with the measured response of two wall panel specimens. The numerically predicted response with inelastic stud behavior (i.e., bilinear behavior with limited stud tension and compression capacities) agrees well with the measured response of the double side sheathed specimen, which suffered from stud buckling during load testing. Utilizing linear-elastic wall studs in the model increases the wall lateral load capacity, as evident in the figure. In this case, no limit was imposed on stud elements and wall load capacity was dictated by

the behavior of the equivalent brace elements. It is interesting to note that the wall response obtained from the model utilizing linear-elastic stud elements agrees perfectly well with twice the measured response of specimen S1, which was tested with sheathing on one side. The plot obtained by doubling the load values resisted by specimen S1 hypothetically represents the response of a double side sheathed wall with no stud buckling. As evident in Figure 5.16, the behavior of such a wall can be captured with the numerical model by utilizing a linear-elastic behavior for stud elements.

Table 5.1 Details of specimens

Specimen	Anchor rod	Controlled yielding?	Gravity Load (kN/m)
S1[a]	Ø16_threaded, Steel Batch A (F_y=480 MPa, F_u=580 MPa)	No	-
S2	Ø16_threaded, Steel Batch A (F_y=480 MPa, F_u=580 MPa)	No	-
S3	Ø24_threaded, Steel Batch B (F_y=500 MPa, F_u=575 MPa)	No	-
S4	Ø15, Steel Batch B (F_y=500 MPa, F_u=575 MPa)	Yes	-
S5	Ø13 - 1 m length, Steel Batch B (F_y=500 MPa, F_u=575 MPa)	Yes	-
S6	Ø15, Steel Batch C (F_y=415 MPa, F_u=645 MPa)	Yes	-
S7[b]	Ø13, Steel Batch C (F_y=415 MPa, F_u=645 MPa)	Yes	25.7
S8	Ø24_threaded, Steel Batch B (F_y=500 MPa, F_u=575 MPa)	No	25.7
S9[c]	Ø24_threaded, Steel Batch B (F_y=500 MPa, F_u=575 MPa)	No	25.7

[a] Specimen failed without completing drift cycles
[b] Bottom 35 cm part of wall on one side was sheathed with a separate OSB panel
[c] Two shear anchors connecting wall panel to base were not present

Table 5.2 Results of tests

Specimen	P_peak (kN/m)		Δ_peak (mm)		Δ_u (mm) / % drift				P_yield (kN/m)		Δ_y (mm)		K_e (kN/mm/m)		
	Push	Pull	Push	Pull	Push		Pull		Push	Pull	Push	Pull	Push	Pull	Average
S1	31.7	-30.2	97.3	72.0	97.6	4.0	73.2	3.0	29.0	26.0	50.3	39.8	0.58	0.65	0.62
S2	30.0	-29.0	48.8	46.2	61.2	2.5	48.8	2.0	28.5	26.1	37.0	28.0	0.77	0.93	0.85
S3	47.0	-47.0	71.2	70.6	87.6	3.6	87.7	3.6	42.8	42.8	47.7	47.8	0.90	0.90	0.90
S4	37.6	-41.6	73.2	65.0	87.2	3.6	73.2	3.0	33.8	37.0	36.0	40.0	0.94	0.93	0.94
S5	26.2	-25.0	49.8	47.8	57.6	2.4	48.8	2.0	24.2	22.7	31.2	22.7	0.78	1.00	0.89
S6	40.0	-40.0	88.0	94.0	97.6	4.0	97.6	4.0	35.7	34.1	44.6	46.8	0.80	0.73	0.77
S7	37.2	-33.0	97.4	97.0	97.6	4.0	97.6	4.0	30.8	28.0	35.2	33.8	0.87	0.83	0.85
S8	44.8	-41.8	63.3	64.4	67.0	2.7	73.2	3.0	38.8	39.1	34.3	41.6	1.13	0.94	1.04
S9	42.5	-39.4	65.0	49.5	69.0	2.8	67.0	2.7	37.0	35.8	34.8	34.9	1.06	1.03	1.05

Grey shaded rows indicate wall panels that were able complete 4% drift cycles in both loading directions

Table 5.3 Drift capacities of wall panels in database

Study	Number of wall specimens	Specimen Details		Drift ratio at peak load (%)		Maximum drift ratio (%)	
				Push	Pull	Push	Pull
Nguyen et al. (1996)	4	WD: 1.22x2.44 m FS: 50/300, 75/300, ST: 0.9 mm OSBT: 11 mm	Min:	1.7	2.1	2.0	2.5
			Max:	2.6	2.4	3.0	2.7
			Avg:	*2.2*	*2.3*	*2.6*	*2.6*
Serrette (1997)	4	WD: 1.22x2.44 m FS: 50/300, 75/300, ST: 1.1 mm OSBT: 11 mm	Min:	1.7	1.7	1.9	1.7
			Max:	2.1	2.1	2.5	2.5
			Avg:	*1.9*	*1.9*	*2.2*	*2.0*
Morgan et al. (2002)	8	WD: 1.22x2.44 m FS: 50/300 mm ST: 1.4 mm, 1.7 mm OSBT: 11 mm 4 specimens double-sided	Min:	0.8	0.7	1.0	0.8
			Max:	1.5	1.4	2.1	2.2
			Avg:	*1.2*	*1.1*	*1.5*	*1.5*
Li (2012)	2	WD: 1.22x2.44 m FS: 50/300 ST: 1.1 mm OSBT: 11 mm	Min:	2.6	2.1	2.6	2.1
			Max:	2.9	2.7	3.3	2.8
			Avg:	*2.8*	*2.4*	*3.0*	*2.5*
Branston (2004)	3	WD: 1.22x2.44 m FS: 75/300 ST: 1.1 mm OSBT: 11 mm	Min:	1.2	1.0	1.7	1.3
			Max:	1.9	1.8	2.2	2.1
			Avg:	*1.6*	*1.3*	*2.0*	*1.6*
Blais (2006)	3	WD: 1.22x2.44 m FS: 75/300 ST: 1.1 mm OSBT: 9 mm	Min:	1.3	1.2	1.6	1.6
			Max:	1.6	1.3	2.3	1.9
			Avg:	*1.4*	*1.3*	*2.0*	*1.7*
Hikita (2006)	3	WD: 1.22x2.44 m FS: 75/300 mm ST: 1.1, 1.4 mm OSBT: 11 mm GL: 14.8 kN/m	Min:	1.1	1.1	1.6	1.1
			Max:	1.7	1.3	1.7	1.9
			Avg:	*1.4*	*1.2*	*1.7*	*1.4*

Table 5.4 Seismic response parameters for specimens

Specimen	μ			R_μ			R_o		
	Push	Pull	Average	Push	Pull	Average	Push	Pull	Average
S1	1.94	1.84	**1.89**	1.70	1.64	**1.67**	1.09	1.16	**1.13**
S2	1.65	1.74	**1.70**	1.52	1.58	**1.55**	1.05	1.11	**1.08**
S3	1.84	1.83	**1.84**	1.63	1.63	**1.63**	1.09	1.10	**1.09**
S4	2.42	1.83	**2.13**	1.96	1.63	**1.80**	1.11	1.12	**1.12**
S5	1.85	2.15	**2.00**	1.64	1.82	**1.73**	1.08	1.10	**1.09**
S6	2.19	2.09	**2.14**	1.84	1.78	**1.81**	1.12	1.17	**1.15**
S7	2.77	2.89	**2.83**	2.13	2.19	**2.16**	1.21	1.18	**1.19**
S8	1.95	1.76	**1.86**	1.70	1.59	**1.65**	1.15	1.07	**1.11**
S9	1.98	1.92	**1.95**	1.72	1.69	**1.70**	1.15	1.10	**1.12**

Table 5.5 Monotonic and cyclic Pinching4 parameters used in computational
models

		Fastener-based model		Equivalent brace model
		Monotonic	Cyclic	Wall Panel S1
N	**ePf1**	210	400	5720
	ePf2	1300	930	33,360
	ePf3	1720	1385	43,160
	ePf4	1200	1240	41,930
mm	**ePd1**	0.06	0.5	0.0006
	ePd2	4.4	2.8	0.0062
	ePd3	8.7	7.0	0.0085
	ePd4	12.7	10.5	0.0116
N	**eNf1**		-350	-5880
	eNf2	-	-795	-34,880
	eNf3		-1160	-41,210
	eNf4		-975	-39,690
mm	**eNd1**		-0.5	-0.0005
	eNd2	-	-2.8	-0.0059
	eNd3		-7.0	-0.0084
	eNd4		-10.5	-0.0116
-	**rDispP**	-	0.6	0.6
	rForceP	-	0.01	0.1
	uForceP	-	0.001	0.01
	rDispN	-	0.6	0.6
	rForceN	-	0.3	0.1
	uForceN	-	0.001	0.01
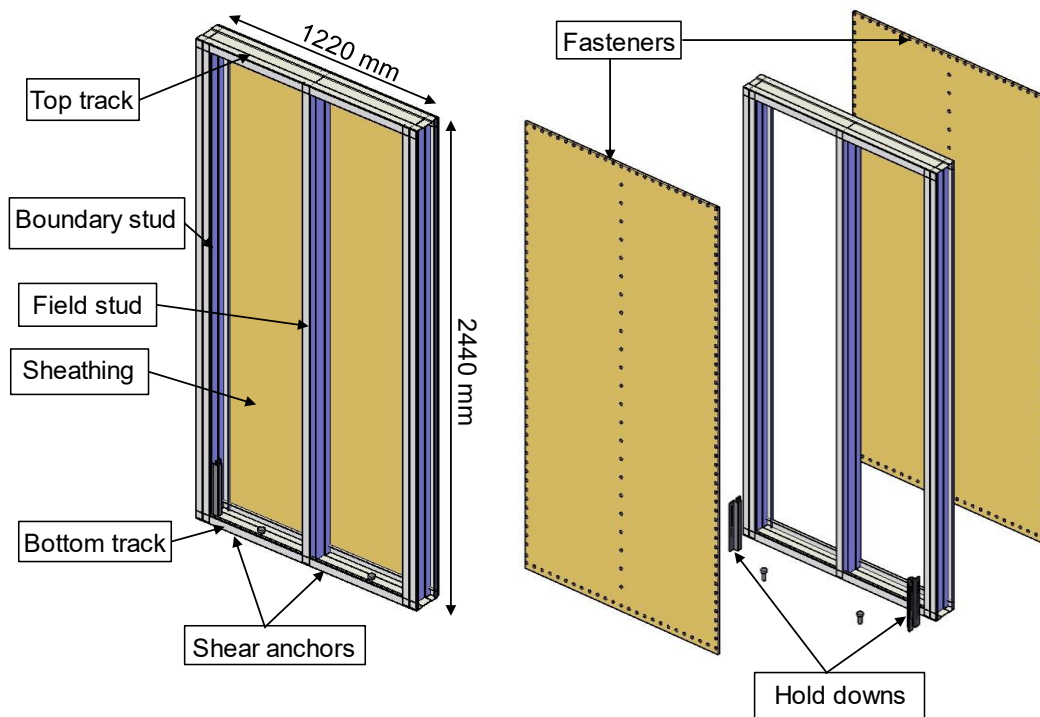
Figure 5.1 General framing details of wall panels
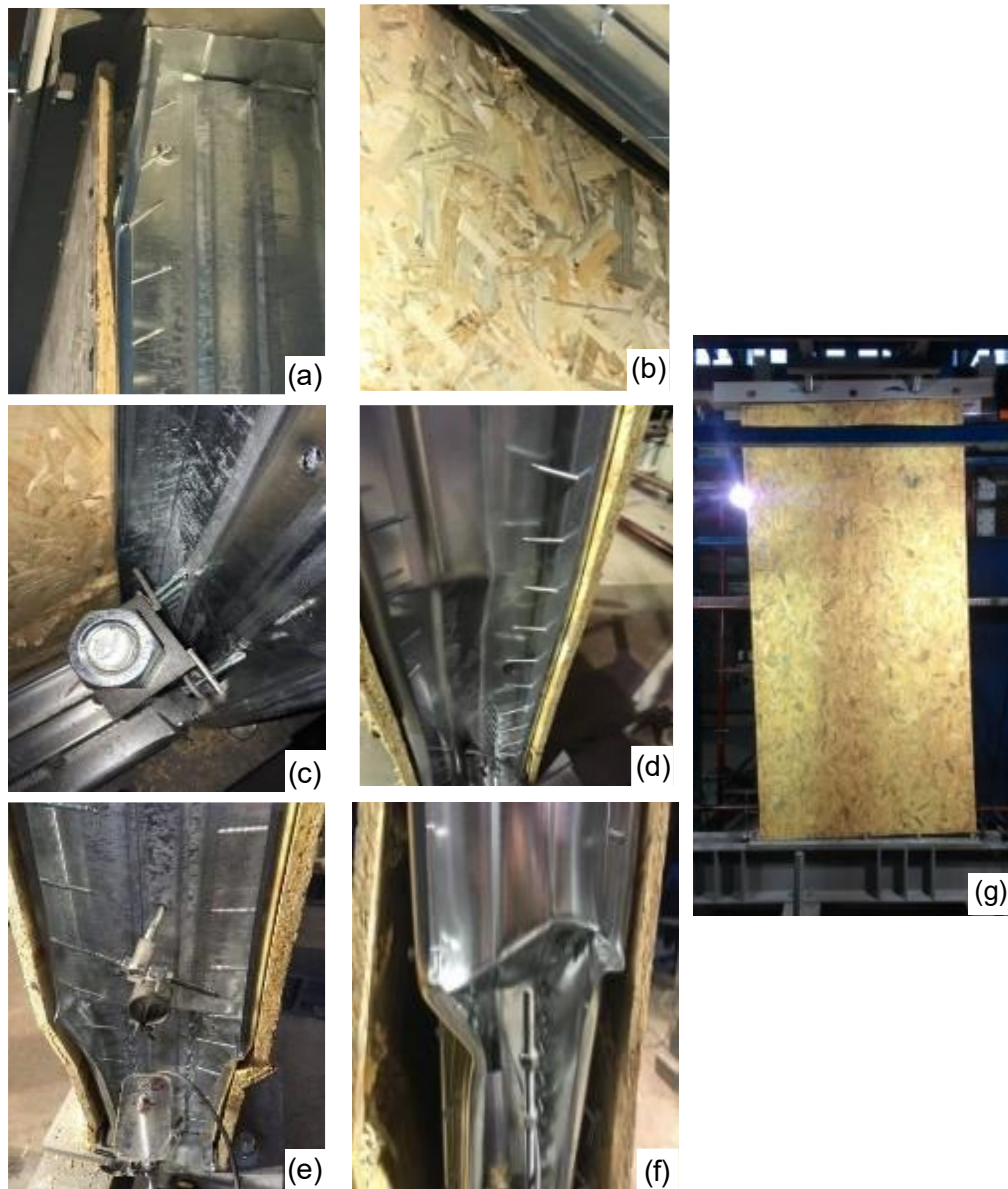
Figure 5.2 Deformations observed on wall panel specimens: (a), (b) tilting of screws and pulling of screw heads; (c) bending of hold down and anchor rod; (d) local/distortional buckling of boundary stud near wall mid-height; (e), (f) local/distortional buckling of boundary studs near wall base; (g) overall failure mode of wall panel
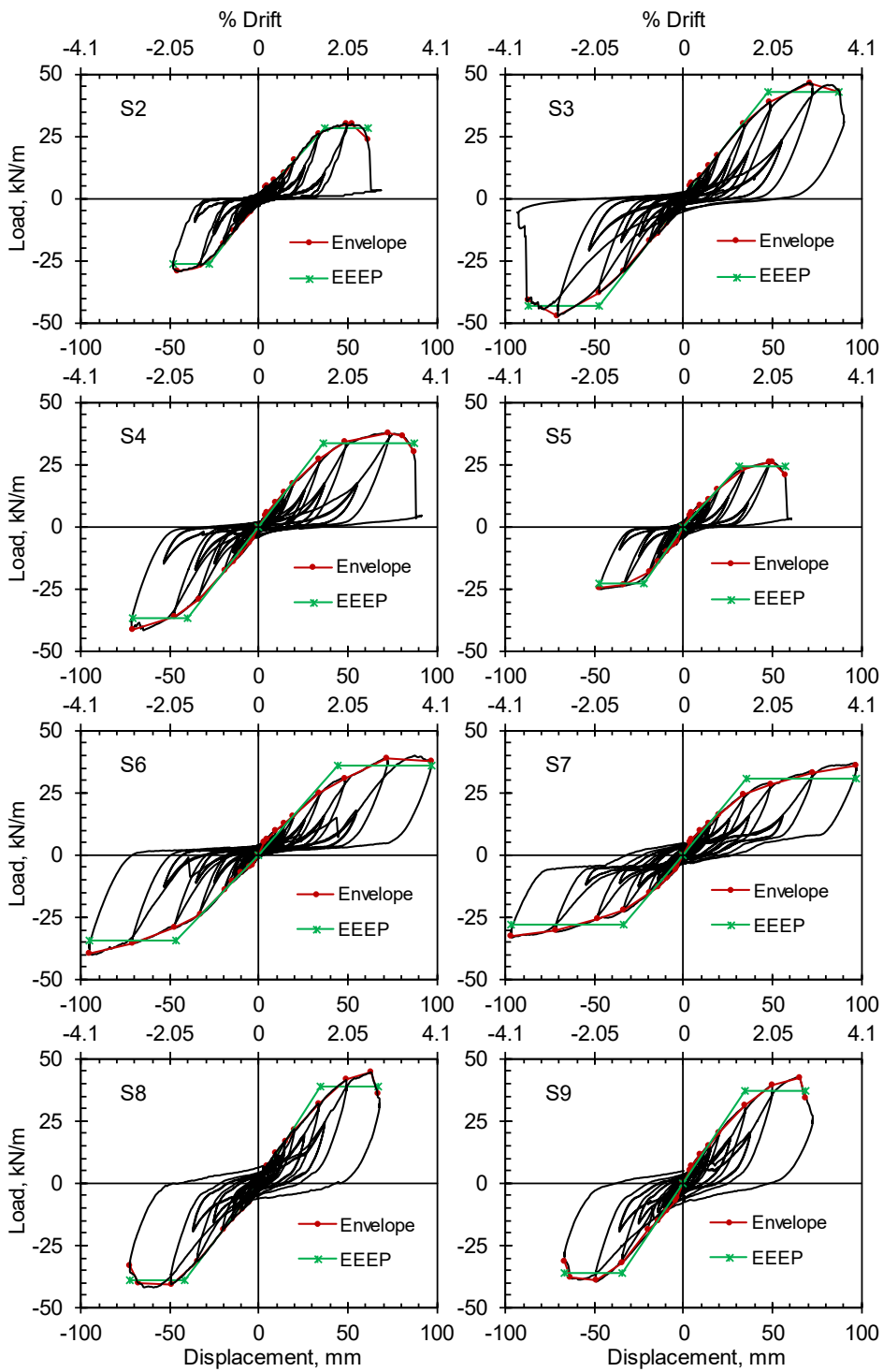
Figure 5.3 Load-displacement behavior of walls with double sided OSB sheathing
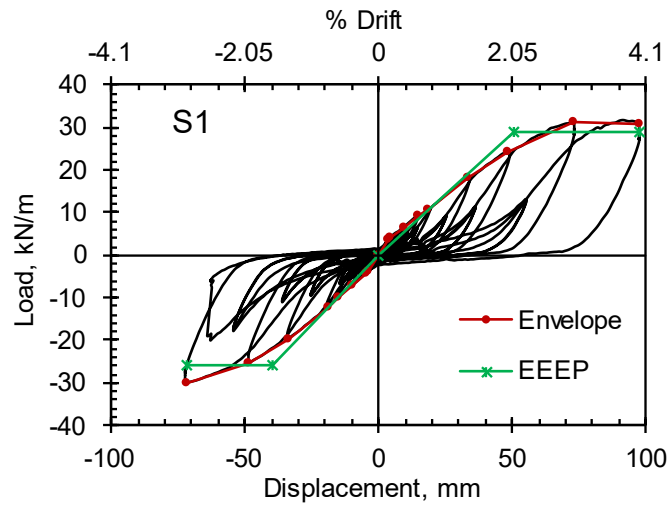
Figure 5.4 Load-displacement behavior of wall with single sided OSB sheathing
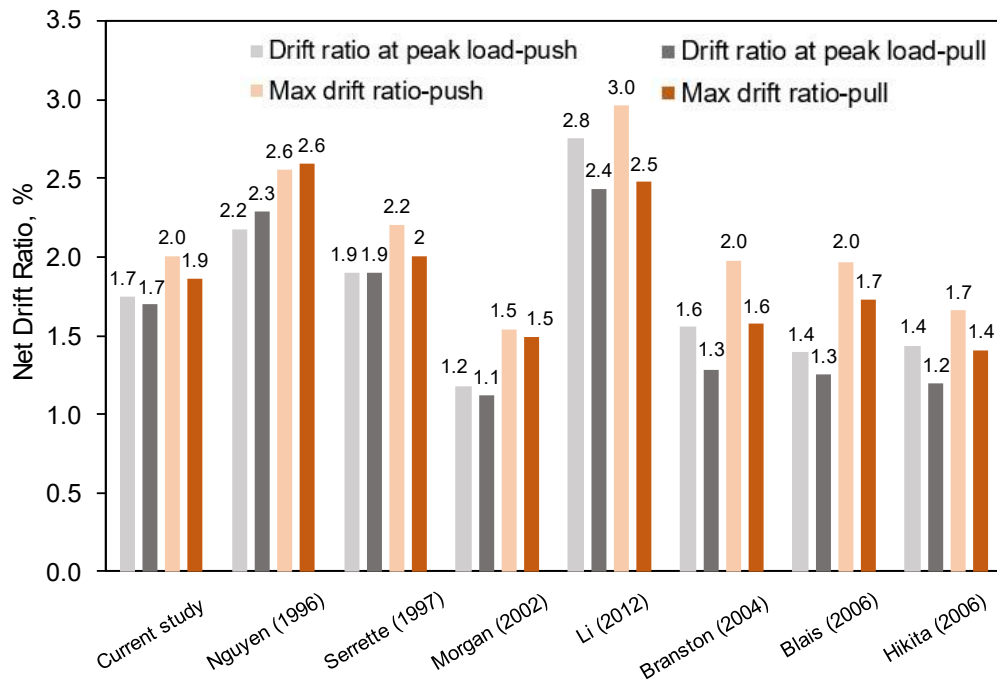
Figure 5.5 Comparison of wall net drift capacities with earlier studies

121
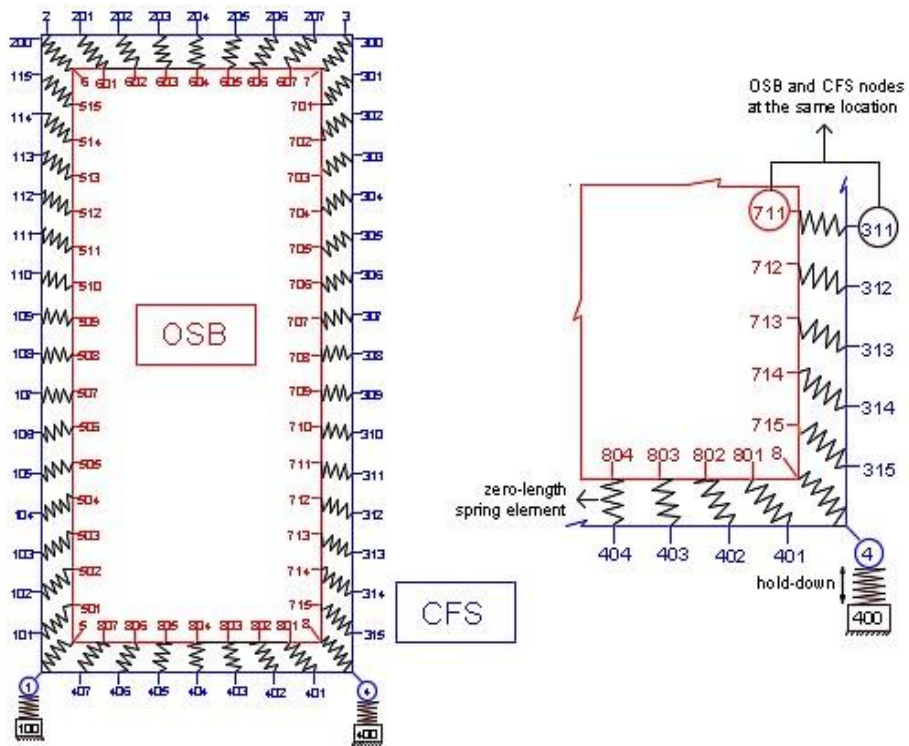
Figure 5.6 General layout of fastener-based wall model (Topçuoğlugil, 2019)

122
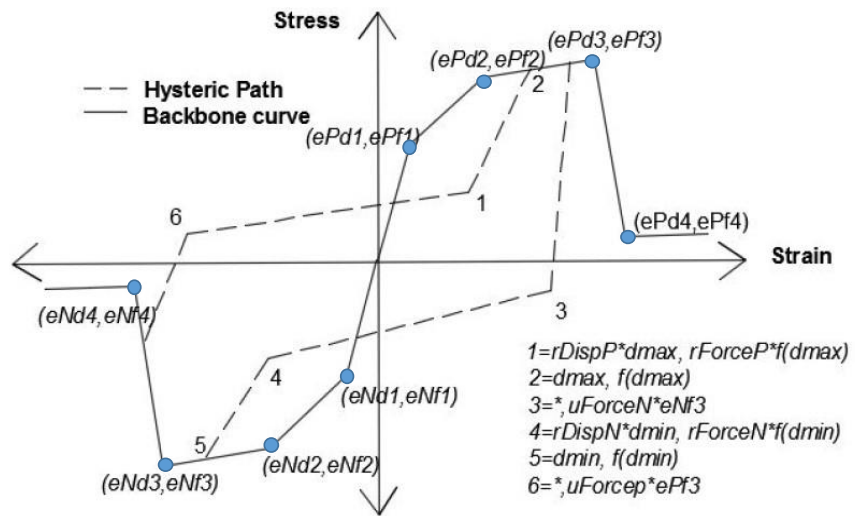
Figure 5.7 Pinching04 material model available in OpenSees (McKenna, 2011)
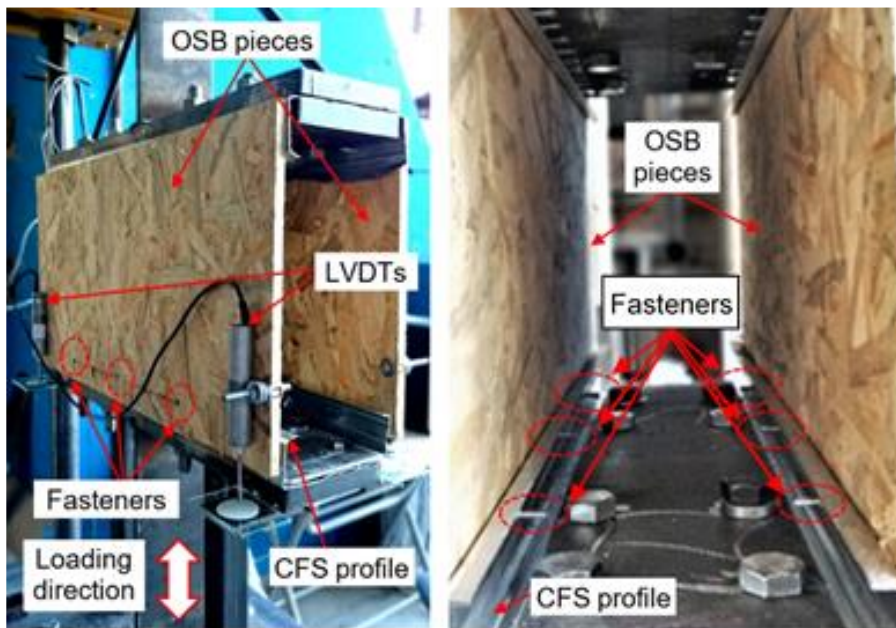
Figure 5.8 Setup used for fastener tests (Topçuoğlugil, 2019)
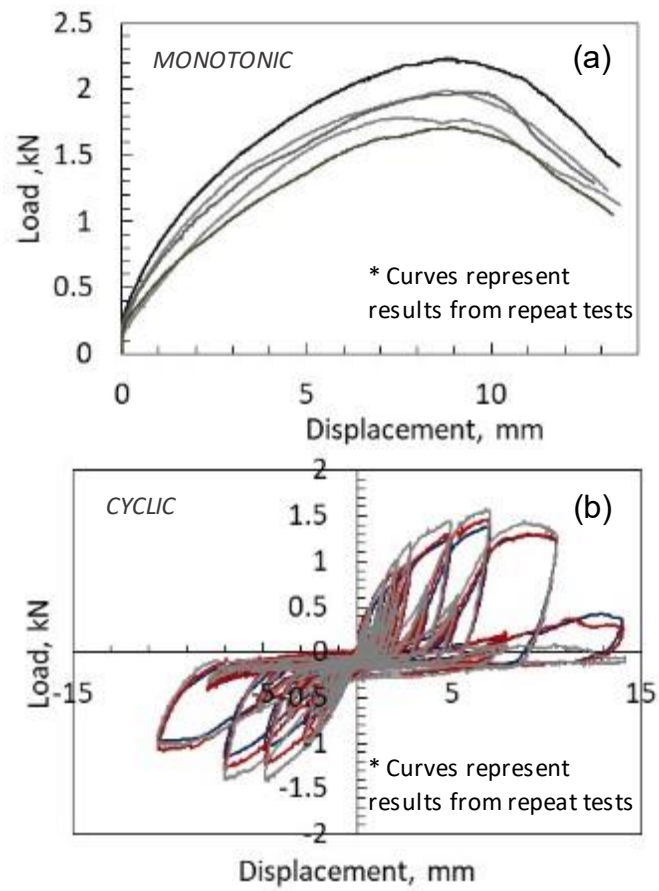
Figure 5.9 Load-displacement response from fastener tests under: (a) monotonic
loading; (b) cyclic loading (Topçuoğlugil, 2019)

124
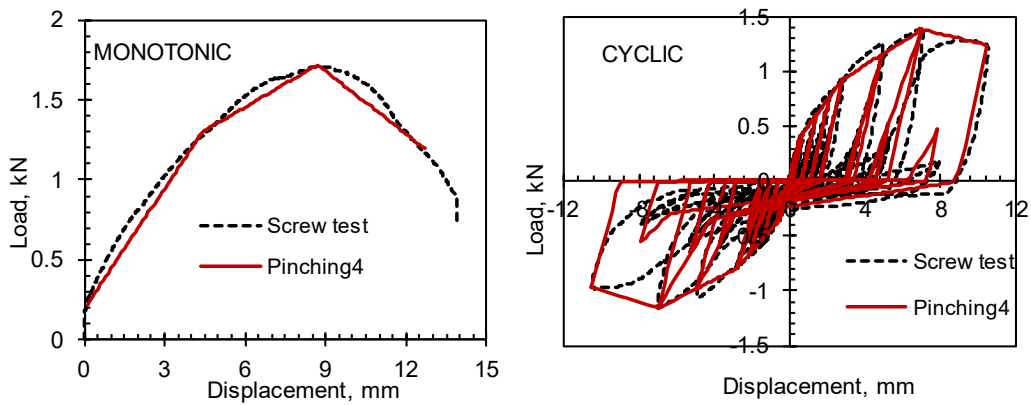
Figure 5.10 Monotonic and cyclic fastener material models based on screw test data (Topçuoğlugil, 2019)
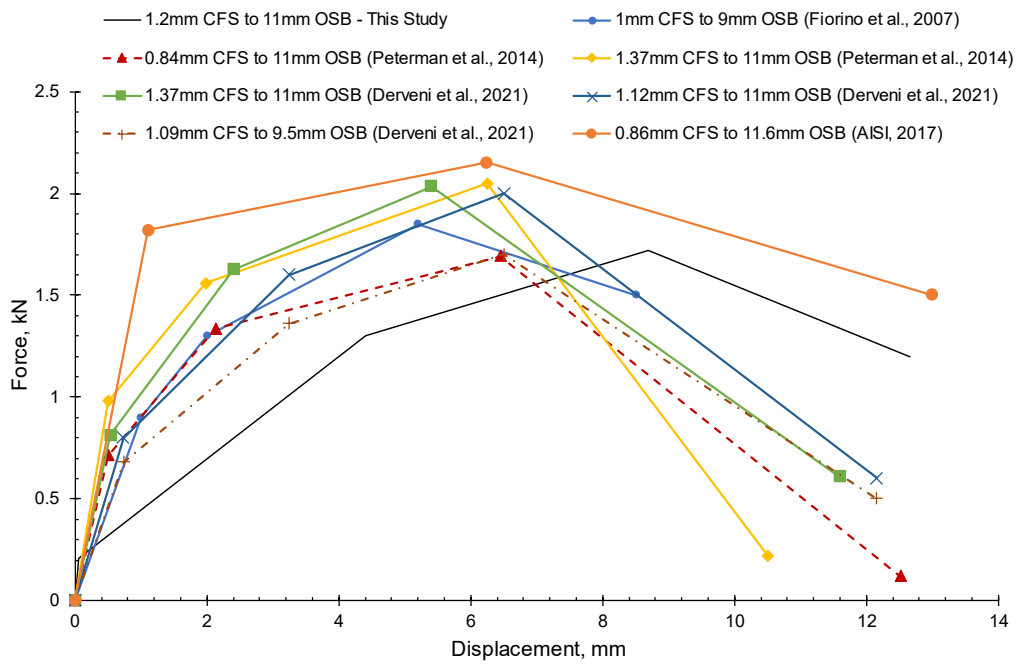
Figure 5.11 Load–displacement envelope curves for local fastener response from earlier studies
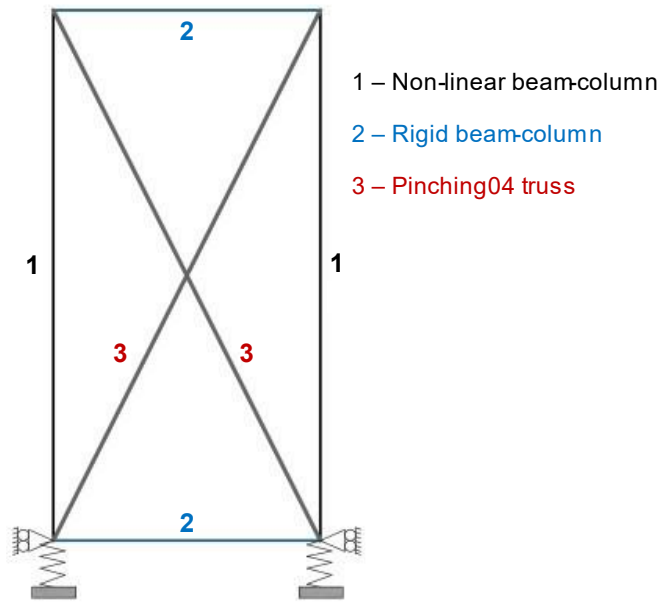
Figure 5.12 Schematic representation of equivalent brace wall model
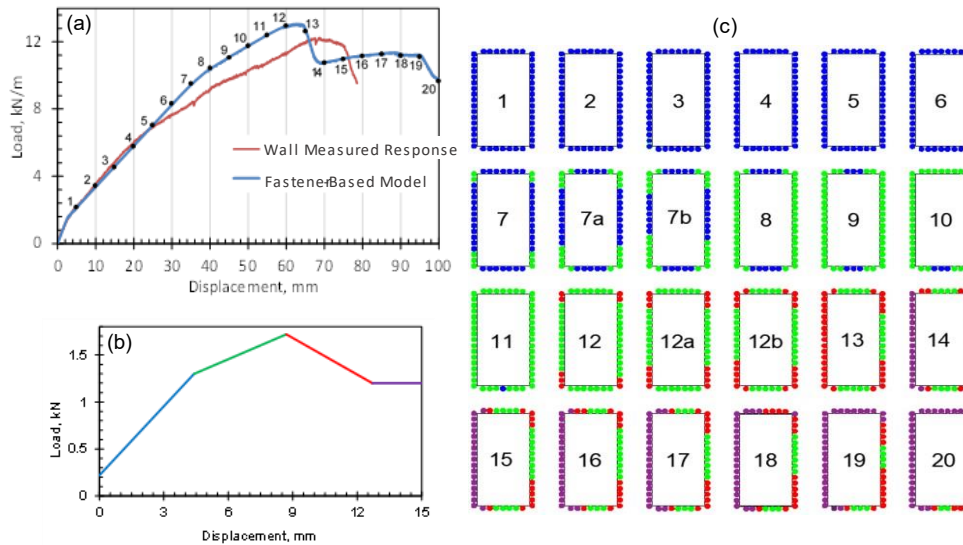
Figure 5.13 Monotonic response from fastener-based model: (a) comparison of experimental and numerical wall load-deflection responses; (b) Pinching4 material model used for fasteners; (c) progression of fastener damage (Topçuoğlugil, 2019)

126
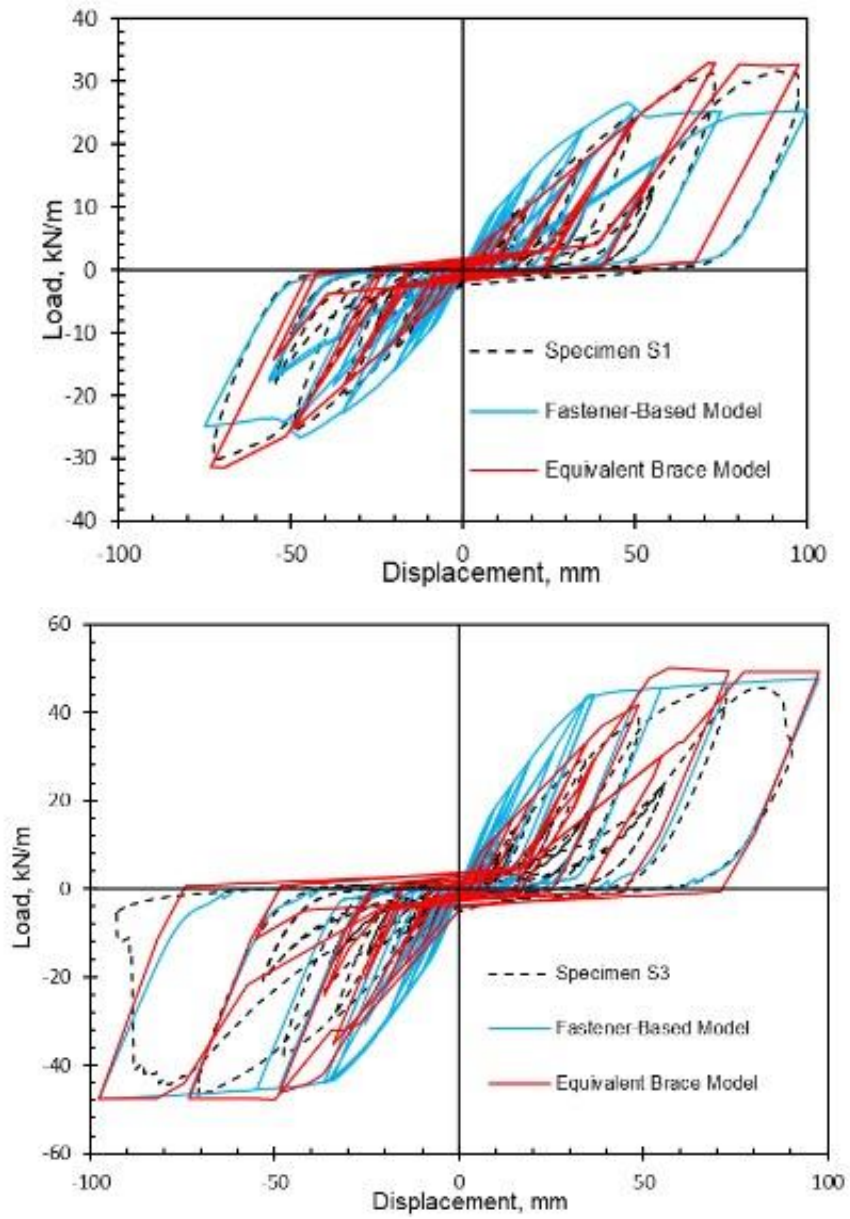
Figure 5.14 Comparison of measured and predicted wall responses
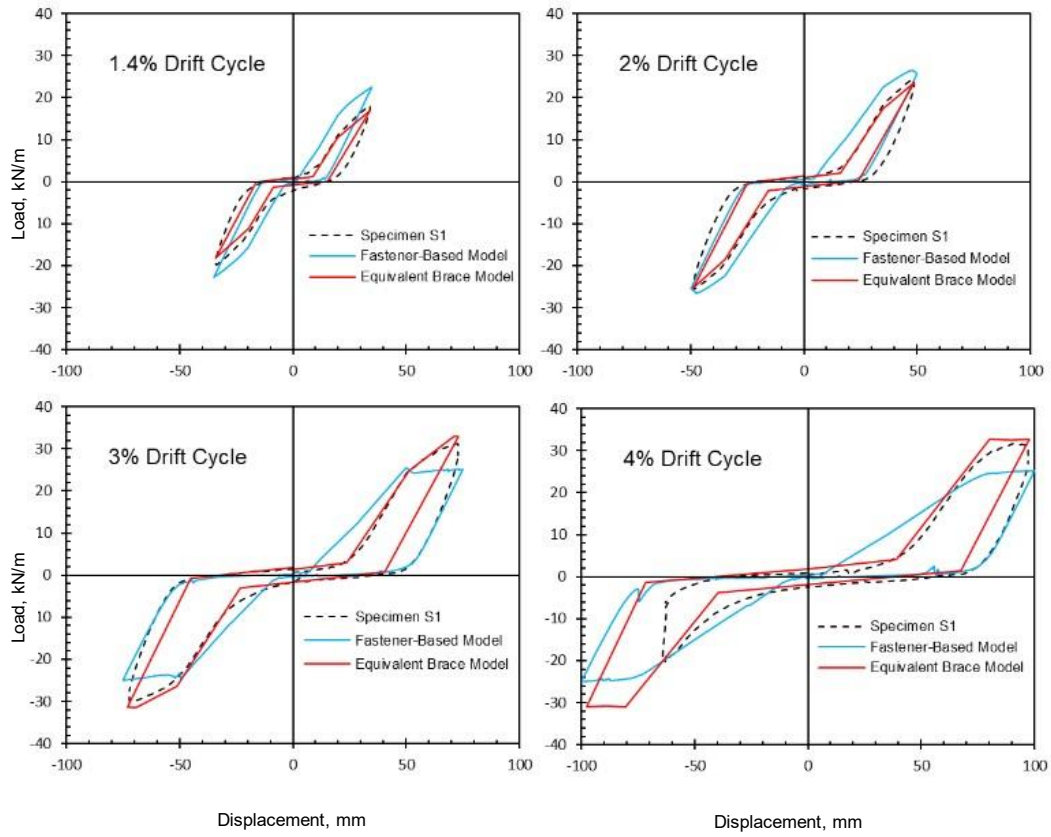
Figure 5.15 Comparison of measured and predicted hysteresis curves
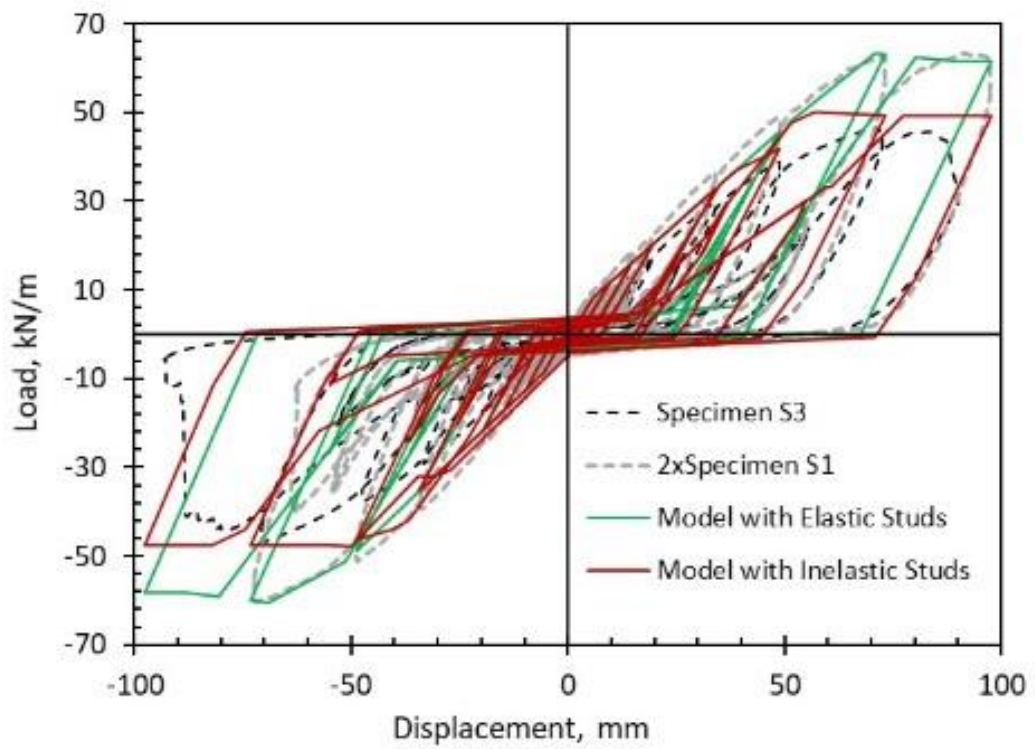
Figure 5.16 Effect of stud inelastic behavior on wall response

CHAPTER 6

LATERAL LOAD BEHAVIOR OF OSB SHEATHED COLD-FORMED STEEL FRAMED MULTI-PANEL SHEAR WALLS

6.1   Introduction

Depending on the architectural layout of building and location of walls on floor plan, the length wall segments in CFS building systems can vary significantly. The lateral load behavior of a wall segment is expected to be affected from its length. The limited stiffness and strength of relatively narrow wall segments is acknowledged in the North American Standard for CFS Framing, AISI S213 (2007) by limiting the maximum height/length ratio of CFS framed shear wall segment to 4:1. A reduction is also specified in AISI S213 (2007) for the tabulated shear strength values for walls with height/length ratio between 2:1 and 4:1. For that reason, the behavior of relatively narrow walls (i.e., walls with height/length ratio exceeding 2:1) has been studied extensively (Dolan and Easterling, 2000; Nava and Serrette, 2015; Serrette, 1997; Tarpy and McBrearty, 1978; Yan et al., 2021). In addition to that, studies on the effect of aspect ratio of CFS shear walls also includes relatively wider CFS walls (i.e., walls with height/length ratio of 1:1 and lower) (COLA-UCI, 2001; Liu et al., 2014; Nava and Serrette, 2015; Nguyen et al., 1996; Salenikovich et al., 1999), however the relation between the strength and stiffness response of these walls, as well as the assembly details and various parameters such as sheathing quantity and spacing of connection fasteners were not investigated in detail. Generally, scope of the studies in the literature was limited with the effect of aspect ratio on load capacity or the effect of openings in shear walls. Furthermore, the offsite fabrication of CFS wall segments requires the use of different techniques to provide connection between

neighboring wall segments to form a long wall. Effects of such connections and wall configurations on the overall response of CFS shear walls were not considered as an influencing parameter and not investigated in any of the studies in the literature, as well as not included in the studies that review the subject (Sharafi et al., 2018; Zhang et al., 2021). The presented work in this chapter investigates the cyclic lateral load behavior of OSB sheathed CFS framed walls with different lengths. The differences in the response of walls utilizing a single CFS framing and those that are formed by connecting individual wall segments have been investigated. These parameters were studied with the combinations of one-sided sheathing and coarse fastener layout, as well as double-sided sheathing and dense fastener layout.

6.2   Shear Wall Test Program

The test program included reversed cyclic load testing of eight full scale CFS wall panel specimens. Typical detailing of a wall panel specimen is shown in Figure 6.1a. Framing details and parameters used in wall panel specimens are listed in Table 6.1. Six of the tested specimens were 2.44 m long and 2.44 m tall corresponding to an aspect ratio of 1.0, while two specimens were 4.88 m long and 2.44 m tall with an aspect ratio of ½. Similar to shear wall specimens presented in previous chapters, CFS framing in all specimens included 1.2 mm thick and 140 mm deep C-shaped section shown in Figure 6.1b. Relevant to common practice, boundary studs comprised of two back-to-back C-shaped sections while single C-shaped sections were used for interior stud and track members. All CFS members had a specified yield strength of 350 MPa.

Three types of wall panel configurations shown in Figure 6.2 were considered in the study, which are denoted as types A, B and C. Type A specimens include a single 2.44 m long panel with two end studs and three interior studs. These studs were connected to 2.44 m top and bottom track members to form the wall framing, and

the framing were sheathed with two 1.22 m long OSB panels either on one side or both sides (Figure 6.2a). Types B and C specimens consist of segmented walls that were formed by connecting either two or four 1.22 m long individual wall panels.

As illustrated in Figure 6.2b, for type B specimens, connection between the individual 1.22 m long shear wall segments were provided through the OSB sheathing panels without any direct connection between the studs of neighboring panels. Total of three OSB pieces were utilized on each side for these specimens. A 1.22 m long OSB panel was placed at the middle of the framing and connected to internal studs of both wall segments to provide the connection. Two 0.61 m long OSB panel pieces were used at the sides of the framing to provide sheathing for these parts. For type C specimens (Figure 6.2c), each individual 1.22 m long wall panel was sheathed with 1.22 m long OSB panels separately and the force transfer between the individual wall panels occurs through 6.3 mm diameter self-tapping screws provided between the studs of neighboring panels. These screws were placed in two rows at 15 cm spacing.

All of the wall panels were sheathed with 11 mm thick OSB sheets. Sheathing panels were attached to either one side or both sides of the CFS framing members by using 4.2 mm diameter self-tapping screws. For specimens sheathed on single side, 150 mm and 300 mm screw spacings were used on boundary framing members and interior studs, respectively (i.e., 150/300 screw layout). Whereas for wall panels that were sheathed on both sides, the screw spacing was 50 mm on boundary framing members and 100 mm on interior studs (i.e., 50/100 screw layout). This way, the performance of the force transfer mechanism was tested both with the combination of one-sided sheathing and coarse fastener layout, and with the combination of double-sided sheathing and dense fastener layout, which creates a much higher force demand than the former configuration. The 150 mm and 50 mm boundary framing members screw spacing values utilized in wall specimens represent the upper and

the lower bound spacing values specified in Nominal Shear Strength Table E1.3-1 in North American Standard for Seismic Design of Cold-Formed Steel Structural Systems, AISI S400-15 (2015).

Connection of wall panels to the foundation was provided by using the hold down device that was investigated in Chapter 4. Regardless of the wall length, two hold downs were used in each wall specimen and they were attached to boundary studs with twenty 6.3 mm diameter self-tapping screws (Figure 6.3b). Connection of hold downs to the foundation base plate was provided by 24 mm diameter threaded anchor rods with measured yield and tensile strengths of Fy = 500 MPa and Fu = 575 MPa. In addition to hold down devices, two 16 mm diameter shear anchors were used in each 1.22 m long wall panel segment in order to connect bottom track members to the foundation base plate (Figure 6.3c). In other words, for 2.44 m and 4.88 m long specimens respectively, a total of four and eight shear anchors were used.

6.2.1   Test Setup, Instrumentation and Loading Protocol

Wall specimens were subjected to lateral loading in a reversed cyclic manner using the test setup shown in Figure 6.4. Walls were placed on a 20 mm thick steel foundation plate that was attached to the laboratory's strong floor. A hydraulic actuator having 300 kN load capacity and ± 250 mm stroke was used to apply lateral loading at the top level of walls. Load transfer to walls was achieved with the help of a load distribution beam that was attached to the top track members by self-tapping screws. Ball bearing rollers were used on each side of walls in order to provide lateral stability in the out-of-plane direction. Lateral force applied on wall, lateral displacement at the top of wall, lateral slip at wall base, and base uplift at hold down locations were measured during testing.

Similar to previous tests on CFS shear walls, all of the wall specimens shown here were also tested under reversed cyclic loading with a loading rate of 1 mm/sec and loading history defined by the CUREE specification (Krawinkler et al., 2001) was utilized as the cyclic loading protocol.

6.3   Test Results

6.3.1   Damage and Failure Modes

Two main damage mechanisms were observed during cyclic load testing of wall specimens. Examples of these deformation modes are shown in Figure 6.5. For wall panels sheathed on one side, tilting and pull through of the screws between OSB sheathing panels and CFS framing members was the main failure mechanism. For wall panel specimens that were sheathed on both sides, on the other hand, failure usually occurred as a result of local/distortional buckling in the vicinity of hold down location. Initiation of such buckling was observed to occur at approximately 2% drift ratio with wall failures occurring at approximately 3% drift ratio.

Another important observation regarding the damage behavior of wall specimens is the presence of excessive base slip in double side sheathed wall specimens. This type of damage was especially significant in specimen MP-6, as shown in Figure 6.5f. This specimen had a 4.88 m of wall length and utilized two hold downs and eight shear anchors. The 4.88 m wall length together with the double sided sheathing and dense fastener layout resulted in a significantly large shear force demand at wall base. The main reason for longer walls being more susceptible to excessive base slip than the shorter ones is related with the fact that the increase in shear capacity at wall base does not increase linearly with wall length. As mentioned earlier, a standard 1.22 m long wall panel was attached to the foundation base plate with two hold downs and two shear anchors. For 2.44 m and 4.88 m long walls, even though the

number of shear anchors was increased to four and eight, respectively, the number of hold downs was not increased. A common design assumption is that shear force demand at wall base is met entirely by shear anchors and that hold downs are responsible for only resisting the uplift effects. In reality however, due to their relatively high stiffness, hold downs contribute to the shear force capacity at wall base. Therefore, between 1.22 m and 2.44 m long walls, the shear force demand at wall base is almost doubled, but the increase in resistance remains smaller since two hold downs are used for both wall lengths. The same relation is valid between 2.44 m and 4.88 m wall panels. Hence, for the 4.88 m long wall specimen that was sheathed on both sides with a dense fastener layout (i.e., specimen MP-6) the shear capacity at wall base remained below the shear force demand, while such a problem did not occur for the companion specimens with a smaller wall length (i.e., specimens SP-2, MP-2 and MP-4).

6.3.2   Load-Displacement Behavior

Figure 6.6 and Figure 6.7 show the lateral load versus top displacement response of all wall panel specimens. Load values for wall panels are presented in terms of 1 m of wall length. The severely pinched response evident in the plots is a characteristic property of CFS framed shear walls. Figure 6.6 and Figure 6.7 also display cyclic backbone curves based on primary loading cycles and bilinear Equal Energy Elastic-Plastic (EEEP) curves as specified in AISI S400-15 (2015).

Table 6.2 shows results for wall panel specimens in terms of their load capacities, maximum drift ratios as well as the yield load capacities and yield displacement values determined based on the EEEP model approach. Results from two 2.44x1.22 m shear walls tested in the previous parts of the study are also included in the table for the purpose of comparison with the recently tested shear walls. Labeled as S3 and S8, these wall specimens utilized double side sheathing with 50/100 mm screw

spacing and single side sheathing with 150/300 mm screw spacing, respectively. Cyclic load-displacement behavior and EEEP bilinear response of these walls are provided in Figure 6.8.

Comparison of wall response based on the sheathing condition (i.e., single side or double side) and fastener spacing is provided in Figure 6.9 in terms of cyclic envelope and EEEP curves. For single side sheathing and 150/300 mm fastener spacing, change in wall length and connection detail between individual wall segments did not cause any appreciable difference in wall response. For walls with double side sheathing and 50/100 mm spacing, there was a marked increase in wall stiffness with an increase in wall length from 1.22 m to 2.44 m.

6.3.2.1   Load Capacity

As per AISI-15 Standard, the expected nominal shear strength values for single side sheathed walls are 12 kN/m for 150/300 mm fastener spacing, and 30 kN/m for 50/100 mm fastener spacing. With the presence of sheathing on both sides of walls, these capacities are expected to double. In other words, for double side sheathed walls with 50/100 mm fastener spacing the expected shear strength is 60 kN/m. As shown in Figure 6.10, the measured load capacity of wall specimens with single side sheathing and 150/300 mm fastener spacing changes between 10.5 kN/m and 12.9 kN/m. These reported values are the average of capacities obtained in push and pull directions. For double side sheathed walls with 50/100 mm fastener spacing the measured load capacities are between 46.7 kN/m and 50.6 kN/m, except for specimen MP6. Buckling of boundary studs in the latter group of walls resulted in load capacities to be significantly smaller than the code specified values.

Load capacity normalized by wall length varies slightly among walls tested with the same sheathing condition (i.e., single side or double side) and fastener spacing, as

shown in Figure 6.10. For the case of single-sided sheathing and loose fastener layout, there is a slight increase in normalized load capacity when the wall length is increased from 1.22 m to 2.44 m and then to 4.88 m. Providing a single 2.44 m long CFS panel or connecting two 1.22 m long panels with two different methods did not cause a major change in the load capacity of wall specimens. For the case of double-sided sheathing and dense fastener layout, on the other hand, increasing the wall length from 1.22 m to 2.44 m resulted in a slight increase in normalized capacity, but further increasing the wall length to 4.88 m led to a premature failure at wall base. In this case, the normalized load capacity dropped significantly compared to the walls tested with a smaller length, as a result of excessive slip at wall base. Tearing of the bottom track member shown in Figure 6.5f is an indication of premature failure at wall base in specimen MP-6. As mentioned earlier, the main cause behind this type of response is the shear capacity at wall base remaining below the shear force demand in specimen MP-6 due to the increase in shear capacity at wall base being smaller than the rate of increase in wall length.

Among all walls tested in the present study, specimen MP-1, which had two wall segments connected by OSB sheathing acquired the minimum normalized load capacity of 10.5 kN/m. The highest normalized load capacity of 50.6 kN/m was obtained in specimen MP-2, which utilized the same connection method between wall segments but was tested with double side sheathing and a dense fastener layout. In terms of maximum drift ratios, majority of wall specimens were able to reach 3% drift ratio. Specimen MP-4 is the only specimen able to reach the targeted 4% drift ratio in both loading directions. Specimen MP-3 on the other hand, were only able to reach 2% drift ratio in both directions. Failure of this specimen is due to the deformations shown in Figure 6.5a.

6.3.2.2   Hold Down Forces

During load testing of wall specimens, forces in hold down anchor rods were measured by load cells placed between the top end of each hold down device and anchor rod (Figure 6.3b). Considering the moment equilibrium of shear wall specimens, the hold down force is expected to be approximately equal to the horizontal load applied on the wall panel (i.e., wall base shear) for 2.44 m long walls and half of the horizontal load for 4.88 m long walls. Figure 6.11 presents measured hold down force vs base shear plots for four representative wall specimens sheathed on both sides with 50/100 mm fastener spacing. Expected behavior is also indicated by dashed red lines corresponding to the required base shear to hold down force ratio. Linear behavior between hold down force and wall base shear is an indication that anchor rods remained linear-elastic during wall loading tests. As evident in the plots, the measured hold down tensile forces are in accordance with the expected levels for both push and pull directions. This observation indicates that hold down force demand decreases with increasing wall length.

6.3.2.3   Ductility Ratio
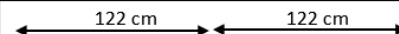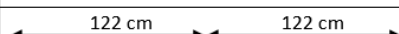
Ductility ratio for each wall specimen was calculated as the ratio of the ultimate displacement Δ_u to the yield displacement Δ_y by utilizing the values reported in Table 6.2. For all wall lengths studied and connection details utilized between individual wall segments, wall sheathed on single side with 150/300 mm fastener spacing possessed larger ductility ratio than the companion wall sheathed on both sides with 50/100 mm fastener spacing, as shown in Figure 6.12. It is noteworthy that as the response of wall specimen MP-6 was mostly governed by slip at wall base, the ductility ratio of 4.0 shown in the figure for this specimen does not reflect the actual wall behavior.

139

When this specimen is excluded, ductility ratios for walls with single side sheathing and coarse fastener layout change between 3.0 and 4.5, while for walls with double side sheathing and dense fastener layout values changes between 1.8 and 2.6. No clear trend exists between ductility ratio and wall length.

6.3.2.4   Energy Dissipation

Energy dissipated by wall specimens at each drift ratio was calculated as the area under the cyclic load-displacement curve at each main cycle of loading. Two different cumulative dissipated energy values are shown in Figure 6.13, one is the dissipated energy at the end of 2% drift cycle and the other one is at the end of loading test. Results indicate that walls sheathed on single side with 150/300 mm fastener spacing dissipated approximately three times more energy at the end of 2% drift cycle than the companion walls sheathed on both sides with 50/100 mm fastener spacing. The relatively high total energy dissipation capacity for specimen MP-4 is due to the fact that among all tested walls this was the only specimen that was able to reach the 4% drift value. Similar to the case with ductility ratio, no clear trend exists between the energy dissipation capacity and wall length.

Table 6.1 Details of specimens

Specimen	Wall Framing Details	Force transfer mechanism between panels	Wall dimensions cm	Sheathing condition	Screw spacing[a] mm
SP-1	244 cm	-	244x244	Single side	150/300
SP-2		-	244x244	Double side	50/100
MP-1	122 cm — 122 cm	OSB sheathing panels	244x244	Single side	150/300
MP-2		OSB sheathing panels	244x244	Double side	50/100
MP-3	122 cm — 122 cm	Fasteners	244x244	Single side	150/300
MP-4		Fasteners	244x244	Double side	50/100
MP-5	122 cm 122 cm 122 cm 122 cm	Fasteners	244x488	Single side	150/300
MP-6		Fasteners	244x488	Double side	50/100

[a] First number indicates screw spacing along boundary framing members, second number indicates spacing along interior studs

Table 6.2 Test results

Specimen	P_{peak} kN/m			Δ_{peak} mm		Δ_u (mm) / % drift				P_{yield} kN/m		Δ_y mm		K_e (kN/mm/m)		
	Push	Pull	Avg	Push	Pull	Push		Pull		Push	Pull	Push	Pull	Push	Pull	Avg
SP-1	12.2	9.2	10.7	47.5	48.6	69.0	2.8	55.5	2.3	9.5	8.0	19.5	18.2	0.5	0.4	0.5
SP-2	49.0	44.3	46.7	65.2	66.0	74.0	3.0	71.0	2.9	43.0	40.7	33.5	35.6	1.3	1.1	1.2
MP-1	10.6	10.4	10.5	49.0	49.0	65.0	2.7	65.0	2.7	8.8	8.9	17.5	12.2	0.5	0.7	0.6
MP-2	52.6	48.5	50.6	73.0	68.6	73.3	3.0	73.0	3.0	45.0	37.5	34.8	34.4	1.3	1.1	1.2
MP-3	12.5	10.0	11.3	46.5	34.0	48.8	2.0	48.8	2.0	10.3	8.6	14.4	14.4	0.7	0.6	0.7
MP-4	49.0	52.0	50.5	97.0	72.5	98.0	4.0	98.0	4.0	43.6	46.8	36.3	38.3	1.2	1.2	1.2
MP-5	13.8	12.0	12.9	49.0	49.0	72.0	3.0	72.0	3.0	11.2	9.6	21.1	14.2	0.5	0.7	0.6
MP-6	37.6	36.0	36.8	72.0	49.0	83.0	3.4	98.0	4.0	34.3	30.5	27.3	19.5	1.3	1.6	1.4
S3	46.6	47.0	46.8	71.2	70.6	87.7	3.6	87.7	3.6	42.8	42.8	47.7	47.8	0.9	0.9	0.9
S8	11.6	9.6	10.6	63.7	64.0	72.5	3.0	71.5	2.9	10.0	8.4	26.0	21.8	0.4	0.4	0.4
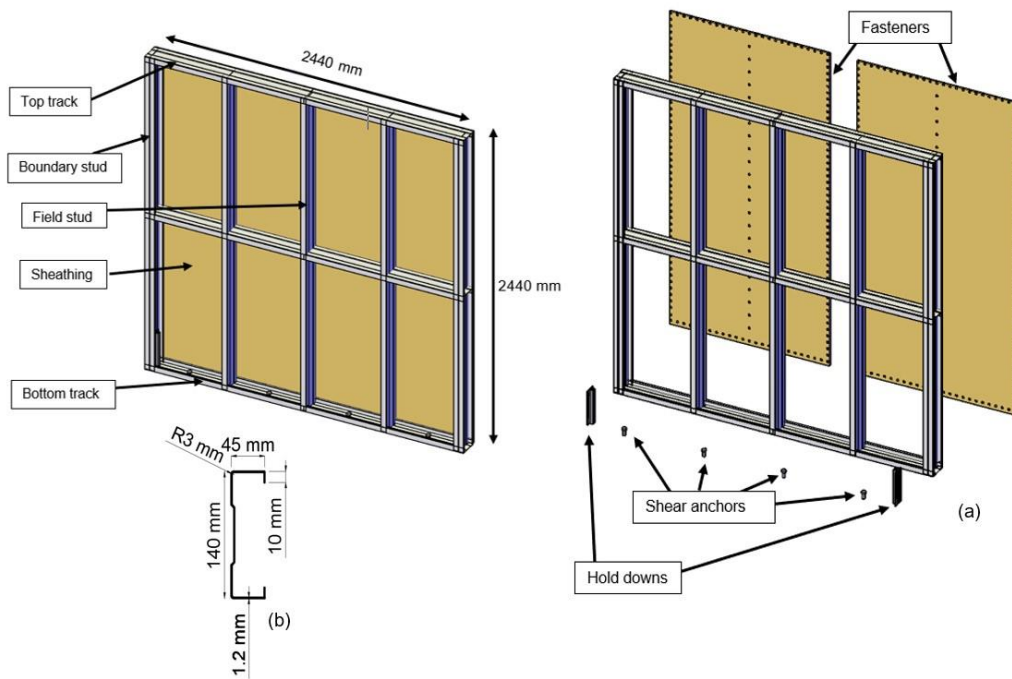
Figure 6.1 (a) General framing details of wall panels; (b) CFS section used for wall panel tracks and studs
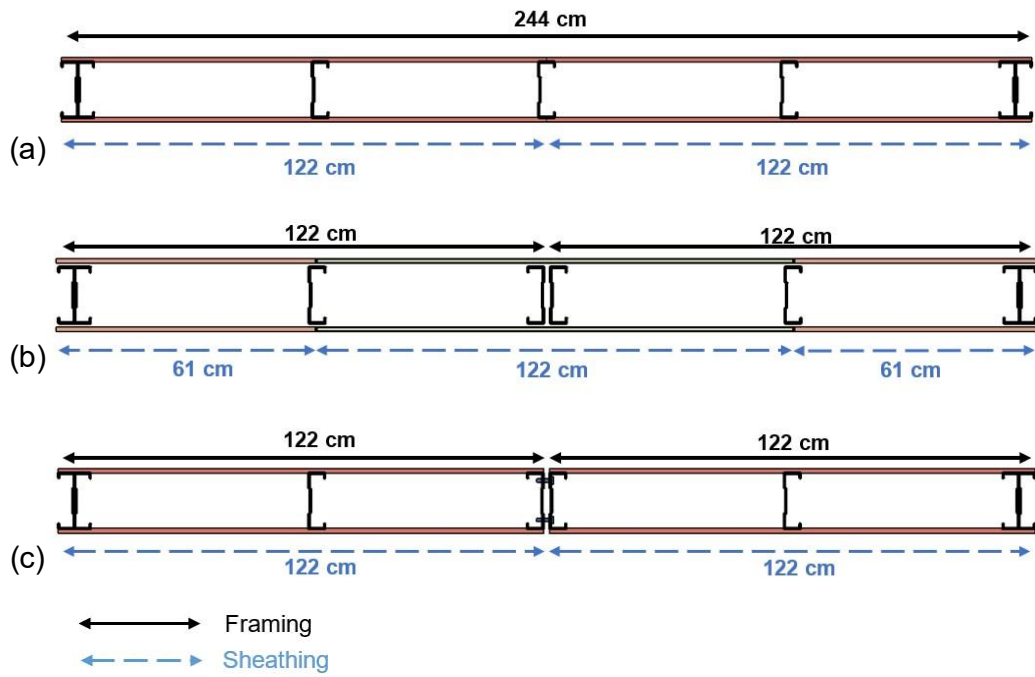
Figure 6.2 Shear wall connection configurations: (a) single framing (Type A); (b) wall segments are connected by OSB sheathing (Type B); (c) wall segments are connected by fasteners (Type C)
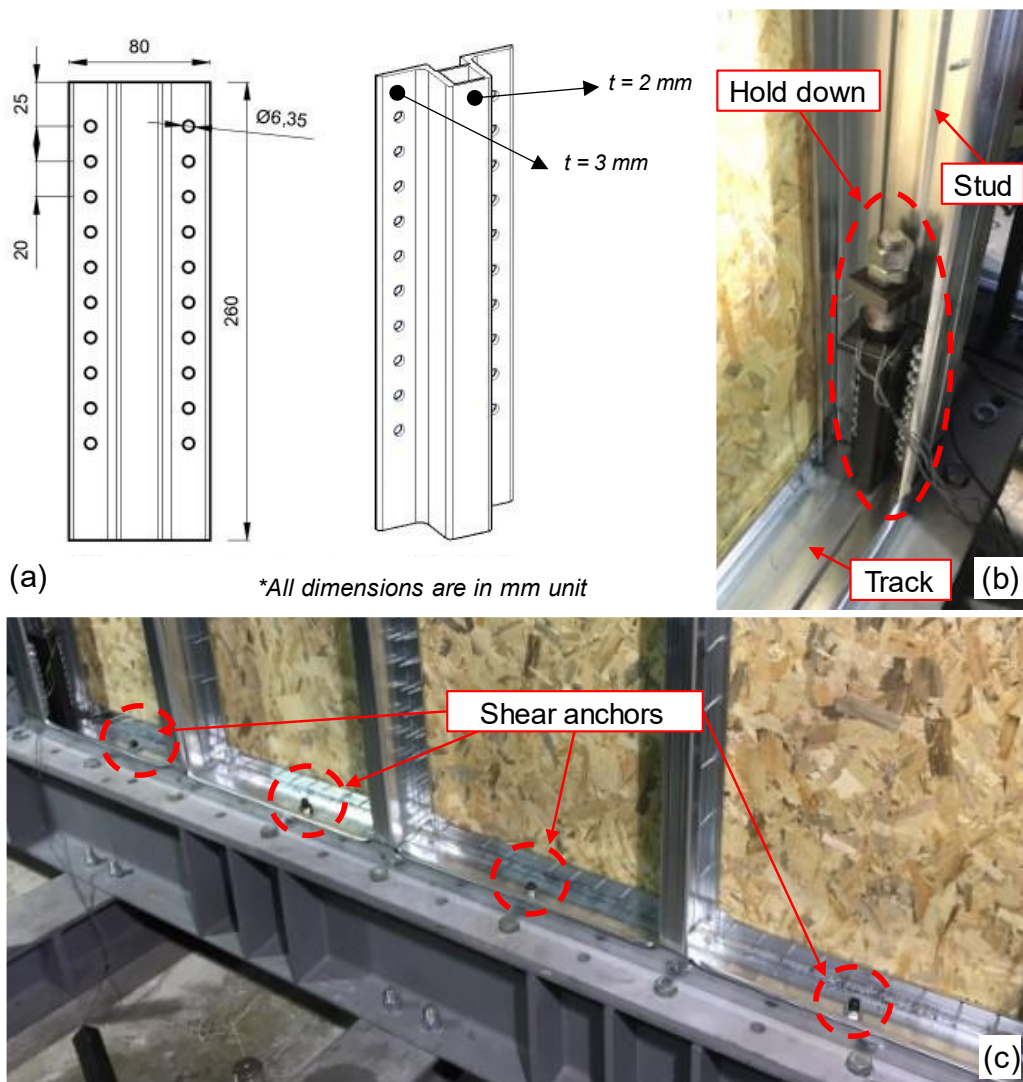
Figure 6.3 Connection of wall panels to the foundation: (a) details of hold down device; (b) hold down attached to an end stud; (c) shear anchors

Figure 6.4 Details of wall panel test setup
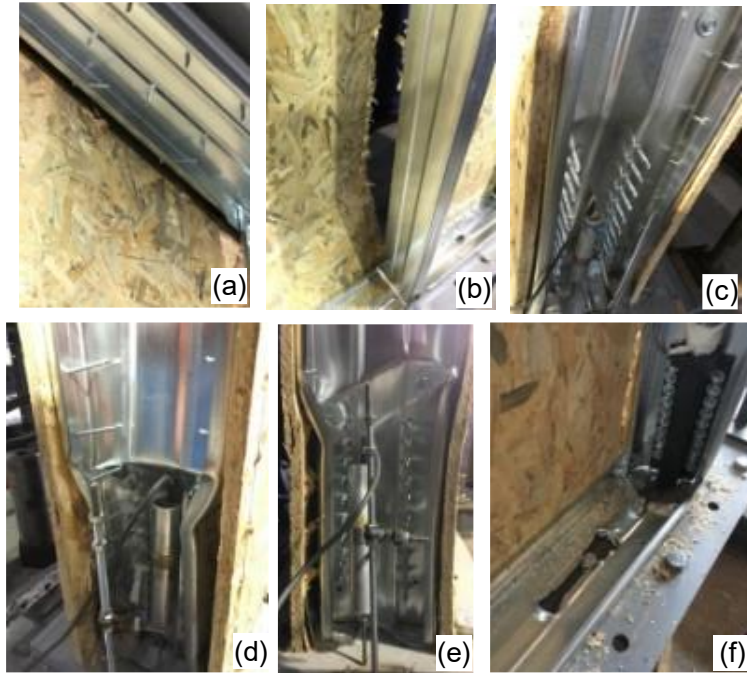
Figure 6.5 Observed deformations on wall specimens: (a) screw tilting, (b) screw head pull through; (c) initiation stud buckling; (d), (e) local/distortional buckling of boundary stud near wall base; (f) slip deformation and damage in bottom track around shear anchor and hold down in specimen MP-6
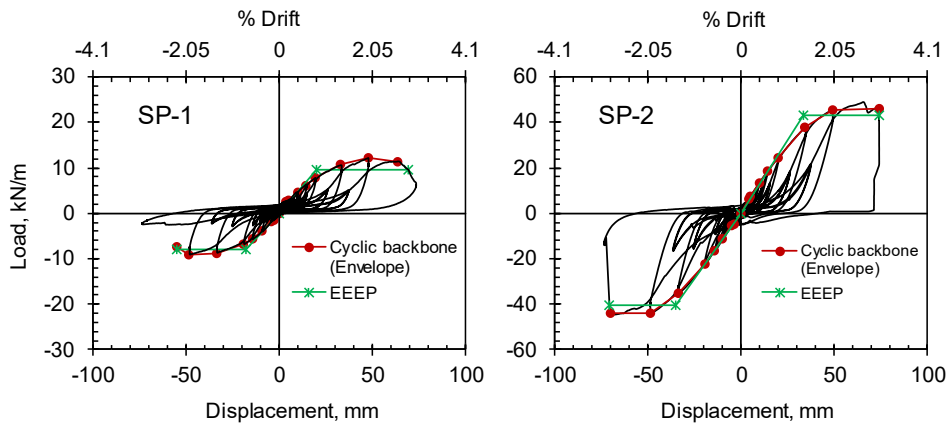
Figure 6.6 Load-displacement behavior of single panel walls
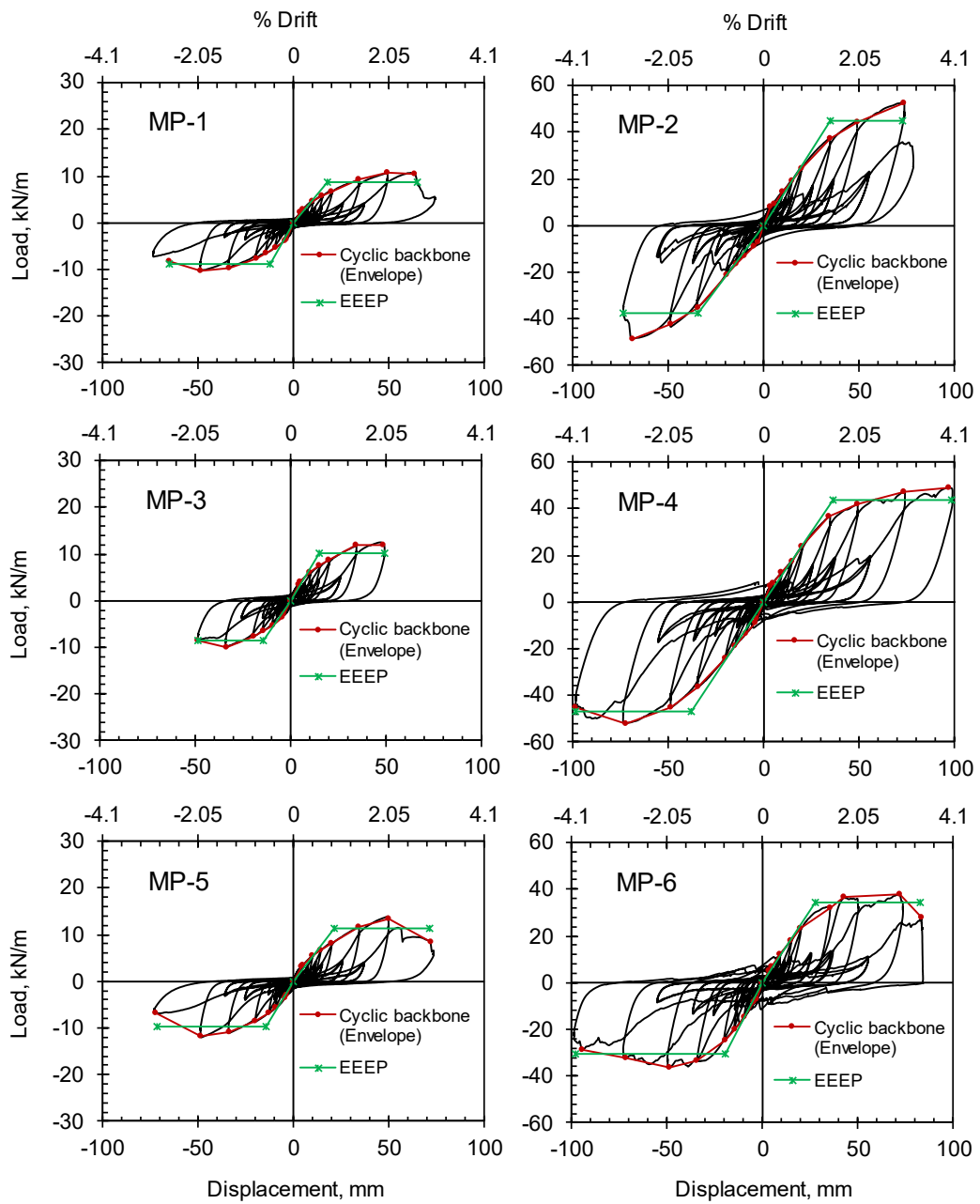
Figure 6.7 Load-displacement behavior of multi-panel walls
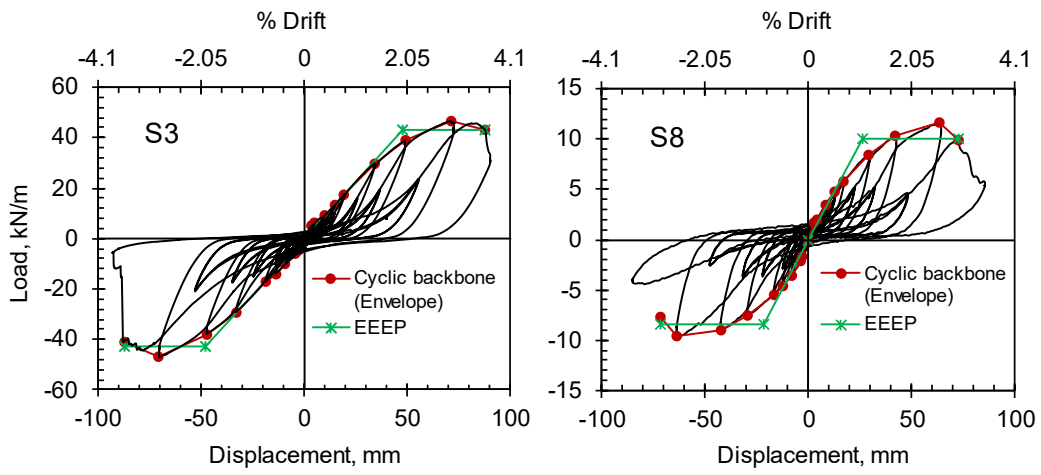
Figure 6.8 Load-displacement behavior of 2.44x1.22 m shear walls
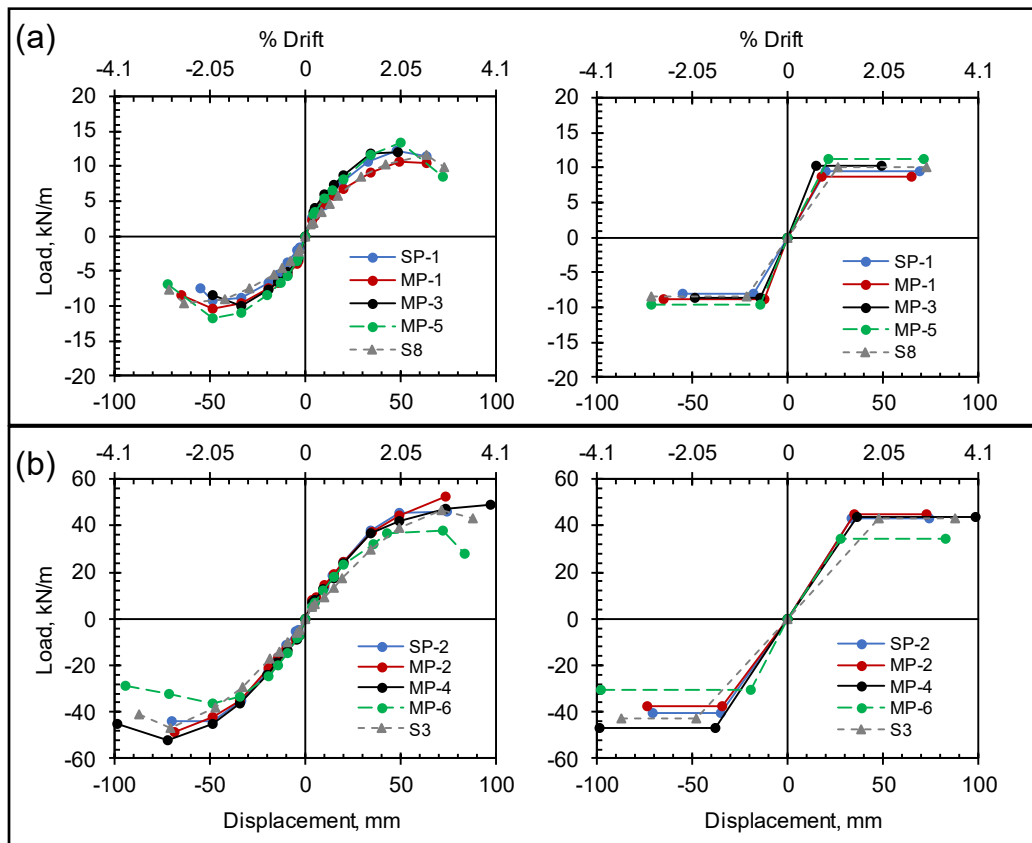
Figure 6.9 Comparison among walls in terms of cyclic envelope curves and EEEP curves: (a) walls with single side sheathing and 150/300 mm fastener spacing; (b) walls with double side sheathing and 50/100 mm fastener spacing
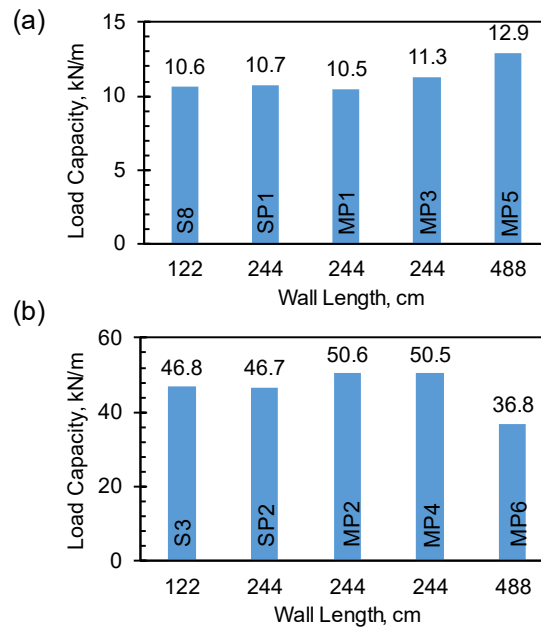
Figure 6.10 Variation of load capacity with wall length: (a) walls with single side sheathing and 150/300 mm fastener spacing; (b) walls with double side sheathing and 50/100 mm fastener spacing

150
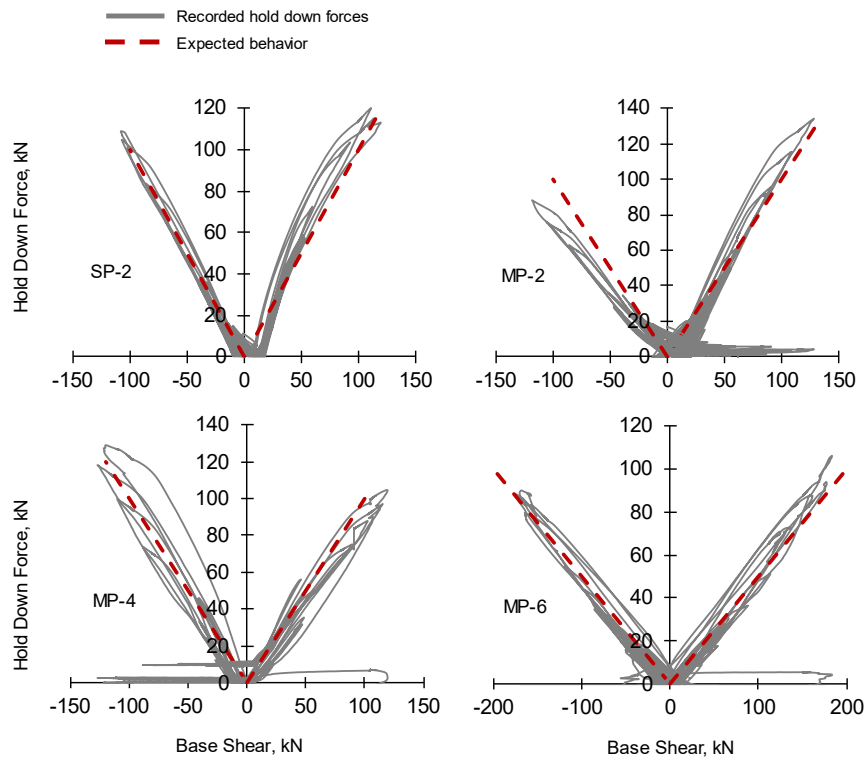
Figure 6.11 Hold down force responses in walls with double side sheathing and 50/100 mm fastener spacing
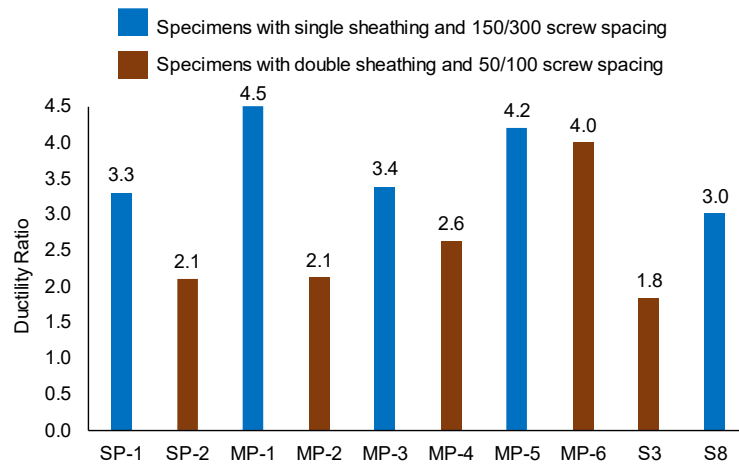
Figure 6.12 Ductility ratio of wall specimens
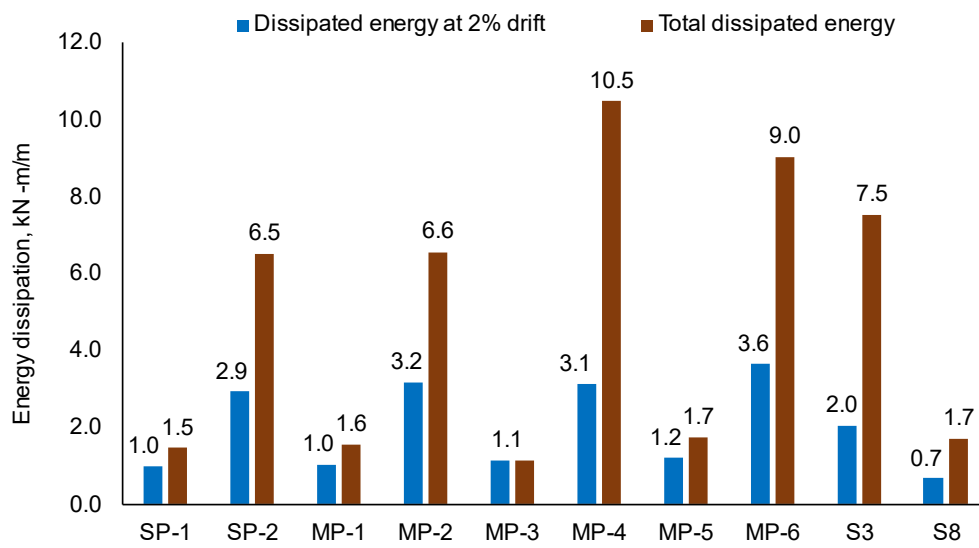
Figure 6.13 Energy dissipation of wall specimens

CHAPTER 7

LATERAL LOAD BEHAVIOR OF OSB SHEATHED COLD-FORMED STEEL FRAMED TWO STORY SHEAR WALLS

7.1 Introduction

In CFS structural systems, detailing of the floor system is an important factor affecting the structural performance. Since floor system is placed between shear walls of neighboring stories in a CFS structure, connection between floors and shear walls, as well as connection between story walls are important details to be considered. In order to ensure the transfer of horizontal and vertical loads, proper force transfer mechanisms should be provided between floors and shear walls.

In common practice, two different framing options are considered between floors in CFS structures named as; (i) platform framing and (ii) ledger framing. The main difference between these two choices is the continuity of shear walls throughout the height of the structure. In platform framing, shear walls are terminated at floor levels and floor system rests direcetly on these walls. In ledger framing, on the other hand, shear walls are continuous at floor levels and the floor systems is connected to the side of walls with ledger members. These two framing options create different force transfer mechanisms udner seismic loading and also require different connection details.

In this chapter of the thesis, results of experiments on two story shear wall assemblies utilizing both platform and ledger framing details are presented.

7.2   Shear Wall Test Program

7.2.1   Wall Specimens

Experimental program included eight full scale two-story shear wall specimens. Details and considered parameters are summarized in Table 7.1. All specimens were designed as two-story shear walls and total of three different framing details were considered. Framing details used for wall specimens are shown in Figure 7.1 and Figure 7.2. Specimens P1-1, P1-2 and P1-3 represent shear walls with platform framing detail where a filler truss member was placed between walls. In this detail, floor beams rest on shear walls with a short filler truss fabricated with CFS profiles placed between two neighboring floor beams. Specimens P2-1, P2-2 and P2-3 were prepared with a different platform framing detail, where additional CFS members were provided at the top of the first floor wall panel in order to form a gap to accept the floor beams. It is worth to mention that this detail has a common use in CFS construction in Turkey. Specimens L-1 and L-2 represent the ledger framing detail and were created by placing second floor shear wall panel directly on top of the first floor shear wall panel.

Tested shear walls were fabricated in such a way that each framing detail was represented by two sheathing and fastener combinations. For the first configuration, walls were sheathed on one side with a screw spacing of 150 mm along boundary studs and 300 mm along field studs (i.e., 150/300 mm spacing configuration). Second combination included double side sheathing with 50 and 100 mm screw spacing along boundary and field studs, respectively (i.e., 50/100 mm spacing configuration). As explained in the previous chapters of the thesis, the 50 and 150 mm boundary stud spacing values represent respectively the lower and upper bound spacing values specified in Nominal Shear Strength Table E1.3-1 in North American Standard for Seismic Design of Cold-Formed Steel Structural Systems, AISI S400-15 (2015).

Additionally, two specimens with platform framing detail (i.e., specimens P1-3 and P2-3) were designed in such a way that instead of sheathing each floor wall separately, a 2440 mm long sheathing was connected to both lower wall, upper wall and platform framings. This way, an additional connection between two shear walls was created. This type of sheathing configuration can be seen in Figure 7.3.

All of the wall specimens had 1220 mm width and 4880 mm height, as shown in Figure 7.2. Specimens with platform framing detail-1 included a 2440 mm high first floor wall, 300 mm high platform part and 2140 mm high second floor wall. Specimens with platform framing detail-2 consisted of a 2740 mm high first floor wall and 2140 mm high second floor wall. The wall at the first floor was manufactured such that in the top 300 mm part gaps were provided for the placement of floor beams in the framing of the wall. Specimens with ledger framing included two wall panels of 2440 mm height placed on top of each other. Similar to the specimens discussed in previous parts of the thesis, all CFS framing members used in two story wall specimens were made of 1.2 mm thick 140 mm deep C-shaped section with a specified yield strength of 350 MPa. In accordance with the common practice, field stud and track members were comprised of a single C-shaped CFS section and boundary studs were produced from back-to-back double C-shaped sections. Wall panel specimens were sheathed with 11 mm thick OSB sheets. All of the sheathing panels were connected to the CFS framing members using self-tapping screws having 4.2 mm diameter and 25 mm length.

In order to provide connection between first and second floor shear walls and allow for the transfer of vertical shear wall forces, two different connection details were utilized for platform and ledger framings, as shown in Figure 7.4. As described in NEHRP Seismic Design Technical Brief document (Madsen et al., 2016), a traditional tie-down device is usually considered for platform framing option since continuity of shear walls are prevented by floor beams.

For shear wall specimens utilizing platform framing detail-1, two tie-down devices were connected to each shear wall on both sides and a 24 mm diameter steel anchor rod was used to connect the tie-downs attached to the bottom of the second floor wall and top of the first floor wall (Figure 7.4a). In the case of wall specimens with platform framing detail-2 and ledger framing option, a simple steel strap tie having 50 cm length was utilized to provide connection between first and second floor shear walls (Figure 7.4b). Both tie-down devices and steel straps were connected to shear walls by using 6.3 mm diameter self-tapping screws. In addition to connection provided by tie-downs and steel strap ties, wall panels were connected to platform framing detail or to each other by using two lines of 6.3 mm diameter self tapping screws with 15 cm of spacing as shown in Figure 7.5. This connection is responsible for transfer of shear forces between neighboring floors. Moreover, an OSB was placed between first and second floor wall panels or between second floor wall panel and platform framing in an attempt to represent sheathings used as part of the floor construction.

For the connection of shear wall specimens to foundation base plate, hold down devices investigated in Chapter 4 were utilized together with shear anchors, similar to the other shear wall specimens tested in the thesis work.

7.2.2 Test Setup, Instrumentation and Loading Protocol

Test setup used for two-story shear walls is shown in Figure 7.6. Specimens were supported by a 20 mm thick steel foundation plate. This plate was securely attached to I-shaped steel floor beams that were connected to the laboratory's strong floor. Lateral loading was applied at the top level of wall specimens with a single hydraulic actuator which has 300 kN of load capacity and ±250 mm stroke. The actuator was attached to a 1.6 m long load distribution beam that was connected to top track member of second floor shear wall by self-tapping screws. The out of plane stability

of specimens were provided by two ball bearing rollers placed on each side of wall panels at the top level. In addition to that, two steel box profiles were placed at the middle height of specimens again on both sides. These profiles were covered with Teflon sheets to allow for friction free sliding of specimens.

Similar to all shear wall specimens tested in the study, CUREE (Krawinkler et al., 2001) loading history was used as the reversed cyclic loading protocol for specimens considered here also. During tests, lateral deformation of shear walls was measured with six linear variable displacement transducers (LVDT) placed throughout the height of specimens, as shown in Figure 7.7. This way, displacement profile of shear walls was obtained. In addition to that, lateral slip at wall base, base uplift at hold down locations and vertical separation between lower and upper wall panels were also measured during tests.

7.3 Test Results

7.3.1 Overall Observations and Failure Modes

7.3.1.1 Specimens with Platform Framing Detail-1: P1-1, P1-2 and P1-3

The shear wall specimen P1-1 with single side sheathing and 150/300 mm screw spacing were able to reach the last primary cycle without any major damage or failure. During the last cycle, where specimen was expected to reach 4% drift ratio based on the top-level displacement, screws connecting the sheathing to upper shear wall's boundary studs were pulled-through as shown in Figure 7.8. As a result, specimen was able to reach 3.8% and 3.2% drift ratios in push and pull directions, respectively.

For specimen P1-2, which utilized double side sheathing and 50/100 mm screw spacing, main failure mechanism was the buckling of lower shear wall's boundary studs. When the top-level drift was around 2%, local distortions were observed at the filler truss element provided between the lower and upper shear walls (Figure 7.9a). In addition to that, several rivets connecting the truss element's members together sheared off. As the top-level drift ratio was increased up to 3%, local/distortional buckling was initiated at the boundary studs of the lower wall panel. During last primary cycle that was aimed at 4% drift ratio, both end studs were completely buckled near hold down locations and total collapse of the specimen was observed (Figure 7.9b).

Loading test on the wall specimen P1-3, which was the last tested specimen with the first platform framing detail, was completed without any significant damage on the shear wall. During the last primary cycle, pull-through of several screws were observed at the lower shear wall but that was merely effective on the overall behavior of the wall specimen.

7.3.1.2   Specimens with Platform Framing Detail-2: P2-1, P2-2 and P2-3

Specimen P2-1 with one side sheathing and 150/300 mm fastener spacing was the first tested specimen with platform framing detail-2. This specimen was able to reach 2% top level drift without experiencing any damage. When the top-level drift got closer to 3%, extensive damage occurred at the part of the specimen between the upper and lower wall panels. Several of the rivets connecting profiles together in this part of the specimen sheared off (Figure 7.10a). In addition to that, boundary studs of the lower shear wall locally buckled at various locations (Figure 7.10b). As a result, wall specimen was able to reach 3% top level drift for both push and pull directions before overall failure.

For specimen P2-2, which was tested with double side sheathing and 50/100 mm screw spacing, observed behavior was essentially similar to that of specimen P2-1. However, this specimen was only able to reach 2% of top-level drift before failure. Similar to the previous specimen with platform framing detail-2, failure of rivets and local deformation of framing members were observed with in the part between the lower and upper shear walls. Moreover, chord studs of the lower shear wall buckled near top of the wall (Figure 7.11).

Third specimen with platform framing detail-2 included additional connection between upper and lower shear walls by the OSB sheathing panel. This panel was also connected to profiles of the platform framing part located between shear walls. As a result of the additional reinforcement effect provided by the sheathing panel, the way that this wall specimen failed was different than the previous two specimens in this group. During load testing, no damage was observed within the connection part between wall panels and specimen was able to reach 3% top level drift ratio without any significant damage. When the last primary cycle was underway however, connection screws of the lower shear wall were pulled-through at several locations near wall base (Figure 7.12).

7.3.1.3   Specimens with Ledger Framing Detail: L1 and L2

Specimen L1, which was tested with single side sheathing and 150/300 mm screw spacing, was able to reach 3.5% and 3% top level drift ratios respectively in push and pull directions. Wall specimen did not show any signs of damage or failure until the last primary cycle during the load test. Failure mode of the specimen was screw pull-through occurring at the first story shear wall near the top part (Figure 7.13a). As a result, sheathing framing connection lost its integrity and wall specimen could not handle higher deformation levels.

159

The second specimen with ledger framing (specimen L2) was able to reach 3% top level drift ratio in both directions before failure. Given that this wall specimen was prepared with double side sheathing and 50/100 mm fastener spacing, load levels that the shear wall was able to achieve was relatively higher. Boundary stud of the lower shear wall buckled suddenly near hold down locations when drift ratio reached 3% (Figure 7.13b).

7.3.2   Load-Displacement Behavior

Figure 7.14 shows the load-displacement curve for each shear wall specimen under cyclic loading. In these curves, load is the total shear force and displacement is the lateral displacement recorded at the top of upper shear wall. Lateral load values displayed on these plots are for 1 m of wall length. Load-displacement curves of first and second story shear walls of each specimen are also given in Figure 7.15. Displacement values in these plots represent the relative lateral displacement between the top and bottom levels of the first and second story walls. The severely pinched response of specimens is evident in each hysteresis curve. As mentioned in previous chapters, this type of behavior is a characteristic property of CFS framed shear wall systems and mainly results from the local behavior of connection screws between sheathing panels and CFS framing members. Plots provided in Figure 7.15 indicate that for all specimens except for P1-2 the first and second story shear walls exhibited similar response. This may be due to the fact that with double sided sheathing and reduced screw spacing, wall panels of specimen P1-2 became more rigid and platform framing part acted as the weakest link in the specimen. The excessive deformation of this part along with the uplift deformations between the platform framing and upper shear wall resulted in the difference of wall responses.

Hysteresis plots in Figure 7.14 also display cyclic backbone curves based on primary loading cycles and bilinear Equal Energy Elastic-Plastic (EEEP) curves as specified

in AISI S400-15 (2015). Details about the EEEP model, which creates a bilinear curve describing the linear elastic behavior of a shear wall up to a yielding point and perfectly plastic behavior until the failure, and its calculation method were explained in Chapter 4 of the thesis.

7.3.2.1 Evaluation of Test Results

Load capacities and design parameters obtained from the EEEP model approach, such as elastic stiffnesses, yield loads and yield displacement values for each specimen are presented in Table 7.2. Reported values are calculated from overall response of each specimen, as well as response of both story shear walls. As it can be seen, all shear wall specimens were able to reach 3% or more top level drift ratio, except the specimen P2-2 utilizing platform framing detail-2. In terms of load capacities, wall specimens that were sheathed on one side with 150/300 mm fastener spacing acquired values ranging between 10.2 to 14.2 kN/m. For specimens P1-2, P2-2 and L-2, which were tested with double sided sheathing and 50/100 mm fastener spacing, measured load capacities were 24.7, 12.5 and 25.4 kN/m, respectively. Although it was sheathed on both sides with a dense fastener layout, specimen P2-2 obtained a relatively low load capacity value of 12.5 kN/m, almost identical to the wall specimen P2-1 which is sheathed with a single OSB panel. This is due to the fact that the connection part between upper and lower walls of this specimen was not sheathed. During load testing, excessive damage occurred in framing members within this connection region resulted in premature failure of the specimen.

In order to evaluate the obtained load capacity values of shear wall specimens, a comparison can be made with nominal shear strength values per AISI S400-15 (2015). According to the specification, nominal shear strength value for a CFS framed shear wall that is OSB sheathed on one side with 150/300 fastener spacing is

12 kN/m. For a shear wall that was sheathed on both sides with OSB panels and with 50/100 fastener spacing, expected nominal shear strength is 60 kN/m. However, since wall specimens in the study have an aspect ratio of 4, an additional reduction should be made when calculating expected nominal strength values. AISI S400-15 (2015) suggests for shear walls with aspect ratio values between two and four, nominal strength shall be calculated as follows:

$$V_n = v_n w(\frac{2w}{h})$$ [7.1]

As a result, code specified values would be 6 kN/m for single side sheathed walls with 150/300 mm fastener spacing and 30 kN/m for double side sheathed walls with 50/100 mm fastener spacing. In that case, load capacity values of single side sheathed specimens were two times the code specified value, whereas for double side sheathed specimens P1-2 and L-2, load capacities fall below the code specified value. This can be attributed to the different mechanisms in the tested specimens. Since specimens were consisted of two shear walls connected with various framing options, behavior of floor framing and connection between first and second story walls affected the overall behavior. In addition to that, especially for double sided specimens with dense fastener layout, where the demand for force is higher, buckling of external studs and distortion of platform framing members were observed, eventually resulting in failure before expected load levels were reached. The difference between obtained load capacities and codified nominal shear strength values for wall specimens P1-1, P1-3, P2-1, P2-3 and L-1 could be resulted from the reduction method defined in the design provision. This subject had previously been investigated (Nava and Serrette, 2015) and it was reported that especially for shear walls with aspect ratios equal to or greater than 4, codified strength reduction expression is somewhat overly conservative.

7.3.3 Comparison of Response among Wall Panels

In order to investigate the effect of different framing options, several comparisons were made by making use of the measured response of specimens. Cyclic backbone and EEEP curves of specimens P1-1, P2-1 and L-1, which are walls that were sheathed with a single OSB panel and had loose fastener layout, are given in Figure 7.16. Provided in the same figure are the plots for double side sheathed specimens with dense fastener layout (P1-2, P2-2 and L-2). As evident, first group of specimens obtained very similar results, indicating both platform framing and ledger framing options resulted in similar behavior. In the case of the second group, specimen P1-2 with platform framing including a filler truss member and specimen L-2 with the ledger framing option showed similar performances, whereas specimen P2-2 exhibited lower load capacity and drift values compared to other two. The reason for this response is the excessive deformations occurred at the framing members within the connection between the first and second floor walls, as explained before.

Another parameter investigated in the study was the presence of sheathing for the connection region in two specimens. Wall specimens P1-3 and P2-3 were built this way, but other than that they were identical with specimens P1-1 and P2-1 in terms of sheathing, fastener layout and platform framing detail. Figure 7.17 shows cyclic backbone and EEEP curves for wall pairs P1-1 – P1-3 and P2-1 – P2-3 to demonstrate the effect of sheathing the platform framing part of specimens. For both types of platform framing options, presence of OSB sheathing for the connection region in two specimens enhanced the behavior as expected. For platform framing detail-1, where a filler truss member is present, a slight increase in load capacity was observed. For platform framing detail-2, on the other hand, the load capacity was increased by almost 40% with a significant increase in overall stiffness as well.

Displacement profiles of each specimen are created and provided in Figure 7.18. These profiles are based on the peak displacement values obtained in both push and pull directions throughout the height of each wall specimen for the last three primary cycles of the CUREE loading history. First observation that can be deducted from the deformation profiles of specimens is the difference between two platform framing options. Comparing wall specimen pairs P1-1 – P2-1 and P1-2 – P2-2, it can be seen that for platform framing detail-2, where upper part of the first floor shear wall was modified for the placement of floor beams, lateral displacements are larger within the connection region when compared to wall specimens utilizing platform framing detail-2. When specimens P1-1 and P1-2 with the platform framing detail that includes a filler truss member are considered, the second story shear walls of these specimens experienced larger story displacements when compared to specimens P2-1 and P2-2. While specimens with different platform framing options reached similar target displacement values, for specimens P1-1 and P1-2 the uplift displacement between the filler truss member and the second story wall was greatly contributed to the total lateral displacement. In the case of specimens P2-1 and P2-2, vertical displacement between first and second story shear walls were not as much, but this time larger contribution to the overall lateral displacement resulted from the deformation of the platform framing part of the specimens. When two wall specimens with ledger type of framing are considered, it can be seen that displacement profiles show a more linear behavior throughout the entire height of walls. Same linearity is also valid for platform framing specimens P1-3 and P2-3, in which connection regions were sheathed with OSB panels. It can be concluded that these panels were able to reinforce the relatively weak connection region and helped to achieve a more uniform behavior by connecting the first and second story shear walls.

Table 7.1 Details of specimens

Specimen	Framing Detail	Sheathing	Screw spacing (mm)
P1-1	Platform framing detail-1	Single side	150/300
P1-2	Platform framing detail-1	Double side	50/100
P1-3	Platform framing detail-1 w/ sheathing connection	Single side	150/300
P2-1	Platform framing detail-2	Single side	150/300
P2-2	Platform framing detail-2	Double side	50/100
P2-3	Platform framing detail-2 w/ sheathing connection	Single side	150/300
L-1	Ledger framing	Single side	150/300
L-2	Ledger framing	Double side	50/100

Table 7.2 Test results

Specimen		P_peak (kN/m)		Δ_peak (mm)		Δ_u (mm) / % drift				P_yield (kN/m)		Δ_y (mm)		K_e (kN/mm)		
		Push	Pull	Push	Pull	Push		Pull		Push	Pull	Push	Pull	Push	Pull	Average
P1-1	*Overall*	11.4	-11.4	**145.0**	**145.0**	**185.0**	**3.8**	**155.0**	**3.2**	**9.6**	**9.0**	**80.0**	**63.0**	**0.12**	**0.14**	**0.13**
	1st story			53.3	57.8	60.4	2.5	57.8	2.4	9.3	8.8	27.7	26.2	0.34	0.34	0.34
	2nd story			74.7	73.0	103.0	4.2	82.5	3.4	9.8	9.2	40.7	31.2	0.24	0.29	0.27
P1-2	*Overall*	24.7	-24.0	**168.0**	**145.0**	**179.0**	**3.7**	**182.0**	**3.7**	**20.0**	**20.2**	**83.0**	**85.0**	**0.24**	**0.24**	**0.24**
	1st story			49.4	42.8	55.7	2.3	47.2	1.9	22.0	22.0	26.0	29.4	0.84	0.75	0.80
	2nd story			88.2	88.8	88.2	3.6	88.8	3.6	20.2	20.4	45.6	47.0	0.44	0.43	0.44
P1-3	*Overall*	12.8	-12.4	**183.0**	**194.0**	**183.0**	**3.8**	**194.0**	**4.0**	**10.9**	**10.5**	**94.0**	**70.5**	**0.12**	**0.15**	**0.14**
	1st story			85.7	96.5	85.7	3.5	96.5	4.0	10.8	10.8	41.0	31.4	0.27	0.34	0.31
	2nd story			82.3	94.0	82.3	3.4	94.0	3.9	10.7	10.8	40.7	34.0	0.26	0.32	0.29
P2-1	*Overall*	10.2	-9.4	**123.0**	**131.0**	**147.0**	**3.0**	**147.0**	**3.0**	**8.4**	**8.2**	**55.0**	**55.0**	**0.15**	**0.15**	**0.15**
	1st story			54.2	56.0	69.0	2.8	56.0	2.3	8.3	7.9	21.4	20.7	0.38	0.38	0.38
	2nd story			40.4	36.6	49.7	2.0	47.0	1.9	8.3	8.4	20.4	24.7	0.40	0.34	0.37
P2-2	*Overall*	12.5	-11.3	**68.0**	**68.0**	**99.0**	**2.0**	**95.0**	**1.9**	**11.0**	**10.0**	**49.8**	**46.8**	**0.22**	**0.21**	**0.22**
	1st story			24.5	24.0	24.5	1.0	24.0	1.0	10.0	9.0	15.0	15.0	0.66	0.60	0.63
	2nd story			23.3	27.0	25.0	1.0	29.2	1.2	11.0	9.0	18.7	17.9	0.59	0.50	0.55
P2-3	*Overall*	14.2	-13.5	**145.0**	**174.0**	**162.0**	**3.3**	**175.0**	**3.6**	**11.5**	**11.4**	**70.0**	**51.7**	**0.16**	**0.22**	**0.19**
	1st story			67.2	86.0	80.0	3.3	101.0	4.1	11.6	11.5	31.2	22.4	0.37	0.50	0.44
	2nd story			63.4	73.5	68.0	2.8	82.6	3.4	11.3	11.6	30.5	24.4	0.37	0.47	0.42
L-1	*Overall*	12.0	-12.3	**143.0**	**145.0**	**170.0**	**3.5**	**145.0**	**3.0**	**9.8**	**10.6**	**73.0**	**70.0**	**0.13**	**0.15**	**0.14**
	1st story			64.0	66.0	94.0	3.9	66.0	2.7	9.3	10.8	32.0	31.8	0.29	0.33	0.31
	2nd story			68.7	69.0	82.7	3.4	69.0	2.8	10.1	10.5	36.0	34.0	0.28	0.30	0.29
L-2	*Overall*	25.4	-25.2	**124.0**	**121.0**	**143.0**	**2.9**	**140.0**	**2.9**	**21.6**	**22.0**	**79.0**	**84.0**	**0.27**	**0.26**	**0.27**
	1st story			51.5	47.3	60.3	2.5	56.0	2.3	21.6	20.8	31.0	26.0	0.70	0.80	0.75
	2nd story			61.0	63.3	67.4	2.8	72.0	3.0	22.5	23.4	43.2	52.3	0.52	0.45	0.49
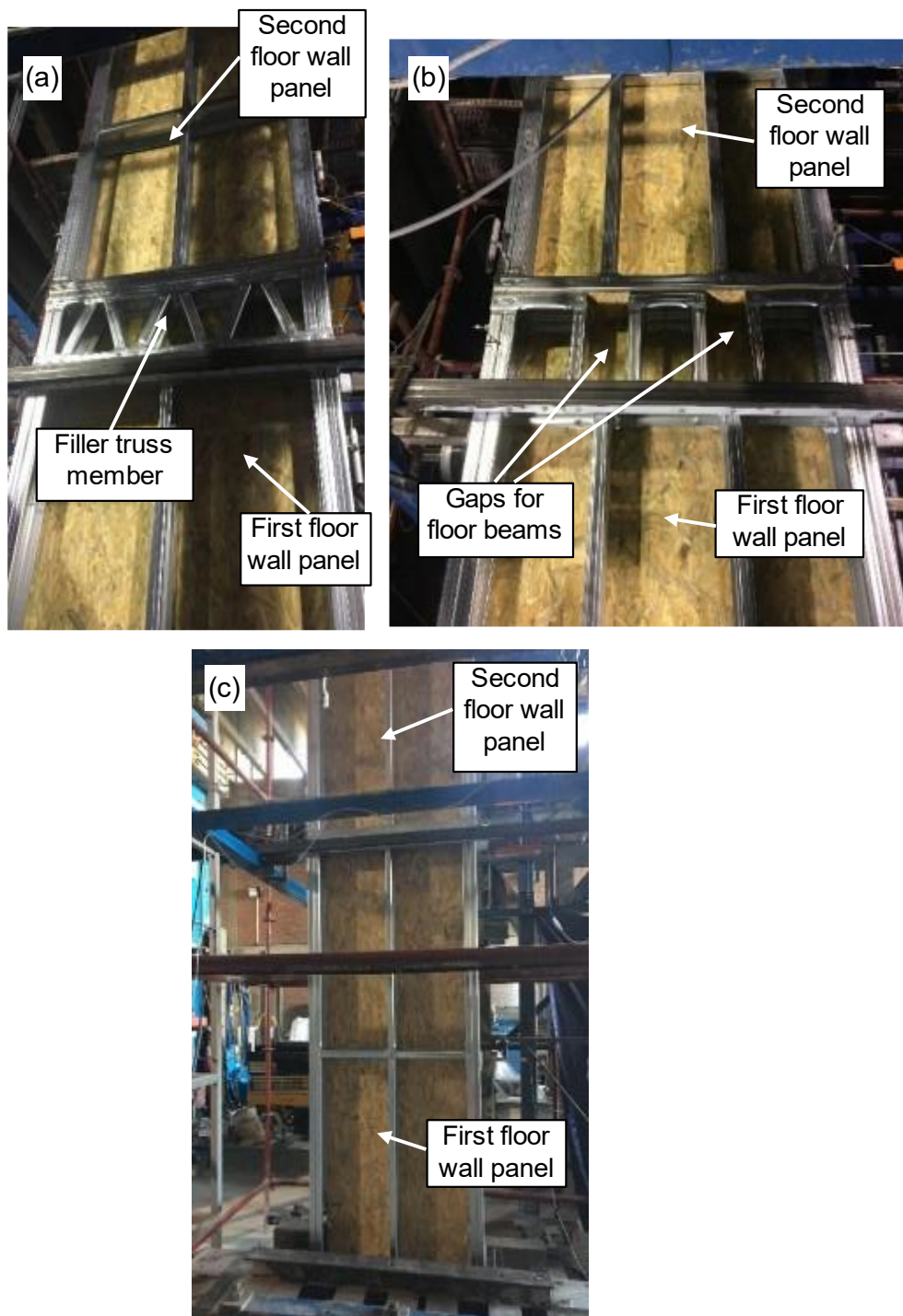
Figure 7.1 Framing details of wall specimens: (a) platform framing detail-1; (b) platform framing detail-2; (c) ledger framing detail
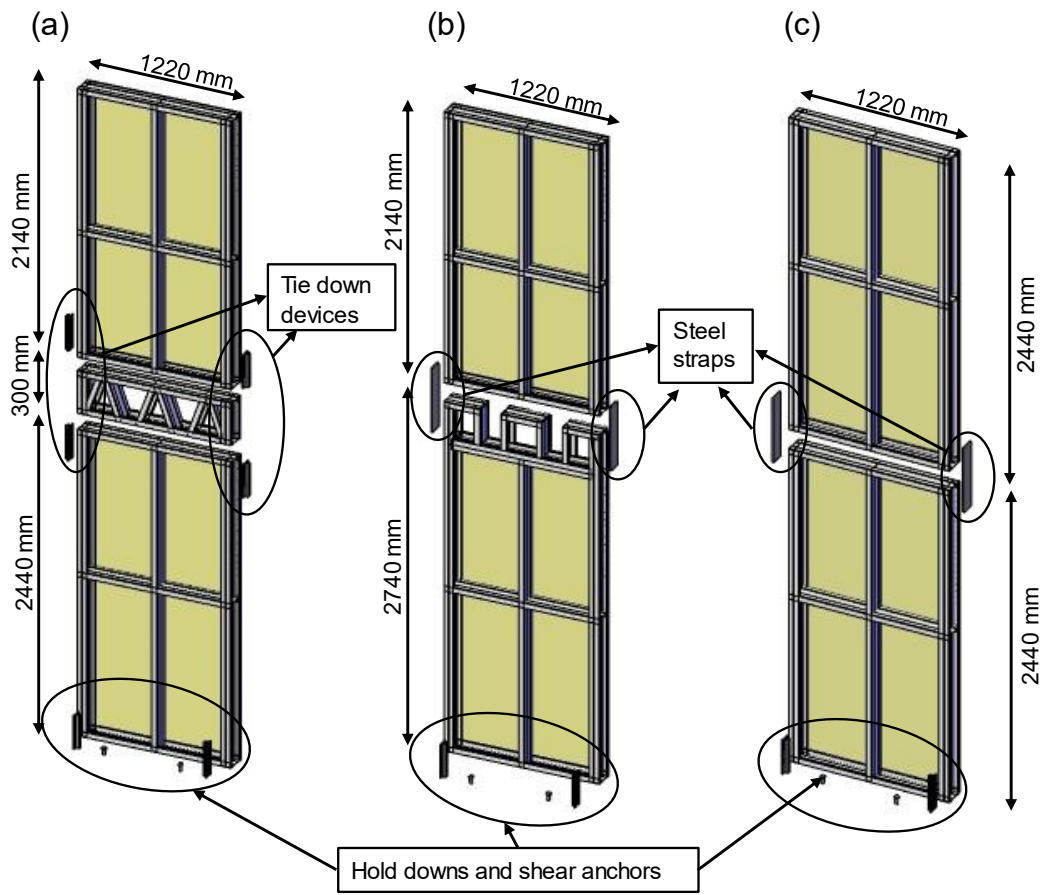
Figure 7.2 General configurations of shear wall specimens: (a) platform framing detail-1; (b) platform framing detail-2; (c) ledger framing detail
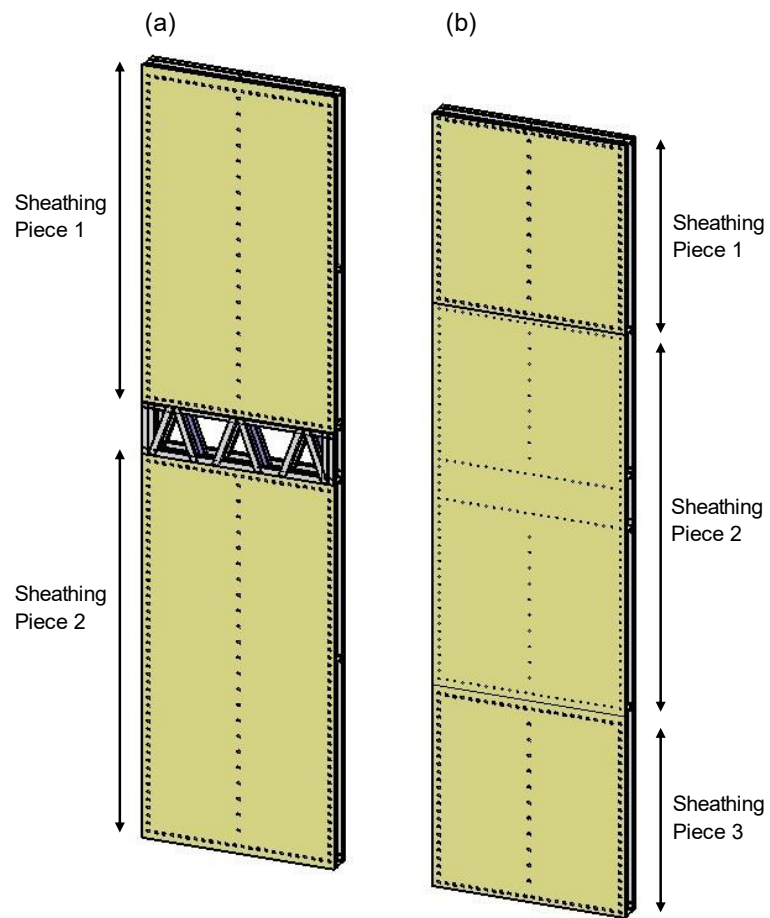
Figure 7.3 Two different sheathing configurations used for specimens: (a) sheathing each floor wall panel; (b) connecting wall panels with a sheathing
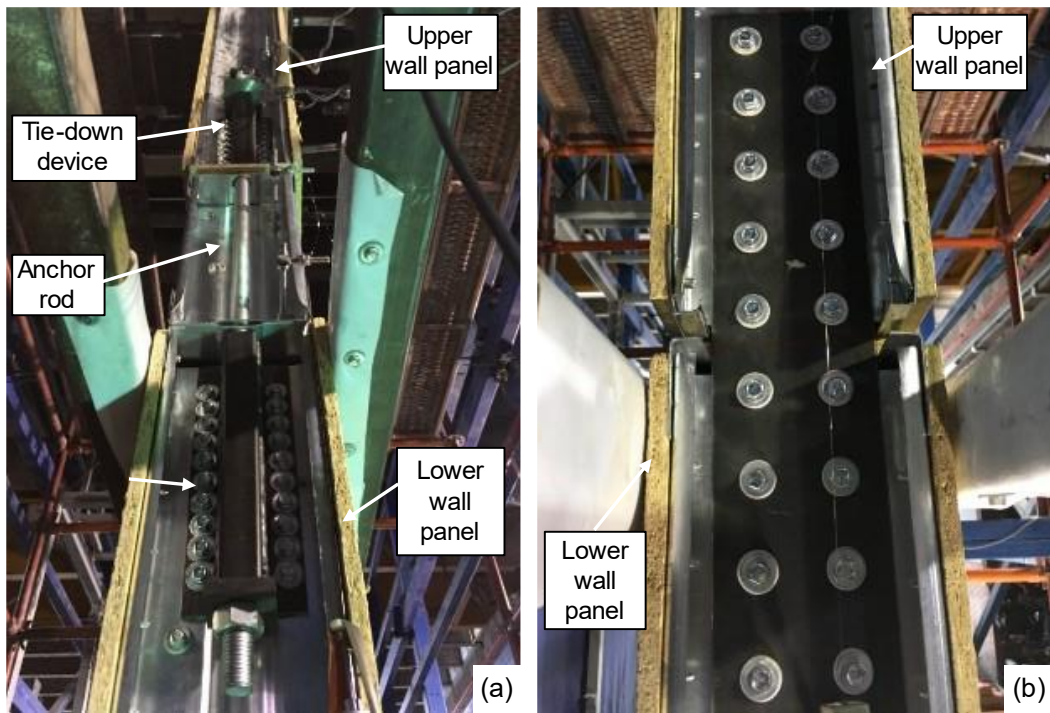
Figure 7.4 Connections between first and second floor shear walls: (a) tie-down
connection for platform framing; (b) steel strap tie connection for ledger framing
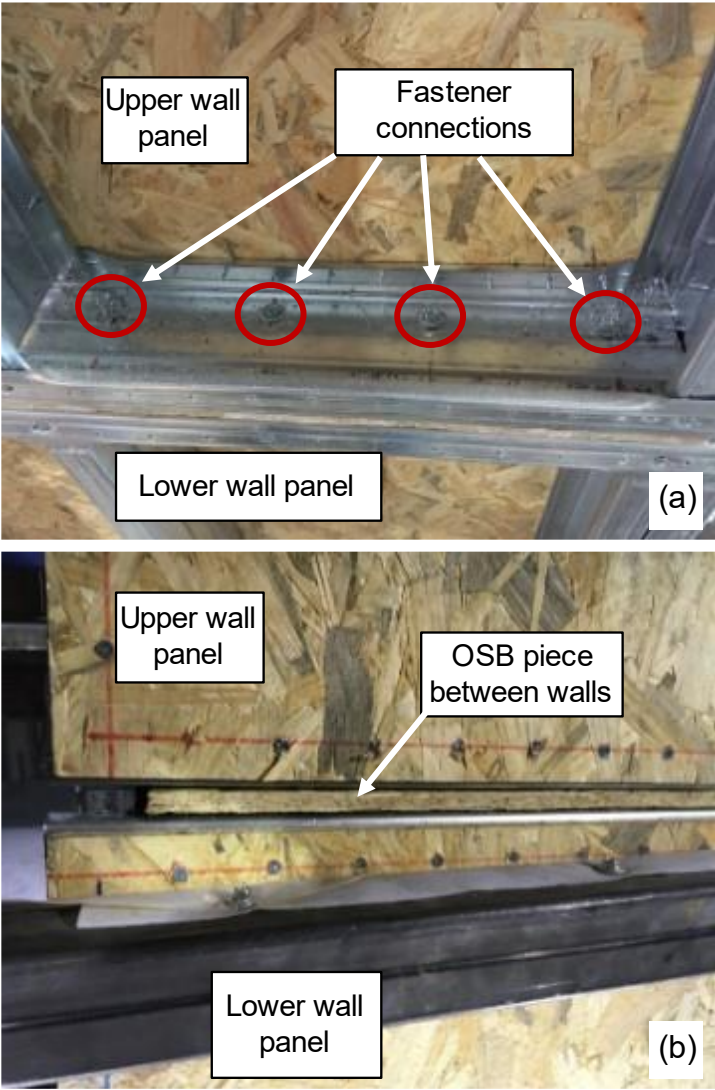
Figure 7.5 (a) Additional fastener connection between upper and lower shear walls;
(b) OSB piece placed between walls
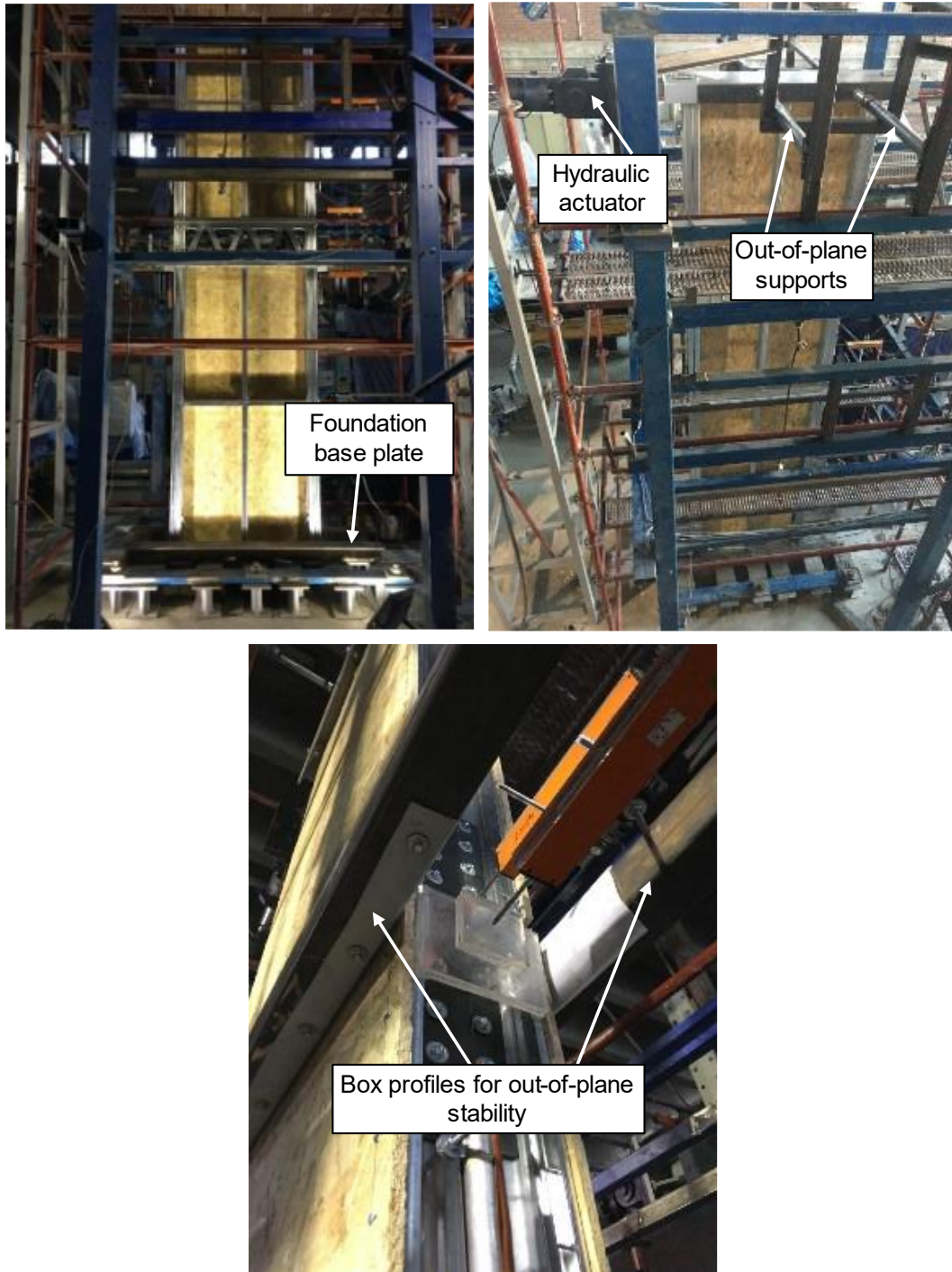
Figure 7.6 Details of two story shear wall test setup
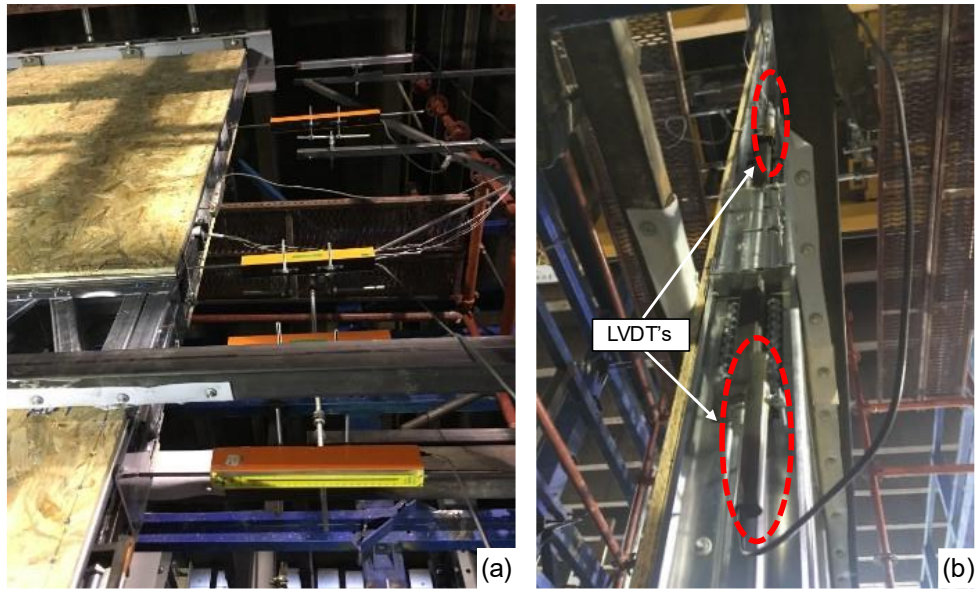
Figure 7.7 (a) LVDT's placed for obtaining lateral displacement profile; (b) measuring vertical displacement between upper and lower shear walls
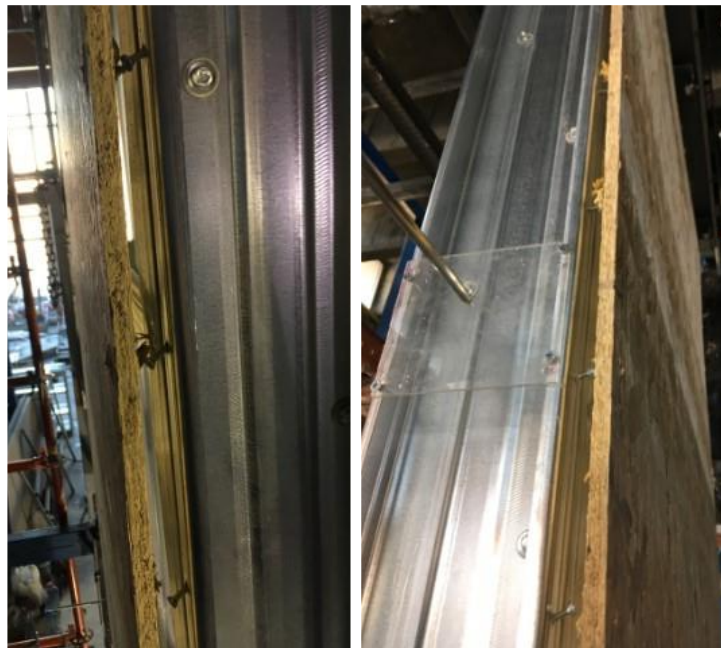
Figure 7.8 Screw pull-through failure observed in specimen P1-1
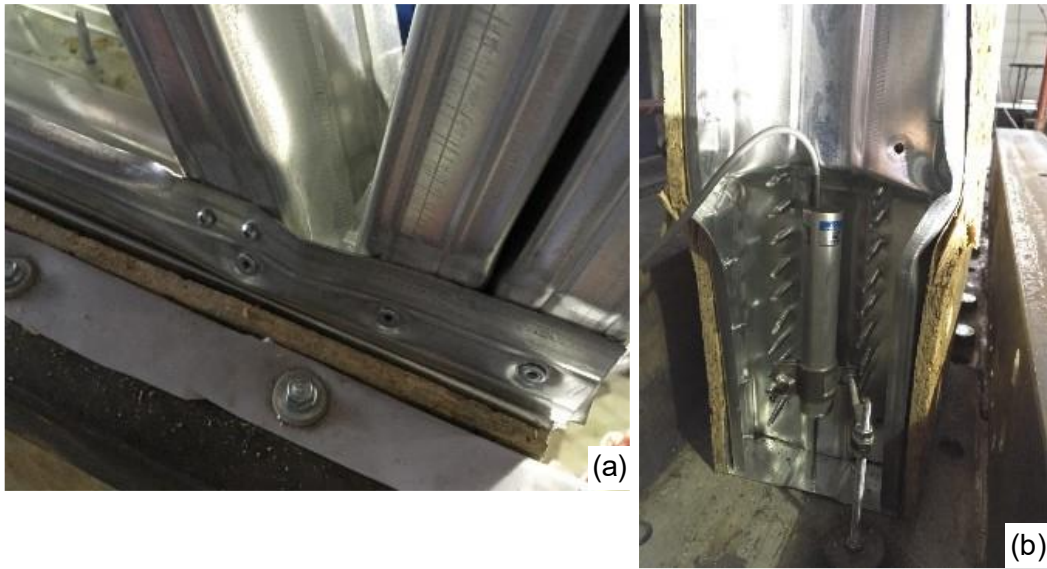
Figure 7.9 Deformations observed in specimen P1-2: (a) local damage on filler truss member; (b) local deformation of boundary stud
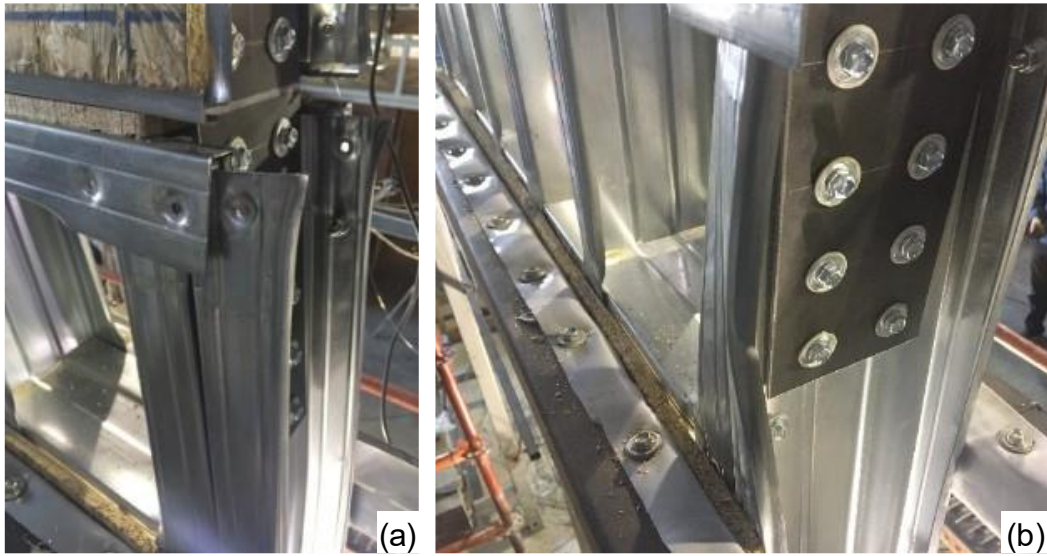
Figure 7.10 Deformations observed in specimen P2-1: (a) failed rivets; (b) local buckling of stud

Figure 7.11 Deformations observed in specimen P2-2
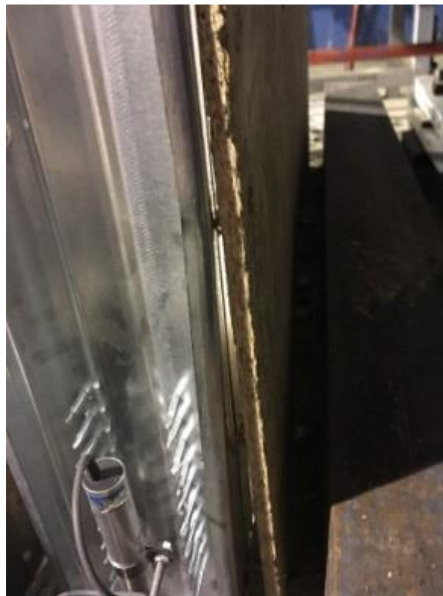
Figure 7.12 Deformation observed in specimen P2-3
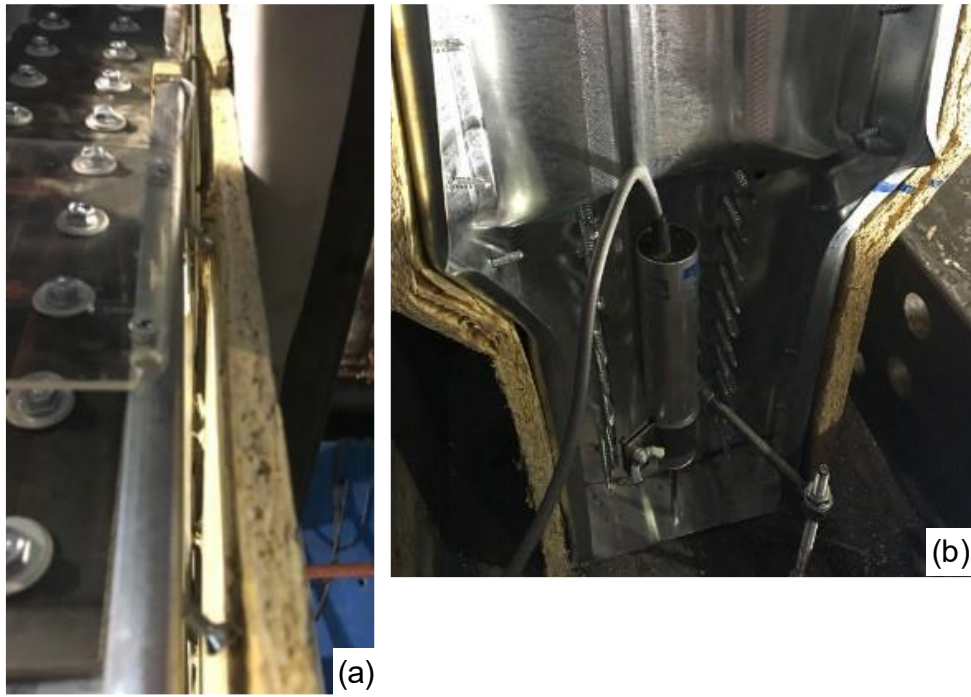
Figure 7.13 Deformations observed in ledger framing specimens: (a) specimen L1;
(b) specimen L2
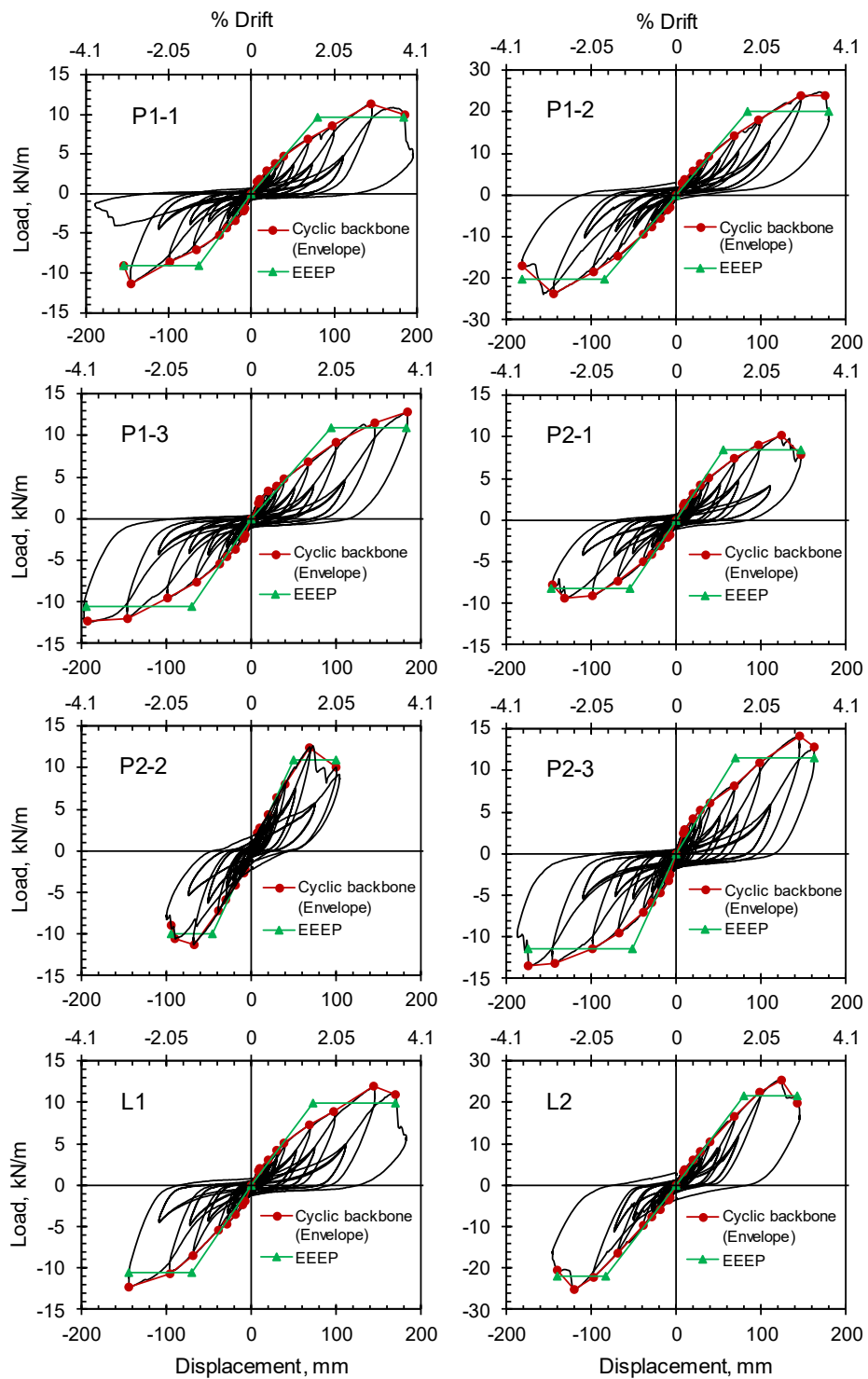
Figure 7.14 Load versus top displacement behavior of two story shear walls
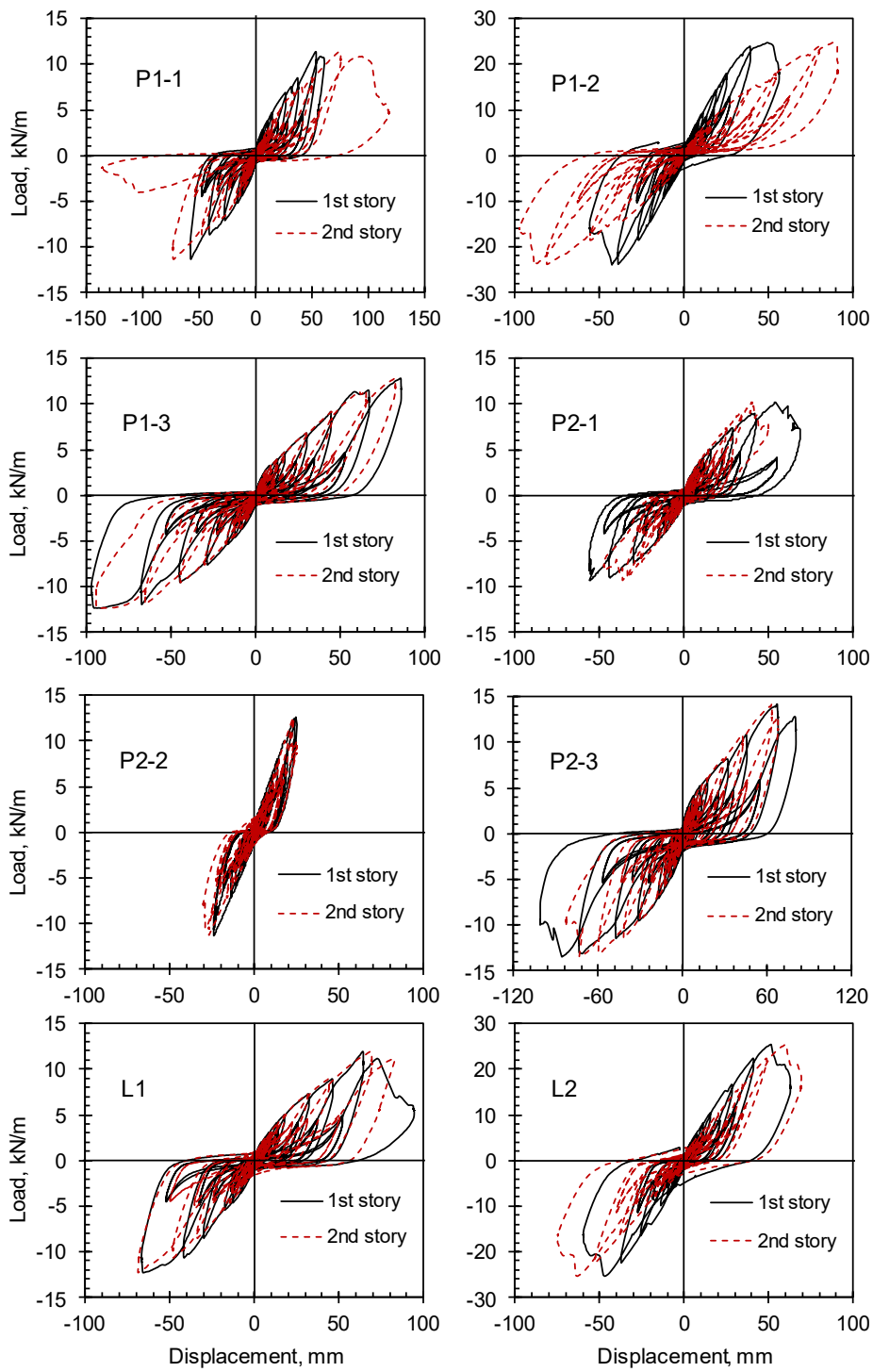
Figure 7.15 Load-displacement behavior of first and second story walls of specimens
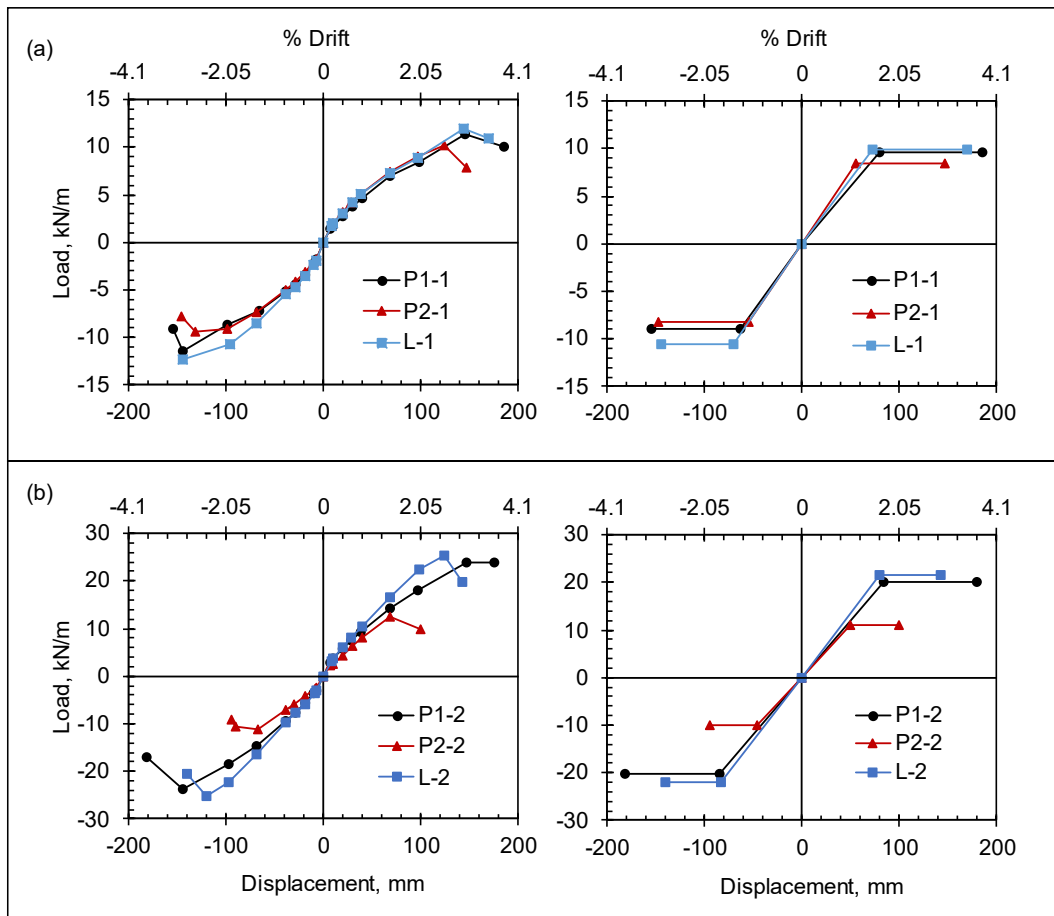
Figure 7.16 Cyclic backbone and EEEP curves for specimens: (a) specimens sheathed on single side with coarse fastener layout; (b) specimens sheathed on two sides with dense fastener layout

179
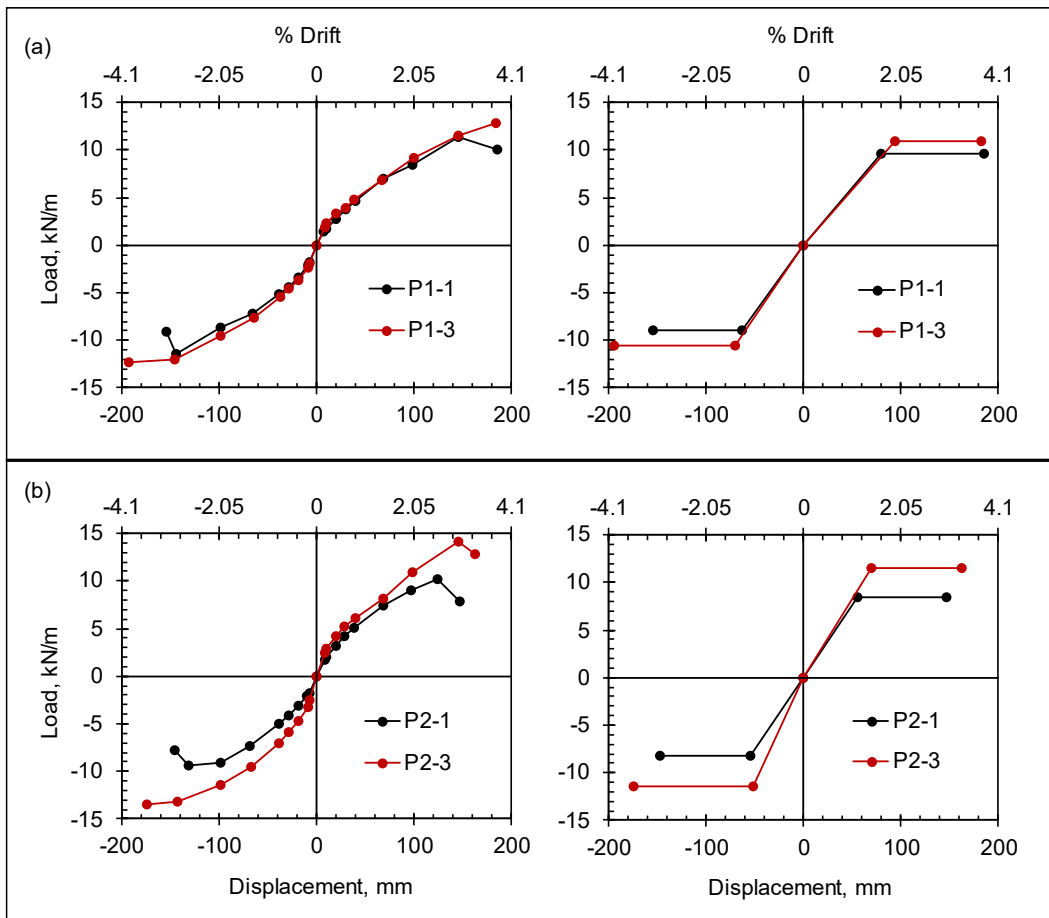
Figure 7.17 Comparison of specimens with two sheathing panel configurations: (a) specimens with platform framing detail-1; (b) specimens with platform framing detail-2
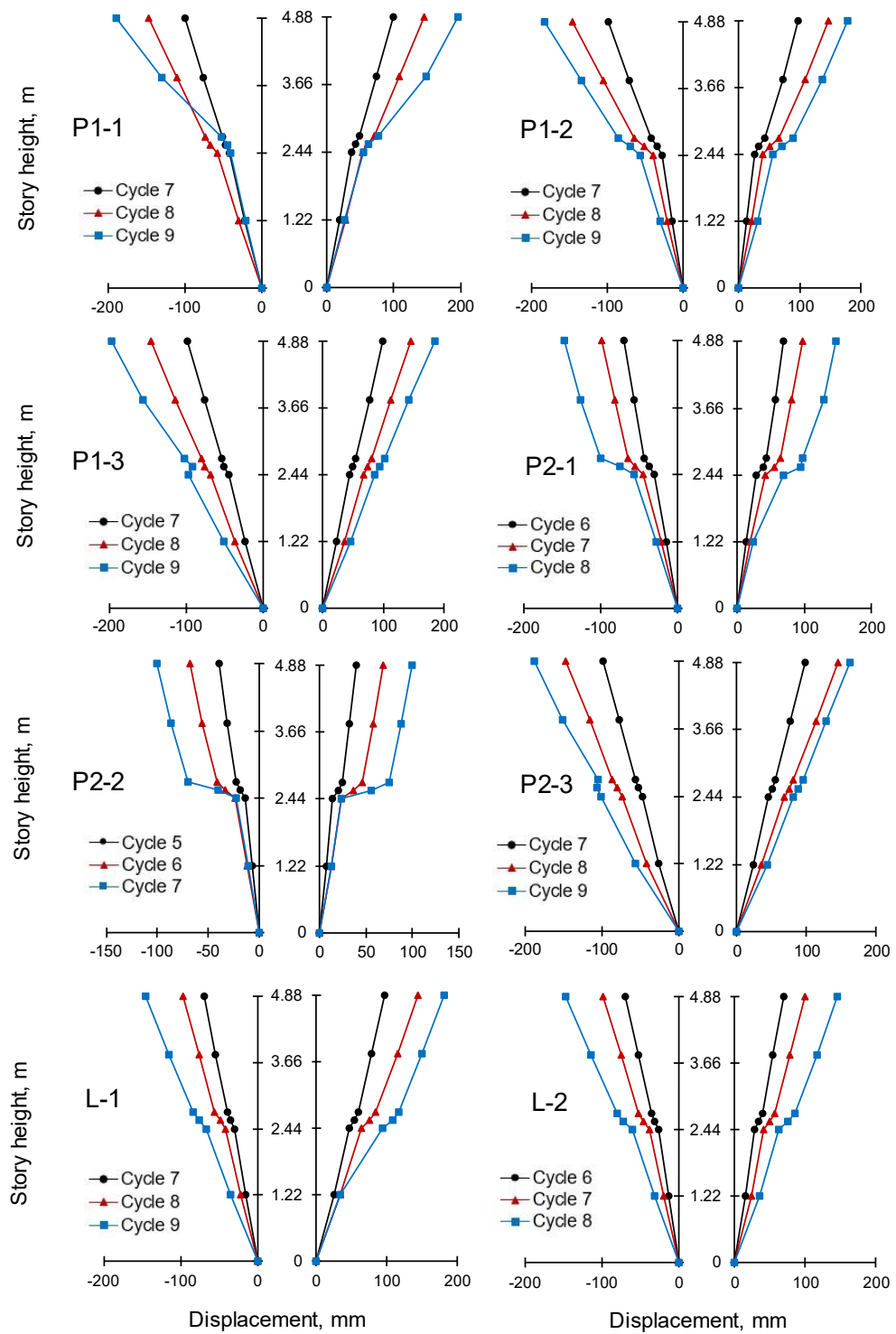
Figure 7.18 Displacement profiles of two story wall specimens

CHAPTER 8

LATERAL LOAD BEHAVIOR OF THREE-DIMENSIONAL CFS SHEAR WALL ASSEMBLIES

8.1   Introduction

This part of the thesis describes the load tests performed on three-dimensional CFS structural asssemblies. These assemblies consisted of two shear walls and a floor system made of three floor trusses along with a sheathing.

8.2   Shear Wall Test Program

8.2.1   Wall Specimens

For this part of the experimental program, total of eight three-dimensional CFS shear wall assembly specimens were created and tested under cyclic loading conditions. General view of a typical specimen is given in Figure 8.1. Each specimen consisted of two 2.44 m tall and 1.22 m long CFS framed OSB sheathed shear wall panels that are placed parallel to each other. Like rest of wall specimens considered in the study, CFS framing members were made of 1.2 mm thick and 140 mm deep C-shaped sections. After the placement of wall panels for the lower story, floor system was placed directly on top of these walls. In order to simulate the effect of shear walls attached to the floor system from above, 1.22 mm tall and 1.22 mm long wall panels were utilized as the upper story walls. Floor system consisted of three floor trusses of 3.7 m length for platform framing detail and 3.4 m length for ledger framing detail and OSB sheathing placed and fastened on top of these trusses. This type of system

represents the commonly used floor construction utilized in CFS buildings in Turkey, as well as in Australia and New Zealand. One important detail that needs to be addressed is that OSB sheathing panels used for the flooring was 18 mm thick, different than the 11 mm thick OSB panels used for shear walls tested in all phases of this study.

Details of specimens and considered parameters are given in Table 8.1. The main investigated parameter in specimens was the different floor framing details. As explained in the Chapter 7 of the thesis, two options are generally considered as floor framings in CFS structures; platform and ledger framings. In accordance with the experimental study on two story shear walls, the same framing details were also utilized in the three-dimensional assembly specimens. Accordingly, three of the specimens included platform framing detail-1, next three specimens included platform framing detail-2 and the other two specimens included ledger framing detail. Photographs showing the specimens utilizing these three framing details provided in Figure 8.2. As it can be seen, for specimens with platform framing details, floor trusses were placed on top of shear walls and connected to the top track of each wall using 6.3 mm diameter fasteners. Platform framing detail-1 included filler truss members placed between floor trusses which were also connected to both wall panels and flooring (Figure 8.2a). The assembly of platform framing detail-2 included CFS shear wall framing with 2.74 m long exterior studs. Several CFS profiles were connected between these exterior studs to form a platform framing detail that included slots for the placement of floor trusses (Figure 8.2b). Floor trusses were placed inside these slots and connected to wall framing both vertically and horizontally with fasteners. The ledger framing detail includes a 1.2 mm thick supporting steel sheet connected to the inner side of lower story shear walls (Figure 8.2c). This steel sheet (i.e., ledger member) was 35 cm high and 122 cm long and bottom 5 cm of it was bent in order to support the floor trusses. Ends of floor trusses were fastened to the ledger members though their bottom chord. As shown in Figure

8.2c, angle brackets, which were bent from 1.2 mm thick steel sheets, were used at the end of floor trusses on both sides in order to provide additional connection between truss ends and ledger members.

In addition to different floor framing options, several other parameters were also investigated with three-dimensional assembly tests. Similar to the shear walls tested in other parts of the study, single or double sided sheathing for shear walls as well as fastener spacings of 150/300 mm and 50/100 mm were also considered. Another parameter used in the test program was the level of gravity loading applied on specimens before lateral loading. Amount of the gravity load was 32 kN for specimen WA-6, whereas it was 16 kN for all other specimens. 16 kN of gravity load was selected based on the AISI Standard for Cold-Formed Steel Framing – Prescriptive Method for One and Two-Family Dwellings (2015). This value was doubled for specimen WA-6 in order to investigate the effect of increased vertical load on the behavior of shear wall assembly.

Base of the lower story shear walls was connected with two hold down devices to the foundation base plate. A 24 mm diameter anchor rod was used with each hold down device. The hold down used in these specimens was the device presented in Chapter 4. In addition to the hold downs, two 16 mm diameter shear anchors were also used at the base of each hear wall.

The 1.22 mm tall and 1.22 mm long wall panels used as the upper story walls were placed on top of the floor system for specimens utilizing platform framing detail and placed on top of first story shear walls for specimens utilizing ledger framing detail. Their connection at the base was provided with 6.3 mm diameter self-tapping screws.

8.2.2 Test Setup, Instrumentation and Loading Protocol

Details of the test setup used for testing three-dimensional shear wall assemblies is shown in Figure 8.3 and Figure 8.4. Different than the setups used for testing of earlier wall specimens, the hydraulic actuator with 1000 kN load capacity was not connected to specimens directly. Instead, actuator was placed right above the specimens and connected to a readily available steel framing, as shown in Figure 8.3. A steel profile acting as a load transferring link was attached to the column in the framing at one end and connected to specimens through a swivel joint and a load cell at the other end. This way, reversed cyclic loading was applied to the steel frame by the actuator and this loading was transferred to the specimens. The load transferring link was attached to a U-shaped steel load spreader beam, which itself was connected to the ends of four other U-shaped profiles. These four profiles rested on top of the floor system and connected to floor sheathing with fasteners, resulting in the lateral load transfer on the plane of the flooring.

The two lower story walls were placed on 20 mm thick steel plates that were connected to steel box shaped profiles, which themselves rested on support beams as shown in Figure 8.5. These support beams were fixed to the strong floor. In order to provide the stability of specimens in the plane perpendicular to loading, steel cables were used as shown in Figure 8.4. Steel blocks were placed on the floors as shown in Figure 8.6 in order to simulate the gravity.

Lateral force applied on specimens was measured by a load cell that was placed between the link profile and specimens, as mentioned before. In order to measure the lateral displacement of specimens, five LVDT's were used. Three of these LVDTs were placed at the floor level, measuring displacements at two sides and the middle. Two LVDT's were placed at the top level of each shear wall to record lateral deformation of walls. Lateral slip at wall bases and base uplifts at hold down

186

locations were also measured with LVDTs. Similar to the reversed cyclic load tests conducted in other parts of the study, loading history of the cyclic tests was defined according to the CUREE specification (Krawinkler et al., 2001)

8.3   Test Results

8.3.1   Overall Observations and Failure Modes

8.3.1.1   Specimens with Platform Framing Detail-1: WA-1, WA-2 and WA-3

The first specimen WA-1 included wall panels with single side sheathing and 50/100 mm fastener spacing. An important detail in this specimen is that filler truss members used in the platform framing, as well as floor trusses were left over from other experimental studies going on in the laboratory. The main purpose of this specimen was to evaluate the design and construction of the test setup. Although that's the case, since wall specimens were able to reach 2% drift in push direction and 1.7% drift in pull direction without any premature failure, results are presented here. Loading test was concluded with excessive deformation at filler truss members of the platform framing as shown in Figure 8.7.

Specimen WA-2 included wall panels with single side sheathing and 150/300 mm fastener spacing. The two shear walls of the specimen reached different drift ratio values. One shear wall was able to reach 2.6% and 1.75% drift ratio in push and pull directions respectively, while the other wall experienced 3% drift in both directions. This difference may be caused due to errors occurred during the preparation of shear walls, especially for the sheathing fasteners. Since screw connections between sheathing and CFS framing are directly affect the response of shear walls and

sometimes it is possible to damage the sheathing at fastener locations while providing screws, it may be possible that one wall panel experienced such damage that resulted in the altered response. Another possible reason may be damage occurred at filler truss members of the platform framing detail. These members of a shear wall may be damaged and resulted in the different response. The main failure mechanism observed in this specimen was the pull through of screws connecting OSB sheathing to CFS framing in one of the walls, without any other damage on framing members (Figure 8.8)

The third specimen with platform framing detail-1 (i.e., specimen WA-3) included wall panels with single side sheathing and 50/100 mm screw spacing. Similar to the previous specimen, uneven behavior of wall panels was also observed for this specimen. While one shear wall was able to reach 3% drift ratio in push and 3.8% drift ratio in pull direction, the other wall experienced only 2.3% and 2.5% drift ratios in push and pull directions, respectively. Loading test was terminated when excessive damage was observed at OSB sheathing panels with pull through of connection screws. In addition to that, filler truss members of the platform framing locally buckled and failed (Figure 8.9).

8.3.1.2   Specimens with Platform Framing Detail-2: WA-4, WA-5 and WA-6

Specimen WA-4 included wall panels with single sided sheathing and 50/100 mm screw spacing. Both wall panels of this specimen were able to reach approximately 3% drift in push and 2.5% drift in pull directions. The main failure mechanism observed in this specimen was the global buckling of one of the wall panel studs. As the buckling initiated, connection screws were also pulled through and resulted in excessive damage on the OSB sheathing, eventually causing the shear wall to lose its integrity as shown in Figure 8.10.

Specimen WA-5 was similar to specimen WA-4 but included wall panels with double sided sheathing. At the end of the loading test, both wall panels of the specimen were able to reach 2.5% drift ratio in push direction and 2% drift ratio in pull direction. Given that the walls were sheathed on both sides, no damage was observed on them and the failure mechanism localized at the platform framing detail. With increasing lateral displacement, screws connecting OSB sheathing to the CFS members within the top 30 cm part of the lower shear wall pulled off, as shown in Figure 8.11.

Specimen WA-6 was identical to specimen WA-5, but tested with 32 kN of gravity load instead of 16 kN. Both shear walls of the specimen were able to reach 2.2% and 2% drift ratio values in push and pull directions, respectively. The main failure mechanism was also similar with the previous specimen and concentrated on the platform framing part, as shown in Figure 8.12.

8.3.1.3 Specimens with Ledger Framing Detail: WA-7 and WA-8

Specimens with ledger framing WA-7 and WA-8 included shear walls with double sided sheathing and 50/100 mm fastener spacing. Specimen WA-8 was almost identical with the WA-7, except one detail. For specimen WA-7, since the supporting steel sheet of the ledger framing was connected to top tracks of wall panels, OSB sheathing was not able to be fastened to this track member of CFS framings. For specimen WA-8, an additional CFS profile was connected to wall framings as shown in Figure 8.13, so that OSB sheathing can be fastened.

Specimen WA-7 was able to experience maximum drift ratio values of 3.6% and 3% in push and pull directions, respectively. Specimen WA-8 experienced approximately 3% drift ratio in both directions. During load testing, no damage or excessive deformation was observed at connections between shear walls and the

floor system in both of these specimens. In that manner, it can be said that the ledger framing detail performed satisfactorily. Because these specimens experienced high levels of lateral load, buckling of shear wall studs was observed during the last cycle of loading, as shown in Figure 8.14.

8.3.2   Load-Displacement Behavior and Evaluation of Test Results

Figure 8.15 shows the load-displacement curve of the two lower story shear walls for each specimen. The load values presented in these plots are the total lateral forces applied by the actuator to the specimens divided by the 1.22 m length of wall panels, while the displacement values are the lateral displacements recorded at the top level of each wall panel. Design parameters obtained using the EEEP model, load capacities and displacement values are presented in Table 8.2. These values were calculated considering both shear walls of each specimen. Maximum drift ratio values and load capacities per sheathing are also shown in Figure 8.16 for an easier comparison.

The plots in Figure 8.15 and Figure 8.16 indicate that specimens, WA-5, WA-6, WA-7 and WA-8 possessed higher load capacity than the others. In terms of lateral displacement, specimens WA-1, WA-5 and WA-6 experienced smaller deformation capacity than the rest of the specimens. Specimen WA-2 obtained lower load capacity values compared to the other specimens, given that only this specimen utilized shear walls with 150/300 mm fastener spacing. Comparing load values per sheathing for other specimens, it can be seen that specimens with two side sheathed shear walls (WA-5, WA-6, WA-7, WA-8) acquired lower load capacity values. This is due to the fact that wall panels with double sided sheathing generally fails due to buckling of boundary stud members. As a result, when load capacity per sheathing values are compared, specimens with single side sheathed shear walls obtained higher load capacity values.

190

A comparison of specimens utilizing shear walls with double sided sheathing and 50/100 mm screw spacing indicate that the load capacity values for these specimens are quite similar, while the same is not valid for drift capacities. Specimens WA-7 and WA-8, which utilized ledger framing, were able to reach higher drift values compared to specimens WA-5 and WA-6, which utilized platform framing detail-2. This can be attributed to the difference in the force transfer mechanism for these two types of framing details. In the case of ledger framing, there is a more direct lateral load transfer from floor members to shear walls than in platform framing. Moreover, in the case of platform framing, multiple members within the floor-wall connection region experience deformations, which negatively affects the overall structural performance.

Comparison of cyclic backbone and EEEP curves for wall panels of specimens WA-3 and WA-4 are presented in Figure 8.17. These two specimens represent platform framing detail-1 and detail-2, respectively and both of them consisted of wall panels with single side sheathing and 50/100 mm screw spacing configurations. It can be seen that based on the cyclic backbone and EEEP curves, these two specimens showed quite similar results. However, the displacement experienced by the floor system in these two specimens differ significantly. Displacement experienced by the floor system was determined by calculating the difference between lateral displacements measured at floor level and at the top level of shear walls. Deformation of the floor system was smaller for specimen WA-4, which utilized platform framing detail-2. The reduced deformation of the floor system in the specimen with platform framing detail-2 than that with platform framing detail-1 is because of the fact that CFS profiles located within the floor-wall connection region in platform framing detail-2 were fastened to floor trusses and sheathed with OSB board.

In order to compare the responses with platform framing detail-2 and ledger framing, results obtained from specimens WA-5, WA-7 and WA-8 are presented in Figure 8.18. It can be seen that specimens with ledger framing acquired slightly higher load capacity and drift ratio values. Additionally, lateral deformation of the floor system was higher for specimen WA-5, which utilized platform framing. Between the two specimens with ledger framing, the floor system in WA-8 experienced smaller lateral deformation than that in WA-7, which can be attributed to the presence of the additional CFS profile at the bottom level of the ledger member in specimen WA-8.

Table 8.1 Details of 3-d assembly specimens

Specimen	Floor Framing Detail	Sheathing	Screw spacing (mm)	Gravity load (kN)
WA-1	Platform framing detail-1	Single side	50/100	16
WA-2	Platform framing detail-1	Single side	150/300	16
WA-3	Platform framing detail-1	Single side	50/100	16
WA-4	Platform framing detail-2	Single side	50/100	16
WA-5	Platform framing detail-2	Double side	50/100	16
WA-6	Platform framing detail-2	Double side	50/100	32
WA-7	Ledger framing	Double side	50/100	16
WA-8	Ledger framing	Double side	50/100	16

Table 8.2 Test results for 3-d assembly specimens

Specimen		P_{peak} (kN/m) Push	P_{peak} (kN/m) Pull	Δ_{peak} (mm) Push	Δ_{peak} (mm) Pull	Δ_u (mm) / % drift Push		Δ_u (mm) / % drift Pull		P_{yield} (kN/m) Push	P_{yield} (kN/m) Pull	Δ_y (mm) Push	Δ_y (mm) Pull	K_e (kN/m/mm) Push	K_e (kN/m/mm) Pull	K_e (kN/m/mm) Average
WA-1	Wall 1	45.0	-40.0	49.7	40.0	50.0	2.0	41.0	1.7	34.7	31.0	23.5	17.7	1.50	1.70	1.60
	Wall 2			51.0	43.0	51.6	2.1	43.8	1.8	37.9	31.3	32.8	19.4	1.15	1.60	1.38
WA-2	Wall 1	25.0	-19.0	73.0	64.0	73.0	3.0	64.0	2.6	19.3	16.2	32.3	26.4	0.60	0.61	0.61
	Wall 2			64.0	36.0	64.0	2.6	43.5	1.8	19.3	15.4	24.2	14.8	0.80	1.00	0.90
WA-3	Wall 1	53.0	-50.0	73.2	73.0	75.6	3.1	93.0	3.8	44.0	44.2	35.8	35.0	1.23	1.26	1.25
	Wall 2			56.0	57.6	56.0	2.3	62.0	2.5	42.5	42.5	28.0	27.3	1.53	1.56	1.55
WA-4	Wall 1	58.0	-45.0	73.3	58.0	73.3	3.0	58.0	2.4	46.0	38.5	36.6	25.7	1.26	1.50	1.38
	Wall 2			66.2	64.0	67.7	2.8	64.0	2.6	44.8	39.4	29.2	26.8	1.50	1.50	1.50
WA-5	Wall 1	73.0	-68.6	61.0	49.0	61.0	2.5	49.0	2.0	62.8	58.0	37.0	34.2	1.70	1.70	1.70
	Wall 2			59.4	48.5	59.4	2.4	48.5	2.0	63.8	58.7	39.3	32.5	1.63	1.80	1.72
WA-6	Wall 1	70.4	-70.0	54.7	49.0	54.7	2.2	49.0	2.0	59.0	59.3	32.0	35.2	1.85	1.70	1.78
	Wall 2			54.5	48.0	54.5	2.2	48.0	2.0	64.6	57.2	40.4	25.8	1.60	2.20	1.90
WA-7	Wall 1	79.7	-76.7	72.3	72.5	84.0	3.4	72.5	3.0	71.2	68.3	47.4	51.2	1.50	1.30	1.40
	Wall 2			77.8	72.0	90.0	3.7	72.0	3.0	70.8	63.2	49.0	35.8	1.40	1.80	1.60
WA-8	Wall 1	82.5	-78.2	68.6	64.0	68.6	2.8	64.0	2.6	73.2	74.0	50.0	50.0	1.46	1.48	1.47
	Wall 2			67.5	77.0	67.5	2.8	77.0	3.2	72.2	74.0	44.6	52.0	1.62	1.42	1.52
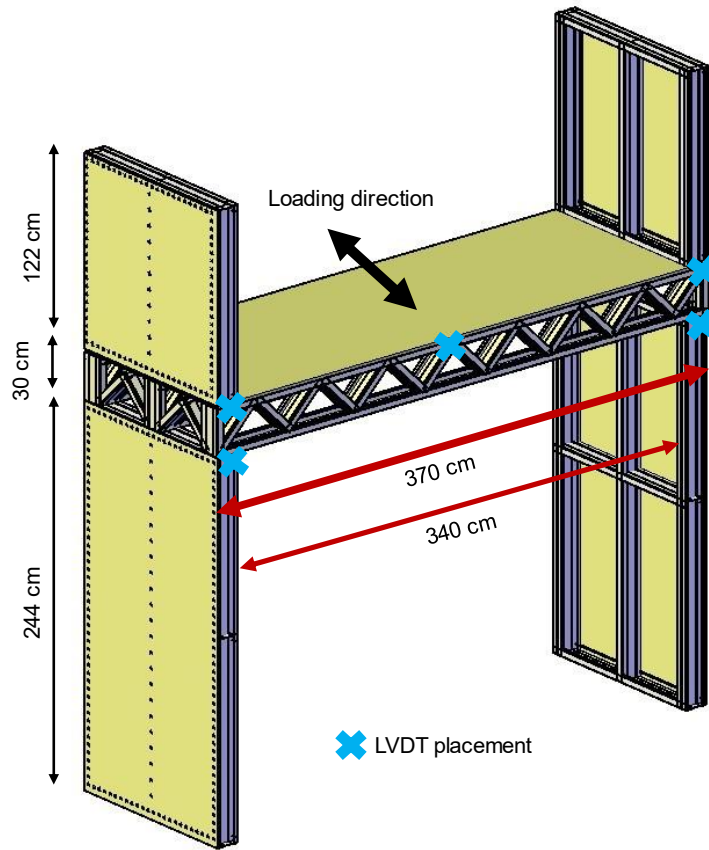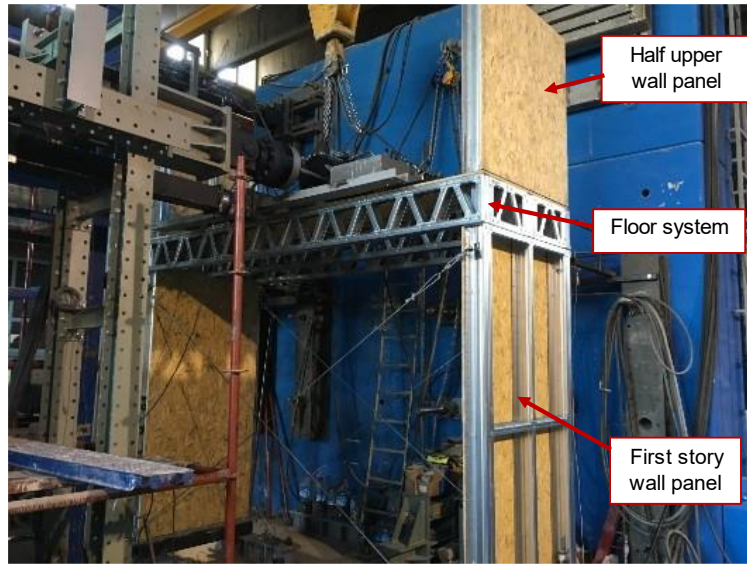
Figure 8.1 General view of a 3-d assembly specimen
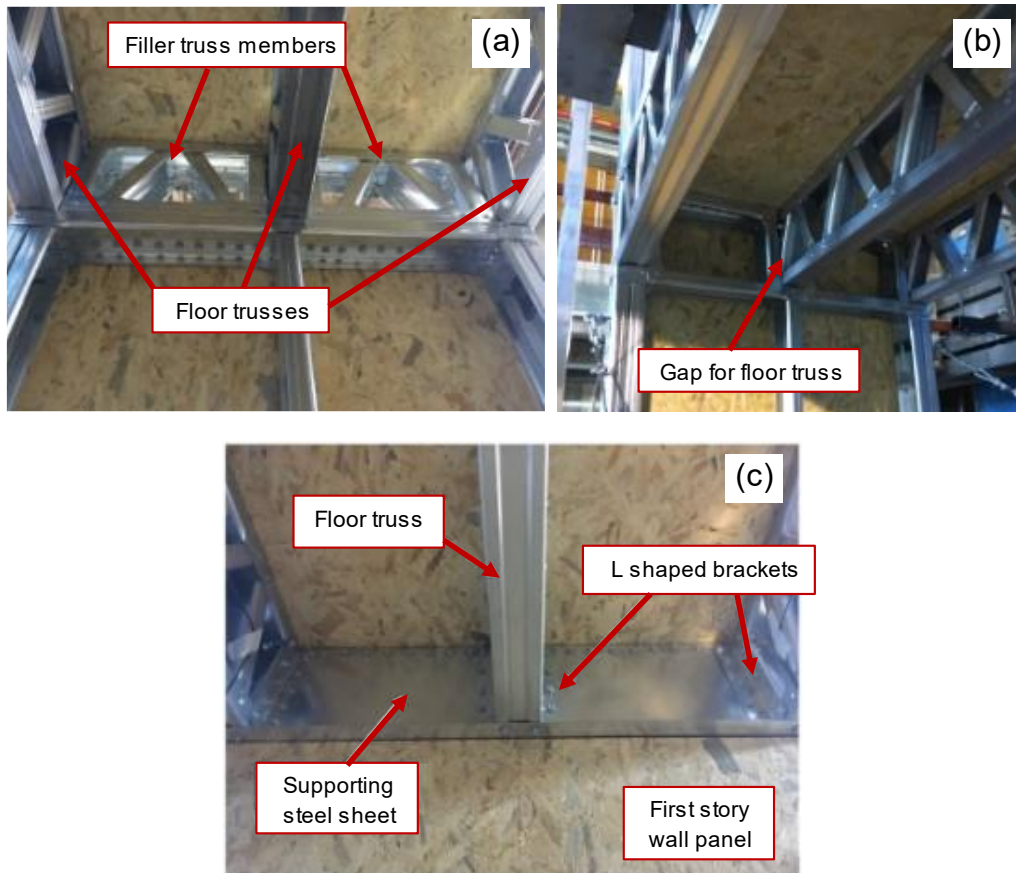
Figure 8.2 Details of different floor framings: (a) platform framing detail-1; (b) platform framing detail-2; (c) ledger framing
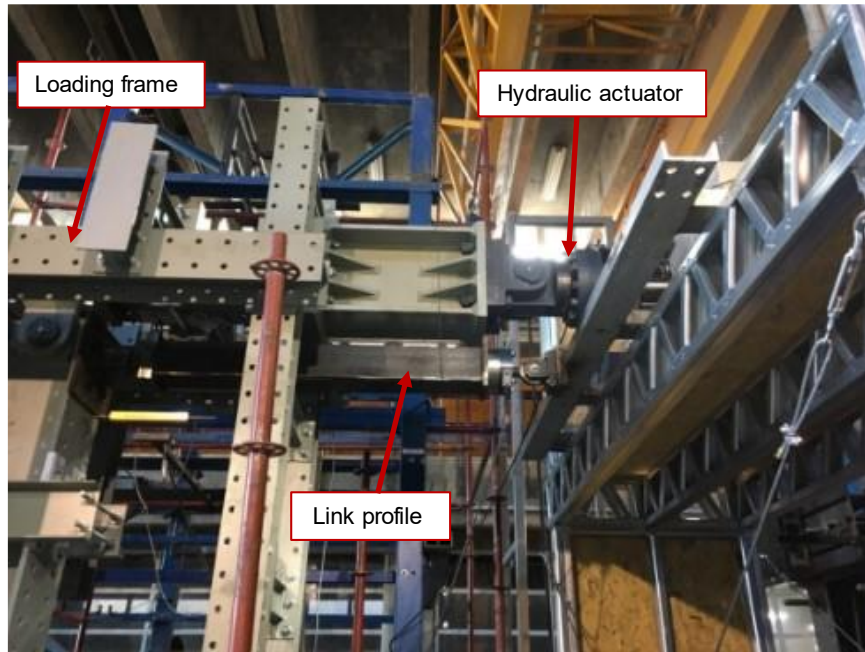
Figure 8.3 Test setup details

Figure 8.4 Steel cables used for out-of-plane stability
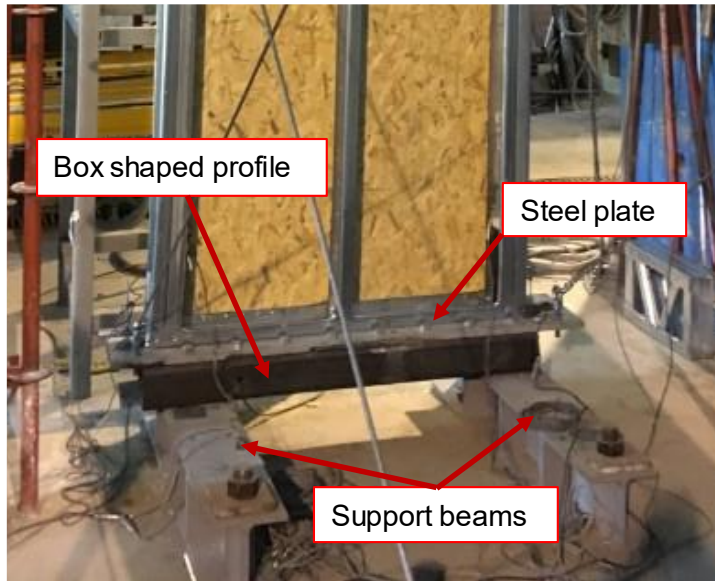
Figure 8.5 Details of wall panel-strong floor connection
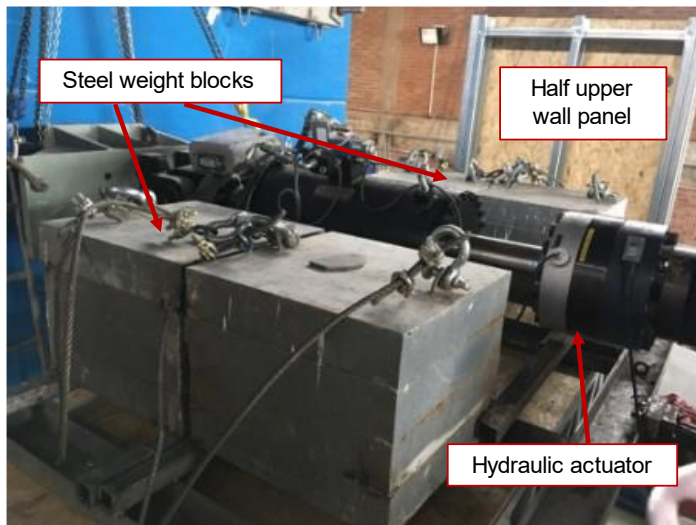
Figure 8.6 Placement of gravity loads

Figure 8.7 Deformations observed in specimen WA-1

First story
wall panel
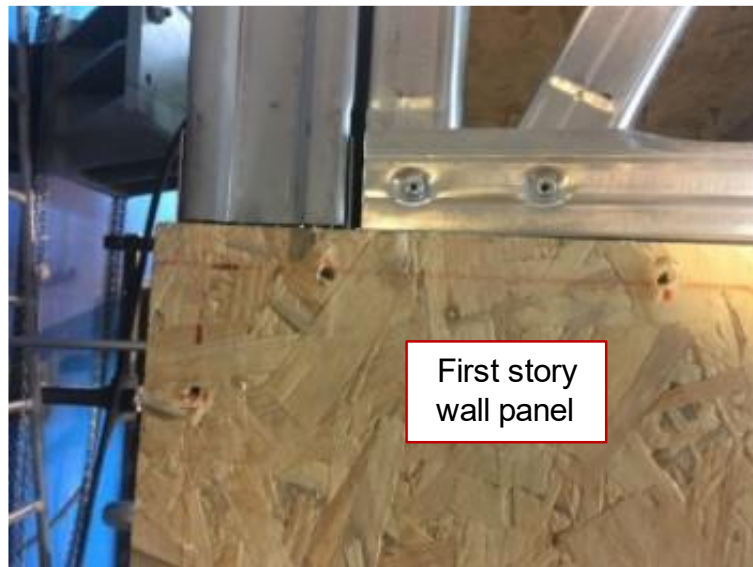
Figure 8.8 Pull through of screws in specimen WA-2
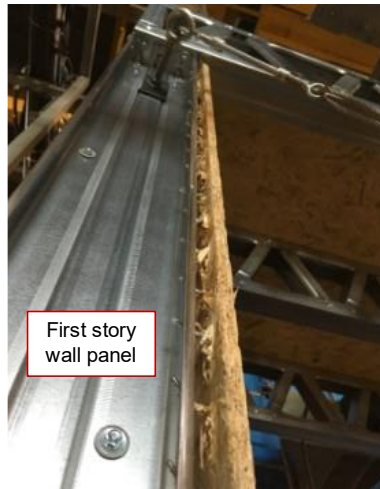
Figure 8.9 Failures observed in specimen WA-3

Figure 8.10 Failure of specimen WA-4

Figure 8.11 Deformations observed at platform framing of specimen WA-5
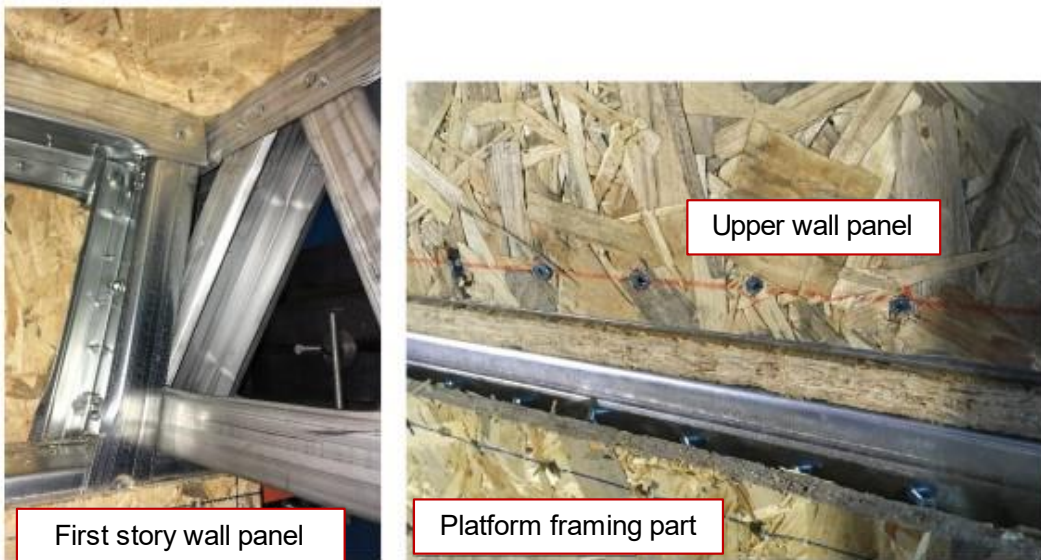
Figure 8.12 Failure of specimen WA-6
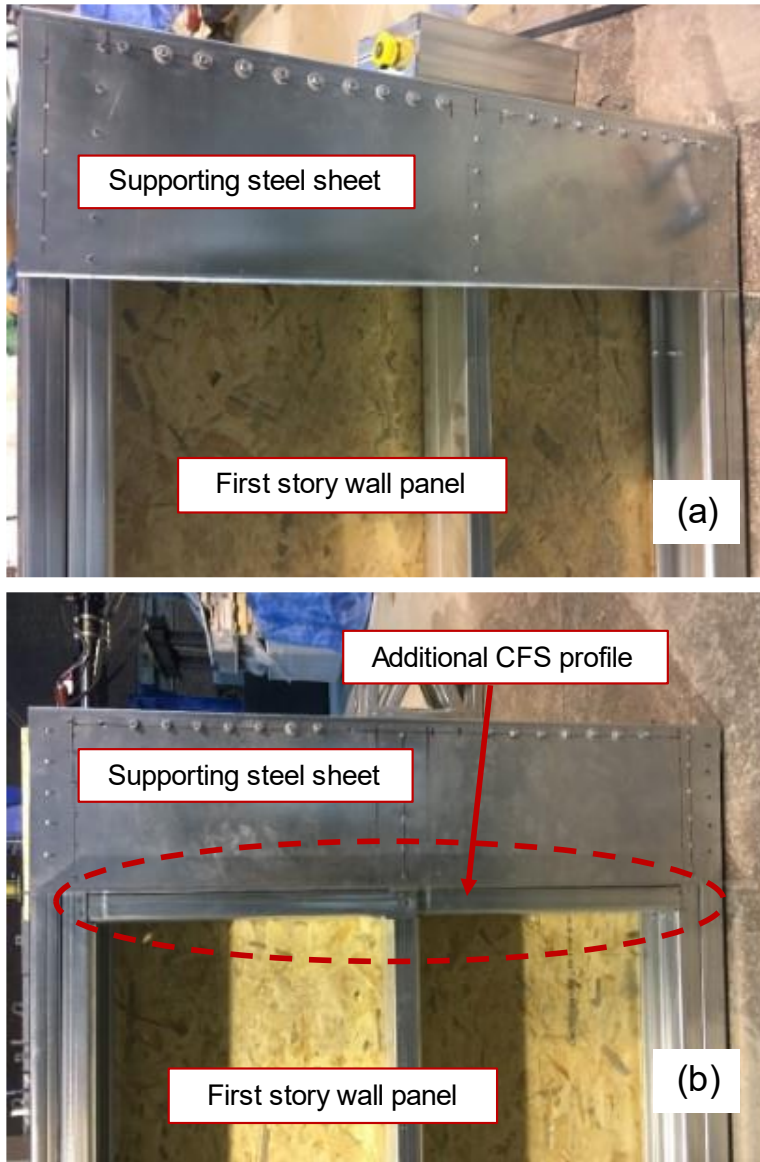
Figure 8.13 Ledger framing detail used: (a) for specimen WA-7; (b) for specimen WA-8

Figure 8.14 Buckling of studs observed in specimen WA-7
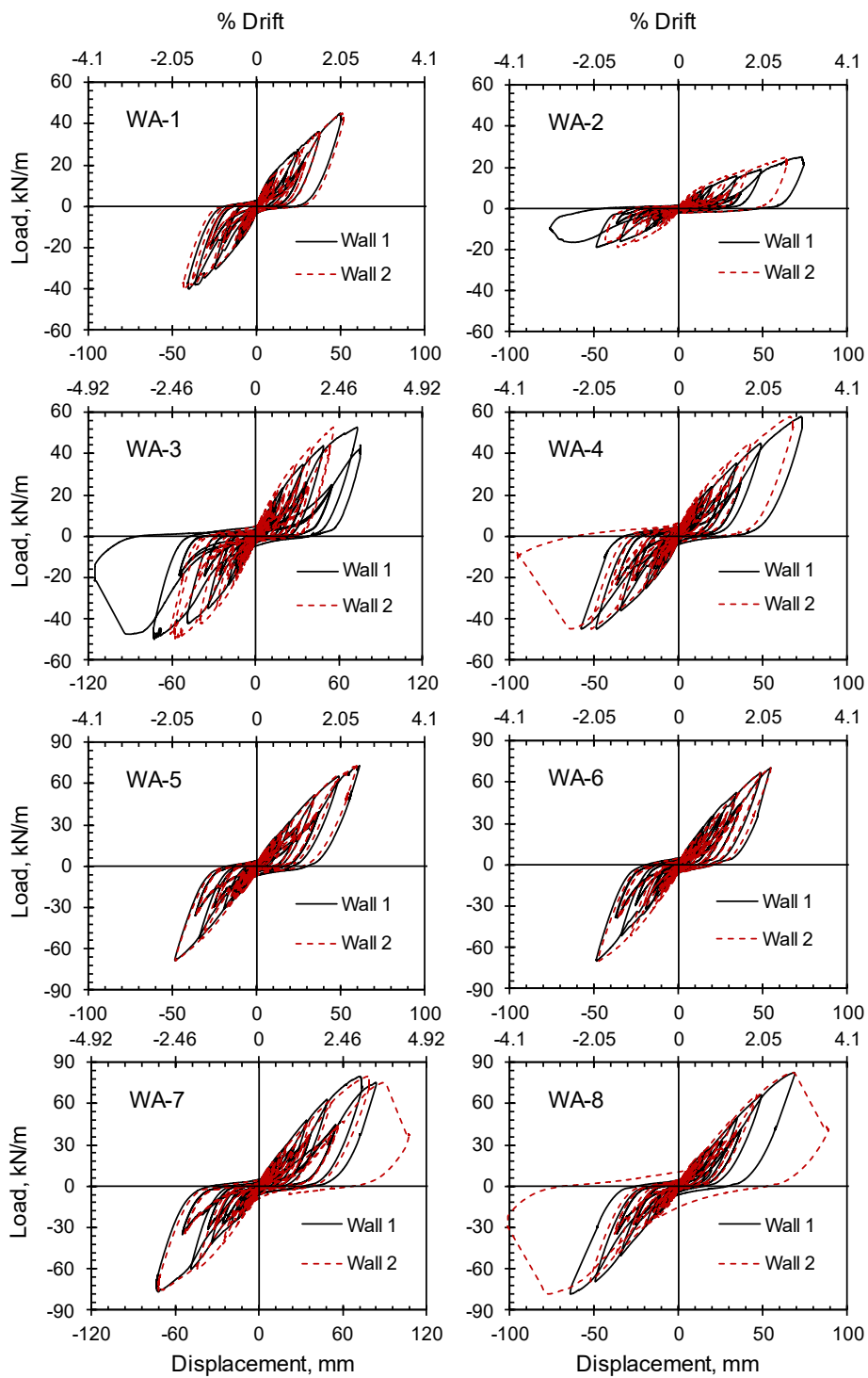
Figure 8.15 Load-displacement behavior of 3-d assembly specimens
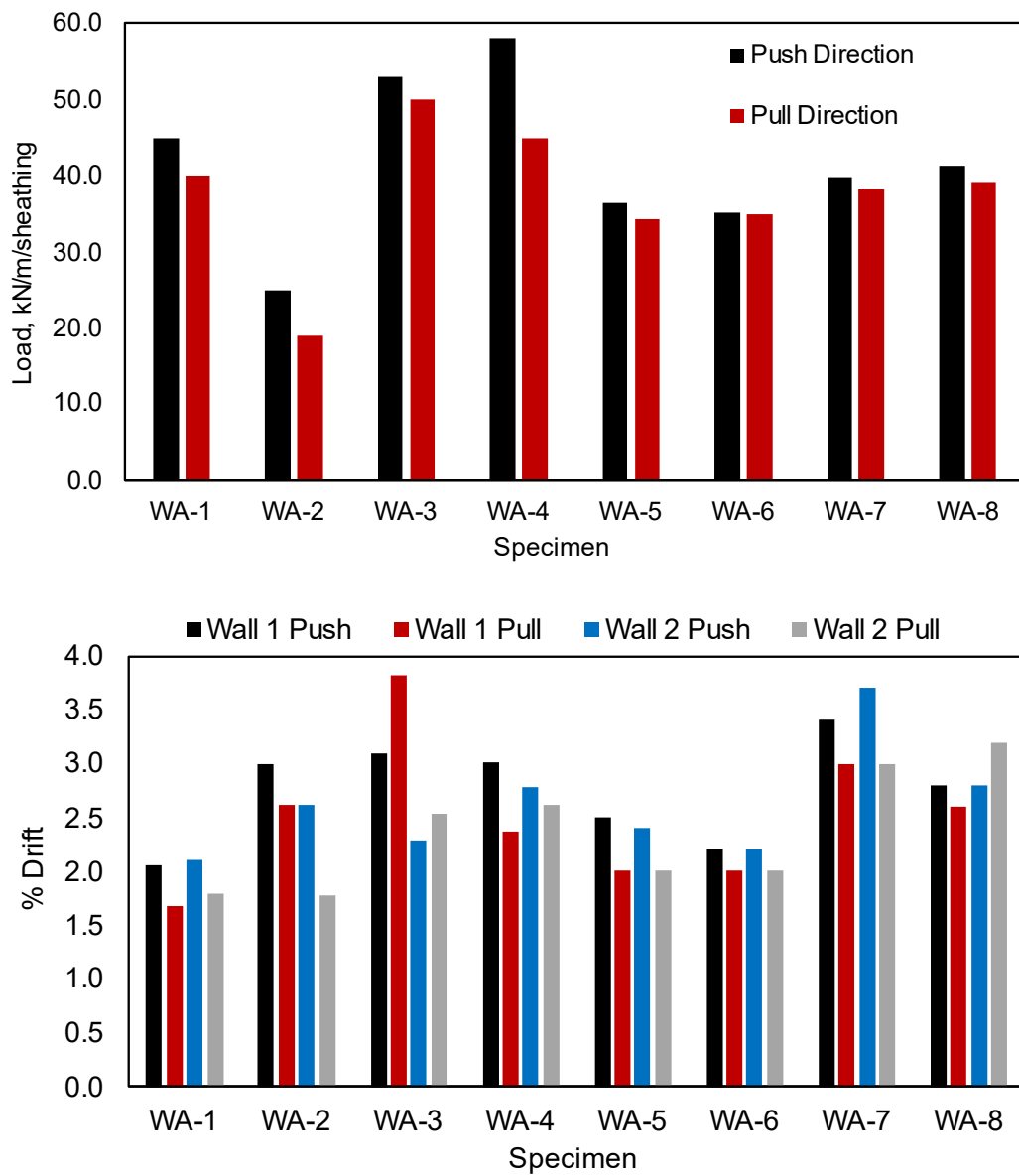
Figure 8.16 Load capacity and maximum drift ratio of 3-d assembly specimens
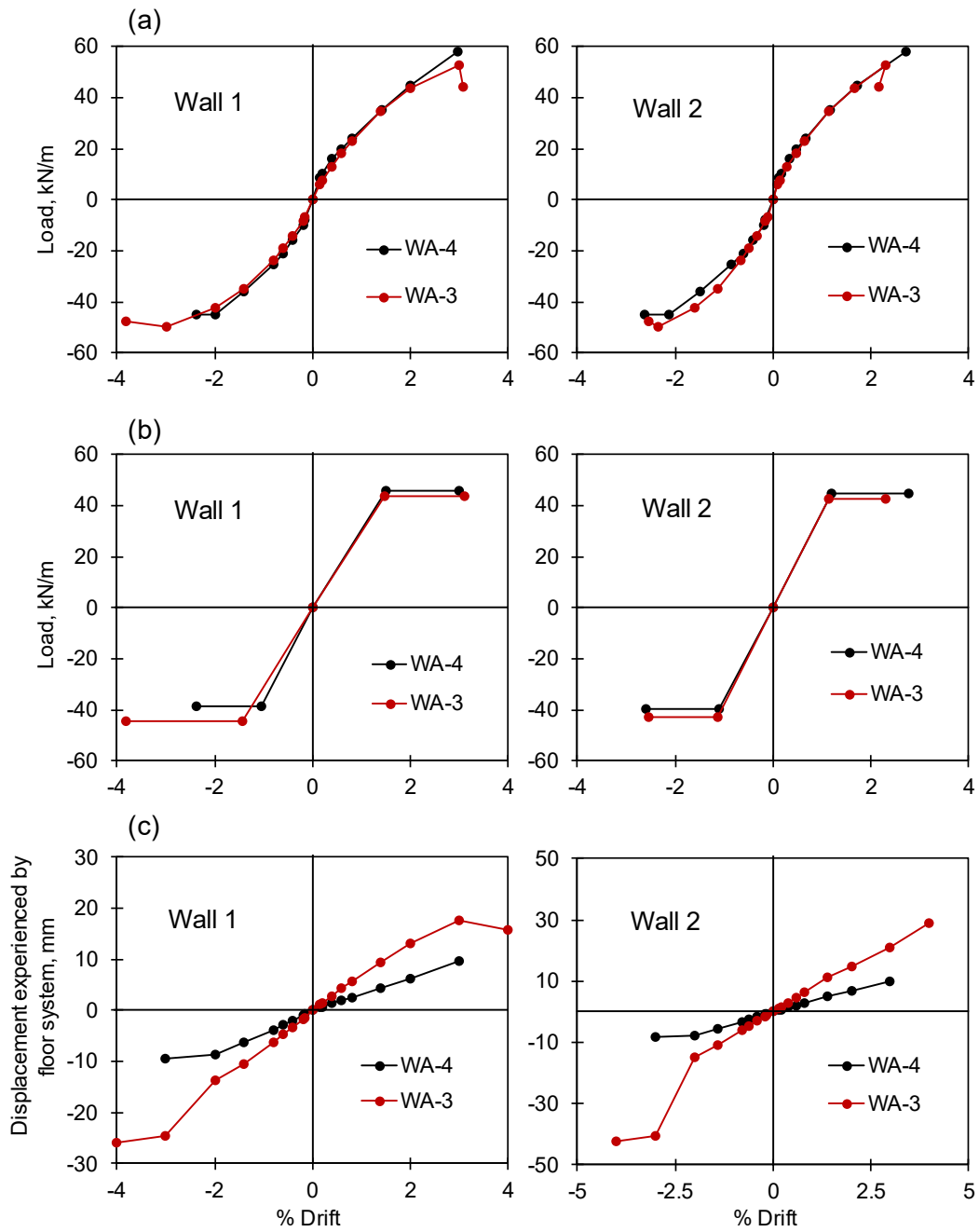
Figure 8.17 Comparison of specimens WA-3 and WA-4: a) cyclic backbone curves; b) EEEP curves; c) displacement experienced by floor system
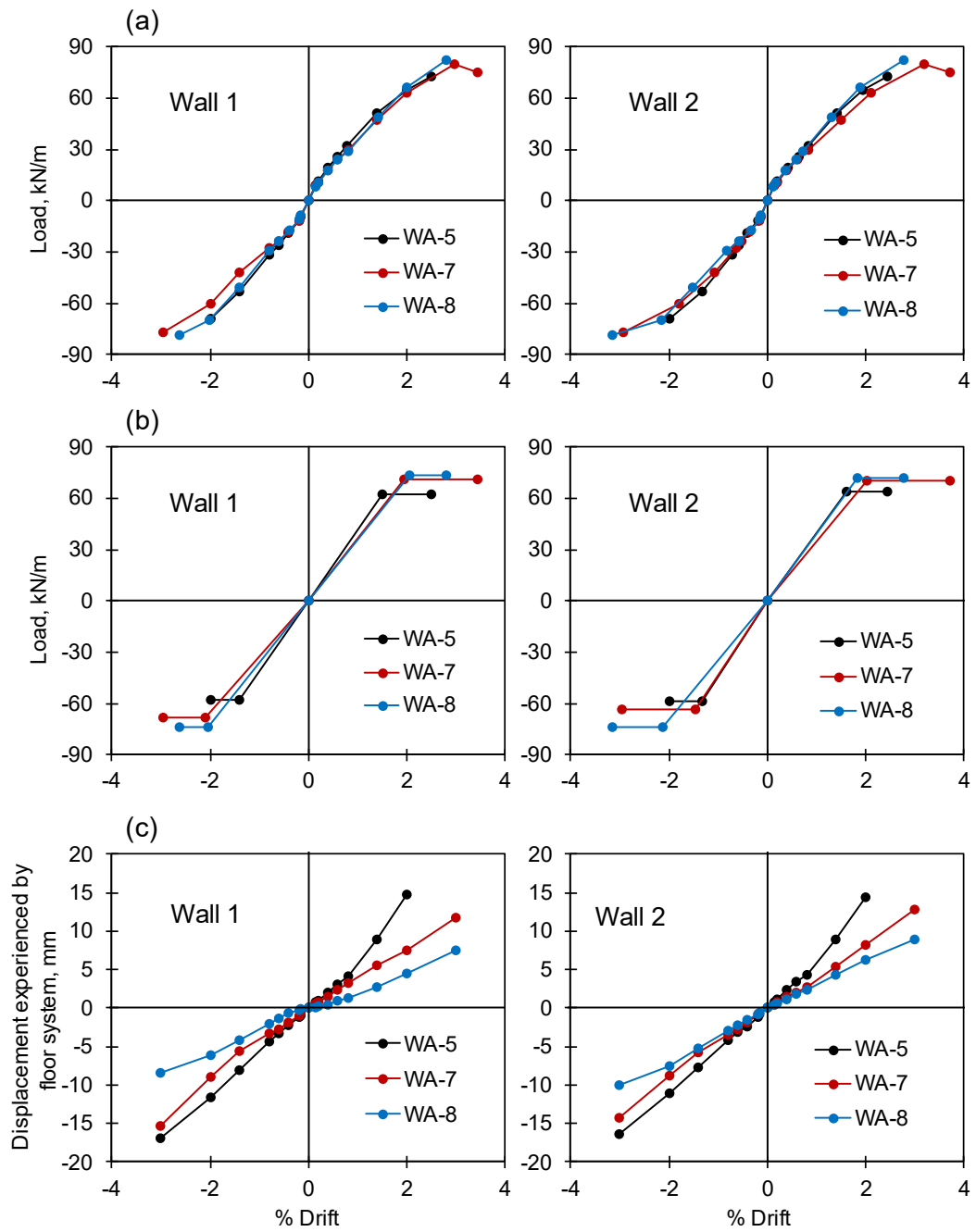
Figure 8.18 Comparison of specimens WA-5, WA-7 and WA-8: a) cyclic backbone curves; b) EEEP curves; c) displacement experienced by floor system

CHAPTER 9

SEISMIC PERFORMANCE EVALUATION OF COLD-FORMED STEEL BUILDINGS WITH DIFFERENT SHEAR WALL STRENGTHS AND STIFFNESSES ACCORDING TO FEMA P695 METHODOLOGY

9.1   Introduction

Seismic design provisions for CFS framed buildings are provided by several design standards around the world. These standards adopt capacity design rules in order to ensure elastic response of non-dissipative elements and sufficient energy dissipation in selected elements to develop plastic mechanisms, eventually resulting in a ductile behavior of the structure. The standards also describe a force reduction factor to be used in design against seismic actions to account for overstrength and ductility of the selected lateral force resisting system. This force reduction factor is described as response modification coefficient (R) in North American Standard for Seismic Design of CFS Structures AISI S400 (2015) and ASCE 7 (2017), while it is described as behavior factor (q) in Eurocode 8 (EN 1998-1, 2004). It is worth mentioning that while ASCE 7 specifies R values for CFS lateral force resisting systems, EN 1998-1 does not explicitly detail the seismic design procedure for structures with CFS walls.

North American standards specify the seismic design parameters to be used for structures with CFS framed wood sheathed shear walls. In USA and Mexico, it is allowed to use the response modification coefficient (R) as 6.5, system over-strength factor (Ω_o) as 3 and deflection amplification factor (C_d) as 4. In Canada, R value is designated as 4.25, C_d as 4.25 and Ω_E as 1.33. In the latest edition of the Turkish Seismic Design Code for Buildings (TBDY, 2018) R and Ω_o values are given as 4 and 2, respectively. The deflection amplification factor C_d is implicitly taken to be

equal to *R*. These values differ from the corresponding values in the North American standards, even though the majority of the provisions specified for CFS building systems in TBDY 2018 were adopted from these standards.

Federal Emergency Management Agency FEMA P695 (2009) methodology describes analytical methods and a procedure to evaluate the seismic performance of building systems. The procedure involves structural design of archetype buildings according to relevant specifications and by using selected response modification coefficient. Nonlinear models of these archetypes are then subjected to pushover analyses for determination of overstrength and ductility. The same archetypes are also subjected to nonlinear dynamic analyses with multiple ground motion records for evaluation in terms of collapse capacity. The FEMA P695 methodology allows for the evaluation of selected response modification coefficient for the selected lateral force resisting system.

The present study aims to investigate the seismic response of CFS framed archetype buildings utilizing OSB sheathed wall panels with different sheathing and fastener configurations (i.e., with different levels of wall strength and stiffness). Studies on seismic collapse analysis of buildings with OSB sheathed CFS framed shear walls are either limited with walls sheathed on one side with 150/300 mm fastener spacing (Landolfo et al., 2022b; Leng et al., 2020; Shakeel et al., 2020b), or do not provide an analysis of the influence of shear wall strength and stiffness on building response (Kechidi et al., 2017). The current study aims to fill this gap in the literature. Objectives of this study can be summarized as follows: (i) evaluate the seismic performance of CFS buildings through nonlinear dynamic analyses, (ii) determine the effect of utilizing shear walls sheathed with OSB panels on both sides and closely spaced fasteners on collapse performance and response modification coefficient of building system, (iii) conduct FEMA P695 collapse performance evaluation and obtain suitable seismic response parameters for such building systems. In order to

reach these goals, a numerical study has been conducted on a total of 28 archetype buildings. Load-displacement hysteresis behaviors of wall panels measured in a recent experimental study were adopted to simulate the shear wall response in the numerical models utilized in the present study.

9.2   Details of Archetypes

The response modification coefficient, occupancy type, number of stories, number of sheathing panel and number of fasteners were considered as variables in the design of archetypes. A total of 28 archetypes, details of which are given in Table 9.1, were taken into account. Archetypes were designed to have either office type or residential type of occupancies. Most of the archetypes had two stories, while some three story residential archetypes were also considered. These variables were also considered while naming the archetypes such as; "O" stands for office, "R" stands for residential, "W" describes the type of shear wall used in the building and S indicates the number of stories for residential type archetypes. In nine of the office archetypes different types of wall panels were utilized in two floors. In these cases, wall panels with smaller strength and stiffness were considered at the second floor than those at the first floor. Variation in wall strength and stiffness was achieved by changing the number of sheathing panel as well as the number of fasteners providing connection between CFS framing and sheathing panels, as discussed earlier.

The archetype naming convention given in table indicates the occupancy type, the response modification coefficient used in design, the type of shear walls and the number of floors. For example, O6.5W3-1 designates the office type archetype designed with a response modification coefficient of R=6.5 and includes SW3 type shear walls at the first floor and SW1 type shear walls at the second floor. Similarly, R3S-4W2 designates the three-story residential archetype designed with a response modification coefficient of R=4 and with W2 type shear walls at all floors.

9.2.1 Occupancy Type and Height of Buildings

Two types of occupancies, namely office and residential were considered for archetype buildings with different structural plans, framing span lengths and live loads acting on the structure. Floor plans shown in Figure 9.1 were considered for office and residential buildings based on the floor plans used in earlier studies (Landolfo et al., 2022b; Shakeel et al., 2020b). A typical story height of 2.74 m (i.e., 2.44 m wall height and 0.3 m floor height) was considered in building designs. All office building archetypes had two stories with a total height of 5.48 m, while residential building archetypes had either two or three stories with a total height of either 5.48 m or 8.22 m.

9.2.2 Seismic Hazard Level

FEMA P695 describes three main Seismic Design Categories (SDC) as B, C and D in accordance with ASCE 7-16. The methodology also describes earthquakes at two levels; Design Earthquake (DE) and Maximum Considered Earthquake (MCE) for each seismic design category. In the regular methodology, analyses are repeated for low, medium and high seismicity levels, however in the present study all archetypes were considered to be located in a high seismicity location. The analyses were conducted considering Seismic Design Category D_{max}, which represents the highest possible seismic condition. For SDC D_{max}, values of the MCE spectral response acceleration parameter S_{MS} and design spectral response acceleration parameter S_{DS} were adopted respectively as 1.50g and 1.0g.

9.2.3   Details of Shear Walls

Three different CFS shear wall types, whose load-displacement behavior under lateral loading were investigated in the previous parts of the thesis and designated as SW1, SW2 and SW3 were used for the lateral load resisting system of archetype structures. As described before, each wall panel is 1.22 m in length and 2.44 m in height and sheathed with 11 mm thick OSB panels that are connected to wall framings with 4.2 mm diameter screws. Framing of wall panels consists of 1.2 mm thick 140 mm deep C-shaped sections that are made of S350 grade steel. Each shear wall type represents a different level of shear strength and stiffness. SW1 has single-sided OSB sheathing with 150 mm screw spacing at panel edges. This spacing represents the maximum spacing value provided in AISI S400-15 Nominal Shear Strength Table E1.3-1 and results in the lowest shear strength among three shear walls utilized in the present study. Shear wall SW2 has single-sided OSB sheathing with a relatively small screw spacing of 50 mm. Shear wall SW3 on the other hand, has OSB sheathing on both sides of the panel with 50 mm screw spacing, producing the largest shear strength and stiffness of all three wall configurations. The experimentally determined load-displacement hysteresis behaviors of the three shear walls are given in Figure 9.2. Superimposed on the plots in Figure 9.2 are cyclic backbone curves and bilinear load-displacement curves determined based on the Equal Energy Elastic-Plastic (EEEP) method as specified in AISI S400-15 (2015). The relatively flexible response of shear walls is evident in the plots. For the three wall panels, the drift ratio at first yield ranges from 1.0% to 2.0% and the drift ratio at maximum load capacity ranges from 2.6% to 3.0%.

Since the OSB sheathed CFS shear walls constitute the main lateral load resisting components in the investigated archetype buildings, their behavior in terms of stiffness and shear strength directly affects the overall seismic performance of buildings. The experimentally determined stiffness and shear strength of the three

shear wall types considered for the analyses are given in Table 9.2. The table presents elastic stiffness K_e, yield load capacity P_y and design load capacity P_{design} obtained from the EEEP approach (AISI S400-15, 2015). The maximum load capacity P_{max} obtained from tests and nominal shear strength calculated according to AISI S400-15 (2015) are also provided. Load capacities obtained for shear walls SW1 and SW2 are in good agreement with codified values. AISI S400-15 (2015) suggests that with double-sided sheathing, load capacity of a wall panel can be considered to be two times the nominal shear strength of a single side sheathed panel provided that minimum stud and track thickness and fastener size requirements are satisfied. For shear wall SW3 however, buckling of end studs prevented the wall panel to reach the codified shear strength value as explained in previous chapters. It should be noted that the amount of changes in wall stiffness and shear strength differ among the three wall panels. For instance, decreasing the screw spacing from 150 mm (in SW1) to 50 mm (in SW2) results in three times increase in shear strength of the wall panel, however the increase in wall stiffness is only 1.6 times. The relation between shear wall stiffness and load capacity is a parameter of significant importance for performance evaluation of CFS building systems, and the effect of this parameter has not been investigated so far. For this reason, the shear wall type was considered as the main parameter in the current study.

9.3   Archetype Design

All archetype structures were designed using relevant parts of ASCE 7-16 (2017), AISI S100 (2016) and AISI S400-15 (2015). As defined in ASCE 7, a floor live load of 2.4 kPa was considered for office buildings, whereas for residential buildings a floor live load of 1.9 kPa was used. In addition to that, roof slab in residential buildings was considered to be accessible while an inaccessible roof slab was considered for office buildings. Roof live load was taken as 1.9 kPa and 1.0 kPa,

respectively for residential and office buildings. Two sets of dead loads were adopted for office and residential buildings as shown in Table 9.3. These values are similar to the loadings used earlier by other researchers in analysis of CFS building systems (Landolfo et al., 2022b; Shakeel et al., 2020b; Shamim and Rogers, 2015a).

The archetypes were designed by adopting three different response modification coefficients of $R = 6.5$, 5 and 4, and with a deflection amplification factor $C_d = 4$. The R values of 6.5 and 4 are upper and lower bound values described in specifications covering CFS wood sheathed shear walls (i.e. $R = 6.5$ for the USA, $R = 4.25$ for Canada and $R = 4$ for Turkey). The deflection amplification factor C_d is specified as 4 for the USA and Turkey and 4.25 for Canada. In the current study the value of $C_d = 4$ was adapted.

As part of the seismic design procedure, the required number of shear walls for each archetype structure was determined based on the calculated base shear. The approximate fundamental period T_a was calculated for two and three story archetype buildings as 0.17 s and 0.24 s respectively, by using Equation 9.1. With these period values the designed archetypes remain in the constant acceleration region of the response spectrum. Accordingly, seismic response coefficient C_s was calculated for each archetype building with the selected response modification coefficient by using Equation 9.2 and total base shear was calculated by using Equation 9.3. The number of required shear walls in each direction was then determined by dividing the base shear to design shear strength of selected wall panel type. The design shear strength of wall panels was calculated by multiplying the yield load capacities obtained from the EEEP method with the code specified resistance factor of 0.60. With the number of shear walls determined this way, an initial 3-D analysis model of each archetype building was created. As the second step, linear elastic analysis was performed for each archetype model with the seismic forces distributed over the height of building according to Equation 9.4.

$$T_a = C_t h_n^x \qquad\qquad\qquad\qquad [9.1]$$

$$C_s = \frac{S_{DS}}{\left(\frac{R}{I_e}\right)} \qquad\qquad\qquad\qquad [9.2]$$

$$V = C_s W \qquad\qquad\qquad\qquad [9.3]$$

$$F_x = V_d \frac{w_x h_x}{\sum_i^n w_i h_i} \qquad\qquad\qquad\qquad [9.4]$$

In Equations 9.1-9.4 C_t and x are approximate period parameters taken respectively as 0.0488 and 0.75, h_n is the structural height, S_{DS} is the design spectral response acceleration and was taken as 1.0 g, R is the response modification coefficient, I_e is the importance factor and was taken as 1, W is the effective seismic weight, V_d is the total design base shear, w_i and w_x are seismic weights assigned to level i and x, h_i and h_x are heights to level i and x from the base.

Interstory drift values obtained from elastic analysis were amplified by a deflection amplification factor of C_d=4 and were checked against the allowable interstory drift of 0.025h_{sx} per Table 12.12-1 of ASCE 7-16, where h_{sx} is the story height and taken as 2.74 m for all archetypes. The number of shear walls was increased as required to satisfy the interstory drift requirement. Other than archetypes in which shear wall type SW1 was used, interstory drift limit happened to be the governing criteria, and the number of shear walls was increased beyond what was required for strength requirement for these archetype buildings. For three office and two residential buildings with SW1 type shear walls, the number of shear walls calculated based on the base shear for each horizontal direction already satisfied the interstory drift limit. Table 9.1 shows number of shear walls provided for each archetype along with design base shear values and design shear strength of wall panels used at the first floor of the relevant building. The required number of shear walls decreases with

increasing values of response modification coefficient, as shown in the table. In addition to that, archetypes designed with SW1 type walls required approximately two times more shear walls than those with SW2 type walls. Utilizing SW3 type walls further decreased the required number of shear walls slightly when compared to the archetypes with SW2 type walls.

9.4   Numerical Modeling of Archetypes

For a structure with CFS framed sheathed wall panels as the main lateral load resisting system, the overall nonlinear seismic response is dictated by the response of individual wall panels. For this reason, accurate representation of the nonlinear hysteretic response of wall panels has a crucial importance in numerical modeling. In the present study, nonlinear analysis of archetype buildings was conducted by using SAP2000 computer program. Modeling process consisted of two steps. First, single wall models for all three shear wall panels were created with available experimental data. Following that, these single wall models were utilized to create three dimensional models of archetype buildings.

9.4.1   Single Wall Panel Models

Single shear wall models were created for walls SW1, SW2 and SW3, and were calibrated with the available experimental test results. A representation of the numerical model is shown in Figure 9.3. Diagonal nonlinear link elements were used with a pivot type hysteresis behavior to represent pinched cyclic behavior of shear walls. Pivot model utilizes several parameters to create pivot points and control the degrading hysteretic loop. Points on the backbone curve along with model parameters were defined for each shear wall type to represent the cyclic behavior. The parameters used in the current study to define the pivot hysteresis model are

α_1=10, α_2=10, β_1=0.5, β_2=0.5, and η=0. Force and displacement values obtained from experimental testing were transformed by using Equations 9.5-9.7 and were used for calibration of hysteresis parameters.

$$cos\theta = \frac{W}{\sqrt{W^2 + H^2}} \qquad\qquad [9.5]$$

$$f = \frac{P}{2cos\theta} \qquad\qquad [9.6]$$

$$d = \Delta \times cos\theta \qquad\qquad [9.7]$$

where, θ, W, H, f, P and Δ are as indicated in Figure 9.3.

Linear frame elements with corresponding CFS section properties were used to represent stud and track members. Hold downs that are connecting shear walls to the foundation were modeled as zero-length nonlinear link elements. Multilinear elastic material property was assigned to these link elements based on the available experimental data on hold down devices. Hold down device presented in Chapter 4 was utilized in shear wall models. A tensile stiffness value of 10 kN/mm, which was determined based on experimental results, was used to represent the behavior of the hold down. In compression, a relatively large stiffness of 10000 kN/mm was used for hold down elements.

Load-displacement responses obtained from numerical models are compared with the experimentally determined responses in Figure 9.4 for all three wall panels. In order to facilitate the direct comparison between the two sets of results, the same cyclic loading protocol that was used in experimental testing was also utilized in wall numerical models.

9.4.2 Three-Dimensional Building Models

All structural elements, including CFS shear walls, studs, tracks and floor system were included in the building numerical models. All elements other than the shear walls were represented with linear elastic frame elements. A rigid diaphragm was defined at floor levels. Moment releases were defined at the ends of stud members to prevent any moment transfer from floor system to these members. Base of wall panels were connected to link elements that are representing hold down devices, while pin support condition was adopted at the base of the gravity load carrying studs. A representative building numerical model is shown in Figure 9.5.

Gravity loading consisting of 100% of dead load and 50% of live load was applied to each shear wall stud and gravity load carrying stud at story levels based on their tributary areas. Similarly, seismic mass, which was taken as 100% of dead load as per ASCE 7-16 (2017), was equally distributed to the top joint of each stud element. P-delta effect was included in all lateral load analyses. For dynamic analyses, Rayleigh damping ratio was considered to be 5%, which is the value adopted in previous studies (Kechidi et al., 2017; Leng et al., 2017, 2020).

9.5 Nonlinear Analyses

9.5.1 Nonlinear Static Analyses

According to FEMA P695 methodology, the first step in the evaluation of building performance is to perform a pushover analysis in order to determine archetype overstrength and period-based ductility. The period-based ductility is then used to determine spectral shape factor (SSF) that is used in dynamic analyses. Pushover analyses were conducted for each archetype by utilizing a lateral load distribution across height that is in proportion to the fundamental mode shape. Displacement-

controlled analysis was conducted with the central node at the top of the building being the controlling point.

Results from pushover analysis of nine office archetype buildings utilizing different wall panel types and designed with different response modification coefficients are presented in Figure 9.6 and Table 9.4. The pushover curves resemble the backbone curves defined for shear walls, as expected. This is due to the fact that the shear walls are the main lateral load resisting elements and the only source of nonlinearity in building models. However, it should be noted that the pushover curves shown in Figure 9.6 indicate the combined response from the first and second floor shear walls. The steep decline in the shear strength after the peak point for office archetypes with SW2 and SW3 type shear walls is related with the shape of backbone curves utilized for these walls. The sudden failure of walls SW2 and SW3 evident in Figure 9.4 leads to the abrupt reduction in lateral load capacity of corresponding buildings in Figure 9.6.

The design base shear, fundamental period and base shear obtained from analysis as well as overstrength and period based ductility for each archetype building are presented in Table 9.4. Overstrength factor Ω is the ratio of the maximum base shear obtained from pushover analysis V_{max} to design base shear V_d (Equation 9.8).

$$\Omega = \frac{V_{max}}{V_d} \qquad [9.8]$$

Another parameter that is obtained from pushover analysis is the period based ductility μ_T, which is defined as the ratio of ultimate roof displacement δ_{max} to the effective roof yield displacement $\delta_{y,eff}$ (Equation 9.9).

$$\mu_T = \frac{\delta_{max}}{\delta_{y,eff}} \qquad [9.9]$$

220

Ultimate roof displacement δ_{max} is the displacement at roof level at the point of 20% strength loss from maximum base shear on pushover curve (i.e. at a base shear of $0.8V_{max}$). Effective roof yield displacement $\delta_{y,eff}$ is computed using Equation 9.10 as defined in FEMA P695.

$$\delta_{y,eff} = C_0 \frac{V_{max}}{W} \left[\frac{g}{4\pi^2} \right] (\max(T, T_1))^2 \qquad [9.10]$$

Pushover analyses were conducted separately for the two principal directions of buildings, as indicated in FEMA P695. The Ω and μ_T values reported in Table 9.4 are the average of the values obtained in two principal directions. It should be mentioned that values obtained in two directions are almost the same due to the number of walls being identical in both directions for each archetype building.

Pushover analysis results indicate that the building models utilizing shear wall types SW2 and SW3 possess higher overstrength than those utilizing shear wall type SW1. This is due to the archetype design being governed by the strength requirement with SW1 shear walls and by the interstory drift requirement with SW2 and SW3 shear walls. Providing additional shear walls in order to meet the interstory drift requirement resulted in larger overstrength in the structural system in building models utilizing shear wall types SW2 and SW3. Overstrength values for each archetype are presented in Figure 9.7. As evident, while the archetypes utilizing only SW1 type shear walls possess overstrength factors of 2.1 – 2.3, utilizing SW2 and SW3 type shear walls leads to higher overstrengths of 3 – 3.8.

9.5.2   Nonlinear Dynamic Analyses

The second step of the performance evaluation in the framework of FEMA P695 is to perform non-linear dynamic analyses in order to determine collapse capacities of archetype buildings. The methodology utilizes incremental dynamic analysis (IDA),

in which selected ground motions are applied on archetype buildings with increasing scale of intensities. The median collapse intensity S_{CT} and the collapse margin ratio (CMR) values are then determined from the IDA results. S_{CT} is defined as the earthquake intensity level at which half of the applied ground motions cause collapse of the building. CMR is the ratio of S_{CT} to the maximum considered earthquake S_{MT}. CMR value is modified by spectral shape factor (SSF) to calculate adjusted collapse margin ratio (ACMR). ACMR of the archetype is compared with the target ACMR value to evaluate the performance of the building.

The approach that was used for dynamic analyses and performance evaluation in the present study is slightly different than the general FEMA P695 procedure. Instead of performing incremental dynamic analysis, in which archetypes are analyzed under a set of scaled ground motions, the ground motions were scaled up to the collapse level earthquake with a collapse margin ratio of 20%. This corresponds to the performance level defined by FEMA P695 as $ACMR_{20\%}$. While IDA is an effective method for design of new structural systems, scaling the ground motions with a predefined scaling factor deemed sufficient for the evaluation of existing buildings. Therefore, the latter approach was adopted in the current study. According to the FEMA P695 methodology, each individual archetype building is expected to have ACMR values larger than $ACMR_{20\%}$. The methodology describes another performance level corresponding to 10% collapse probability, indicated as $ACMR_{10\%}$. The average value of ACMR for a performance group is expected to be greater than $ACMR_{10\%}$. In the present study, each archetype building was analyzed individually without being part of a performance group due to varying shear wall types and different response modification coefficients. For this reason, only $ACMR_{20\%}$ level scaling was considered for performance evaluation. A similar approach has been adopted by other researchers for seismic performance evaluation of various structural systems (Kuşyılmaz and Topkaya, 2016; Landolfo et al., 2022b).

The far-field record set of FEMA P695 was used for dynamic analysis of archetype buildings. Far-field record set consists of 22 pairs of ground motions that were recorded at sites located greater than or equal to 10 km from the fault rupture. The ground motion pairs utilized in dynamic analyses are listed in Table 9.5. Response spectra for these 22 pairs of ground motions are shown in Figure 9.8a. Scaling of ground motion records starts by normalizing each ground motion record with respect to peak ground velocities using normalization factors defined in FEMA P695. Following this normalization, the ground motions were scaled up to MCE level, which is represented by $S_{MT} = 1.5$g at the approximate fundamental period T_a. An example MCE level ground motion scaling is given in Figure 9.8b. As evident, the median spectrum of the record set was anchored to MCE response spectra of seismic design category D_{max} at a period of $T_a = 0.175$ second. The MCE scaling factors were further increased by the calculated collapse margin ratios to reach collapse level earthquake with $CMR_{20\%}$. FEMA P695 provides Equation 9.11 in order to calculate collapse margin ratios. The 1.2 value in this equation is an amplification factor that is applied to CMR when dynamic analyses were executed with three-dimensional models, as suggested by FEMA P695. SSF is the spectral shape factor, which is a function of period-based ductility μ_T, and the fundamental period T_1. ACMR is dependent on total system collapse uncertainty β_{TOT}, which is calculated with Equation 9.12.

$$CMR = \frac{ACMR_{20\%}}{1.2 \times SSF} \tag{9.11}$$

$$\beta_{TOT} = \sqrt{\beta_{RTR}^2 + \beta_{DR}^2 + \beta_{TD}^2 + \beta_{MDL}^2} \tag{9.12}$$

The value of β_{TOT} depends on four uncertainty parameters; record-to-record uncertainty β_{RTR}, uncertainty due to design requirements β_{DR}, test data uncertainty

β_{TD} and modeling uncertainty β_{MDL}. In the present study quality rating of (B) Good was adopted, which led to β_{DR}, β_{TD} and β_{MDL} values to be equal to 0.2. The value of β_{RTR} was taken as 0.4, as the period based ductility values for all archetypes were larger than 3. As a result, total system collapse uncertainty was calculated to be 0.53, which corresponds to $ACMR_{20\%}$ value of 1.56 based on the Table 7-3 of FEMA P695. The SSF values and scaling factors determined with this procedure for each archetype are given in Table 9.4. Both SSF values and scaling factors do not change considerably between archetypes. SSF values range between 1.19 and 1.23, and scaling factors range between 1.90 and 2.08.

9.6   Analysis Results

9.6.1   Lateral Drift Response of Archetypes with Different Shear Wall Types

Nonlinear time history analysis results for one office archetype (O6.5W2) and one residential archetype (R3S-6.5W2) are provided in Figure 9.9 and Figure 9.10 as examples. Both of these two archetypes utilized SW2 type shear walls in all floors. The ground motion record pair selected to demonstrate the response of archetype buildings is ground motion #17, which is the record pair from the Superstition Hills 1987 Earthquake (i.e., records SUPERST/B-POE270 and SUPERST/B-POE360 records in Table 9.5). It should be mentioned that the response spectra for these two records closely follow the median response spectrum of the far-field record set, as shown in Figure 9.11. Interstory drift ratio time histories, overall base shear versus roof drift response of buildings, as well as the force versus drift response of individual shear walls in both principal directions are presented in Figure 9.9 and Figure 9.10, respectively for archetypes O6.5W2 and R3S-6.5W2. For both archetypes in both directions, first floor experienced higher seismic demand

224

compared to the other floors. Maximum recorded interstory drift ratios are 3.0% and 2.1% for office and residential archetypes, respectively. The response of the building in the long and short directions varies since ground motion records consist of two horizontal components with different response spectra. It should be mentioned that, even though the building responses shown in Figure 9.9 and Figure 9.10 represent one horizontal component of ground motion #17 acting in the long direction of archetype and the other component acting on the short direction, same results were obtained when two components of the ground motion changed directions, given that the same number of shear walls were provided for both long and short directions of each archetype as explained before.

The recorded drift profiles of office and residential archetypes at the instant of peak roof displacement are given, respectively in Figure 9.12a and Figure 9.12b. It is evident that an irregular drift profile occurs with lateral displacement localizing at the first floor when shear wall SW1 is utilized in both floors. In cases where SW2 or SW3 type shear walls are used at first floor and SW1 type shear wall is used at second floor, significantly larger drifts occur at second floor than at first floor. On the other hand, utilizing SW2 or SW3 type shear walls either alone or in combination results in regular distribution of lateral displacements among floors. Displacement profiles for office archetypes utilizing all three types of shear walls and designed with R values of 6.5, 5 and 4 are given in Figure 9.13. Irrespective of the R value adopted in design, lateral displacement is localized at first floor with SW1 type shear wall, while a more favorable drift distribution is obtained with shear walls SW2 and SW3. Detrimental effect of using SW1 type shear wall in second floor of an office archetype is shown in Figure 9.14. Significantly large lateral displacements experienced by these walls led to collapse of the second floor, indicated by large residual interstory drifts.

9.6.2   Performance Evaluation of Archetypes

Result of each of the 22 time history analyses conducted on each archetype building with ground motions scaled up to $ACMR_{20\%}$ level was evaluated by checking whether the analyzed archetype reached the failure condition. It should be noted that, due to the number of shear walls being the same in two principal directions, each ground motion component produces identical building responses in the long and short directions. For that reason, 22 time history analyses were performed for each archetype with each ground motion component acting in one principal horizontal direction. Previous studies in the literature on OSB sheathed CFS framed shear walls reported maximum drift ratios varying between 2 to 4%. A 4% drift ratio was achieved by individual shear walls utilizing 150 mm screw spacing in the study of Liu et al. (2014). Li (2012) reported the drift level of 3% for shear walls with 50 mm of screw spacing. Test results provided in Figure 9.2 also show that shear walls with single and double side sheathing and 50 mm screw spacing sustained drift values close to 4%. The same maximum drift ratio was also obtained with double side sheathed wall panels as described in Chapter 5. Moreover, the 4% interstory drift ratio limit was also utilized in previous numerical studies for OSB sheathed CFS framed shear walls (Landolfo et al., 2022b; Leng et al., 2020; Shakeel et al., 2020b). In order to be consistent with the current literature, the collapse criterion was adopted as the interstory drift ratio of 4% in this study. Table 9.6 and Table 9.7 summarize the results of nonlinear dynamic analyses, respectively for office and residential archetypes utilizing different shear wall types and designed with different response modification coefficients. The tables present the number of ground motion pairs that caused collapse for each archetype building. According to the methodology, the archetype fails to satisfy the target performance level when at least half of the ground motions cause collapse. Therefore, the archetypes were considered to fail when the 4% interstory drift ratio limit is exceeded for at least 11 pairs of ground motions.

As evident in Table 9.6 and Table 9.7, all archetype designs utilizing SW1 type shear walls failed to satisfy the performance criterion, irrespective of the response modification coefficient used at the design stage. This result is valid for both office and residential occupancies. As discussed earlier, these archetypes possess smaller overstrength than the rest of the buildings due to their design being governed by the lateral strength criterion as opposed to drift criterion. It is noteworthy that with the use of SW1 type shear walls as the lateral load resisting system, utilizing even a relatively small response modification coefficient of $R = 4$ results in inadequate design. Based on this observation, it can be stated that caution should be taken when using CFS shear walls sheathed with OSB panels on one side with 150 mm spaced fasteners as the sole lateral load resisting members in building systems. The unfavorable response of the SW1 type shear wall results from its relatively low lateral load capacity compared to its lateral stiffness in relation to the SW2 and SW3 type walls. Utilizing SW1 type shear walls also resulted in overstrength factors smaller than the code recommended value 3, which may prevent these buildings to achieve sufficient performance levels even with relatively small R values. The analysis results indicate that utilizing shear walls with smaller load capacity and stiffness at the second floor is generally an acceptable method. However, the use of SW1 type shear walls in combination with the other wall types adversely affected the building performance and the required collapse performance level was not satisfied for some of the investigated archetypes.

The results presented in Table 9.6 and Table 9.7 indicate that for buildings utilizing SW2 or SW3 type shear walls, response modification coefficients of $R = 5$ and 6.5 seem to be appropriate with a deflection amplification factor of $C_d = 4$, respectively for the office and residential archetypes. However, as shown in Table 9.6, the archetype O6.5W2 experienced collapse under 12 ground motion records out of the complete set of 22 motions. The response of this office building under ground motion record pair #7 is further investigated in Figure 9.15 in comparison with the

227

companion residential building (R2S-6.5W2). For the ground motion component acting in the long direction, neither building experienced failure, and responses are quite similar. In the short direction analysis, up to the maximum interstory drift values close to approximately 3.5%, the two buildings exhibited very similar responses with the office building experiencing slightly larger lateral displacements than the residential building. Such a slight difference in the lateral displacements led to the interstory drifts remaining below the 4% limit in the residential building while the office building passed beyond this limit. As evident in Figure 9.15b, reaching the 4% interstory drift value resulted in shear wall collapse in the office building and from that point forward the building experienced increasing drifts as the lateral load resisting mechanism was basically lost. Because the office archetype O6.5W2 experienced very similar response as the companion residential archetype R2S-6.5W2 with a slight difference in story drifts, O6.5W2 can also be considered as a "near pass". In that case, all office and residential archetypes designed with a response modification coefficient of $R = 6.5$ by utilizing SW2 and SW3 types of shear walls satisfy the FEMA P695 acceptability criteria.

It should be noted that the consideration of the deflection amplification factor C_d and the inelastic drift limit for buildings affected the results obtained in the present study. For archetype buildings where the number of wall panels is governed by drift limitation instead of strength requirement, overstrength values range between 3 and 3.75, and the average value is 3.3. This value is in good accordance with the code specified system overstrength value of $\Omega_o = 3.0$.

Using a relatively large R value, such as 6.5 as used in North America, is expected to result in a drift governed design, which eventually leads to higher overstrength. In a study by Shakeel et al. (2020), where OSB sheathed wall panels are used as lateral load resisting mechanism for CFS framed buildings similar to the present study, the reported overstrength values for archetypes that were designed with a behavior factor

228

2.5 range between 1.06 to 1.33. The discrepancy in the overstrength values from the current study and those reported by Shakeel et al. (2020) is due to the adaptation of drift requirement in the current study. The number of shear walls in some of the archetypes had to be increased due to the imposed drift requirement, which in turn led to higher overstrength levels. The R factor of 6.5 together with an overstrength of 3 indicates a ductility based response modification factor of 6.5/3 = 2.16. In the study by Shakeel et al. (2020) the corresponding ductility based response modification factor is 2.5/1.2 = 2.08. These results indicate that this type of structural system possess a ductility based response modification factor of approximately 2.0.

Table 9.1 Details of archetype buildings

Archetype	R	Wall Configuration	Occupancy Type	Building Height	Number of walls for each direction	Design shear strength of wall panel (kN)	Design base shear V_d (kN)
O6.5W1	6.5	SW1			24	6.75	150
O6.5W2	6.5	SW2			12	20.12	150
O6.5W3	6.5	SW3			10	31.70	150
O6.5W2-1	6.5	SW2-SW1			12	20.12	150
O6.5W3-1	6.5	SW3-SW1			12	31.70	150
O6.5W3-2	6.5	SW3-SW2			10	31.70	150
O5W1	5	SW1			30	6.75	194
O5W2	5	SW2			16	20.12	194
O5W3	5	SW3	Office	5.48 m (2-story)	12	31.70	194
O5W2-1	5	SW2-SW1			16	20.12	194
O5W3-1	5	SW3-SW1			14	31.70	194
O5W3-2	5	SW3-SW2			12	31.70	194
O4W1	4	SW1			36	6.75	243
O4W2	4	SW2			20	20.12	243
O4W3	4	SW3			14	31.70	243
O4W2-1	4	SW2-SW1			20	20.12	243
O4W3-1	4	SW3-SW1			18	31.70	243
O4W3-2	4	SW3-SW2			14	31.70	243
R2S-6.5W1	6.5	SW1			14	6.75	90
R2S-6.5W2	6.5	SW2			8	20.12	90
R2S-6.5W3	6.5	SW3		5.48 m (2-story)	6	31.70	90
R2S-4W1	4	SW1			22	6.75	147
R2S-4W2	4	SW2	Residential		12	20.12	147
R2S-4W3	4	SW3			10	31.70	147
R3S-6.5W2	6.5	SW2			12	20.12	142
R3S-6.5W3	6.5	SW3		8.22 m (3-story)	10	31.70	142
R3S-4W2	4	SW2			18	20.12	231
R3S-4W3	4	SW3			14	31.70	231

Table 9.2 Shear wall stiffness and strength values

	SW-1	SW-2	SW-3
K_e (kN/mm)	0.47	0.75	1.10
P_{yield} (kN)	11.25	33.54	52.80
P_{design} (kN)	6.75	20.12	31.68
P_{max} (kN)	14.15	38.7	57.34
Nominal shear strength per AISI (kN)	14.64	36.60	73.20

Table 9.3 Dead load values used in archetypes

Office				Residential			
Floor DL (kPa)		Roof DL (kPa)		Floor DL (kPa)		Roof DL (kPa)	
Floor system	1.4	Roof system	1.0	Floor system	1.2	Roof system	1.3
Vertical partitions	0.6	Ceiling	0.1	Vertical partitions	0.6	Ceiling	0.1
Ceiling	0.1			Ceiling	0.1		
Total	**2.1**	**Total**	**1.1**	**Total**	**1.9**	**Total**	**1.4**

Table 9.4 Nonlinear static analysis results, SSF values and scaling factors for archetypes

Archetype	T_1 (sec)	V_d (kN)	V_{max} (kN)	Ω (overstrength)	$\delta_{y,eff}$ (mm)	δ_u (mm)	μ_T	SSF	Scaling Factor
O6.5W1	0.55	150	341	2.3	22.0	77	3.5	1.21	1.93
O6.5W2	0.52	150	462	3.1	32.2	124	3.9	1.21	1.93
O6.5W3	0.52	150	563	3.8	39.8	133	3.4	1.20	1.95
O6.5W2-1	0.57	150	450	3.0	37.8	149	3.9	1.23	1.90
O6.5W3-1	0.54	150	495	3.3	39.0	137	3.5	1.21	1.93
O6.5W3-2	0.53	150	555	3.7	40.0	146	3.7	1.21	1.93
O5W1	0.50	194	428	2.2	21.7	75	3.5	1.20	1.95
O5W2	0.46	194	614	3.2	33.0	116	3.5	1.20	1.95
O5W3	0.47	194	669	3.4	37.8	136	3.6	1.20	1.95
O5W2-1	0.50	194	603	3.1	38.0	140	3.7	1.21	1.93
O5W3-1	0.49	194	583	3.0	36.0	136	3.8	1.21	1.93
O5W3-2	0.48	194	680	3.5	39.6	142	3.6	1.20	1.95
O4W1	0.40	243	510	2.1	21.0	73	3.5	1.20	1.95
O4W2	0.40	243	768	3.2	31.4	114	3.6	1.20	1.95
O4W3	0.44	243	782	3.2	41.0	133	3.2	1.19	1.97
O4W2-1	0.43	243	729	3.0	37.0	143	3.9	1.22	1.92
O4W3-1	0.44	243	753	3.1	38.0	138	3.6	1.20	1.95
O4W3-2	0.45	243	778	3.2	40.0	148	3.7	1.21	1.93
R2S-6.5W1	0.53	90	199	2.2	25.7	79	3.1	1.19	1.97
R2S-6.5W2	0.53	90	307	3.4	37.6	135	3.6	1.21	1.93
R2S-6.5W3	0.56	90	334	3.7	45.6	142	3.1	1.19	1.97
R2S-4W1	0.42	146	314	2.1	23.5	78	3.3	1.19	1.97
R2S-4W2	0.43	146	461	3.1	38.6	130	3.4	1.20	1.95
R2S-4W3	0.42	146	557	3.8	43.0	139	3.2	1.19	1.97
R3S-6.5W2	0.67	142	454	3.2	55.4	167	3.0	1.21	2.04
R3S-6.5W3	0.68	142	540	3.8	67.0	210	3.1	1.21	2.04
R3S-4W2	0.54	231	693	3.0	54.2	170	3.1	1.19	2.08
R3S-4W3	0.56	231	762	3.3	65.0	200	3.1	1.19	2.08

Table 9.5 FEMA P695 far-field ground motion record set

ID	Earthquake				Normalization Factor
	Magnitude	Name/Year	Component 1	Component 2	
1	6.7	Northridge/1994	NORTHR/MUL009	NORTHR/MUL279	0.65
2	6.7	Northridge/1994	NORTHR/LOS000	NORTHR/LOS270	0.83
3	7.1	Duzce,Turkey/1999	DUZCE/BOL000	DUZCE/BOL090	0.63
4	7.1	Hector Mine/1999	HECTOR/HEC000	HECTOR/HEC090	1.09
5	6.5	ImperialValley/1979	IMPVALL/H-DLT262	IMPVALL/H-DLT352	1.31
6	6.5	ImperialValley/1979	IMPVALL/H-E11140	IMPVALL/H-E11230	1.01
7	6.9	Kobe, Japan/1995	KOBE/NIS000	KOBE/NIS090	1.03
8	6.9	Kobe, Japan/1995	KOBE/SHI000	KOBE/SHI090	1.10
9	7.5	Kocaeli,Turkey/1999	KOCAELI/DZC180	KOCAELI/DZC270	0.69
10	7.5	Kocaeli,Turkey/1999	KOCAELI/ARC000	KOCAELI/ARC090	1.36
11	7.3	Landers/1992	LANDERS/YER270	LANDERS/YER360	0.99
12	7.3	Landers/1992	LANDERS/CLW-LN	LANDERS/CLW-TR	1.15
13	6.9	Loma Prieta/1989	LOMAP/CAP000	LOMAP/CAP090	1.09
14	6.9	Loma Prieta/1989	LOMAP/G03000	LOMAP/G03090	0.88
15	7.4	Manjil, Iran/1990	MANJIL/ABBAR--L	MANJIL/ABBA--T	0.79
16	6.5	SuperstitionHills/1987	SUPERST/B-ICC000	SUPERST/B-ICC090	0.87
17	6.5	SuperstitionHills/1987	SUPERST/B-POE270	SUPERST/B-POE360	1.17
18	7.0	CapeMendocino/1992	CAPEMEND/RIO270	CAPEMEND/RIO360	0.82
19	7.6	Chi-Chi, Taiwan/1999	CHICHI/HY101E	CHICHI/CHY101-N	0.41
20	7.6	Chi-Chi, Taiwan/1999	CHICHI/TCU045-E	CHICHI/TCU045-N	0.96
21	6.6	San Fernando/1971	SFERN/PEL090	SFERN/PEL180	2.10
22	6.5	Friuli, Italy/1976	FRIULI/A-TMZ000	FRIULI/A-TMZ270	1.44

Table 9.6 Nonlinear dynamic analysis results for office archetypes

Office Structure						
	SW1	**SW2**	**SW3**	**SW2&1**	**SW3&1**	**SW3&2**
R = 6.5 *C_d = 4*	**O6.5W1**	**O6.5W2**	**O6.5W3**	**O6.5W2-1**	**O6.5W3-1**	**O6.5W3-2**
	18 / 22 - FAIL	**12 / 22 - FAIL**	5 / 22 - PASS	**13 / 22 - FAIL**	**15 / 22 - FAIL**	5 / 22 - PASS
R = 5 *C_d = 4*	**O5W1**	**O5W2**	**O5W3**	**O5W2-1**	**O5W3-1**	**O5W3-2**
	14 / 22 - FAIL	5 / 22 - PASS	3 / 22 - PASS	11 / 22 - PASS	**12 / 22 - FAIL**	3 / 22 - PASS
R = 4 *C_d = 4*	**O4W1**	**O4W2**	**O4W3**	**O4W2-1**	**O4W3-1**	**O4W3-2**
	13 / 22 - FAIL	2 / 22 - PASS	2 / 22 - PASS	4 / 22 - PASS	8 / 22 - PASS	2 / 22 - PASS

Table 9.7 Nonlinear dynamic analysis results for residential archetypes

Residential Structure					
	2 - Story			**3 - Story**	
	SW1	**SW2**	**SW3**	**SW2**	**SW3**
R = 6.5 *C_d = 4*	**R2S-6.5W1**	**R2S-6.5W2**	**R2S-6.5W3**	**R3S-6.5W2**	**R3S-6.5W3**
	19 / 22 - FAIL	6 / 22 - PASS	4 / 22 - PASS	4 / 22 - PASS	3 / 22 - PASS
R = 4 *C_d = 4*	**R2S-4W1**	**R2S-4W2**	**R2S-4W3**	**R3S-4W2**	**R3S-4W3**
	12 / 22 FAIL	2 / 22 - PASS	1 / 22 - PASS	1 / 22 - PASS	4 / 22 - PASS

(a)

(b)
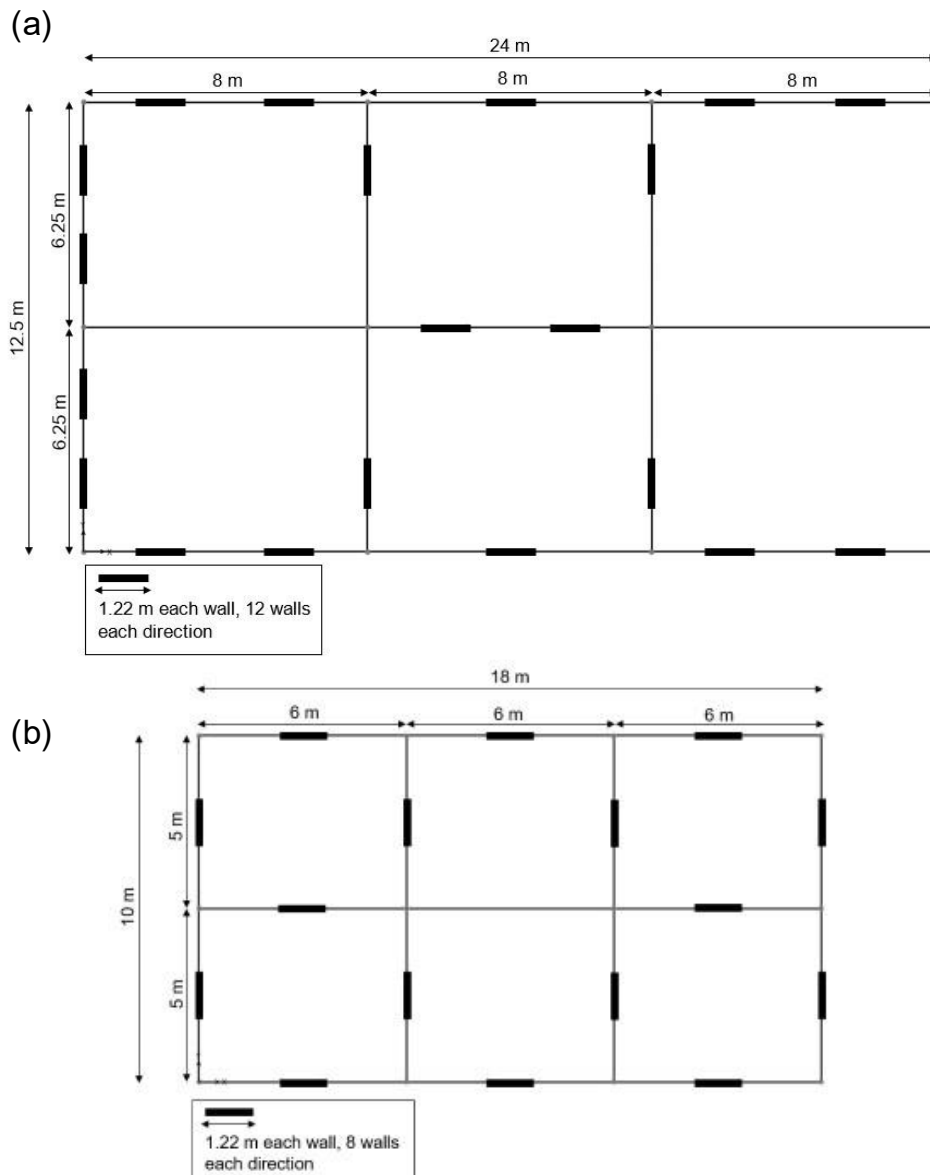
Figure 9.1 Floor plan of an example a) office building; b) residential building

235
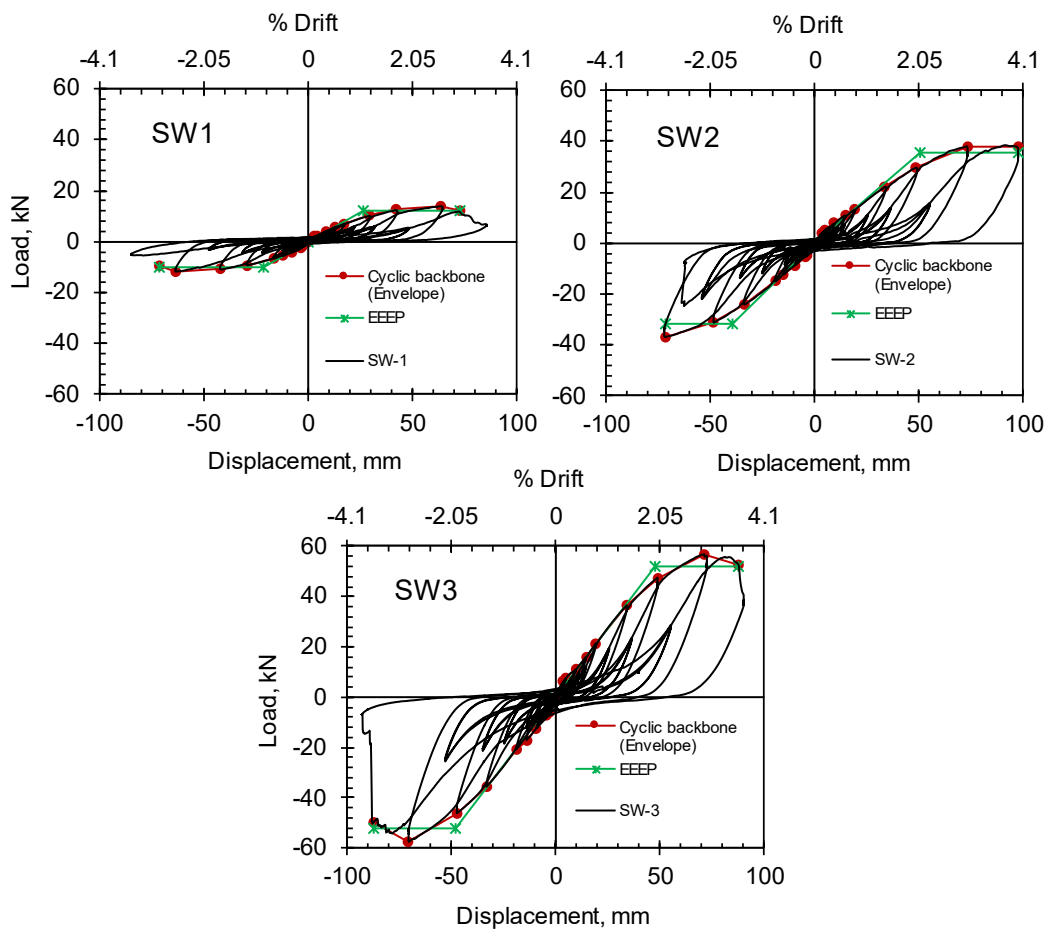
Figure 9.2 Load-displacement behavior of CFS shear walls used in archetype
buildings
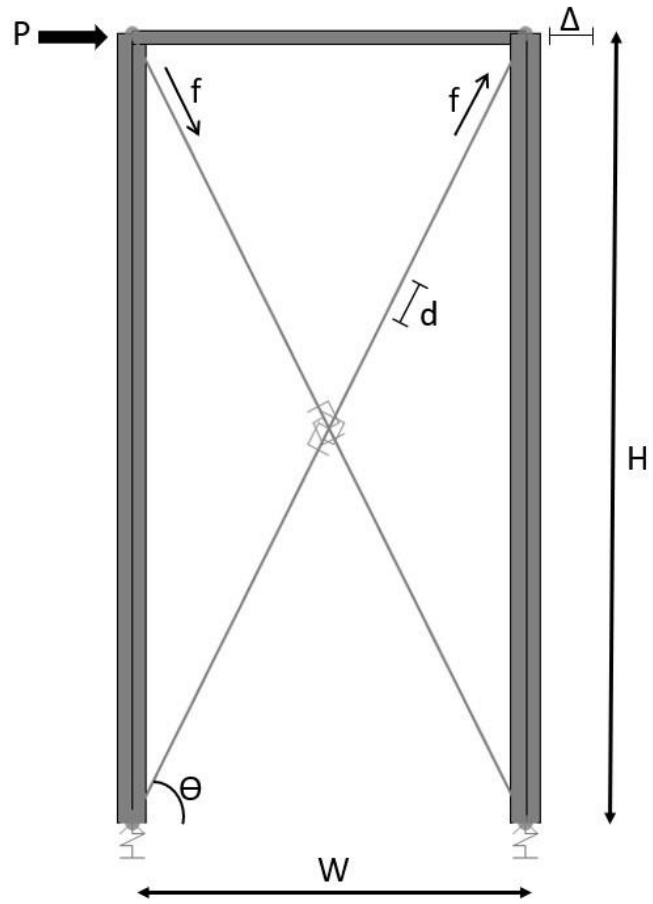
Figure 9.3 Single wall numerical model
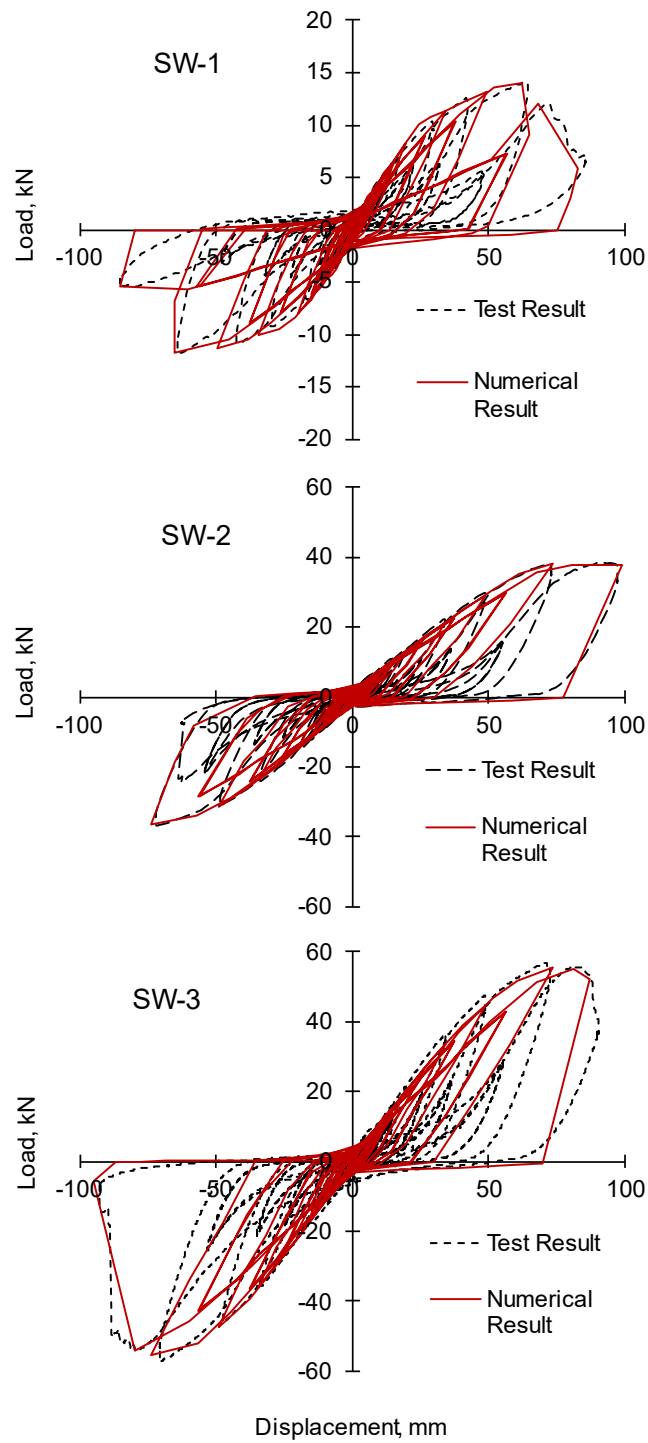
Figure 9.4 Comparison of predicted and measured wall panel behaviors
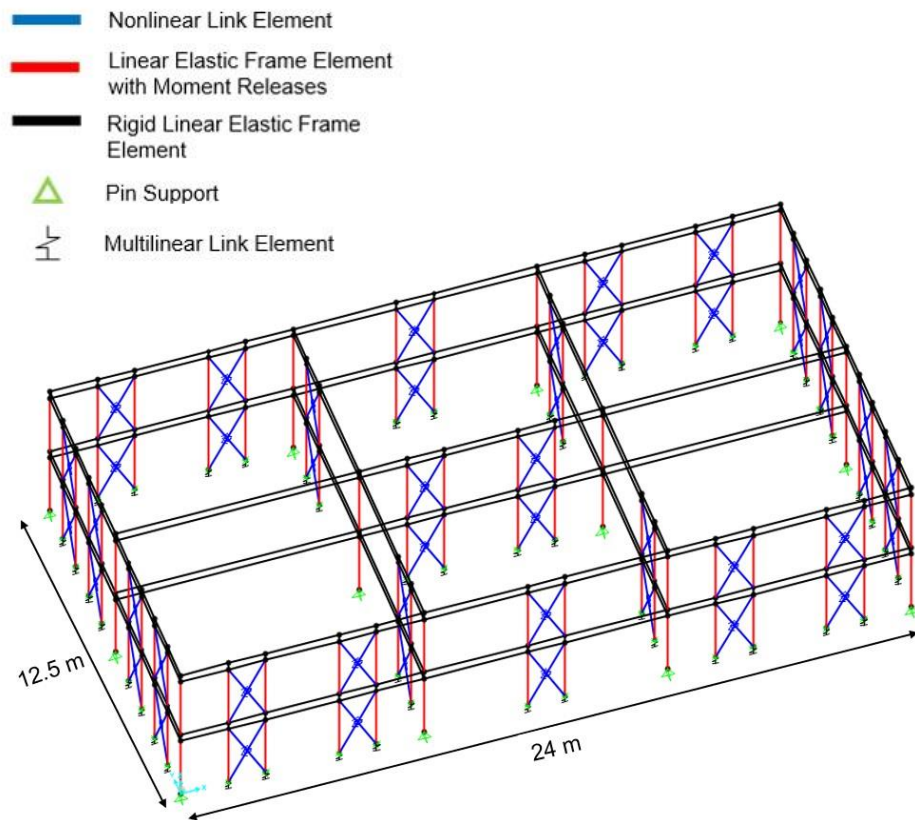
Figure 9.5 Representation of archetype building numerical model
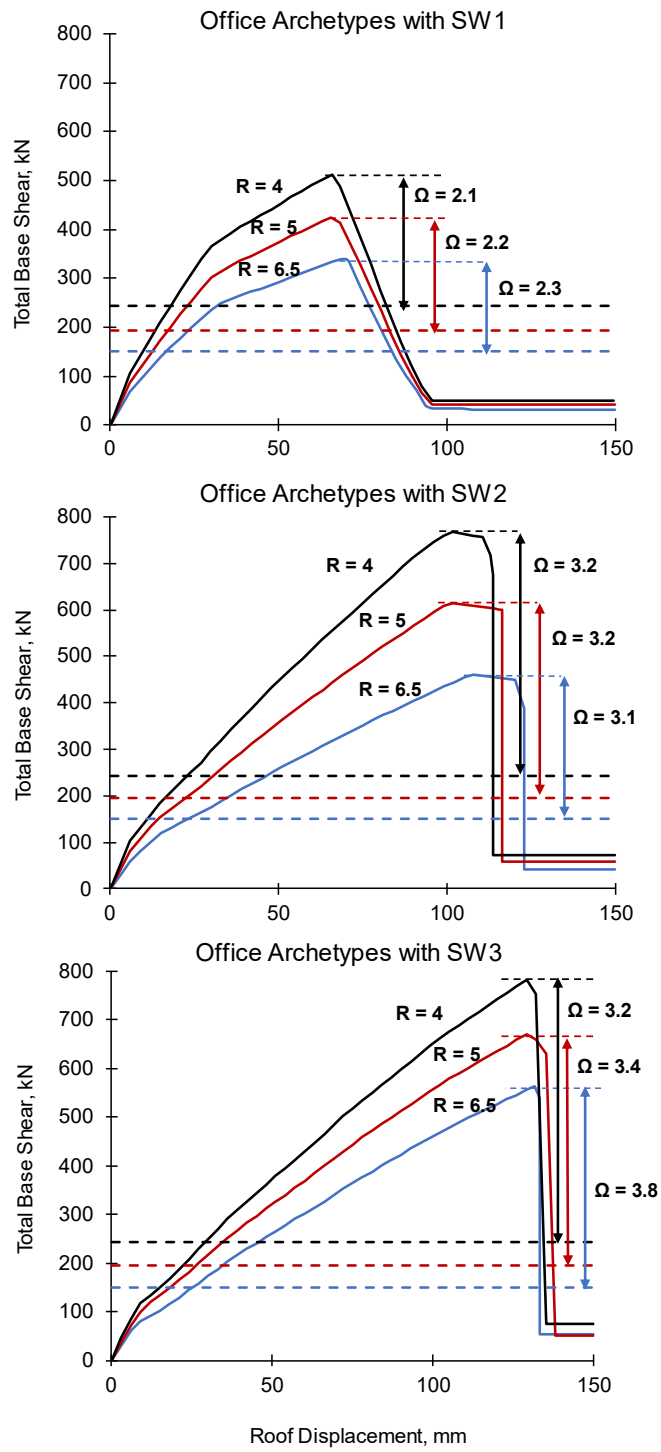
Figure 9.6 Pushover analysis results for office archetypes
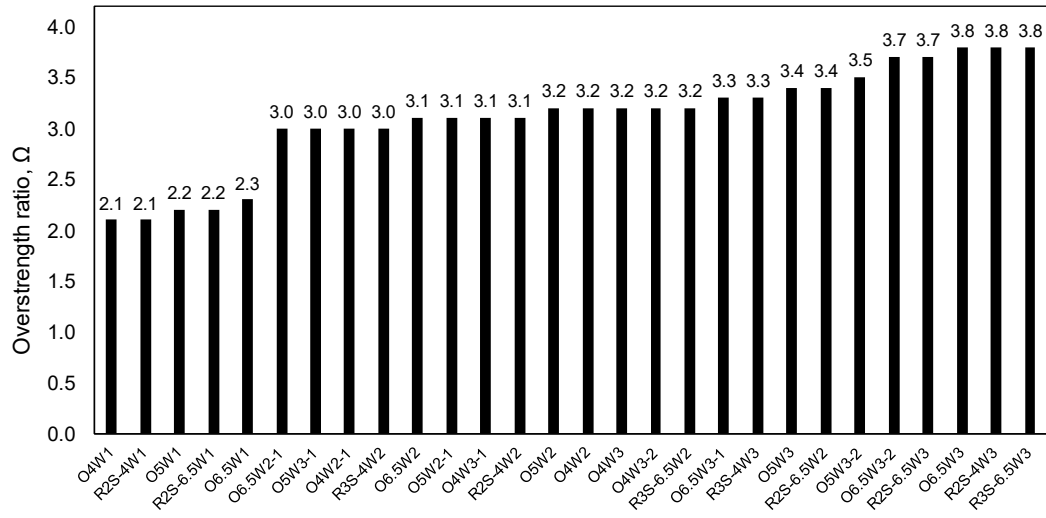
Figure 9.7 Overstrength factor values of archetype buildings
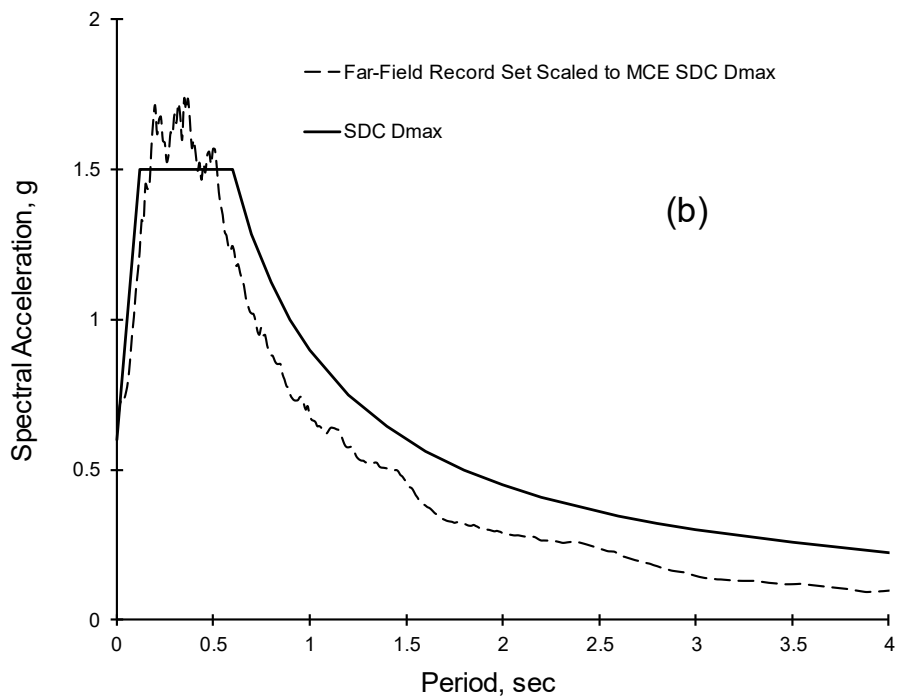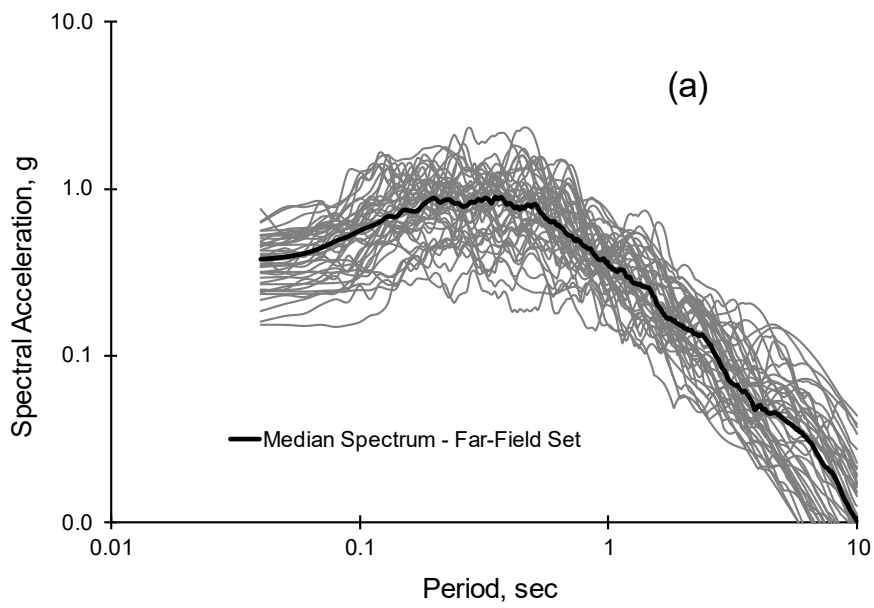
Figure 9.8 Response spectra for far-field ground motion record set: (a) response spectra; (b) anchoring far-field record set to MCE spectral demand
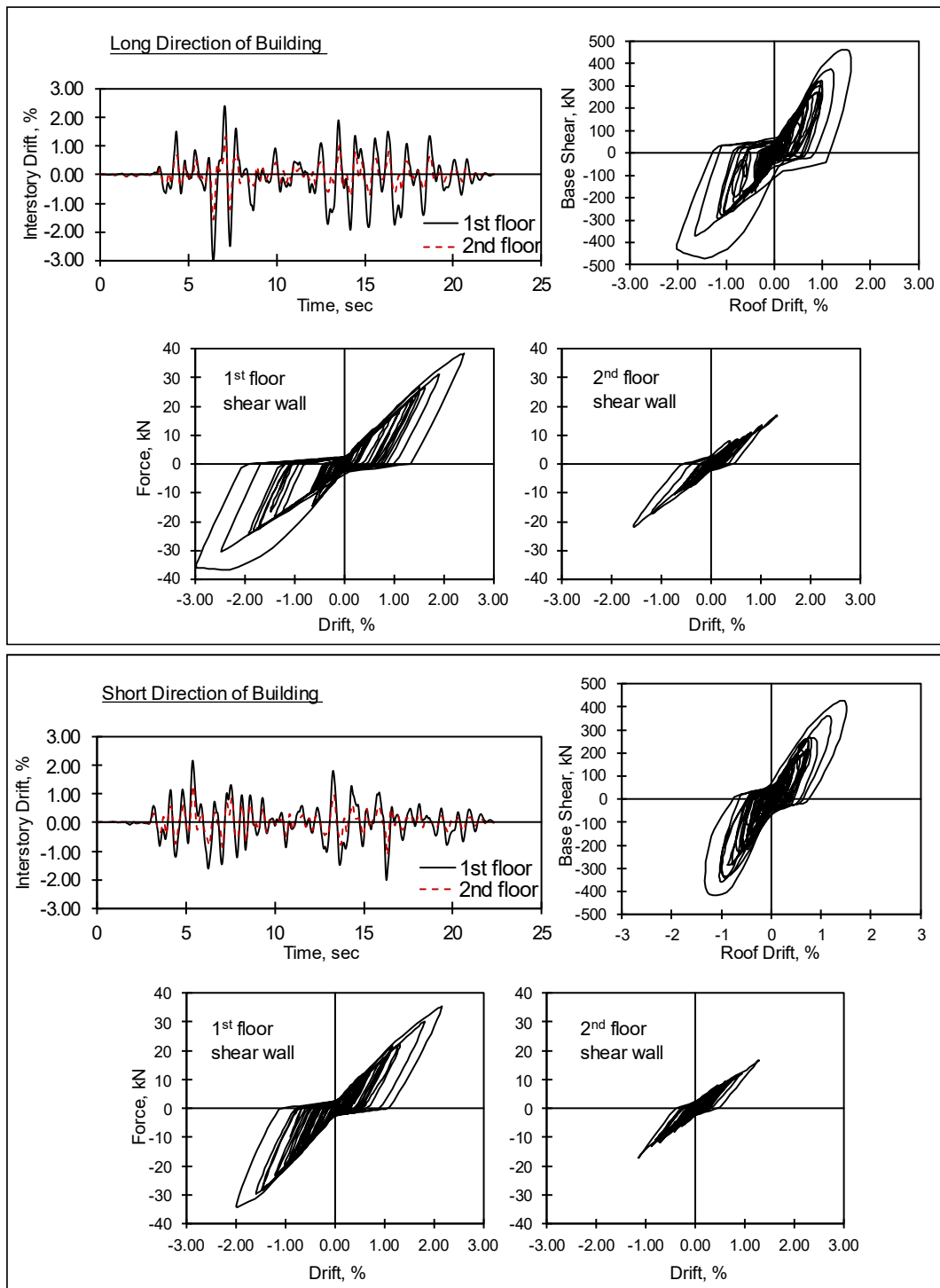
Figure 9.9 Nonlinear time history analysis results for archetype O6.5W2

243
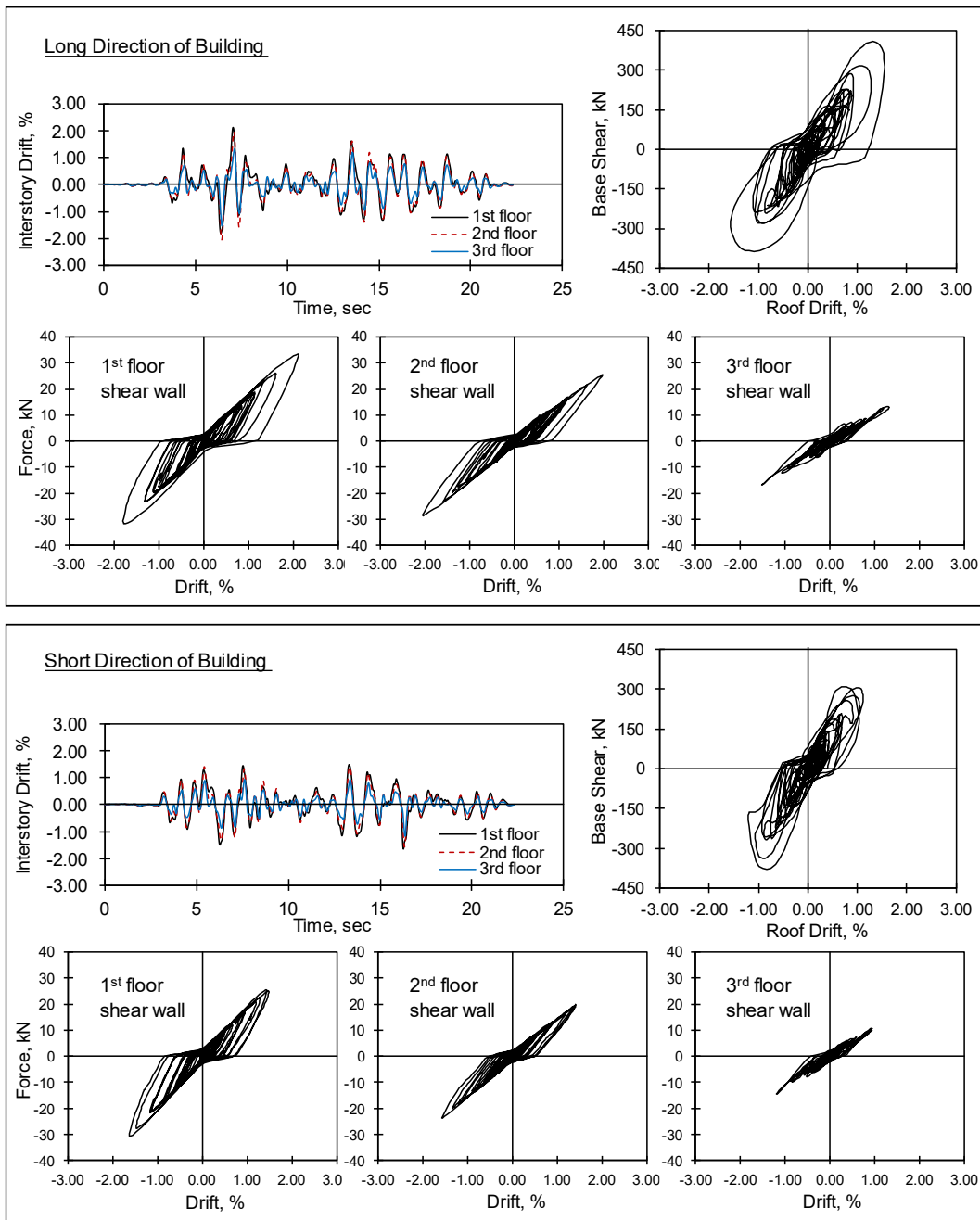
Figure 9.10 Nonlinear time history analysis results for archetype R3S-6.5W2

244
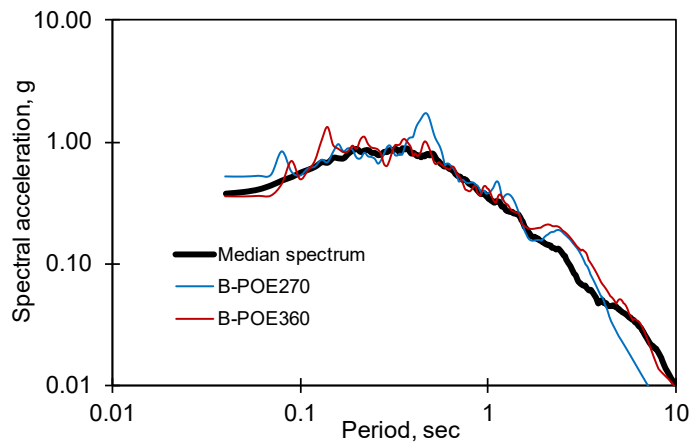
Figure 9.11 Comparison of the response spectrum of records from ground motion #17 and the median spectrum of the far-field record set
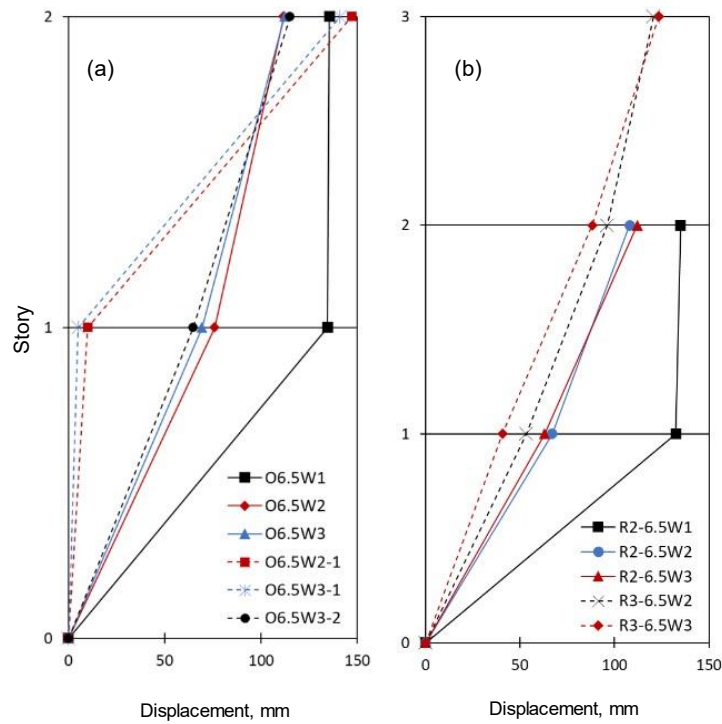
Figure 9.12 Displacement profiles for archetypes: (a) office buildings; (b) residential buildings, under ground motion #17
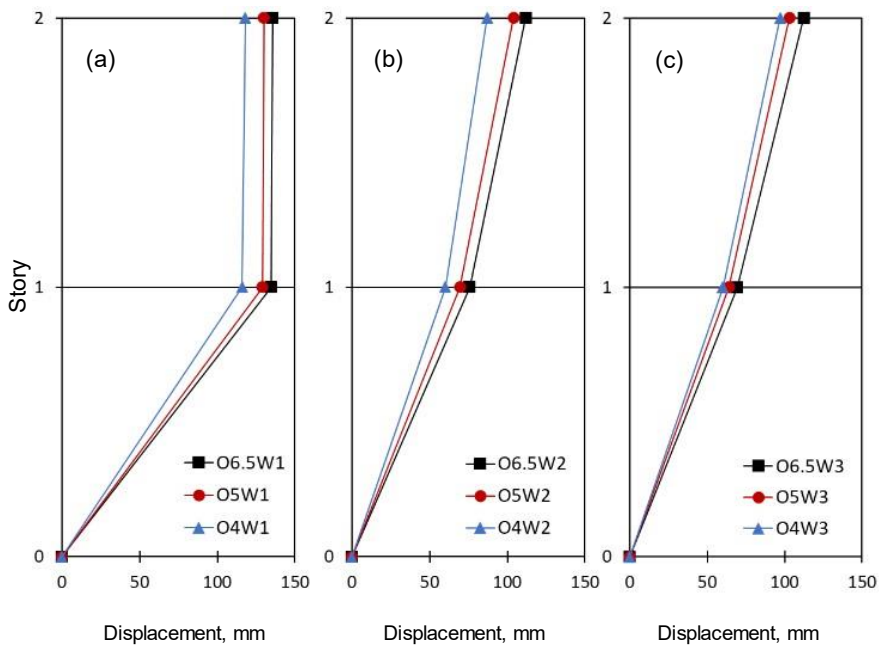
Figure 9.13 Displacement profiles for office archetypes with shear walls: (a) SW1;
(b) SW2; (c) SW3, under ground motion #17
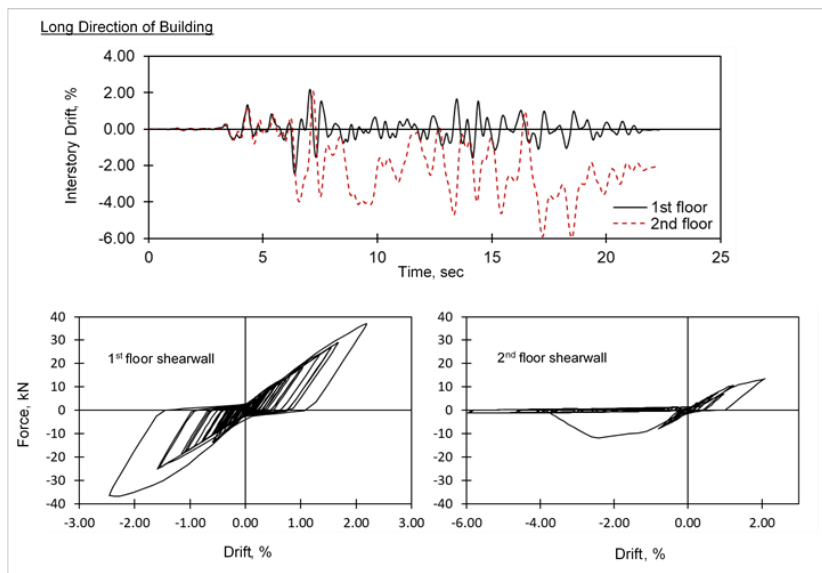
Figure 9.14 Nonlinear time history analysis results for archetype O6.5W2-1
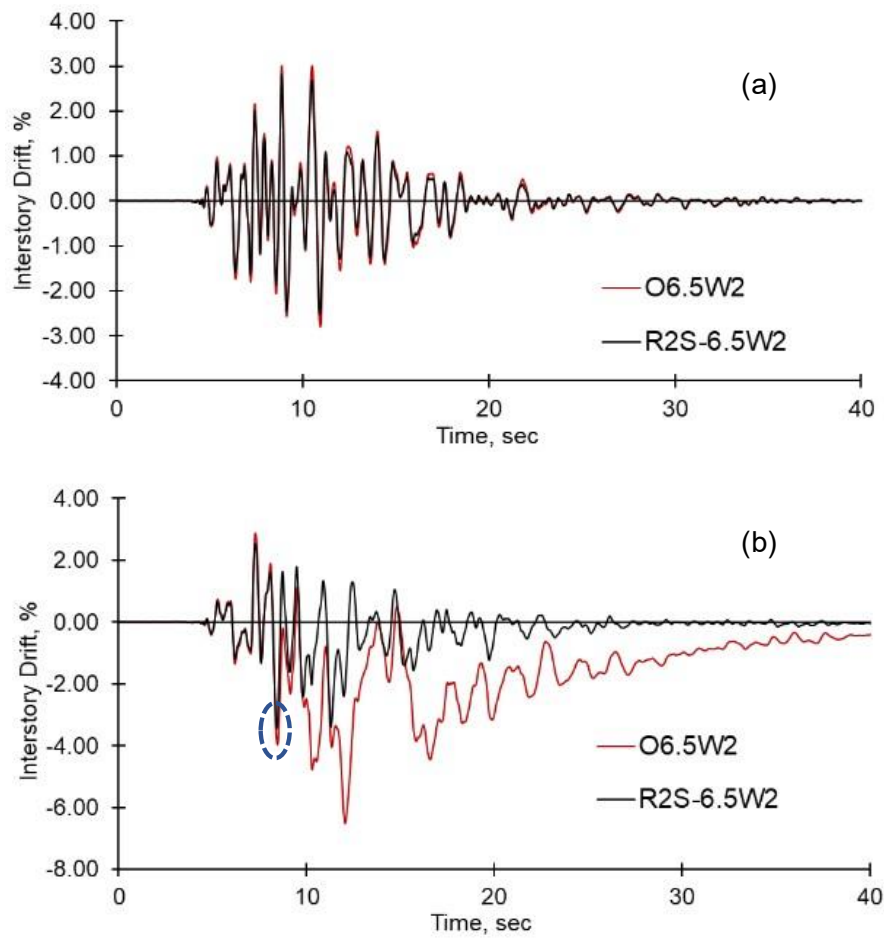
Figure 9.15 Nonlinear time history analysis results for archetypes O6.5W2 and
R2S-6.5W2 under ground motion #7: (a) long direction; (b) short direction

CHAPTER 10

CONCLUSIONS

In this thesis, outcomes of an extensive experimental research program on CFS framed sheathed shear walls are presented. While the main concern of the presented work was the behavior of CFS shear walls under applied lateral loads, various other aspects of these systems were also investigated in detail. These aspects include behavior of hold down devices that are connecting wall panels to rigid foundation, different sheathing and fastener spacing configurations used in shear walls, connection details between multiple walls whether they are placed horizontally or vertically and behavior of shear walls when utilized in a three dimensional structural assembly along with a floor system.

In addition to the experimental part, a numerical study is also included in the scope of this work. By using the experimental findings and load-displacement behavior data obtained from CFS shear walls, both single wall panels and full scale buildings were modeled and analyzed.

All of these different parts of the study are presented in several previous chapters and similarly, conclusions obtained from each part are given seperately as follows.

10.1   Conclusions Regarding Hold Down Devices

This part of the study was conducted in order to evaluate the performance of various types of hold downs in terms of strength and stiffness, as well as to demonstrate that simple hold down geometries that are relatively easy and less costly to fabricate can substitute or be an alternative to the widely used devices. Even though patented off-

the-shelf hold down devices are available in the market in some countries these devices usually employ a special and sometimes complex geometry to meet the stiffness and strength requirements. Manufacturing of such devices requires a special production line for cutting and bending of plates, drilling of holes and other necessary operations. For economies where CFS construction is limited, development of such production lines becomes infeasible. In order to reveal new and more affordable hold down geometries a new hold down device that consists of a hot rolled steel angle section was manufactured and tested as a part of the experimental program. The advantage of this angle type hold down is that it does not require costly bending or welding operations which are required for the other hold down types.

In the first phase of this part of the study, eleven monotonic and three cyclic loading tests on seven different types of hold down devices were completed. Loading tests proved that the angle type of hold down device not only behaves properly in terms of strength and stiffness, but also outperforms hold downs obtained from various manufacturers.

In addition to testing different types of hold down devices, additional parameters such as the number and size of connection screws, placement of hold down and applications to reduce screw tilting were also investigated. Loading tests showed that the number and size of connection screws are crucial parameters that increase both the load capacity and the stiffness of hold down assemblies, especially when the hold down device itself possess relatively high strength and stiffness.

Hold down assembly tests revealed that hold down devices HD-1 and HD-2, which have been used in CFS construction, exhibited very poor behavior. These hold downs were observed to undergo significant deformations under tensile loading and as a result had limited load capacities. Load capacity of some of these devices remain well below the force demand levels typically occur in CFS wall systems. The limited load capacity and stiffness obtained during load tests make some of these devices

250

unsuitable for CFS structural systems for the purpose of transferring the wall panel chord stud forces to the foundation system at the wall base.

The experimentally observed deformation mode of all hold down device types was correctly captured by the FE models. For devices where the response is mainly controlled by the deformation of the hold down itself, the numerically obtained load-displacement response agrees well with the experimentally determined response of test specimens. For hold downs with relatively high strength and stiffness, the main deformation mechanism becomes tilting and shear deformation of connection screws as well as the bearing deformation of vertical CFS framing member localized around these screws. Finite element analysis indicates substantially high initial stiffness for these devices and the numerically obtained response overpredicts the stiffness as compared to the experimentally determined response of test specimens. The discrepancy between the numerical and experimental response of these devices arises from the deformation of components that were not present in FE models.

In the second phase, angle type hold down devices were used in two CFS framed OSB sheathed wall panel specimens. The wall panels were subjected to cyclic lateral loading. The intent was to investigate the behavior of these hold down devices when used as part of a wall panel. The close agreement between the wall panel test results and those obtained from the hold down assembly tests indicated that the specimen geometry and loading method used in the assembly tests accurately represent the conditions that these hold downs are subjected to when used in wall panels.

 Load capacity of the two wall panel specimens tested in the current study is in good agreement with load capacities presented in the AISI S400-15 (2015) Specification as well as the measured load capacity of OSB sheathed CFS wall panels tested by other researchers. This observation indicates that the angle type hold down device enables proper load transfer between the wall panel and the foundation system, and has adequate mechanical performance to develop the expected strength of wall panel.

It can be concluded that this type of hold down device, which requires less workmanship and fabrication cost than some of the widely used devices, is promising and can be an alternative to more traditional hold down devices currently being used in CFS structural systems.

For the angle type hold downs tested in this study the maximum number of screws that can be placed on one leg of steel angle sections were used and the layout of these screws was such that they are uniformly distributed within the angle leg. The response of angle type hold downs with fewer screws and with different screw layout can be the subject of a future study.

Study on hold down devices continued with a two-phase experimental investigation for the development and evaluation of a hold down device that has energy dissipating feature and aimed to be a cost-effective alternative for CFS structures. Focus of the first phase was the development of the device itself, while the second phase concentrated on the investigation of the performance of this device when used in a sheathed CFS wall panel that is subjected to reversed cyclic lateral loading.

A total of twelve hold down subassembly specimens were tested under monotonic and cyclic loading. The main varying parameter was the number of screws connecting the hold down device to the CFS framing member. Results indicate that the load capacity of the hold downs is mostly limited by the shearing capacity of the connection screws. Increasing the number of connection screws results in an increase in hold down load capacity but the rate of change gets smaller as the number of screws is increased. The hold down devices themselves were observed to remain mostly undamaged. No distinct difference was observed on deformation response of specimens tested under monotonic and cyclic loading. Comparison of the hold down response obtained in this study with several other types of hold downs available in the literature shows that the proposed device is superior in terms of structural behavior while offering a simple geometry.

As part of the second phase, cyclic lateral load tests were conducted on seven CFS framed sheathed wall panels in order to study the energy dissipation ability of the proposed hold down device when used in CFS wall systems. Aligned with this focus, the anchor rods used to connect the hold downs to the foundation system in wall panel specimens were altered mainly by reducing the rod diameter within the middle portion over a certain length to provide controlled rod yielding under tensile forces. In other words, anchor rods were used as structural fuses in order to limit the damage on wall panel itself.

Specimens tested with conventional approach, i.e. constant diameter anchor rod, were observed to fail at load levels significantly below the expected strengths of wall panels either due to fracture of the anchor rod on tension side or buckling of the CFS chord member on compression side. Among specimens tested with controlled yielding concept, i.e. anchor rod diameter reduced within the middle portion, rod fracture occurred before reaching the target 4% drift ratio when rods made of steel with relatively low tensile strength to yield strength ratio were used. The anchor rods in these specimens exhibited somewhat non ductile response by fracturing shortly after the onset of yielding. Replacing the anchor rods with the ones with more favorable material properties together with the controlled yielding concept, the rod fracture was eliminated and the wall specimens were able to maintain the target 4% drifts in both loading directions. Controlled yielding of anchor rods reduces the drift demands imposed on wall panels due to seismic effects, resulting in a minimal damage on wall panels themselves.

The maximum load values for Specimens S4–S7, which were tested with the controlled rod yielding concept, are very close to the expected capacities based on anchor rod fracture. This is an indication that the proposed method produces predictable lateral response with limited damage on wall panel itself. It should be mentioned that even though the use of such structural fuses reduces the drift demands

imposed on wall panels and results in limited damage on wall panel itself, the overall load capacity and stiffness of the wall system decreases because of the use of weakened anchor rods.

10.2   Conclusions Regarding Shear Walls with Two-Sided Sheathing

This part of the thesis work included an integrated experimental and numerical study that was conducted to investigate the lateral load response of CFS-framed wall panels sheathed on both sides with relatively small fastener spacing. The experimental investigation included cyclic tests on nine 1220 mm wide by 2440 mm high shear wall panels. Wall panels were sheathed with 11 mm thick OSB sheets on both sides, with the exception of one supplementary specimen that was sheathed on one side. The following conclusions can be made from this work.

- The deformation modes commonly observed during load testing of wall panels were tilting and pull through of the screws between sheathing panels and CFS framing members, tilting and pull out of the screws connecting hold downs to boundary studs, and distortion of boundary studs in the vicinity of hold down locations.

- The average maximum drift ratios of all cyclic tests were 3.2% and 3.0% in two loading directions. The corresponding average drift ratios at peak load capacity were 2.9% and 2.7%. Among all tested wall panels, only the panels tested with the controlled yielding concept and with anchor rods made of AISI 1040 grade steel were able to complete the 4% drift cycles in both loading directions.

- Providing double-sided sheathing resulted in less than two times improvement in wall response when compared to the corresponding single-sided sheathing case due to deformation of other components of the wall panel.

- The average ductility related modification factor and the corresponding average material related overstrength factor for the tested wall panels were determined to be 1.75 and 1.12, respectively.

- The fastener-based and the equivalent brace modeling approaches involves different levels of modeling effort. The fastener-based approach is not as computationally efficient as the equivalent brace approach due to the need for modeling of each individual connection fastener. On the other hand, with the fastener-based approach, the experimental data required for the calibration of the material model can be obtained more easily with small scale fastener tests. The material model for equivalent brace elements has to be calibrated with data from load testing of full scale wall panels, which involves a significant effort. From this perspective, the equivalent brace method would be more suitable for modeling of large scale and three dimensional CFS structures than the fastener-based method, provided that the material model for the brace elements are calibrated with data from wall panel testing.

10.3   Conclusions Regarding Multi-Panel Shear Walls

Cyclic loading tests were conducted on eight OSB sheathed cold-formed steel shear walls that with 2.44 m x 2.44 m and 2.44 m x 4.88 m dimensions. Wall specimens were formed either from a single CFS framing or by connecting individual wall panel segments. Two connection types were investigated; (1) segments connected by fasteners through stud members and (2) segments connected by OSB sheathing panels. Walls were tested with single side sheathing with 150/300 mm fastener spacing and double side sheathing with 50/100 mm fastener spacing.

During load tests, pull-through of the screws between sheathing panels and CFS framing members were observed especially for wall specimens that were sheathed

on one side with 150/300 mm fastener spacing. For specimens with double side sheathing and dense fastener layout, commonly observed failure mode was the distortion and eventually local buckling of boundary studs at locations close to hold downs. Excessive slip at wall base was also observed when 4.88 wall length was used together with double side sheathing and dense fastener layout.

Majority of the tested walls were able to reach 3% drift ratio. For single side sheathing and 150/300 mm fastener spacing, change in wall length and connection detail between individual wall segments did not cause any appreciable difference in wall response. For walls with double side sheathing and 50/100 mm spacing, there was a marked increase in wall stiffness with an increase in wall length from 1.22 m to 2.44 m. Load capacity normalized by wall length varies slightly among walls tested with the same sheathing condition (i.e., single side or double side) and fastener spacing. Providing a single 2.44 m long CFS panel or connecting two 1.22 m long panels with two different methods did not cause a major change in the load capacity of wall specimens. Load capacity of double side sheathed walls with 50/100 mm fastener spacing remained below the code specified strength as a result of stud buckling occurred in these walls.

For all wall lengths studied and connection details utilized between individual wall segments, wall sheathed on single side with 150/300 mm fastener spacing possessed larger ductility ratio than the companion wall sheathed on both sides with 50/100 mm fastener spacing. No clear trend exists between ductility ratio and wall length. Results indicate that walls sheathed on single side with 150/300 mm fastener spacing dissipated approximately three times more energy at the end of 2% drift cycle than the companion walls sheathed on both sides with 50/100 mm fastener spacing. Similar to the case with ductility ratio, no clear trend exists between the energy dissipation capacity and wall length.

Based on the experimental findings, no appreciable difference in terms of load capacity and overall behavior was observed between different types of shear walls and both selections can be viable options to be utilized in CFS structures. Therefore, if the preferred method in the construction would be manufacturing shorter individual shear walls (1.22 m long for instance) by assembling framing members and sheathing them on one side prior to transfer to the construction site and given that these shear wall segments are properly connected with fasteners (Type C specimens) to provide load transfer as done in this study, resulting structural performance of shear walls would not be different than walls made of from a single framing. This type of segmental construction of shear walls can be a practical solution and prove to be advantageous in terms of reduced construction time and ease of transportation.

10.4 Conclusions Regarding Two-Story Shear Walls and Three-Dimensional Shear Wall Assemblies

Cyclic loading tests were conducted on eight cold-formed steel framed and OSB sheathed two-story shear wall specimens that were 4.88 m tall and 1.22 m long. The main parameter that was investigated in the experimental program was the different floor framing options utilized between first and second story shear walls. Total of three different framings were investigated; (1) a platform framing detail where a filler truss member was placed between walls, (2) another platform framing detail where gaps are present for the placement of floor beams and (3) ledger framing option in which upper story wall is simply placed on top of the first story shear wall. All floor framing options were represented by two wall specimen configurations in terms of sheathing and fastener spacing. First configuration includes single side sheathing with 150/300 mm fastener spacing and second one includes double side sheathing with 50/100 mm fastener spacing. In addition to that, two specimens each

utilizing a different platform framing were included in tests, in which an additional OSB panel was used for the sheathing of platform framing part.

During testing of wall specimens, three major types of failure were observed. Especially for specimens that were sheathed on one side with 150/300 mm fastener spacing, pull-through of screws between OSB panels and framing members was the main failure mechanism. For specimens with double side sheathing and 50/100 mm fastener spacing, distortion and eventually buckling of boundary studs was the main failure mechanism. The third type of failure was observed at the platform framing details. In some specimens, platform framing members were distorted and buckled at several locations.

All specimens except one were able to reach 3% or more drift ratio based on the top level of walls. In terms of load capacities, specimens with single side sheathing with 150/300 mm fastener spacing obtained similar results regardless of the utilized floor framing option. For walls with double side sheathing and dense fastener layout, specimens with first platform framing detail and ledger framing were obtained similar results, whereas the specimen with the second platform framing option failed at a relatively early stage of the test and obtained a low load capacity value, given that the platform framing part was excessively damaged. When this specimen is excluded, tested walls showed similar behavior in overall. Another investigated detail which was the inclusion of sheathing for the platform framing part in two specimens, enhanced the behavior of these walls especially in terms of load capacity values.

In addition to obtained wall responses, deformations were measured throughout the height of specimens to create displacement profiles. These profiles along with the individual responses of first and second story shear walls, several observations are made. In general, lateral deformations for the second type of platform framing were quite large and these deformations greatly contributed to the total lateral

258

displacement of these shear wall specimens. For specimens utilizing the first type of platform framing on the other hand, although lateral deformations at floor framing were not as critical, uplift deformations between filler truss member and second story shear wall were larger. For two specimens with ledger framing and other two including an additional OSB sheathing for floor framing part, obtained displacement profiles resembled a linear and more favorable profile.

Experimental program on three dimensional shear wall assemblies included eight load tested specimens that were formed by two shear walls placed parallel to each other and a floor system made of three floor trusses along with a sheathing. Three different floor framing details utilized for two story shear wall specimens were also used for three dimensional specimens. Three of the specimens included platform framing detail-1, another three specimens included platform framing detail-2 and last two specimens included ledger framing detail. Similar to specimens in other parts of the thesis, single side sheathing with 150/300 mm screw spacing and double side sheathing with 50/100 mm screw spacing configurations were also considered.

Similar failure types as two story shear wall specimens were also observed for three dimensional assembly specimens. Pull-through of screws between OSB panels and framing members was the main failure mechanism especially for specimens having single side sheathing and 150/300 mm screw spacing configuration. For double side sheathed ones, buckling of boundary studs occurred. Damages on platform framing details were also encountered.

Comparing the responses of wall assembly specimens showed that in general, specimens with ledger type of floor framing showed better performance. Although in terms of load capacities, specimens with different framing options obtained similar results, but specimens with ledger framing were able to reach higher drift values. This is possibly caused by the difference in the force transfer mechanism for different framing details. The lateral load transfer from floor members to shear walls is more

direct in the case of ledger framing whereas for platform type framing, multiple members within the floor-wall connection region experience deformations, thus affecting the overall structural performance.

10.5   Conclusions of Numerical Study

A numerical part of the study on the seismic response of CFS structures with OSB sheathed shear walls was conducted following the FEMA P695 methodology. Twenty-eight archetype buildings were designed with various shear wall types and response modification coefficients. The archetypes consisted of office and residential type buildings and were designed by utilizing three shear wall types and three response modification coefficients. Each shear wall represented a different strength and stiffness level; single side OSB sheathed shear wall SW1 with 150 mm screw spacing, single side OSB sheathed shear wall SW2 with 50 mm screw spacing and double side OSB sheathed shear wall SW3 with 50 mm screw spacing. Response modification coefficients of $R = 6.5$, 5 and 4 were adopted in design along with the deflection amplification factor of $C_d = 4$. The following conclusions can be drawn for archetype buildings designed according to the North American specifications:

- Other than archetypes in which shear wall type SW1 was used, interstory drift limit governs the structural design. In these cases, the number of shear walls needs to be increased beyond what is required for strength requirement.
- Overstrength values ranged between 3 and 3.8 with an average value of 3.3 for archetype buildings where the number of wall panels is governed by drift limitation instead of strength requirement.
- Buildings designed with shear wall SW1, which represents a wall with single-sided OSB sheathing with 150 mm screw spacing at panel edges, fail to satisfy the performance criteria regardless of the response modification coefficient used for design.

- For buildings with shear walls SW2 (i.e., wall with single-sided OSB sheathing with 50 mm screw spacing) and SW3 (i.e., wall with double-sided OSB sheathing with 50 mm screw spacing) a response modification coefficient of $R = 6.5$ is appropriate for the studied office and residential buildings. This justifies the response modification coefficient specified in the American specifications, and indicates that those specified in the Canadian and Turkish specifications are conservative.

- Irregular drift profile occurs with lateral displacement localizing at the first floor when shear wall type SW1 is utilized in both floors. In cases where SW2 or SW3 type shear walls are used at first floor and SW1 type shear wall is used at second floor, significantly larger drifts occur at second floor than at first floor. On the other hand, utilizing SW2 or SW3 type shear walls either alone or in combination results in uniform distribution of lateral displacements among floors.

REFERENCES

AISI. (2010). Research Report RP10-4, Cold-formed steel framing seismic design optimization phase 1a: Seismic equivalency parameter evaluation.

AISI. (2017). American iron and steel institute, monotonic and cyclic response of single shear cold-formed steel-to steel and sheathing-to-steel connections, in: AISI Specifications for the Design of Cold-Formed Steel Structural Members, p. 157.

AISI S100. (2016). AISI, S100-16 North American Specification for the Design of Cold-Formed Steel Structural Members, American Iron and Steel Institute (AISI).

AISI S213. (2007). North American Standard for Cold- formed Steel Framing — Lateral Design, AISIS213, Washington, DC, USA.

AISI S400-15. (2015). North American Standard for Seismic Design of Cold-Formed Steel Structural Systems.

AISI S913-13. (2013). Test Standard for Hold-downs Attached to Cold-formed Steel Structural Framing.

Ansys. (2015). ANSYS Academic Research, Release 16.2.

AS1170.4. (1993). Minimum Design Load on Structures, Part 4, Earthquake Load, Standards Association of Australia, Sydney (NSW, Australia).

ASCE 7-16. (2017). SEI/ASCE, ASCE 7-16 Minimum design loads and associated criteria for buildings and other structures.

AUS/NZS 4600. (2005). Cold-formed steel structures, Australian/ New Zealand standard, Sydney (NSW, Australia).

Ayhan, D., Baer, S., Zhang, Z., Rogers, C. A., Schafer, B. W. (2018). Cold-formed steel framed shear wall database, in: International Specialty Conference on Cold-Formed Steel Structures.

Baran, E., Alıca, C. (2012). Behavior of cold-formed steel wall panels under monotonic horizontal loading. Journal of Constructional Steel Research, 79, 1–8. https://doi.org/10.1016/j.jcsr.2012.07.020

Bian, G., Buonopane, S. G., Ngo, H. H., Schafer, B. W. (2014). Fastener-based computational models with application to cold-formed steel shear walls, in: International Specialty Conference on Cold-Formed Steel Structures.

Bian, G., Padilla-Llano, D. A., Leng, J., Buonopane, S. G., Moen, C. D., Schafer, B. W. (2015). Opensees modeling of cold-formed steel framed wall system, in: International Conference on Behavior of Steel Structures in Seismic Areas.

Blais, C. (2006). Testing and analysis of light gauge steel frame/9 mm OSB wood panel shear walls, in: Dept of Civil Eng. and Applied Mechanics (Master's Thesis), McGill University, Montreal, QC, Canada,.

Boudreault, F.-A. (2005). Seismic analysis of steel frame/wood panel shear walls, in: Dept of Civil Eng. and Applied Mechanics (Master's Thesis), McGill University, Montreal, QC, Canada.

Branston, A. E. (2004). Development of a design methodology for steel frame/ wood panel shear walls, in: Dept of Civil Eng. and Applied Mechanics (Master's Thesis), McGill University, Montreal, QC, Canada,.

Branston, A. E., Chen, C. Y., Boudreault, F. A., Rogers, C. A. (2006). Testing of light-gauge steel-frame - Wood structural panel shear walls. Canadian Journal of Civil Engineering, 33(5), 561–572. https://doi.org/10.1139/L06-014

Buonopane, S. G., Bian, G., Tun, T. H., Schafer, B. W. (2015). Computationally efficient fastener-based models of cold-formed steel shear walls with wood sheathing. Journal of Constructional Steel Research, 110, 137–148. https://doi.org/10.1016/J.JCSR.2015.03.008

Chen, C. Y. (2004). Testing and performance of steel frame/wood panel shear walls.

COLA-UCI. (2001). Report of a testing program of light-framed walls with wood-sheathed shear panels. Final report to the City of Los Angeles Department of Building and Safety, Structural Engineers Association of Southern California. Irvine, CA.

Derveni, F., Gerasimidis, S., Schafer, B. W., Peterman, K. D. (2021). High-Fidelity Finite Element Modeling of Wood-Sheathed Cold-Formed Steel Shear Walls. Journal of Structural Engineering, 147(2), 04020316. https://doi.org/10.1061/(asce)st.1943-541x.0002879

Dolan, J. D., Easterling, W. S. (2000). Monotonic and Cyclic Tests of Light-Frame Shear Walls with Various Aspect Ratios and Tie-Down Restraints, Report No. TE-2000-001, Virginia Polytechnic Institute and State University, Blacksburg, VA.

Dubina, D. (2008). Behavior and performance of cold-formed steel-framed houses under seismic action. Journal of Constructional Steel Research, 64(7–8), 896–913. https://doi.org/10.1016/J.JCSR.2008.01.029

EN 1993-1-3. (2006). CEN, EN 1993-1-3 Eurocode 3: Design of steel structures-Part 1-3: General rules-Supplementary rules for cold-formed members and sheeting, European Committee for Standardization, Brussels.

EN 1998-1. (2004). CEN, EN 1998-1 Eurocode 8: Design of Structures for Earthquake Resistance-Part 1: General Rules, Seismic Actions and Rules for Buildings, European Committee for Standardization, Brussels.

FEMA P695. (2009). FEMA, FEMA P695: Quantification of Building Seismic Performance Factors, Washington, DC, USA.

Fiorino, L., della Corte, G., Landolfo, R. (2007). Experimental tests on typical screw connections for cold-formed steel housing. Engineering Structures, 29(8), 1761–1773. https://doi.org/10.1016/J.ENGSTRUCT.2006.09.006

Fiorino, L., Iuorio, O., Landolfo, R. (2009). Sheathed cold-formed steel housing: A seismic design procedure. Thin-Walled Structures, 47(8–9), 919–930. https://doi.org/10.1016/J.TWS.2009.02.004

Fiorino, L., Iuorio, O., Landolfo, R. (2012). Seismic analysis of sheathing-braced cold-formed steel structures. Engineering Structures, 34, 538–547. https://doi.org/10.1016/J.ENGSTRUCT.2011.09.002

Fiorino, L., Macillo, V., Landolfo, R. (2017). Shake table tests of a full-scale two-story sheathing-braced cold-formed steel building. Engineering Structures, 151, 633–647. https://doi.org/10.1016/J.ENGSTRUCT.2017.08.056

Fiorino, L., Shakeel, S., Macillo, V., Landolfo, R. (2017). Behaviour factor (q) evaluation the CFS braced structures according to FEMA P695. Journal of Constructional Steel Research, 138, 324–339. https://doi.org/10.1016/j.jcsr.2017.07.014

Fülöp, L. A., Dubina, D. (2004a). Performance of wall-stud cold-formed shear panels under monotonic and cyclic loading - Part I: Experimental research. Thin-Walled Structures, 42(2), 321–338. https://doi.org/10.1016/S0263-8231(03)00063-6

Fülöp, L. A., Dubina, D. (2004b). Performance of wall-stud cold-formed shear panels under monotonic and cyclic loading: Part II: Numerical modelling and performance analysis. Thin-Walled Structures, 42(2), 339–349. https://doi.org/10.1016/S0263-8231(03)00064-8

Hikita, K. (2006). Combined gravity and lateral loading of light gauge steel frame/wood panel shear walls, in: Dept of Civil Eng. and Applied Mechanics (Master's Thesis), McGill University, Montreal, QC, Canada,.

Iuorio, O., Fiorino, L., Landolfo, R. (2014). Testing CFS structures: The new school BFS in Naples. Thin-Walled Structures, 84, 275–288. https://doi.org/10.1016/j.tws.2014.06.006

Kechidi, S., Banks, N., Iuorio, O. (2021). Contribution of OSB sheathing to racking capacity of cold-formed steel frames, ce/papers. 4 2-4, 393-400.

Kechidi, S., Bourahla, N., Castro, J. M. (2017). Seismic design procedure for cold-formed steel sheathed shear wall frames: Proposal and evaluation. Journal of Constructional Steel Research, 128, 219–232. https://doi.org/10.1016/j.jcsr.2016.08.018

Krawinkler, H., Parisi, F., Ibarra, L., Ayoub, A., Medina, R. (2001). CUREE-development of a testing protocol for woodframe structures-w-02.

Kuşyılmaz, A., Topkaya, C. (2016). Evaluation of seismic response factors for eccentrically braced frames using FEMA P695 methodology. Earthquake Spectra, 32(1), 303–321. https://doi.org/10.1193/071014EQS097M

Landolfo, R., Fiorino, L., Corte, G. D. (2006). Seismic Behavior of Sheathed Cold-Formed Structures: Physical Tests. https://doi.org/10.1061/ASCE0733-94452006132:4570

Landolfo, R., Fiorino, L., Corte, G. D. (2006). Seismic performance of sheathed coldformed shear walls, in: CCFSS Proceedings of International Specialty Conference on Cold-Formed Steel Structures (1971-2018), p. 7. https://scholarsmine.mst.edu/isccss/17iccfss/17iccfss-session8/7

Landolfo, R., Shakeel, S., Fiorino, L. (2022a). Lightweight steel systems: Proposal and validation of seismic design rules for second generation of Eurocode 8. Thin-Walled Structures, 172. https://doi.org/10.1016/j.tws.2021.108826

Landolfo, R., Shakeel, S., Fiorino, L. (2022b). Lightweight steel systems: Proposal and validation of seismic design rules for second generation of Eurocode 8. Thin-Walled Structures, 172. https://doi.org/10.1016/j.tws.2021.108826

Leng, J. (2015). Simulation of Cold-Formed Steel Structures, Johns Hopkins University, Baltimore, MD.

Leng, J., Buonopane, S. G., Schafer, B. W. (2020). Incremental dynamic analysis and FEMA P695 seismic performance evaluation of a cold-formed steel–framed building with gravity framing and architectural sheathing. Earthquake Engineering and Structural Dynamics, 49(4), 394–412. https://doi.org/10.1002/eqe.3245

Leng, J., Peterman, K. D., Bian, G., Buonopane, S. G., Schafer, B. W. (2017). Modeling seismic response of a full-scale cold-formed steel-framed building. Engineering Structures, 153, 146–165. https://doi.org/10.1016/j.engstruct.2017.10.008

Li. (2012). C. Li, Nominal Shear Strength of Cold-Formed Steel Shear Walls using OSB Sheathing (Master's Thesis), University of North Texas,.

Liu, P., Peterman, K. D., Schafer, B. W. (2014). Impact of construction details on OSB-sheathed cold-formed steel framed shear walls. Journal of Constructional Steel Research, 101, 114–123. https://doi.org/10.1016/j.jcsr.2014.05.003

Macillo, V., Fiorino, L., Landolfo, R. (2017). Seismic response of CFS shear walls sheathed with nailed gypsum panels: Experimental tests. Thin-Walled Structures, 120, 161–171. https://doi.org/10.1016/J.TWS.2017.08.022

Madsen, R. L., Castle, T. A., Schafer, B. W. (2016). NEHRP Seismic Design Technical Brief No . 12 Seismic Design of Cold-Formed Steel Lateral Load-Resisting Systems A Guide for Practicing Engineers. 12.

McKenna, F. (2011). Open System for Earthquake Engineering Simulation (OpenSees), Pacific Earthquake Engineering Research Center, Berkeley, CA.

Morgan, K. A., Sorhouet, M. A., Serrette, R. (2002). Performance of Cold-formed Steel-framed Shear Walls: Alternative Configurations. AISI-Specifications for the Design of Cold-Formed Steel Structural Members, 48.

Nava, M., Serrette, R. (2015). Strength Reduction Factors for High-Aspect-Ratio OSB Cold-Formed Steel Frame Shear Walls. Journal of Structural Engineering, 141(5).

Newmark, N. M., Hall, W. J. (1982). Earthquake spectra and design, in: Engineering Monographs on Earthquake Criteria, Structural Design, and Strong Motion Records, Vol. 3, Earthquake Engineering Research Institute, Oakland, CA.

Nguyen, H., Georgi, H., Serrette, R. (1996). Shear wall values for light weight steel framing, in: AISI-Specifications for the Design of Cold-Formed Steel Structural Members. 46.

NRCC. (2015). National Building Code of Canada, National Research Council of Canada (NRCC), Ottawa, ON, Canada.

Padilla-Llano, D. A. (2015). A Framework for Cyclic Simulation of Thin-Walled Coldformed Steel Members in Structural Systems (Ph.D. Thesis), Virginia Polytechnic Institute and State University.

Peterman, K. D. (2014). BEHAVIOR OF FULL-SCALE COLD-FORMED STEEL BUILDINGS UNDER SEISMIC EXCITATIONS.

Peterman, K. D., Nakata, N., Schafer, B. W. (2014). Hysteretic characterization of cold-formed steel stud-to-sheathing connections. Journal of Constructional Steel Research, 101, 254–264. https://doi.org/10.1016/J.JCSR.2014.05.019

Salenikovich, A. J., Dolan, J. D., Easterling, W. S. (1999). Monotonic and Cyclic Tests of Long Steel-frame Shear Walls with Openings, AISI-Specifications for the Design of Cold-Formed Steel Structural Members. https://scholarsmine.mst.edu/ccfss-aisi-spechttps://scholarsmine.mst.edu/ccfss-aisi-spec/66

Schafer, B. W., Ayhan, D., Leng, J., Liu, P., Padilla-Llano, D., Peterman, K. D., Stehman, M., Buonopane, S. G., Eatherton, M., Madsen, R., Manley, B., Moen, C. D., Nakata, N., Rogers, C., Yu, C. (2016). Seismic Response and Engineering of Cold-formed Steel Framed Buildings. Structures, 8, 197–212. https://doi.org/10.1016/j.istruc.2016.05.009

Selvaraj, S., Madhavan, M. (2018). Geometric Imperfection Measurements and Validations on Cold-Formed Steel Channels Using 3D Noncontact Laser Scanner. Journal of Structural Engineering, 144(3), 04018010. https://doi.org/10.1061/(asce)st.1943-541x.0001993

Selvaraj, S., Madhavan, M. (2019a). Improvements in AISI Design Methods for Gypsum-Sheathed Cold-Formed Steel Wall Panels Subjected to Bending. Journal of Structural Engineering, 145(2), 04018243. https://doi.org/10.1061/(asce)st.1943-541x.0002223

Selvaraj, S., Madhavan, M. (2019b). Sheathing braced design of cold-formed steel structural members subjected to torsional buckling. Structures, 20, 489–509. https://doi.org/10.1016/J.ISTRUC.2019.04.015

Selvaraj, S., Madhavan, M. (2021). Direct stiffness-strength method design for sheathed cold-formed steel structural members - Recommendations for the AISI S100. Thin-Walled Structures, 162. https://doi.org/10.1016/j.tws.2020.107282

Serrette, R. L. (1997). Additional Shear Wall Values for Light Weight Steel Framing, Report No. LGSRG-1-97, Department of Civil Engineering, Santa Clara University, SantaClara, CA, USA.

Serrette, R., Member, A., Asce, K. O. (n.d.). SHEAR RESISTANCE OF GYPSUM-SHEATHED LIGHT-GAUGE STEEL STUD WALLS.

Shakeel, S., Fiorino, L., Landolfo, R. (2020a). Behavior factor evaluation of CFS wood sheathed shear walls according to FEMA P695 for Eurocodes. Engineering Structures, 221. https://doi.org/10.1016/j.engstruct.2020.111042

Shakeel, S., Fiorino, L., Landolfo, R. (2020b). Behavior factor evaluation of CFS wood sheathed shear walls according to FEMA P695 for Eurocodes. Engineering Structures, 221. https://doi.org/10.1016/j.engstruct.2020.111042

Shakeel, S., Landolfo, R., Fiorino, L. (2019). Behaviour factor evaluation of CFS shear walls with gypsum board sheathing according to FEMA P695 for Eurocodes. Thin-Walled Structures, 141, 194–207. https://doi.org/10.1016/j.tws.2019.04.017

Shamim, I. (2013). Seismic Design of Lateral Force Resisting Cold-formed Steel Framed (CFS) Structures (Ph.D. Thesis), Department of Civil Engineering and Applied Mechanics, McGill University, Canada.

Shamim, I., Dabreo, J., Rogers, C. A. (2013). Dynamic Testing of Single-and Double-Story Steel-Sheathed Cold-Formed Steel-Framed Shear Walls. https://doi.org/10.1061/(ASCE)

Shamim, I., Rogers, C. A. (2015a). Numerical evaluation: AISI S400 steel-sheathed CFS framed shear wall seismic design method. Thin-Walled Structures, 95, 48–59. https://doi.org/10.1016/j.tws.2015.06.011

Shamim, I., Rogers, C. A. (2015b). Numerical evaluation: AISI S400 steel-sheathed CFS framed shear wall seismic design method. Thin-Walled Structures, 95, 48–59. https://doi.org/10.1016/J.TWS.2015.06.011

Sharafi, P., Mortazavi, M., Usefi, N., Kildashti, K., Ronagh, H., Samali, B. (2018). Lateral force resisting systems in lightweight steel frames: Recent research advances. In Thin-Walled Structures (Vol. 130, pp. 231–253). Elsevier Ltd. https://doi.org/10.1016/j.tws.2018.04.019

Tarpy, T. S., McBrearty, A. R. (1978). Shear Resistance of Steel-Stud Wall Panels with Large Aspect Ratios, Report No. CE-USS-2, Department of Civil Engineering, Vanderbilt University, Nashville, TN.

TBDY. (2018). TBDY 2018, Türkiye Bina Deprem Yönetmeliği.

Topçuoğlugil, Y. (2019). NUMERICAL MODELING OF COLD-FORMED STEEL SHEATHED SHEAR WALLS UNDER LATERAL LOADING.

Usefi, N., Sharafi, P., Ronagh, H. (2019). Numerical models for lateral behaviour analysis of cold-formed steel framed walls: State of the art,

evaluation and challenges. In Thin-Walled Structures (Vol. 138, pp. 252–285). Elsevier Ltd. https://doi.org/10.1016/j.tws.2019.02.019

Vieira, L. C. M., Schafer, B. W. (2012). Lateral stiffness and strength of sheathing braced cold-formed steel stud walls. Engineering Structures, 37, 205–213. https://doi.org/10.1016/j.engstruct.2011.12.029

Vieira, L. C. M., Schafer, B. W. (2013). Behavior and Design of Sheathed Cold-Formed Steel Stud Walls under Compression. Journal of Structural Engineering, 139(5), 772–786. https://doi.org/10.1061/(asce)st.1943-541x.0000731

Yan, Z., Cheng, Y., Shicai, C., Ziqin, J., Wenying, Z. (2021). Shear performance of cold-formed steel shear walls with high-aspect-ratios. Structures, 33, 1193–1206. https://doi.org/10.1016/J.ISTRUC.2021.05.011

Zhang, W., Xu, X., Zheng, Y., Wang, S., Li, Y. (2021). Influencing factors analysis on shear capacity of cold-formed steel light frame shear walls. Structures, 33, 3588–3604. https://doi.org/10.1016/J.ISTRUC.2021.06.064

CURRICULUM VITAE

Surname, Name: Pehlivan, Barış Mert

EDUCATION

Degree	Institution	Year of Graduation
MS	Columbia University Structural Engineering	2014
BS	METU Civil Engineering	2013
High School	Binnaz Ege Rıdvan Ege Anadolu Lisesi, Ankara	2007

FOREIGN LANGUAGES

Advanced English

PUBLICATIONS

1. Pehlivan B.M., Baran E. and Topkaya C. "Testing and analysis of different hold down devices for CFS construction", Journal of Constructional Steel Research, 145 (2018) 97-115.

2. Pehlivan B.M., Baran E. and Topkaya C. "An energy dissipating hold down device for cold-formed steel structures", Journal of Constructional Steel Research, 166 (2020)

3. Pehlivan B.M., Baran E., Topkaya C. and Topcuoglugil Isik Y. "Investigation of CFS shear walls with two-sided sheathing and dense fastener layout", Thin-Walled Structures, 180 (2022)